AD NUMBER

AD442181

LIMITATION CHANGES

TO:

Approved for public release; distribution is unlimited.

FROM:

**Distribution authorized to U.S. Gov't. agencies and their contractors;
Administrative/Operational Use; MAR 1964. Other requests shall be referred to Army Electronic Research and Development Laboratory, Fort Monmouth, NJ.**

AUTHORITY

usaec ltr, 9 dec 1964

[redacted]

442181

meteorology research, inc. & atmospheric research group

2420 n. lake ave. • altadena, calif.

FLAGSTAFF CUMULUS STUDIES

A Joint Report to:

Atmospheric Sciences Section, National Science Foundation
by
Atmospheric Research Group

Final Report under Grants No. NSF G8334 and No. NSF G11969
Covering the Period Spring 1959 - Spring 1964

and

U. S. Army Electronic Research & Development Laboratory
Fort Monmouth, New Jersey
by
Meteorology Research, Inc.

Report No. 4A, Study and Modification of Convective Storms
Contract No. DA 36-039 SC-89066
Order No. 265-62, Project Code No. 8900
Dept. of the Army Project 3A 99-27-005-06
Final Report, Part A
Covering the Period April 1, 1963 - March 31, 1964

Flagstaff Cumulus Studies

A Joint Report

Final Report to Atmospheric Sciences Section, National Science Foundation

Under Grants No. NSF G8334 and No. NSF G11969 to ARG

Covering the Period Spring 1959 - Spring 1964

and

Part A of the Final Report on Study and Modification of Convective Storms

Final Report, Part A, Report No. 4A

Contract No. DA 36-039 SC-89066 with MRI

ARPA Order No. 265-62

Dept. of the Army Project No. 3A99-27-005-06

Project Code No. 8900

Final Report, Part A, covering the period April 1, 1963 to March 31, 1964

Object of the Research: To obtain a quantitative understanding of the physical mechanisms involved in convective storms (nucleation, hydrometeor development, electrification, cloud and storm dynamics), both for natural storms and storms which have been artificially modified.

This report prepared by: Dr. P. B. MacCready, Jr.
Dr. T. B. Smith
Mr. C. J. Todd

TABLE OF CONTENTS

PURPOSE

This basic research program is directed toward obtaining a quantitative and qualitative understanding of the physical mechanisms involved in natural and modified convective storms. The various phases of the convective phenomena are considered from a balanced, integrated viewpoint. The aim is to investigate and understand critical factors such as: nucleation, hydrometeor development, electrification, cloud dynamics, environmental effects, and the complex interrelations between all these separate items. The research technique is built around the concept of an outdoor cloud laboratory, treating the clouds and storms in the simplest possible real situations. Seeding is used as a diagnostic research tool to permit observations of direct and secondary effects on hydrometeor development, electrification, and cloud dynamics.

The program necessarily has entailed the development of equipment and field study techniques. Success of the field program relies on an extensive coordinated effort using radar, other ground observations, and light aircraft systems which probe the dominant factors simultaneously.

ABSTRACT

The Flagstaff Cumulus Studies were initiated in 1959 by Atmospheric Research Group with support from the National Science Foundation. In 1962 the research was expanded with additional sponsorship to Meteorology Research, Inc., affiliated with ARG, coming from the U.S. Army Electronic Research and Development Laboratory. This report covers the field program period from the beginning through 1962 and subsequent related analyses. This is a joint report, constituting the final report by ARG to NSF on Grants No. G8334 and No. G11969, and Part A of the final report by MRI to USAERDL for the second year of Contract DA 36-039 SC-89066. (Part B of the final report by MRI to USAERDL gives results of the 1963 season, and some further analysis of items treated in the present report.)

The Flagstaff Cumulus Studies represent a broad program of investigation into the microphysics and dynamics of cumulus clouds. The program was based on the concept of instrumenting an outdoor laboratory with a coordinated system of aircraft and ground measurement devices of sufficient scope to delineate the dominant factors and interrelations of nucleation, hydrometeor development, electrification, and dynamics. The outdoor laboratory was the area around the isolated San Francisco Peaks in northern Arizona, an area where the regular summer cumulus clouds tend to be cold and thus emphasize the growth of ice phase hydrometeors. The program probed larger and more complex clouds each year as the instrumentation, field techniques, and general understanding of the subject improved; in the final seasons, flights were conducted within major clouds yielding lightning and hail. Cloud seeding by dry ice and silver iodide was used as a research tool to create ice crystals at desired times and places in the test clouds.

Sixteen reports of papers were prepared concerning those studies. Eleven of these have been published or submitted to appropriate journals, and several others are being incorporated into papers on related programs. This final report includes copies of the nine main papers and reports, and summarizes the primary results with respect to the whole program.

New instrumentation techniques were developed as required, the instrumented-outdoor-laboratory concept was developed to an effective operational stage, and the techniques were used to establish certain quantitative aspects of natural and artificial cloud seeding and crystal growth, cloud and cloud-region dynamics, and electrification.

The program provides a basis for certain more specialized investigations, but also, by emphasizing the complex interrelationships of the various factors comprising convective storms, it points out the value of fitting investigations into a broader perspective.

PUBLICATIONS, LECTURES, REPORTS, AND CONFERENCES

The following reports and publications pertain to the initial NSF phase of the Flagstaff Cumulus Studies, relating primarily up to the field season of 1961:

ARG, Progress Report on Field Studies in Cloud Physics (Flagstaff Cumulus Studies) submitted to NSF September 30, 1959.

Todd, C. J., Precipitation Initiation in Summer Cumulus at Flagstaff, Arizona. 8th Weather Radar Conf., San Francisco, April 1960.

MacCready, P. B., Jr., Equipment for Field Studies in Cloud Physics. ISA Preprint 8-SF60, ISA Conference, San Francisco, May 1960.

ARG, Brief Resume Report to the National Science Foundation on Flagstaff Cumulus Studies, Grant No. NSF G8334. Submitted to NSF June 15, 1960.

ARG, Flagstaff Meteorological Studies, Summer 1960. Picture Booklet of exhibit of Museum of Northern Arizona, distributed by ARG, October 1960.

MacCready, P. B., Jr., A Review of Small Cumulus Studies and the Modification of Hail. Nubila, IV, N. 1, 1961 (from International Congress on the Physics of Cloud, Verona, Italy, August 1960).

MacCready, P. B., Jr., Memorandum on Yellowstone Park Studies. Contained in Publication #1, ASRC of the State University of New York, Final Report, 1961 Yellowstone Field Research Seminar, V. J. Schaefer, Chairman.

Todd, C. J., A Study of Cloud Composition. 9th Weather Radar Conf., Kansas City, October 1961.

Todd, C. J., Memorandum on 2nd Yellowstone Field Research Seminar. Contained in Publication #5, ASRC-SUNY, May 1962.

MacCready, P. B., Jr., The Continuous Particle Sampler at the Puy de Dome Comparison Conf. Bulletin de l'Observatoire du Puy de Dome, No. 1, 1962.

Todd, C. J., and E. Hindman, II, Memorandum on 3rd Annual Yellowstone Field Research Seminar. Contained in Publication #13, ASRC-SUNY, March 1963.

The results pertaining to the expanded field operations in 1962 are given by:

MacCready, P. B., Jr., T. B. Smith, C. J. Todd, C. W. Chien, and B. Woodward, Study and Modification of Convective Storms. Final Report, MRI Contract No. DA 36-039 SC-89066, USAERDL, May 1963. AD 415 347.

In addition, there have been prepared the nine papers which appear as appendices in this report (see Table of Contents), seven of which have been submitted to appropriate journals.

MRI has submitted a final report to Naval Research Laboratory - Office of Naval Research on Contract Nonr-3819(00)(X), "Continuous Particle Sampler Study Program", by P. B. MacCready, Jr., and R. E. Williamson, December 1963, which furthered the development of the sampler originally developed by ARG and used on the joint ARG-MRI studies. This project was thus interrelated with the program of this report.

Papers were presented at meetings by Todd (the 8th and 9th Weather Radar Conferences, on the echoes in seeded clouds and the continuous sampler, the 1964 AMS-Los Angeles meeting on ice crystal development in a seeded cloud, and the 1964 AMS-Chicago cloud physics meeting on ice crystal growth and quantitative seeding), and by MacCready (ISA 1960 meeting on instrumentation, 1960 meeting at Verona, Italy, on the general field studies, and 1962 AGU meetings on hydrometeor charge evolution).

NSF field research trips, in addition to the Flagstaff field work, consisted of MacCready visiting Yellowstone Park and attending the sampler comparison program in France, Todd visiting Yellowstone Park twice, and Hindman visiting Yellowstone Park once.

Conferences at Flagstaff in 1962 and 1963 are detailed in the MRI final reports to USAERDL (AD 415 347 for the 1962 season, Part B of the Final Report for the 1963 season).

DISCUSSION

A. Introduction

This is the final report to the Atmospheric Sciences Section of the National Science Foundation under Grants No. G8334 and No. G11969, and Part A of the Final Report to USAERDL by MRI on the 1963-1964 program. This report consists of a summary of activities and results plus appendices which are separate papers on particular subjects. The report is a complete review of the NSF work, and a partial account of the work for USAERDL. This report and the later Part B of the Final Report to USAERDL have some overlap in that each document can separately present a complete picture of results.

The aim of the research has been to advance the physical understanding of natural and modified convective clouds and storms, utilizing the outdoor laboratory afforded by the clouds in the summer at Flagstaff, Arizona. Cloud seeding was sometimes used as a research tool to alter the laboratory setup in a desired way at a desired time. The research technique has been to consider the interrelationships of the various factors which dominate the development of cumulus clouds and their hydrometeors and electrification. Thus the scope of the program has been very broad, including nucleation, hydrometeor growth, cloud dynamics, and electrification, and requiring considerable development of instrumentation and techniques.

The results of the program have depended to a considerable extent on concurrent sponsorship of associated studies. One uniquely valuable program was the related MRI project, "Continuous Particle Sampler Study Program", Contract Nonr-3819(00)(X), from the U.S. Naval Research Laboratory and Office of Naval Research. The Flagstaff Cumulus Studies were preceded by an MRI investigation of electrification due to seeding, "Cloud Electrification Study", Contract No. AT(04-3)-236, from the Atomic Energy Commission. The U.S. Army Electronics Research and Development Laboratory, the Air Force Cambridge Research Laboratories, the University of Chicago, and the University of Michigan all conducted field investigations at Flagstaff during the course of the NSF grants. Many visiting scientists observed the Flagstaff studies in action, and seminars were held regularly at Flagstaff to promote exchanges of ideas between the various scientists and to acquaint students with the subjects.

Atmospheric Research Group employed meteorology students for some of the summer work, and two of the students were able to contribute articles of their own to this program. In addition, for two seasons

Dr. V. J. Schaefer of the New York State University has conducted an atmospheric science field laboratory for advanced young students at Flagstaff, with the students assisting some in the research projects.

B. General Project Background

The Flagstaff Cumulus Studies have been interwoven with the efforts of various research groups for the mutual benefit of all. The interrelated programs were as follows (the programs are listed in the year pertaining to the field effort, although the analysis of the field season may considerably overlap the following field periods):

1956 USFS Project Skyfire introductory program at Flagstaff, some MRI personnel.

1958 MRI AEC-sponsored electrification study (seeding to produce definite electrification), final report July 1959. MRI small service contract with GRD (AFCRL).

1959 ARG-NSF Grant No. NSF G8334. General small cloud studies, traverses, electrification. MRI small service contract with GRD (Anderson). University of Michigan and University of Chicago (Fujita) participating.

1960 ARG-NSF Grant No. NSF G11969. Special emphasis on convective cloud sources and characteristics. GRD (Anderson, Cunningham, Fitzgerald) participating in own program, and Fujita with a major meso-network.

1961 ARG-NSF continued, more seeding, general studies, development of spiral ascent technique. GRD (Atlas, L'Hermitte, Cunningham, Fitzgerald). University of Michigan drop spectrometer. Hallett, UCLA.

1962 ARG-NSF continued, major studies, hydrometeor charging, advanced data reduction, seeding continued. USFS (Fuquay) help in seeding to ARG-MRI. MRI-USAERDL contract for expanded work. Also USAERDL (Weickmann, Kascmir) conducting their own studies. Cooperation with Schaefer advanced student field studies. MRI-NRL-ONR contract for continuous sampler development.

1963 Major MRI-USAERDL programs continued, as well as MRI-NRL-ONR project.

C. The Over-All Project

Obtaining significant physical understanding of the dominant factors in convective dynamics and precipitation necessarily involves a complex group of related studies. An underlying philosophy of this whole program has been to make the study as simple as possible, while realizing that even in the simplest case a convective cloud represents a very complex phenomenon. As the project tools, techniques, and understanding were improved each year, it became possible to study larger and more complex clouds and cloud systems. Thus at the beginning the instrumentation in the aircraft was rudimentary; the aircraft probed the clouds only when they were relatively small; the ground network was limited; and cloud photography was used more than radar. By the final field season the aircraft instrumentation was rather advanced, capable of measuring many variables simultaneously; the aircraft routinely probed moderately severe thunderstorms, flying in strong icing and turbulence conditions, and even in some cases being in hail larger than 1/2-inch diameter; two radars were in use for monitoring the precipitation situation and the aircraft position; and the data reduction and analysis scheme was developed to the point where a complete field test can be quantitatively analyzed in just several man-weeks.

The foundation of this program has rested on the development of appropriate instrumentation. It has been necessary to measure simultaneously the many variables which are major factors in the outdoor laboratory. Whenever standard instruments were not available (which was the case in most instances) new ones were developed. The emphasis has been on simple devices giving reliability, accuracy, and resolution appropriate for this type of field program.

This broad project has succeeded in its aim of advancing the basic understanding of cumulus microphysics and dynamics. It has helped establish the groundwork for quantitative treatment of factors in cloud dynamics, droplet growth, and electrification.

The main project results are given herein as copies of separate papers and reports. Most of these have been submitted for publication; others form the bases of papers which will subsequently be submitted after being augmented by data from other programs. The next section of this report summarizes the program results, putting the various papers in the perspective of the over-all program.

D. Project Results

1. Effect of the San Francisco Peaks on the Development of Convection and Precipitation.

Appendix A is a paper by A. I. Weinstein and T. B. Smith titled "Convective Precipitation in the Lee of an Isolated Peak". The existence of a persistent localized major convective phenomenon has been established, here called the convective mountain wake. The growth of convective cells and convective precipitation is often greater in the wake area, considerably downwind of the Peaks, than it is over the Peaks. The phenomenon stems from the convergence of hot surface air into the zone well behind the Peaks, augmented by the convective release of latent heat of condensation there; it may also include an effect from a dynamic wave set up by the Peaks. The convective wake existed when the wind at 14,000 feet exceeded 9 knots or the wind sheared strongly with height, when the air was convectively unstable, when there was strong solar heating, and when the air was not excessively moist. When the precipitable water was less than 2 cm, convective precipitation would be confined to the wake area; greater moisture produced convective precipitation everywhere.

This paper is being incorporated into a more extensive analysis in Part B of the MRI report to USAERDL on the 1963 season.

This persistent localized convective phenomenon represents the simplest, steadiest, and most predictable large convective regime with which the authors are familiar. It thus suggests itself as an ideal situation for future cloud modification trials on an operationally valuable scale.

2. Convection Structure.

Appendix B is a paper by C. J. Todd, "Aircraft Traverses in a Growing Mountain Cumulus Cloud".

It describes the motions and continuity in a growing cumulus area over the San Francisco Peaks as observed by a systematic sequence of aircraft traverses (17) through the cloud region and by time-lapse photographs of the clouds. The observations showed consistency with the "starting plume" picture presented by R. J. Taylor. There was considerable time continuity to the upcurrent cells. The vertical transport of air past the observation level in a typical cell was 6 times the length of the horizontal cell dimension. Cloud cell top vertical motions showed

velocities about half of the apcurrent strength within the cloud. The initial cloud positions correlated with those high slopes on the mountains which were most heated by the sun.

These observations add information to the over-all question of thermal cell structure.

This paper has been submitted to the Journal of Atmospheric Science

3. Dynamic Effects of Cloud Seeding.

Appendix C is a paper by W. L. Woodley, "Computations on Cloud Growth Related to Seeding". Mr. Woodley is a meteorology student at UCLA who worked on the program during the Summer of 1963. Observations at Flagstaff and by other investigators elsewhere have demonstrated that in some cases the latent heat of fusion released in seeding supercooled clouds can significantly increase the ultimate height of the cloud. This paper represents a statistical study of the magnitude of this dynamic seeding effect which could have occurred at Flagstaff.

One hundred eighty soundings are treated, covering all available data from the Summers of 1961, 1962, and 1963. The cloud top heights are computed, considering the weight of the droplets but with the simplest possible assumptions such as no mixing and no growth above the zero buoyancy level, for two cases: 1) the naturally seeded case, with supercooled water conversion to ice at -30C, and 2) the artificially seeded case, with supercooled water conversion to ice at -10C. The results imply that height increases of over 5000 feet due to seeding can be expected fairly often, and increases over 15,000 feet are sometimes possible. Despite the simplicity of the model, it is felt that the computed height differences quantitatively represent a reasonable measure of the potential for cloud dynamics changes from seeding. Specific observations of cloud growth due to seeding are noted, but can only be considered as consistent with these concepts rather than verifying them.

This investigation represents a further look at the question of the seedability of a particular meteorological situation, considering the cloud dynamics aspect of seedability. The question of seedability has been touched on by others at ARG-MRI in the past, specifically in C. J. Todd's concept of seedability as related to the mechanism of precipitation initiation (MacCready, Smith, Todd, Beesmer, "Nuclei, Cumulus, and Seedability Studies", contained in Vol. II, Final Report of the Advisory Committee on Weather Control, 1957), and by T. B. Smith's analysis of seedability in west coast winter storms as a function of storm stability and moisture supply (Smith, T. B., "Physical Studies of the Santa Barbara Cloud Seeding Project", J. Appl. Meteor., June 1962).

Woodley's paper has been accepted for publication by the Journal de Recherches Atmosphériques.

4. Quantitative Aspects of Crystal Growth in a Seeded Cloud.

Appendix D is a paper by C. J. Todd entitled "Ice Crystal Development in a Seeded Cumulus Cloud". One of the main research techniques for the Flagstaff Cumulus Studies has been to consider the natural clouds as a laboratory, instrument the aircraft for the appropriate quantitative measurements, and then seed to introduce a new parameter at a desired time and place. This paper describes one of the most successful such experiments.

The seeding plane spiraled 1780 meters below the base of a supercooled cloud (cloud base about -9.5C). The "flying laboratory" plane spiraled from below the seeding plane up into the cloud to a height with temperature colder than -16C. There was continuous sampling of the droplet and crystal population with the continuous particle sampler. At low elevations in the cloud the ice crystal regions from the seeding plume were narrow; at the high elevations the ice crystal regions were broad because there had been more time for diffusion, broad enough so there were only small areas without crystals. Considering generator output as a function of temperature and invoking the theory of diffusion in the inertial subrange, the computed crystal concentrations agreed reasonably well with the observed concentrations, and the volumes in which they were found agreed with the expanding plume picture. From careful study of the growth rate of the crystal population, Todd was able to fit the growth into a formula consistent with crystal theory and laboratory measurements, and verify that the growth rate increased five-fold from -9.5C to -13C. This investigation represents the use of a cloud as a full scale cold box for basic crystal studies and for the quantitative study of seeding effectiveness.

Other measurements from the airplane showed that undiluted cores existed in the cloud even at the peak heights reached, and showed the increase of buoyancy associated with the release of heat of fusion as the supercooled water turned to ice.

This paper has been accepted, with revisions, by the Journal of Atmospheric Sciences.

5. Quantitative Calculations of Hydrometeor Development.

Appendix E is a paper by C. J. Todd, "A System for Computing Ice Phase Hydrometeor Development". It represents a beginning in treating cloud modification techniques in the sort of quantitative detail which must be considered in any eventual practical application scheme. The paper touches on the broad aspects of the whole cloud modification picture, and then focuses on the ice phase hydrometeor development. It is a practical assembling of the factors which dominate hydrometeor growth. It draws extensively on the literature, and it utilizes logical extrapolations where literature is lacking. Thus it points out the areas requiring special additional study, while putting present knowledge into some perspective.

The computation method treats the development of ice hydrometeors in non-raindrop clouds from (1) the nucleating agent, (2) the rate of growth of ice crystals as a temperature function, (3) the onset of riming as a function of crystal size, fall velocity, and cloud droplet size, (4) the rate of graupel growth as a function of size, shape, density, fall velocity, and cloud droplet concentration, and (5) the development of hailstones as a function of size, density, shape, surface temperature, fall velocity, and liquid water content of the cloud. The computations are by graphical techniques and are basic to the design of actual seeding techniques. They constitute a starting point for more complex situations wherein electrification, cloud dynamics, and overseeding interference to growth must be considered.

The study emphasizes the importance of the details of the growth rate of crystals, particularly the fast growth observed at the -4C level.

In its present form the paper is too large and detailed for submission to a journal, although it is planned that some extractions from it will be the basis of formal articles.

6. The Continuous Collection of Droplets and Crystals.

Appendix F is a paper titled "Continuous Particle Sampler" by P. B. MacCready and C. J. Todd. It describes an instrument which has proven to be uniquely valuable for these cloud physics studies. The device was developed primarily as an instrument with which to observe the presence of ice crystals coexisting with water droplets. It permits calculation of concentrations and size spectra of liquid droplets and crystals in the general range of 3 to 100 microns.

The sampler captures atmospheric particles in a Formvar solvent liquid film which has been coated on 16 mm movie leader stock. The Formvar solution completely encapsulates the particle; then as the solvent evaporates, the film hardens quickly, preserving a replica of the particle. The replicas from crystals are exact; those from droplets can be somewhat flattened. The amount of flattening of droplet replicas has been determined approximately by a laboratory technique. The collection efficiency of the sampler is computed by standard means.

The film records are analyzed by projecting the film on a screen and manually counting and sizing the images. Rapid methods have been developed for this data reduction.

The sampler invokes various design compromises to overcome, over a broad range of meteorological conditions, problems such as those associated with film coating, droplet encapsulation, droplet migration, and spurious crystal growth. Operation for collecting warm droplets alone is rather simple; operation to get droplets and crystals simultaneously requires critical adjustments.

The continuity for the development of this continuous sampler has been due to the NSF support. Major factors in the development and use of the instrument derive from the support given MRI by NRL-ONR and by USAERDL. This paper has been submitted to the Journal of Applied Meteorology. Additional information on the use of the device is contained in Part B of the MRI report to USAERDL on the 1963 field season.

7. A Formvar Collector for Nuclei and Settling Particles.

Appendix G is a paper by E. E. Hindman, II, titled "Continuous Sampler for Settling Particles". Mr. Hindman is a meteorology student at the University of Utah who has worked for Atmospheric Research Group for several summers, paying particular attention to the Formvar collection techniques. In 1963 he received honorable mention for the Father McElwane award by AMS for the beginning of one of the developments which is included in this paper. This paper describes the development of a continuous collector which uses the Formvar encapsulation principle, and softens the dry Formvar coating by a vapor solvent instead of a liquid solvent. 16 mm leader material with a very thin dry Formvar coating moves slowly horizontally where particles will fall on it -- particles falling from the atmosphere, such as small droplets and ice crystals, or crystals falling down in a cold box. Next the film passes into a vapor chamber with chloroform, which softens the Formvar enough to encapsulate the particles, and then the film is exposed to ambient conditions so the solvent will evaporate.

Records are shown of particles falling from a seeded geyser at Yellowstone.

This paper will appear in the Vol. I, 1964 issue of the Journal de Recherches Atmosphériques.

8. Charging of Melting Hydrometeors, in the Atmosphere and Laboratory.

Appendix H is a paper by P. B. MacCready, Jr., and Alexander Proudfit titled "Observations of Hydrometeor Charge Evolution in Thunderstorms". Potential gradient measurements around and within clouds each year of the project produced rather complex and contradictory data from which no simple pattern could be discerned readily. In 1962 hydrometeor charge equipment was installed on the airplane and a pattern started to emerge. The measurements were made in a rather limited set of meteorological conditions (very cold, entirely supercooled clouds) and so applying the results to other situations may not be warranted. The aircraft would spiral up into the cloud, staying in the rising core until altitudes corresponding to -15 or -17C. The small hydrometeors encountered were found to be predominately positive. The aircraft then would move down into the precipitation area directly under the cloud (or an equivalent cloud) and spiral down through the rain/hail shaft. The ice hydrometeors were generally positive, switching rather abruptly to negative at lower altitudes when the hydrometeors were entirely water; a significant charging mechanism associated with ice hydrometeor melting is thus implied. Similar brief measurements on the MRI-USAERDL project in 1963 showed a more complex hydrometeor charge evolution below the freezing level of clouds with warmer bases than the 1962 conditions.

Appendix I is a paper by MacCready and Proudfit, "Self-Charging of Melting Ice", which describes laboratory measurements made to investigate the phenomena suggested by the flight measurements. Ice pellets, simulating ice hydrometeors, were melted in a small wind tunnel. The resulting charging of the initially uncharged samples was noted. Charging occurred in a reproducible manner, but it was of the opposite sign and of lower magnitude than suggested by the flight measurements. Measurements with real hail in 1963 agreed generally with the results of the tests on the simulated ice hydrometeors. The charging is apparently related to the release of bubbles by melting hail. Hail typically has a great density of bubbles. Hail with few bubbles showed smaller electrification effects.

An earlier version of these two electrification papers was presented at the 1962 AGU meetings in Washington, D.C. The papers have been separated, new data added, and generally revised, and the new versions have been submitted to the Quarterly Journal of the Royal Meteorological Society.

9. Miscellaneous Related Reports.

The following published papers, prepared with major sponsorship from this NSF grant, have previously been submitted to NSF.

A. Todd, C. J., 1960: Precipitation Initiation in Summer Cumulus at Flagstaff, Arizona. Proc. 8th Weather Radar Conference, San Francisco, April. For a series of unseeded, naturally seeded, and dry ice seeded cumulus clouds at Flagstaff the radar reflectivity at the time of the first detectable echo was computed by considering the rate of growth of crystals. This reflectivity was then compared with that observed on the radar. The dry ice seeded clouds showed a first echo in from 4 to 8 minutes of the seeding.

B. MacCready, P. B., Jr., 1960: Equipment for Field Studies in Cloud Physics. ISA Preprint 8-SF60, ISA Conference, San Francisco, May. Items which were presented which relate to the Flagstaff Cumulus Studies were: the whole-sky camera cloud observation system, and the use of the instrumented light plane, together with details of some of the instrumentation.

C. MacCready, P. B., Jr., 1961: A Review of Small Cumulus Studies and the Modification of Hail. Nubila, IV, N. 1, (International Congress on the Physics of Clouds, Verona, August 1960). The beginning of the Flagstaff Cumulus Studies is reviewed, a case of electrification from seeding is described, and possibilities of decreasing hail by seeding is discussed.

D. Todd, C. J., 1961: A Study of Cloud Composition. Proc. 9th Weather Radar Conference, Kansas City, Mo., October. This paper described the earliest version of the continuous particle sampler and presented samples of its use in cumulus clouds.

E. MacCready, P. B., Jr., 1962: The Continuous Particle Sampler at the Puy de Dome Comparison Conference. Bull. Observatoire du Puy de Dome, Paris, 1, 19-30. This paper was the result of an NSF-sponsored trip by MacCready to France to compare the continuous sampler with other droplet collecting and measuring devices. The airborne version of the collector was adapted to ground use by having a small wind tunnel provide the relative air motion. The study provided data on the variability of cloud droplet spectra and gave some first clues as to the calibration factors needed for converting replica diameters to true droplet diameters.

With the support of NSF, Todd and MacCready have participated in the yearly Yellowstone Park winter seminars organized by Dr. V. J. Schaefer. Their activities there are reported in the reports by Schaefer issued by the Atmospheric Sciences Research Center, State University of New York.

Report #1, ASC-SUNY, 1961, MacCready section. Various droplet collection techniques were investigated, with the result that subsequently the Schaefer Formvar method was adopted as the basis of the continuous sampler. The effects of Old Faithful geyser eruptions on the local potential gradient were studied; the local lowering of the potential gradient was of a magnitude which could be accounted for by the induced-charge effect in the geyser liquid which ultimately formed the plume. Charging of a simulated ice hydrometeor moving through a supercooled cloud showed a strong temperature dependence.

Report #5, ASC-SUNY, 1962, Todd Section. The testing and development of the continuous sampler was continued, using different coating techniques. Continuous replication at extremely cold temperatures was obtained.

Report #13, ASC-SUNY, 1962, Todd and Hindman section. The development of the continuous sampler was carried still further, with collection at temperatures as low as -43C. A gravity settling version was tested and was used to get replicas of the particles coming down from Old Faithful geyser eruptions (reported by Hindman in Appendix G). Brief studies on condensation were conducted.

Two other papers by MacCready which were not associated with any sponsored projects benefited from the existence of the NSF-supported work. One was "Improving Thermal Soaring Flight Techniques", in the July 1961 issue of the Swiss Aero-Review. It considered ways of locating thermals from sailplanes, by the understanding of thermal characteristics, using forecasting and direct and indirect measurement techniques. The other is a paper submitted to the Journal of Applied Meteorology titled "Standardization of Gustiness Values for Aircraft". This describes the use of the inertial subrange concept of turbulence to standardize turbulence measuring and reporting, noting that aircraft gust loads come primarily from eddies which, to a first approximation, fit into the inertial subrange. A preliminary relation between the inertial subrange turbulence intensity parameter and the qualitative "feel" of the pilot (light, moderate, etc.) was obtained from records in the NSF-sponsored Flagstaff studies.

The Flagstaff Cumulus Studies involved many separate but related projects and not all could be pursued to the point where they justify a formal report at this time. For completeness, several of such items will be mentioned here.

Freezing nuclei measurements represented one facet of the program which had to be minimized relative to other subjects which loomed as more important. Freezing nuclei counts were made (usually at -20C) at the 10,800-foot Doyle Saddle on 17 days during the 1959 program. Crystal concentrations and time of appearance were made in a dual cold box using the supercooled sugar solution technique. It was noted that the nuclei counts frequently were large during the hours when heating of the mountain slope caused convection currents from lower levels to reach the Saddle area. The clean, non-upslope air showed nuclei counts similar to average low values found elsewhere, of the order of 1 per 5 or 10 liters. Counts more than an order of magnitude higher (2 to 10 per liter) appeared erratically in air moving up the slope. In subsequent years some brief trials using the filter method of collection did not work out because of limitations in the experimental technique as used. Visual observations of clouds at Flagstaff showed that the natural nuclei count there can be variable in both time and space.

Some quantitative effects of seeding are covered in Todd's paper with this report. Qualitative effects of seeding were of course noted each year, visually and by radar. The timing and location of the first radar echoes were consistent with what one would expect considering cloud growth rates and temperatures.. In clouds with any reasonable liquid water content, say with moderate upcurrents and thickness of more than 5000 feet, a first radar echo would appear from dry ice seeding in 4 to 6 minutes if the cloud top was -8C to -12C. Seeding of somewhat warmer clouds produced echoes more slowly. Experience showed that the first radar echo from naturally seeded clouds could be expected about 15 minutes after the cloud top passed the -17C to -20C level (generally around 22,000 - 24,000 feet). Often large seeded clouds showed "feathers" projecting up from their tops presumably due to localized excess buoyancy from localized seeding.

The convective clouds would show significant unmixed regions with the maximum theoretical liquid water content. Turbulence was generally moderate in the clouds. Traverse data (liquid water content, vertical velocity, temperature fluctuations) showed that, in small to moderate cumulus clouds, volumes with homogeneous properties were on the order of 1000 feet across.

E. Instrumentation and Field Techniques

The Flagstaff Cumulus Studies have been based on thorough instrumentation of the natural outdoor laboratory afforded by the San Francisco Peak area. Thus special radars, cameras, ground instruments, and airborne instrumentation had to be developed or adapted to this task. Further, the operational techniques of utilizing these devices in a large coordinated field program had to be created, and methods of analysis developed which could cope with the voluminous and complex data generated. The instrumentation and its utilization in the field necessarily constituted the most expensive part of the work reported here.

Instrumentation methods and techniques of use are described to some extent in the separate papers which are part of this report and in the published papers submitted earlier to NSF. The system improved steadily each year. The over-all measurement and data reduction-analysis system in use in the last field season with NSF sponsorship (1962) (jointly with USAERDL) is reviewed briefly in the MRI Final Report of the USAERDL project (May 1963). The final system will be described in the forthcoming (May 1964) Final Report on the USAERDL project; this will depict the final stage of development of the field system which originated in the NSF-ARG work and evolved considerably thereafter through the USAERDL project.

The main features of the measurement system (essentially the 1962 version used on the joint MRI-ARG Flagstaff project) will be reviewed here.

A most important factor is the instrumented light aircraft. This is flown in systematic patterns probing for particular factors: horizontal traverses through thermals and clouds, vertical spirals up with the thermal core into cumulus clouds and thunderstorm cells, spirals down through hail shafts, and other patterns. Even with the instrumentation designed for minimum power requirements, it is necessary to install a special high-ampere generator in the aircraft. Recording is by the analog chart method, with all data going on a multichannel Brush recorder of 2 or 6 channels. When more channels are desired than are available on the recorder, some of the variables are cycled to share a channel (each variable repeated once per second). Event marks on the recorder chart show the timing of a clock, of all radio and voice data transmissions, of frames of the time-lapse camera looking forward at the clouds and flight instruments, and of footage of the continuous particle sampler. The basic variables recorded are altitude (via light follower potentiometer on a standard mechanical altimeter, giving 1000 feet full scale), temperature (thermistor in a vortex housing, multiscale bridge), turbulence (Universal Turbulence Indicator operating on high frequency, longitudinal velocity fluctuations in the inertial subrange), mixing ratio (MRI phosphorous

pentoxide electrolyzing unit), liquid water content (Johnson-Williams hot wire system), infrared with a Barnes 8-12 μ radiometer, and vertical potential gradient and airplane charge (balanced double radioactive probe sensors, operational amplifiers). Special variables (hydrometeor charge, conductivity, space charge) are added as desired. A magnetic tape recorder records all pertinent verbal information. A continuous particle sampler collects cloud droplets and crystals. The aircraft is equipped with an oil fog generator to make certain air motions visible. The aircraft is linked to ground control by 123.3 mc radios.

A Cessna 180 served as the main research aircraft in 1962. It would operate regularly to 20,000 feet, and was used to above 23,000 feet in rising cells. A supercharged Aero-Commander was partially instrumented and employed at heights to 27,000 feet. The Aero-Commander was equipped to seed by releasing large amounts of pre-crushed dry ice. Small quantities of dry ice pellets were occasionally released by the Cessna 180. Another Cessna 180 with USFS Fuquay acetone-type silver iodide generators provided the main seeding capability. The U.S. Forest Service contributed to the Flagstaff program by supplying the generators and materials, and Mr. Fuquay and several assistants participated in the work at Flagstaff.

The aircraft were tracked with an MR-4 3.2 cm pencil beam radar on PPI -- a difficult procedure requiring considerable skill on the part of the radar operator. In previous years with Air Force participation a radiosonde transmitter was installed on the aircraft and the aircraft tracked satisfactorily with a GMD-1. However, it is most convenient to have the aircraft plotted on a radar screen which also shows precipitation echoes.

The PPI radar and another MR-4 radar used in the RHI mode obtained details of the precipitation distribution related to the clouds being studied.

Standard time-lapse cameras were used, at 10 seconds per frame, at the airport ground control and several other locations. Several whole-sky cameras, at 1 frame per minute, filled in the photographic coverage. Associated with the whole-sky cameras was a network of potential gradient recorders. Freezing nuclei measurements were made at the ground with the supercooled sugar technique with a dual temperature cold box.

Debugging and operating such a complex instrumentation system required the dedicated efforts of a large field crew. The project had its share of frustrations caused both by rapid changes of the weather being studied and by the difficulty of working with new, sometimes unproven equipment. Each summer involved instrumentation system development as well as use of the instrumentation system.

The next stage in the development of such an integrated field investigation system should include slightly more refined aircraft instrumentation, especially with a better de-icing capability, a higher flying but still maneuverable airplane, better tracking of aircraft, and tracking of balloon tracers. The 1963 USAERDL program included some of these improvements, with a supercharged light twin-engined Apache as the main research aircraft, and an M-33 radar for automatic tracking and plotting of aircraft and balloon positions. To simplify the field program there is now more emphasis on concentrating on making the aircraft and the ground control station more versatile, and minimizing the over-all ground network except for a few automatic cameras and recorders.

The next stage in the development of such an integrated field investigation system should include slightly more refined aircraft instrumentation, especially with a better de-icing capability, a higher flying but still maneuverable airplane, better tracking of aircraft, and tracking of balloon tracers. The 1963 USAERDL program included some of these improvements, with a supercharged light twin-engined Apache as the main research aircraft, and an M-33 radar for automatic tracking and plotting of aircraft and balloon positions. To simplify the field program there is now more emphasis on concentrating on making the aircraft and the ground control station more versatile, and minimizing the over-all ground network except for a few automatic cameras and recorders.

F. Conclusions and Recommendations

The Flagstaff Cumulus Studies represent a broad program which rather completely instrumented the natural convection laboratory and which looked simultaneously into many different factors pertaining to clouds, precipitation, and electrification. The separate papers in this report give conclusions and recommendations along specific lines. A few more general comments will be given here:

1. The area around the isolated San Francisco Peaks does constitute a uniquely valuable outdoor laboratory, as was first recognized by Dr. V. J. Schaefer. Meteorologically, it appears ideal as an area in which to investigate ice phase mechanisms and to study the effect of an isolated peak. It also has enough variety in weather to provide a good spectrum of study conditions. It features pleasant living conditions, has facilities for large crews, has a Weather Bureau station, a fine airport, good service facilities, a dense network of roads which even go partially up the peaks, and a helpful research climate with the Research Center of the Museum of Northern Arizona, the Lowell Observatory, the Naval Observatory, and Arizona State College. Most important, there is now a background of experience with the area -- experience which makes each investigation there more productive.

2. The over-all techniques represented by the coordinated airplane and ground instrumentation, the techniques of using the devices, and the data reduction methods have proven generally satisfactory. The techniques of spiraling a slow flying airplane up into the rising core of a cumulus cloud proved to be particularly valuable. Future projects which concentrate on probing the natural outdoor laboratory can fruitfully employ the same methods, with the main change being in using a more versatile, higher flying aircraft, and being able to use instruments which are now more proven.

3. The convective wake behind the San Francisco Peaks offers a relatively large yet steady-state predictable convective system, and therefore presents an unusually good situation for performing modification trials on convective clouds large enough to be of economic significance.

4. Although many continuing basic studies are still desirable, there have been enough advances in the quantitative aspects of nuclei generation, diffusion, crystal growth, coalescence, and buoyancy effects to warrant an initial rather quantitative development of seeding techniques for supercooled clouds without coalescence-type precipitation.

5. Cloud electrification studies will benefit greatly from systematic aircraft probings of charges inside the cores of large convective clouds. Instrumentation improvements are required for space charge measurement.

6. The data which have already been obtained during the Flagstaff Cumulus Studies warrant considerably more analysis than time and funds have permitted so far. Case studies of natural and artificial seeding can be treated by some of the quantitative techniques now available, and the time-lapse photographs and radar records offer a unique fund of data for cloud dynamics investigations.

7. The technique of using seeding as a research tool has worked well, and can fruitfully be applied more extensively for advancing knowledge of cloud microphysics, electrification, and dynamics. The physical evaluation employed in such studies also yields quantitative information on the effects of seeding for practical application.

APPENDIX A

Convective Precipitation in the Lee of An Isolated Peak

A. I. Weinstein and T. B. Smith
Atmospheric Research Group
Altadena, Calif.

January 1964

ARG64 Pa-120

ABSTRACT

Examination of PPI radar records and time-lapse cloud photographs taken during the summers of 1961 and 1962 has verified the existence of a localized convection region, here called the convective mountain wake, downwind of the isolated San Francisco Peaks north of Flagstaff, Arizona. The convective mountain wake represents a persistent localized major convective phenomenon. The downwind distance of the wake shows a weak positive relationship to the wind speed across the peaks. The region is apparently dependent upon (a) inflow of heated surface air into the wake, and (b) the convective release there of latent heat of condensation, and the phenomenon may be linked to the standing wave generated by the peaks. The observations showed the convective mountain wake existed when the 14,000-ft wind speed exceeded 9 knots or the wind sheared strongly with height, when the air was convectively unstable, when there was strong solar heating, and when the air was not excessively moist.

The dependency of the phenomenon upon moisture is examined. It is found that under the proper wind and stability conditions, convective precipitation is confined to the wake region when the precipitable water content of the air is below 2 cm. When the moisture content is above this level, convective precipitation elements are observed to appear randomly distributed over the whole Flagstaff area.

1. Introduction

It is becoming increasingly clear that isolated peaks and low ridges play an important role in the generation of convective clouds and precipitation (Förchtgott 1951, Loewe and Radok 1955, Hosler, Davis and Booker 1962).

Figure 1 is a topographical map of the area near Flagstaff, Arizona. It can be seen that the terrain is characterized by several isolated peaks extending above the surroundings. The most prominent of these is Humphrey's Peak, extending over 5000 ft above the terrain. The topography in this area makes it an ideal location to study the effects of an isolated peak on the micro-meteorology of the region.

In an earlier report, MacCready, Smith, Todd, Chien and Woodward (1963) had shown that under conditions of early morning stability and high wind speed, the San Francisco Peaks may generate observable lee waves, that convective clouds develop in the wave crests, and that a considerable amount of surface air flows around the peaks to converge downstream in a region referred to as the wake. It was suggested that the surface flow pattern serves to collect the available heat from the low levels into the wake region and that this heat plays an important role in the generation of convective clouds.

It is the aim of the present paper to examine the radar echo pattern to determine if it is similarly affected by the peaks, and if so, how the

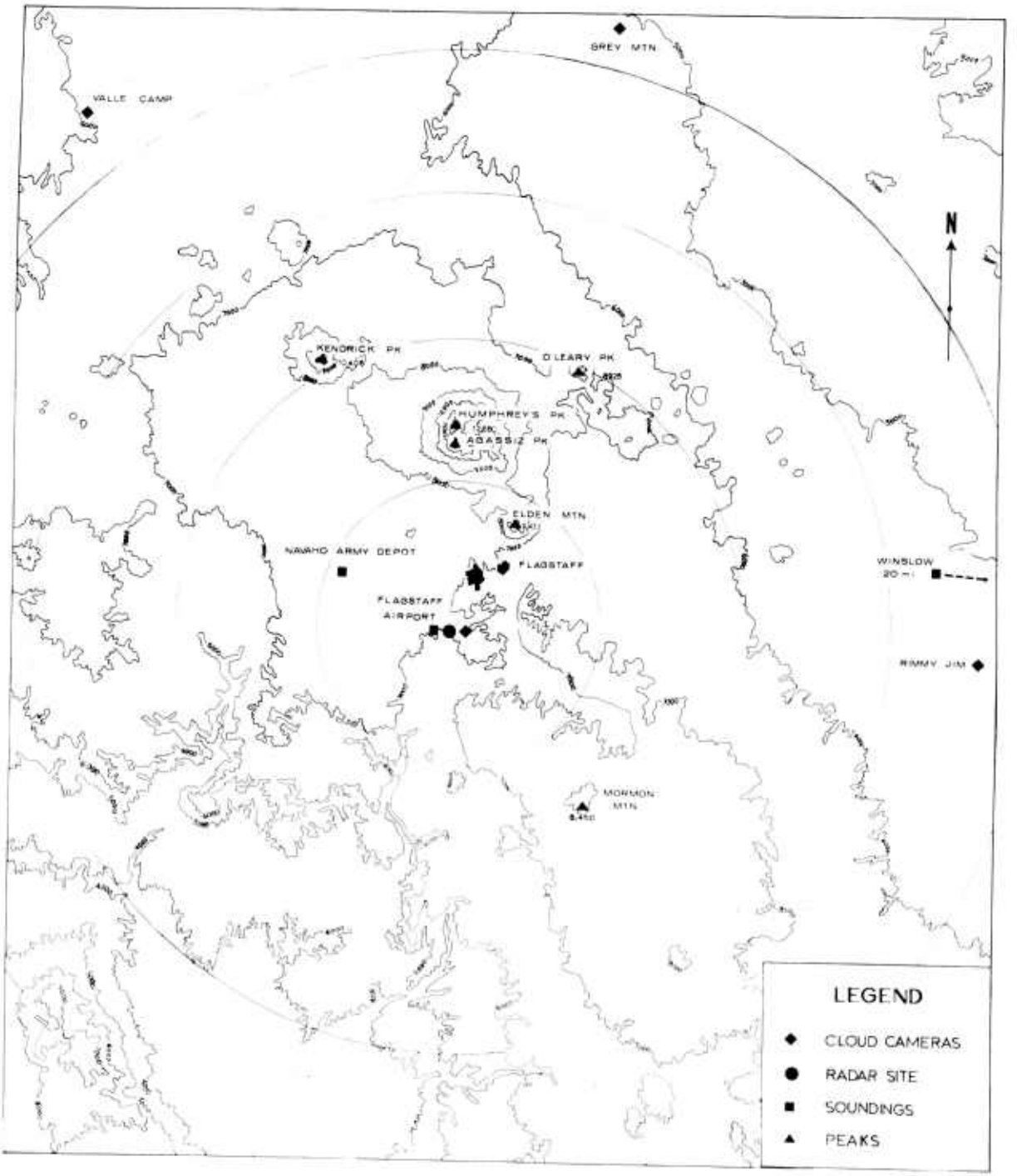

Fig. 1. THE SAN FRANCISCO PEAKS IN NORTHERN ARIZONA.

The range circles are every 10 miles.

wake region might aid in the development of the precipitation. Fig. 2 is presented as a very general picture of the flow pattern deduced from the observations taken by MacCready et al. (1963) and the radar echo pattern observed in the present study. It is not meant as an accurate description of the flow pattern, as the data are not complete enough to draw such a picture. It is instead presented to give the reader a general feeling for the problem at hand and to indicate the important regions to be discussed in the body of the paper. It is noteworthy to state here that by the time a convective cloud has developed to the point at which it can return a coherent radar echo, it has probably drifted somewhat downwind of its surface heat source. In the present study this means that the surface wake may well be upstream of the observed convective echo.

2. Data Sources and Procedure

The data used in this investigation were obtained from three sources: (1) time-lapse film of the MR4 (3 cm) PPI scope, (2) Radiosonde runs taken at Flagstaff Airport in 1961 and at Navajo Ordinance Depot and Winslow in 1962, and (3) time-lapse cloud film taken at Gray Mountain, Valle Camp, Rimmy Jim and Flagstaff Airport. The locations of all of these points are shown in Fig. 1.

The following procedure was employed to reduce the data into useful form:

1) Trace the radar echo outlines every 30 minutes on 8-1/2 x 11-inch acetate overlays, from the time of first echo appearance. When

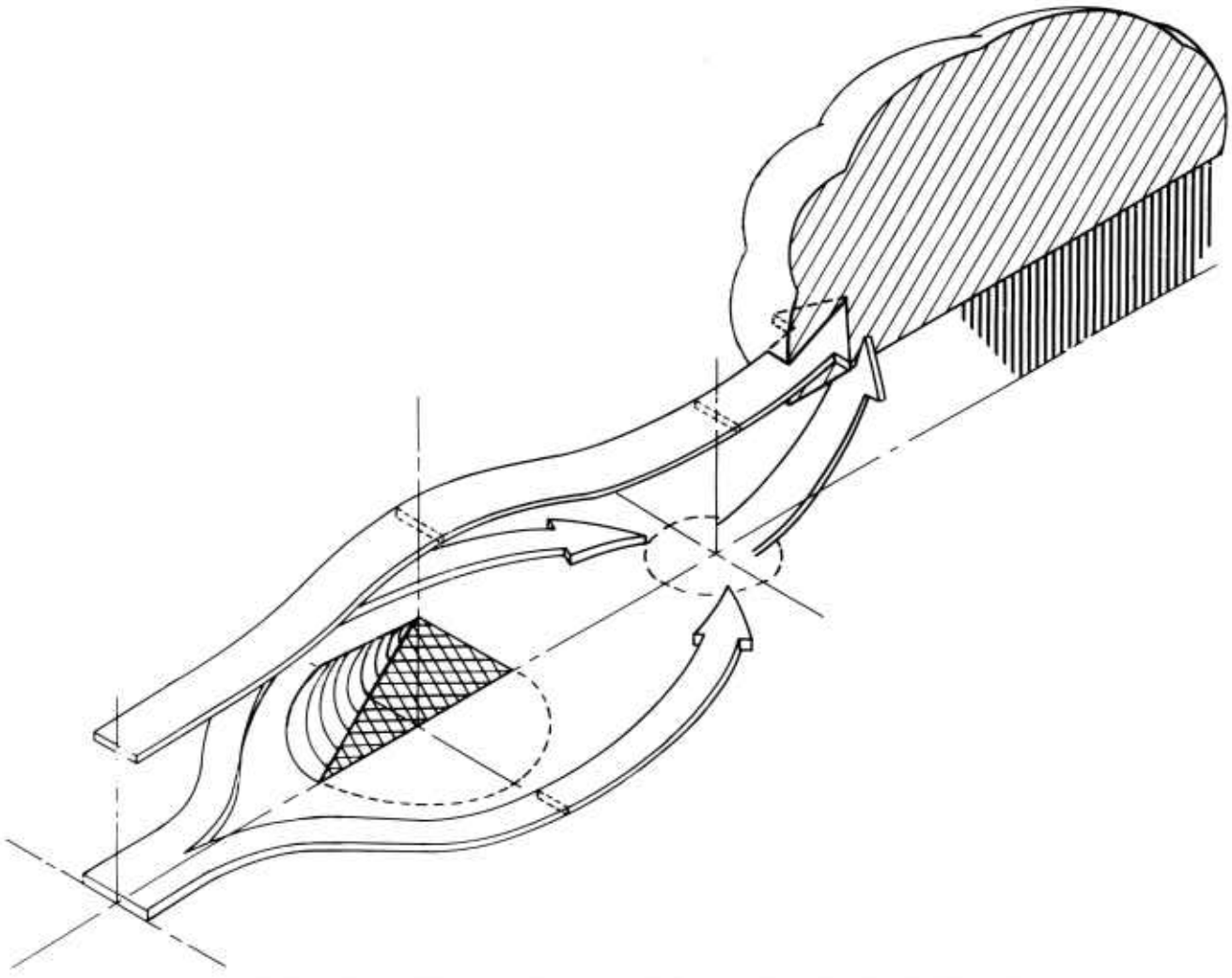

Fig. 2. SUGGESTED PICTURE OF THE CONVECTIVE MOUNTAIN WAKE.

The upcurrent causing precipitation derives from the warm converging surface air and the release of latent heat in the cloud. A standing wave related to the mountain may contribute to positioning the phenomenon.

placed one upon the other, these tracings show the areas of greatest echo occurrence and the general direction of echo movement.

2) Note the direction of movement of the clouds and radar echoes. This is the direction to which the expression "downwind of the peaks" refers.

3) Record the 14,000-ft wind speed from the radiosonde reports. This was the level closest to the top of the peak, at which wind data could be constantly obtained.

4) Compute, from the plotted radiosonde reports, the precipitable water content of the complete column of air.

5) Record the days in which the cloud film indicated convective clouds in the wake of one or more of the peaks. The occurrence of wake clouds was used as the final indicator of the phenomenon.

6) Divide the collected data into two categories. "Wake echo days" are characterized by the appearance of a localized region of echo formation and development downwind of one of the peaks. The "non-wake echo days" are those on which this localized region does not appear.

3. Results

The data collected on the 29 days of 1961 and 1962 are summarized in Table 1. It can be seen that the wake echo days are characterized by

Table 1. Data summary

Wake Echo Days

Date		Downwind distance of echo maximum (Mi)	14,000-ft wind speed (knots)	Precipitable water (cm)	Remarks
17 July		10	4	1.71	
18 July		35	12	1.33	
19 July		20	10	1.24	
20 July	1961	23	24	1.33	
24 July		12	8	1.38	
1 August		3	4	1.45	Strong vertical wind shear aloft
5 August		5	8	1.76	Strong vertical wind shear aloft
17 July		20	27	1.55	
18 July		15	19	1.90	
19 July		9	11	2.00	
20 July		25	24	1.33	
21 July	1962	17	13	1.85	
25 July		20	11	1.55	
27 July		4	5	1.60	
31 July		10	17	1.90	
7 August		12	21	1.15	
10 August		15	20	1.50	

Non-Wake Echo Days

Date		14,000-ft wind speed (knots)	Precipitable water (cm)	Remarks
26 July		4	1.78	Convectively stable
27 July		6	1.99	Convectively stable
28 July	1961	3	2.34	
30 July		6	2.25	
2 August		2	2.47	
23 July		15	2.55	
28 July		6	1.90	Convectively Stable
1 August		3	1.40	Light wind aloft
2 August	1962	10	2.00	
3 August		21	2.05	
13 August		2	2.00	Light wind aloft
14 August		Calm	1.65	Light wind aloft

low moisture content and either high wind speeds or strong vertical wind shear. The non-wake echo days are characterized by high moisture content, convective stability and/or light winds.

10 August 1962 is a good example of a wake echo day in which the wake region displayed an echo maximum for several hours. Fig. 3 is a schematic representation of the PPI scope as it appeared on this day. For simplicity, the representations are shown at one hour intervals, the ground clutter has been removed and the range markers shown for every 10 miles. The local time is shown in the upper right corner. The arrow in the center indicates the mean wind direction as derived from the echo movement. Note that the echo maximum is directly downwind of Humphrey's Peak and that there are few echoes elsewhere on the scope.

26 July 1961 is an illustrative example of a day in which the echoes are not restricted to a localized region downwind of the peaks. Fig. 4 depicts the PPI scope as it appeared on this non-wake echo day. The symbols are the same as those in Fig. 3.

Figure 5 shows a plot of 14,000-ft wind speed versus precipitable water content of the air. Notice that the wake echo days (x) fall in a localized region of the plot outlined by the dashed line. The exact bounds of this region on this plot is as yet not known, but the existence of such a region does seem definite from Fig. 5, and such a region would be expected to exist on the basis of physical reasoning to be given below.

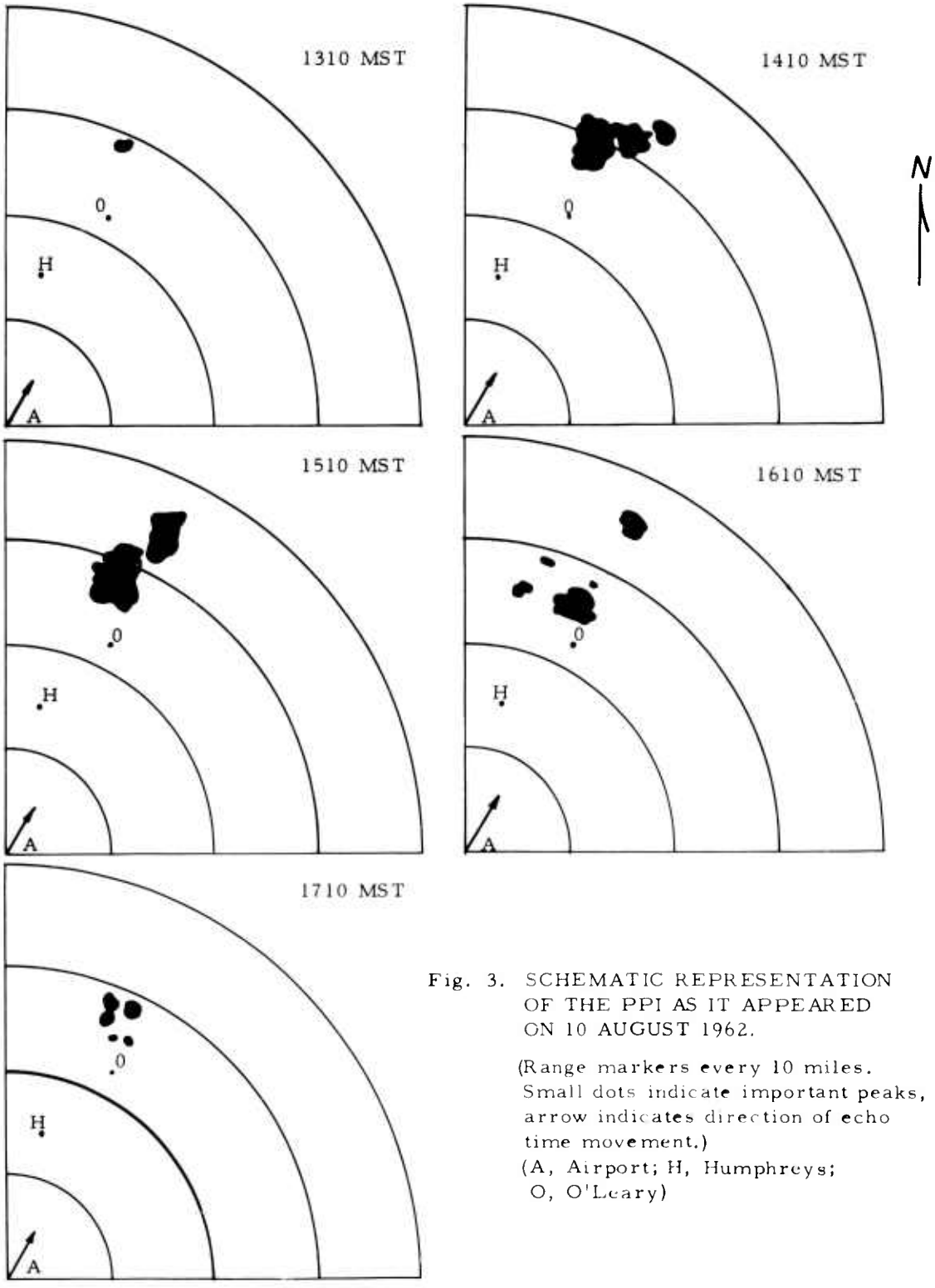

Fig. 3. SCHEMATIC REPRESENTATION OF THE PPI AS IT APPEARED ON 10 AUGUST 1962.

(Range markers every 10 miles. Small dots indicate important peaks, arrow indicates direction of echo time movement.)
(A, Airport; H, Humphreys; O, O'Leary)

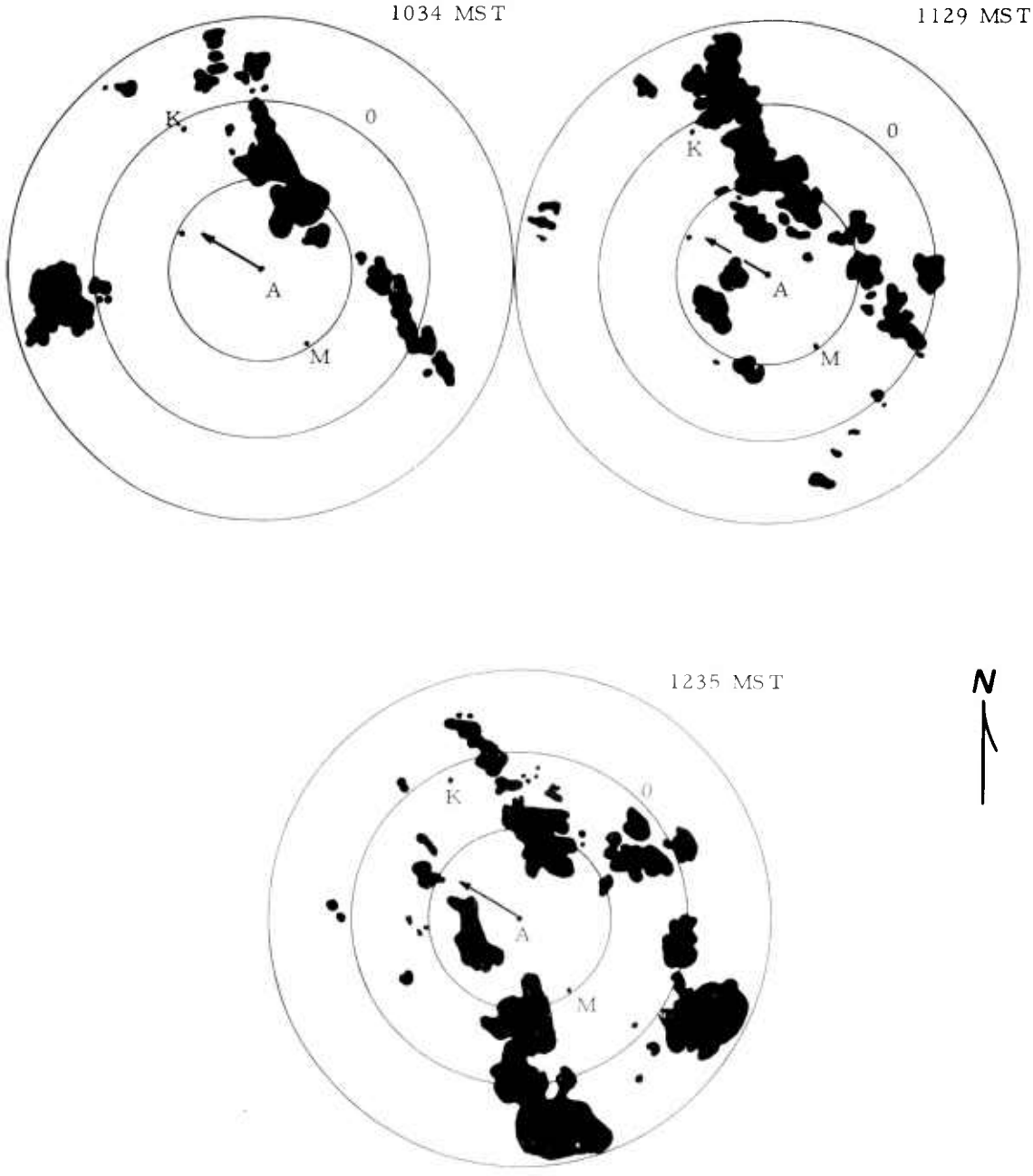

Fig. 4. SCHEMATIC REPRESENTATION OF PPI SCOPE AS IT APPEARED ON 26 JULY 1961.

Symbols same as in Fig. 3. (K, Kendrick; M, Mormon Mt.)

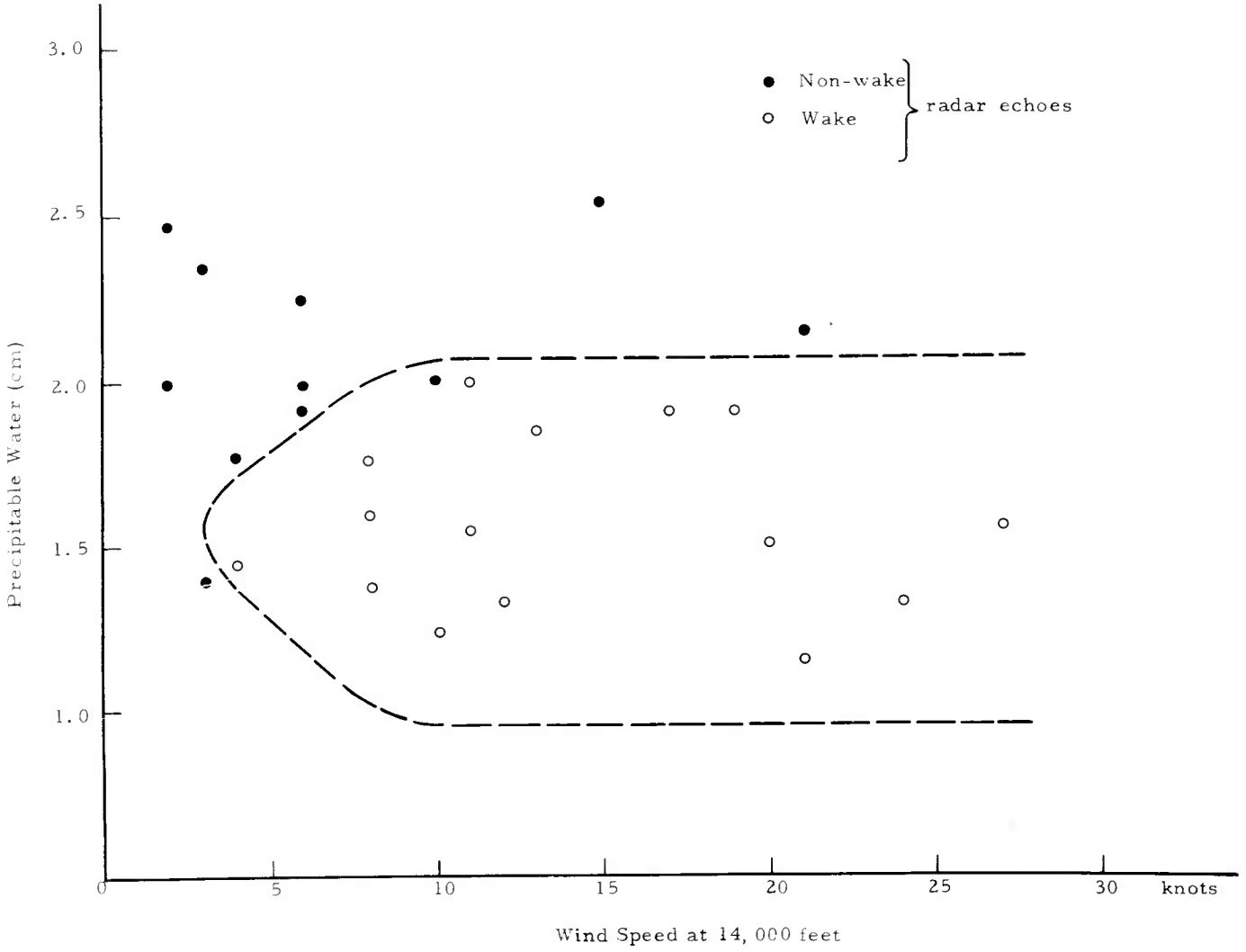

Fig. 5. A PLOT OF PRECIPITABLE WATER VS. HORIZONTAL WIND SPEED OVER THE PEAKS, SHOWING CONDITION OF WAKE ECHO OCCURRENCE.

Figure 6 shows a plot of 14,000-ft wind speed versus downwind distance of the echo maximum. This figure shows a weak positive relationship between the variables.

4. History and Discussion

Since the 1920's, meteorologists have been observing the lee wave phenomenon. The greatest majority of the papers resulting from these observations deal with waves generated by continuous ridges (Kuettner 1939, Manley 1945, Förchtgott 1949, Larsson 1954, Holmboe and Klieforth 1957, Hosler, Davis and Booker 1962). These plus several theoretical studies (Lyra 1943, Queney 1947, Scorer 1949, Corby and Sawyer 1958) have provided a good general picture of the lee waves that exist in the vicinity of long mountain ridges.

The problem of isolated peaks acting as obstacles to the flow of air, however, has not been as clearly defined. Mathematically, the problem is far more difficult as it must be solved in three dimensions. A few attempts have been made in this direction (Scorer 1953, 1954, 1956, Scorer and Wilkinson 1956, Wurtele 1957), but most of the information about this type of disturbance comes from observations (Förchtgott 1951, Loewe and Radok 1955, MacCready, Smith, Todd, Chien and Woodward 1963). It is from these reports that a picture resembling that shown in Fig. 2 has evolved.

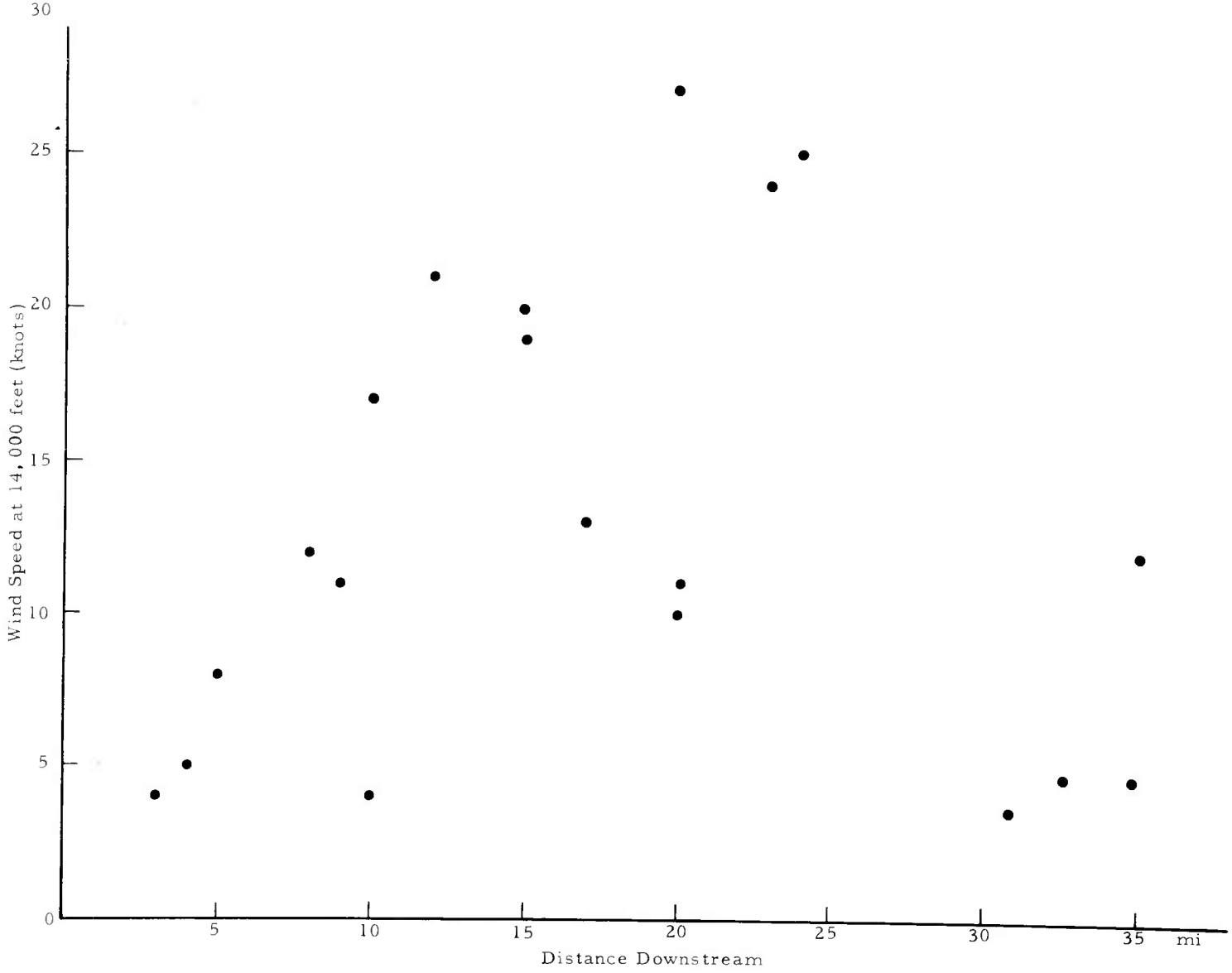

Fig. 6. PLOT OF DISTANCE OF WAKE FROM PEAKS VS. HORIZONTAL WIND SPEED OVER THE PEAKS, SHOWING WEAK POSITIVE RELATIONSHIP.

Silverman (1960) showed that air impinging upon an isolated peak, displays a strong preference to go around rather than over the peak, under the type of stability conditions present in Arizona. While his observations were taken near Tuscon, Arizona, the conditions are similar to those at Flagstaff. This type of flow will bring considerable amounts of surface heat into a localized region of surface convergence, which is referred to as the wake. When supported by upper level divergence, as was shown to exist to the lee of the peaks by Glass and Carlson (1963) (their Fig. 7 shows a divergent wind field as deduced by thermal tuft trajectories) the wake becomes a region of strong persisting updrafts. When a convectively unstable air mass with the correct amount of moisture is introduced into this updraft, convective precipitative elements can be expected to develop. The convective instability requirement is necessary because (1) if the air is absolutely unstable the convective precipitation will break out outside, as well as within the wake and (2) if the air is convectively stable the strong updrafts will have no destabilizing effect. In the first case the wake region will either be masked or even destroyed by mixing. In the second instance the convective elements will not be made buoyant.

Possibly most important, however, is the requirement of correct moisture content of the air. If the air is too dry, it simply is not capable of producing strong convective precipitation even in the presence of strong updrafts. There is not sufficient data present to define this

lower limit of moisture. If the air is too moist, small isolated local heat sources outside the wake will very quickly be aided by latent heat of condensation and convective elements may grow within these. Under these conditions a situation similar to that of absolute instability will result. With precipitable water contents above 2 cm, this condition appears to exist. Within the precipitable water range between the lower limit and about 2.10 cm, and with convectively unstable air flowing around the peaks, the wake region is one of convective precipitation maximum. Fig. 5 shows that at low wind speeds, the range of favorable precipitable water content decreases. This is because at these low wind speeds the convergence of surface heat is not as effective. The lower moisture limit must rise as the updrafts are not as strong as before and the upper limit must fall as surface heat is not as rapidly removed from other potential thermal heat sources.

Little has been said about the role of the lee wave in the development of wake precipitation. At the present time its role is in doubt. Alaka (1958) states that development of waves to the lee of an isolated peak is less likely than in the case of a long ridge, but that their occurrence is possible. Such waves would have a relatively small amplitude and would rapidly die away downstream. It appears that the importance of the wave, if any, is in the development of the upper level divergence, necessary to sustain the updrafts.

9. Conclusions and Recommendations

Under the proper conditions of wind and stability, moisture plays a pivotal role in the confinement of convective echoes to the localized wake downwind of the San Francisco Peaks, Arizona. When the precipitable water content of convectively unstable air flowing around the peaks is between some lower limit, as yet undefined, and about 2 cm, the wake echoes appear.

Little is known about the structure of the wake region beyond the fact that it is an area of low level convergence. It seems necessary that there be an upper level divergence region to sustain the convergence and persistent updrafts. As yet, the depth and limits of the convergence and expected divergence regions are unknown as well as is the quantity of surface heat collected into the wake. At the present time, it is possible only to make a very general three dimensional picture of the flow (Fig. 2).

Little is known about the thermodynamics of the wake clouds except to say that on the wake echo days, the air was convectively unstable.

It is in the above two areas that most of the future work should be centered. Mesoscale observations of surface temperature, pressure and wind, vertical soundings through key places in and around the wake, as well as detailed radar and cloud observations should be made. It would be interesting to make many of the above observations at night or under overcast conditions when the importance of surface heat (or the lack of it) would become apparent.

Finally, it might be useful to model the San Francisco Peaks in the laboratory where the effects of wind, moisture, stability, insolation, etc., could be studied individually.

REFERENCES

Alaka, M. A., 1958: Aviation aspects of mountain waves. Tech. Note No. 18, W. M. O.

_____, (Editor) 1960: The airflow over mountains. Tech. Note No. 34, W. M. O.

Corby, G. A. and J. S. Sawyer, 1958: The airflow over a ridge: The effects of the upper sounding and high level conditions. Quart J. of Roy. Met. Soc., 84, 25-37.

Förchtgott, J., 1949: Wave streaming in the lee of mountain ridges. Bull Met Czech., 3, 49.

_____, 1951: The airflow around a conical hill. Gliding, 2, 147-149.

Glass, M., and T. N. Carlson, 1963: The growth characteristics of small cumulus clouds. Jour. Atmos. Sciences, 20, 397 406.

Holmboe, J., and H. Kliefoth, 1957: Investigations of mountain lee waves and the airflow over the Sierra Nevada. Dept. of Met., University of California.

Hosler, C. L., Davis, L. G., and D. R. Booker, 1962: The role of orographic barriers of less than 3000 ft in the generation and propagation of showers. Progress Report NSF G-7363, Dept. of Meteorology, The Pennsylvania State University.

Kuettner, J., 1939: Inoayagotl Und Fohnwelle. Beitr. Phys. frev. Atmos. 25, 79-114.

Larsson, L., 1954: Observations of lee wave clouds in the Jämtland mountains, Sweden. Tellus, 6, 124-138.

Loewe, F., and V. Radok, 1955: A wave cloud at Heard Island, Weather, 10, 78.

Lyra, G., 1943: Theorie der Stationaren Loewellenstromang in Freier Atmosphäre, Z. Angew. Math. Mech. Berlin, 23, 1.

MacCready, P. B., Smith, T. B., Todd, C. J., Chien, C. W., and E. Woodward, 1963: Study and modification of convective storms. Report No. 2, Meteorology Research, Inc., Contract No. DA36-039 SC89066, U.S. Army Electronics Research and Development Laboratory AD 415 347.

Manley, G., 1945: The helm wind of crossfell, 1937-1939. Quart J. of Roy. Met. Soc., 71, 197-219.

Queney, P., 1947: Theory of perturbations in stratified currents with application to airflow over mountain barriers, University of Chicago Press, Misc. Report No. 23.

_____, 1948: The problem of airflow over mountains: A summary of theoretical studies, Bull Amer. Met. Soc., 29, 16-26.

Scorer, R. S., 1949: Theory of waves in the lee of mountains, Quart.J. of Roy. Met. Soc., 75, 41-56.

_____, 1956: Airflow over an isolated hill, Quart.J. of Roy. Met. Soc., 82, 75-81.

_____, and M. Wilkinson, 1956: Waves in the lee of an isolated hill, Quart. J. of Roy. Met. Soc., 82, 419-427.

Silverman, B., 1960: The effect of a mountain on convection. Cumulus Dynamics, Proc. 1st Conf. on Cumulus Convection, Pergamon Press.

Wurtele, M., 1957: The three dimensional lee waves. Beitr. Phys. frei. Atmos., 29, 242-252.

APPENDIX B

AIRCRAFT TRAVERSES

IN A GROWING MOUNTAIN CUMULUS CLOUD

By

Clement J. Todd

Atmospheric Research Group
Altadena, California

December 1963

Submitted to Journal of Atmospheric Sciences

ARG64 Pa-115

ABSTRACT

During a one-hour interval while a mountain cumulus cloud system was developing into a cumulonimbus, in a light wind condition over an isolated peak, a series of 17 traverses were made through the clouds by an instrumented aircraft. Time-lapse cloud photographs and radar records were available for the same sequence. The observations are presented and briefly analyzed. The cloud towers had active lives which started out at two minutes and increased to more than 30 minutes as the clouds developed. Deep in the cloud the aircraft was able to find the same updrafts on consecutive traverses for from 7 to 18 minutes. The updrafts observed by the aircraft within the cloud had vertical velocities two to three times as great as the maximum rate of rise of the towers. The length of the vertical flow of air past the flight level for a typical updraft was 18, 000 feet or more, while the diameter of the updraft was only 3, 000 feet. The towers broadened somewhat as the cloud developed and became rapidly broader just as the first radar echoes occurred. The gross features of the convective cells were in general agreement with the "starting plume" treated by J. G. Turner.

1. Introduction

During the course of cumulus cloud studies at Flagstaff, Arizona, on 10 August 1960, the meteorological situation, the aircraft positioning, the aircraft measurements, the radar records, and the time-lapse cloud photographs all combined to yield an especially informative observational sequence of cumulus development. The sequence featured a series of systematic aircraft traverses through the cumulus area over the sun-heated slopes of the isolated San Francisco Peaks, north of Flagstaff, on a day with light surface winds. The data particularly illuminated features of the continuity and duration of cumulus cloud updrafts. This paper presents the observations and analyzes them briefly.

Other sequences of aircraft traverses conducted for study of mountain convection have been reported on by Braham and Draginis (1960) and also Silverman (1960). These flights were mainly carried out on relatively cloudless days where only small convective clouds developed over the mountains. The present study, on the other hand, follows through the cloud development to the start of the precipitation stage. This study reinforces some of the findings made in the clear air studies and sheds some light on the questions not answered in these studies. The advantage of this study over the clear air convection studies is the use of time-lapse motion pictures of the clouds in which the aircraft is traversing. A great deal of information about the continuity of the convection was gathered by this technique.

2. Over-all situation.

At Flagstaff August 10 began with clear sky and excellent visibility. 16 mm time-lapse cameras at the Flagstaff Airport showed the first cumulus puffs over the San Francisco Peaks, 13 miles to the north, at 0828 MST. The small cumulus clouds appeared and disappeared until 0952 MST, after which time there were always active towers. The view remained unobstructed until after a radar echo developed at 1034 MST. The cloud observation aircraft, a specially instrumented Cessna 180, started cloud traverses at 0934 MST and continued until 1028 MST when the aircraft descended to de-ice. Seventeen cloud traverses were made over the Peaks in rapid succession from east to west and back again during this interval. These traverses followed virtually the same track but lengthened as the cloud grew wider. It is the duration of the sequence of cloud traverses made in such rapid succession that makes this investigation unique. After the de-icing from 1038 to 1052 MST four additional traverses were made. The cloud situation had become so complex by then that these later traverses are not presented here.

3. Equipment.

The instruments on the Cessna 180 pertinent to this flight were altimeter, thermistor thermometer with 1/2-second time constant, and a Johnson-Williams hot-wire type liquid water instrument. These variables were recorded on a time sharing basis on a 2-channel Brush recorder. The

aircraft flight path was taken from the radar during the parts of the flight that were followed by radar. The rest of the flight path was reconstructed from the observer's log and from the time and location of cloud penetration. Because the cloud had a distinct profile in the direction of flight, it was possible to define the flight path easily.

Time-lapse photographs were taken with two 16 mm cameras from the Flagstaff Airport (Fig. 1, map). Each camera used a 10 mm lens giving a field view of 55°; the cameras' fields overlapped 5° and produced a total view of 105°. Pictures were taken at 30-second intervals before the aircraft started traversing, and after this time the interval was shortened to 12 seconds.

Besides the two 16 mm wide-angle cameras located at the Airport, there were two full-sky cameras operated at one frame per minute. One was just to the south of the peaks and the other was to the west of the Peaks. With these it was possible to locate the first clouds and some features of the cloud bases accurately. The cloud tops, however, were observed only from the Airport and, therefore, were located only approximately in distance. Because of this, the heights and growth rates could have estimated errors on the order of ±10 per cent, an amount of error which would not materially alter any conclusion from these studies.

Two MR-4 X-band radars were used from Flagstaff Airport. One operated in RHI mode and the other in PPI, giving records of both the height and horizontal cross sections of the precipitation areas. The PPI photographic records also showed the aircraft track.

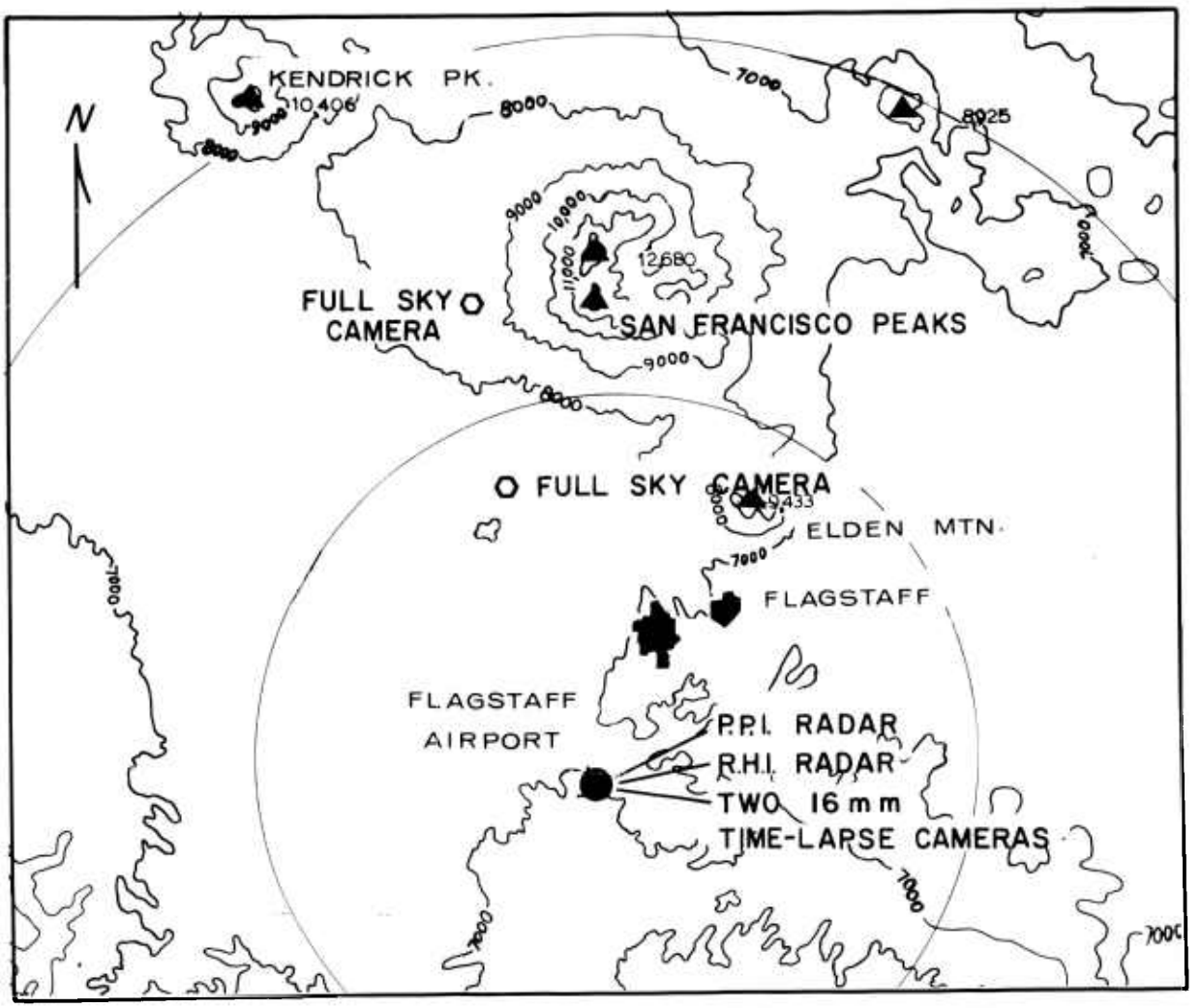

Fig. 1. MAP OF THE FLAGSTAFF AREA SHOWING THE LOCATION OF CAMERAS AND RADAR SITES.

4. Observations.

On August 10 the surface wind measured at the Flagstaff Airport was calm at 0700 MST. Then a wind developed from the south becoming 9 mph by 1000 MST. The wind aloft was light up to about 15,000 feet, at which altitude it backed from the east.

Figure 2a-b is a time diagram of the evolution of the cumulus cloud towers that emerged from the cloud system over the San Francisco Peaks. It begins with the first puff at 0824 MST and follows through until 1045 MST. A profile of the mountains taken from the south serves to orient the cloud development. The east-west positions of the towers are given in their proper locations with respect to the mountain profile. The width of the towers and their drift as they sheared to the west are shown to scale. At the right side of the chart is a height history of the cloud tops given on the same time scale as the east-west histories of the towers. These two can be matched for individual cloud towers.

A general feature shown in Fig. 2a-b is that the cloud system grew in a series of surges. The first visible surge produced just two cloud puffs or towers and lasted for about 5 minutes. The next surge produced five small isolated towers and lasted for 10 minutes. There was another 10-minute surge with two towers, and then the cloud died out. Next, a bigger surge lasted for over 30 minutes and produced 12 towers. After this came a sustained surge that produced over 20 towers which increased progressively in height and breadth for over one hour and 20 minutes and

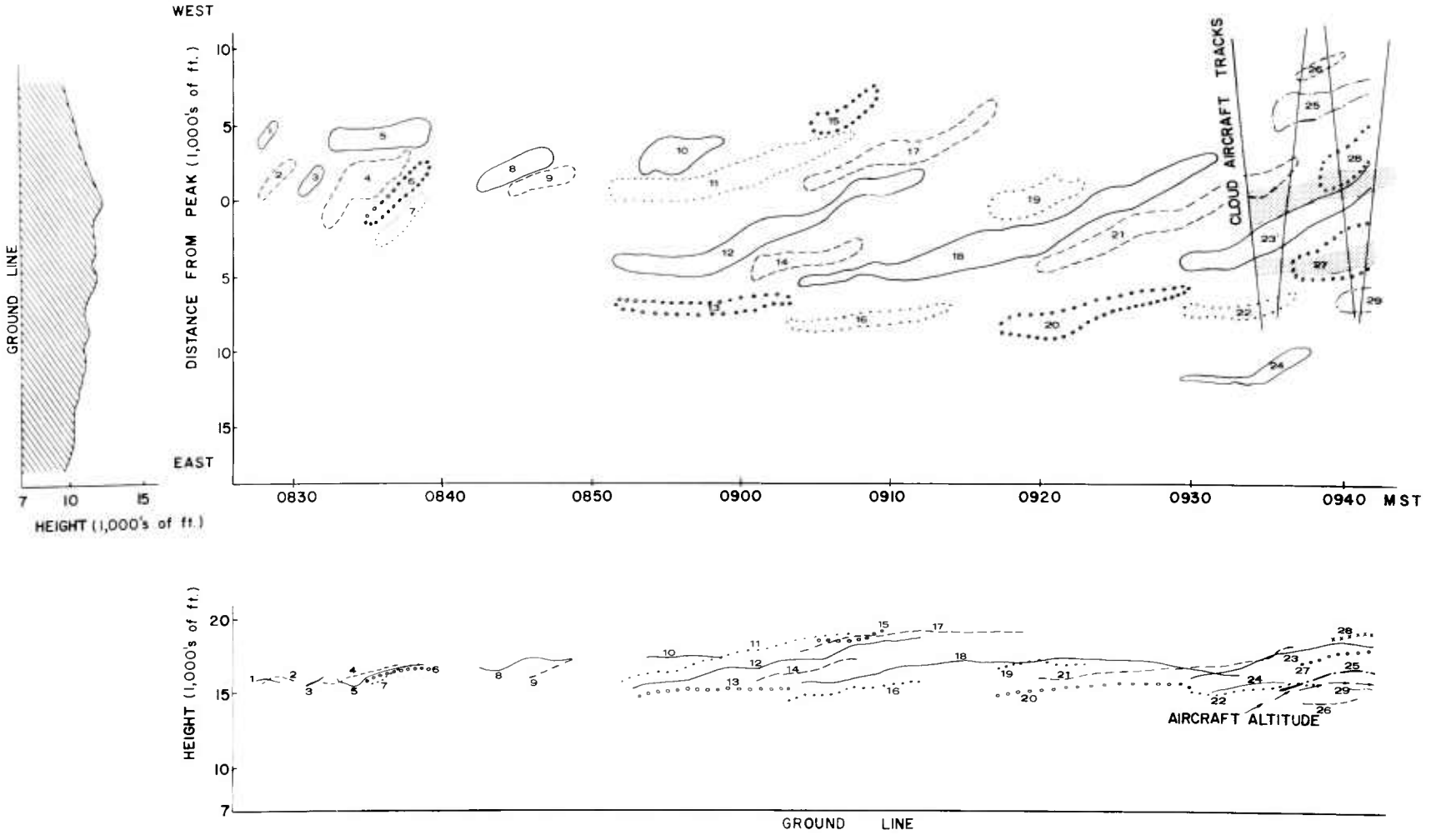

a.

Fig. 2. TIME SECTIONS OF THE CLOUD TOWERS AND AIRCRAFT TRACK.

Upper section shows horizontal location of cloud towers with respect to the Peaks. Shaded areas indicate regions of updrafts within the cloud as found by the aircraft. The lower section shows the time-height histories of cloud towers.

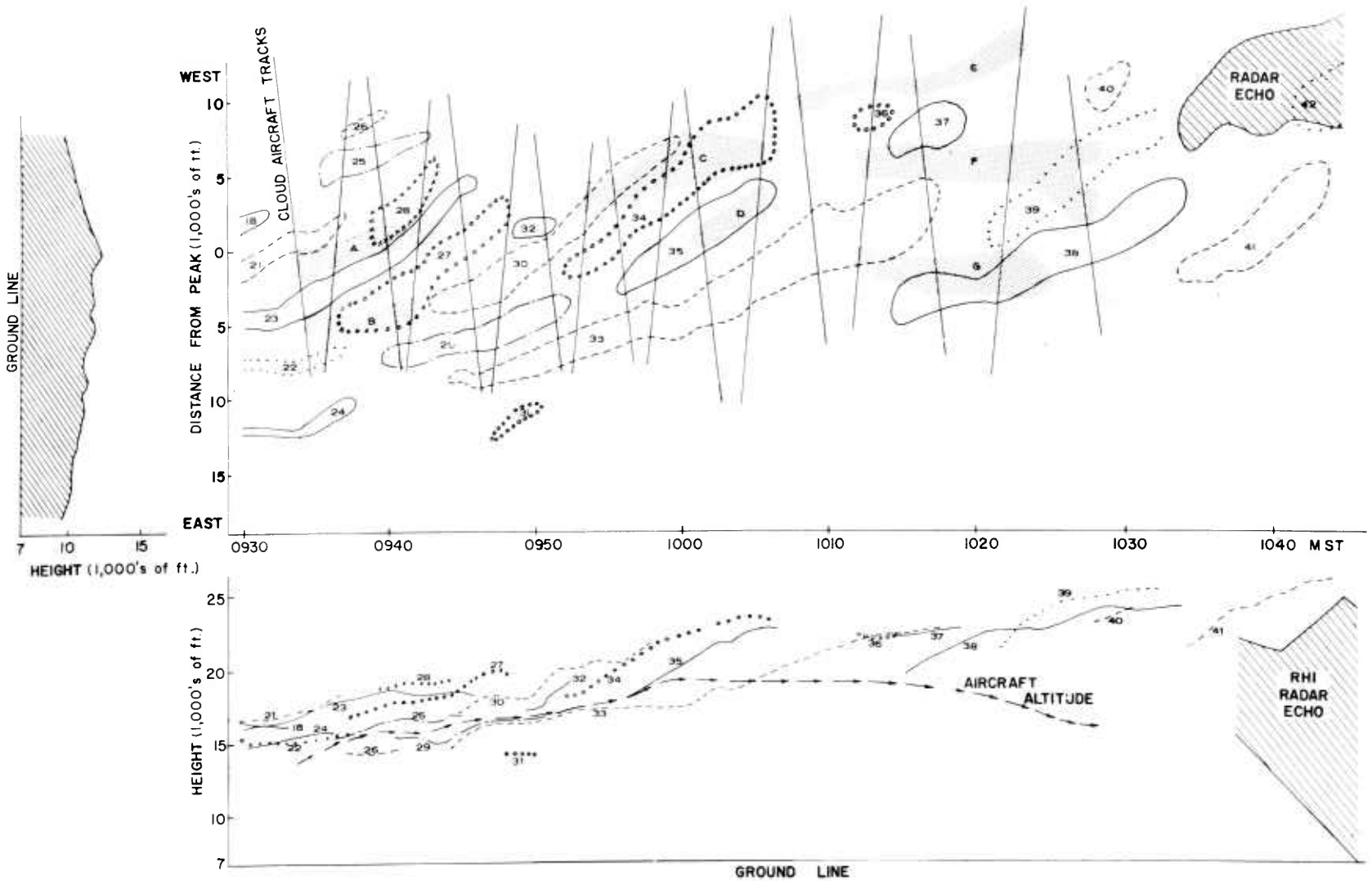

b.

Fig. 2. TIME SECTIONS OF THE CLOUD TOWERS AND AIRCRAFT TRACK.

Upper section shows horizontal location of cloud towers with respect to the Peaks. Shaded areas indicate regions of updrafts within the cloud as found by the aircraft. The lower section shows the time-height histories of cloud towers.

caused rain. As a final result there were broader, taller towers lasting longer and having faster rates of rise as they emerged from the cloud top.

It was quite apparent that the width, duration, and height of the towers all increased with time. A radar echo appeared at 1034 MST. The width, east-west location, and height are shown on the cloud tower chart. It is interesting to note that this echo started when the towers exceeded a cross section of 3000 feet and a height of 25,000 feet MSL. The width of the echo started at 3000 feet and within four minutes spread to 6000 feet.

The aircraft traversed from east to west and west to east over the mountains. Its east-west time position appears on the cloud tower chart, Fig. 2a-b. Its altitude is shown on the time-height chart.

The aircraft was flown at a constant power setting and attitude during the traverses, and being a light aircraft it responded rapidly to the up- and downdrafts. For the purpose of these observations it is assumed that the velocities of the up- and downdrafts can be measured from the slope of the altimeter traces. These velocities are plotted along the flight path (Fig. 3) with the updrafts plotted on the positive side of the line and the downdrafts plotted on the negative side of the line. The updrafts were analyzed for continuity, and those which were considered to be consecutive encounters of the same updraft were joined into shaded areas. These shaded areas of updraft have been added to Fig. 2a-b for comparison with the observed continuity of tower development.

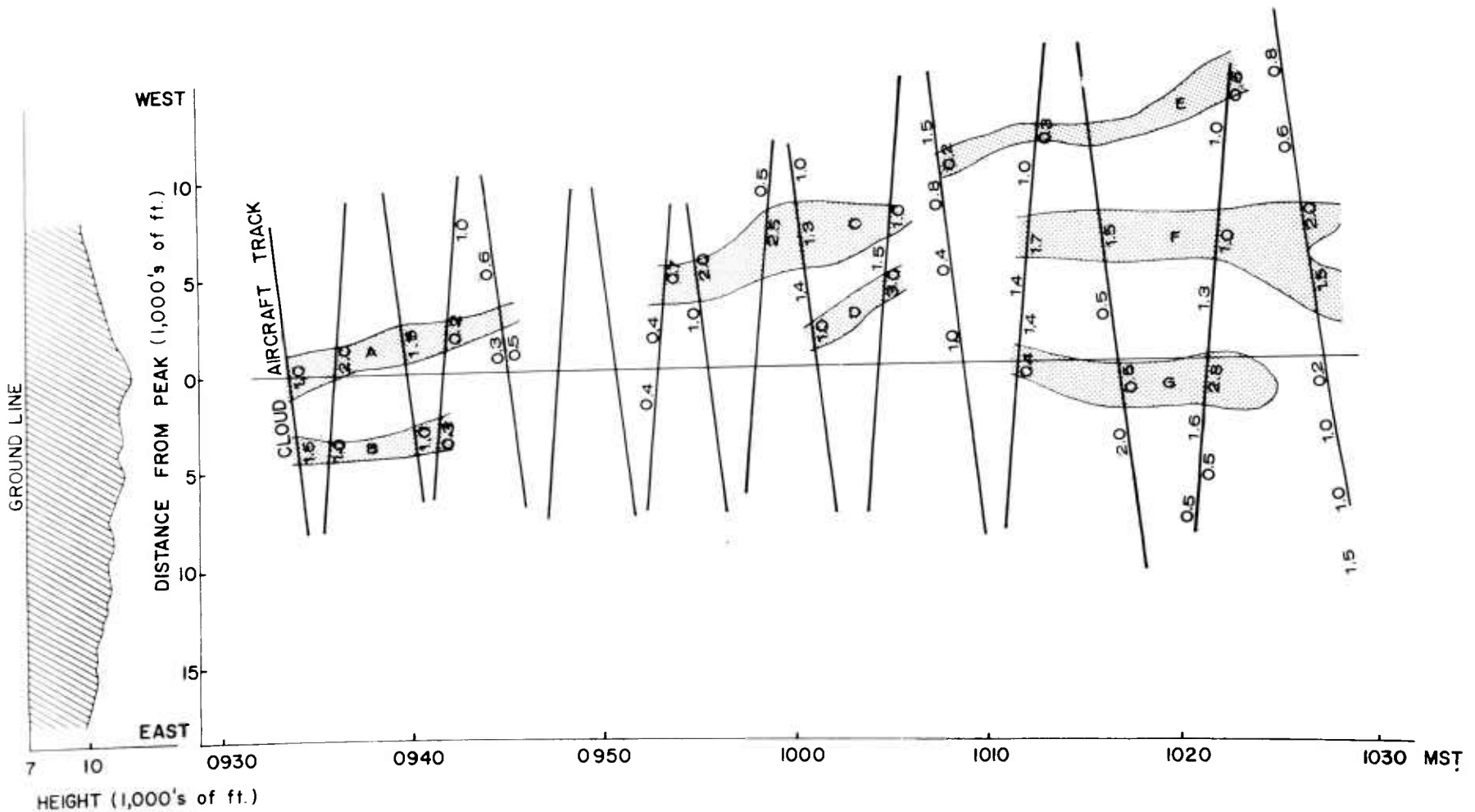

Fig. 3. HORIZONTAL LOCATIONS OF THE VERTICAL CURRENTS FOUND BY THE AIRCRAFT.

The numbers to the right of the lines indicate updraft velocities; the numbers to the left indicate downdrafts (1000 ft min^{-1}). The updraft regions are shaded to show continuity.

5. Analysis.

Figure 4a summarizes the length of time the towers and updrafts can be recognized, and it shows how the towers developed from 2-minute lifetimes to 15- to 20-minute lifetimes with the extreme cases about 30 minutes. "Lifetime" here refers to the time when a tower was identifiable, and so can include some periods when the tower was not growing vigorously. The towers have dimensions similar to those found by Glass and Carlson (1963). Updrafts found by the aircraft shown in Fig. 3 indicate a duration of 7 to 18 minutes. The fact that the aircraft did not intercept a particular updraft in a traverse may merely indicate that the localized upcurrent was missed. The aircraft was able to find that updrafts deep in the cloud had considerable continuity, comparable to the active growth period exhibited by the towers at the top of the cloud.

The evolution of tower widths (Fig. 4b) showed little real increase until after 1000 MST, and these widths were roughly the same as those of the updrafts found by the aircraft deep in the cloud. The widths of the radar echoes, also plotted on Fig. 4b, show that by the time they occurred the convection seemed to be getting broader.

The maximum rate of rise exhibited by the towers is shown as a function of time in the life of the cloud system in Fig. 4c. The observed aircraft updraft velocities are also plotted. These show upward velocities two to three times greater than the rate of rise of tower tops at the same time in the cloud. The tower top rise rates represent averages over

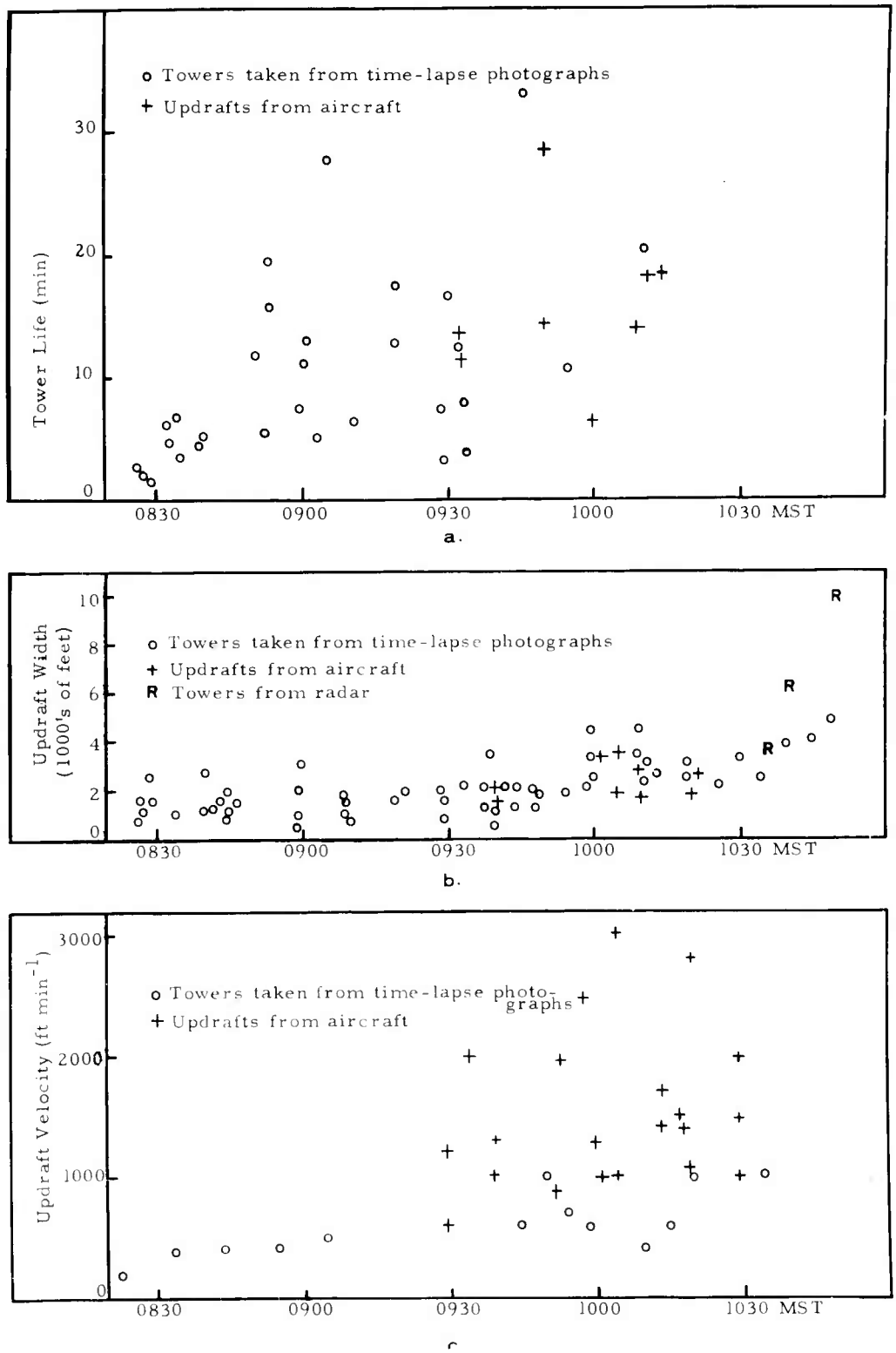

Fig. 4. A SUMMARY OF INFORMATION ON INDIVIDUAL TOWERS AND UPDRAFTS DEPICTED IN FIGS. 2 AND 3.

several minutes; the aircraft vertical velocities represent averages of about 2000 feet of the traverse.

The shear rate of the towers (Fig. 5) varies markedly at low levels suggesting that there is a localized mountain effect on the wind apparently producing a narrow jet as much as 4000 feet above the tops of the San Francisco Peaks (12,680 MSL). There is an apparent minimum wind at 20,000 feet with an increase to 25,000 feet where the wind component from the east is 800 feet min^{-1}.

A study of a typical updraft which reveals some interesting characteristics is shown in Fig. 6. This is updraft C from Fig. 3. The coordinates are width of the updraft versus length of flow. If the length of the stream of air that flows past the flight level is ℓ and the velocity of the updraft as measured by the aircraft is w at time t, then

$$\ell = \int_{\text{start}}^{\text{finish}} w \, dt$$

from the start of the updraft to the finish. For updraft C shown in Fig. 6a, ℓ from start to finish is 18,000 feet while the widest point found by the aircraft is 3000 feet. Time is plotted along the length scale at appropriate points.

Figure 6b shows the liquid water (LW) content plotted on the updraft flow chart for the times of the aircraft traverses. The LW is compared with the adiabatic liquid water content for that altitude above cloud base. When the updraft was first detected at flight level the LW was nearly

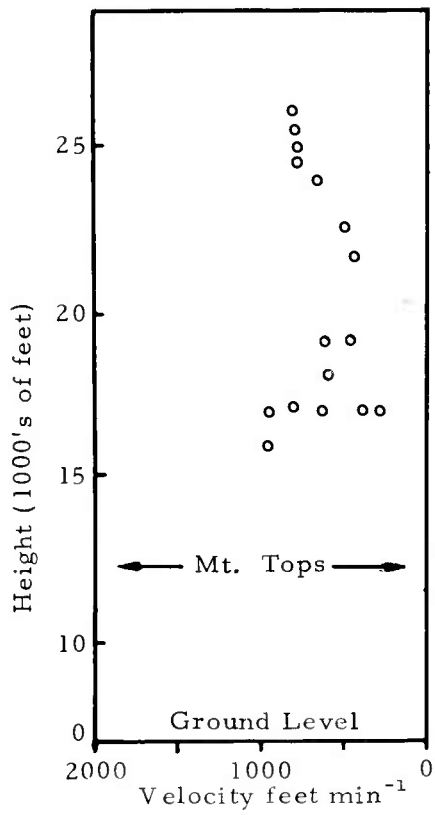

Fig. 5. WESTWARD COMPONENT OF TOWER DRIFT.

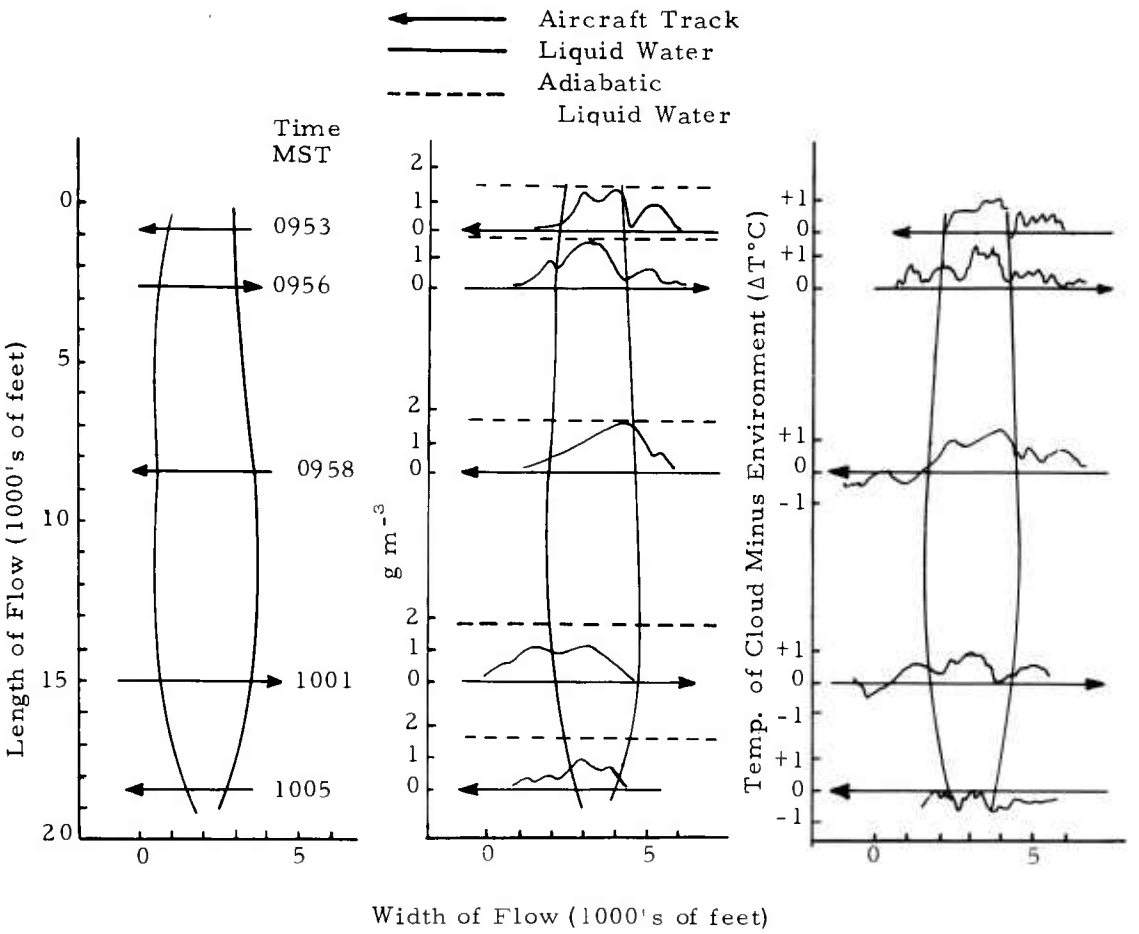

Fig. 6. VARIATIONS DURING THE LIFE OF AN UPDRAFT.

a. The length of flow past the flight level shown with respect to the width of the updraft. b. The liquid water encountered by the aircraft plotted with respect to its location on the length and width of the flow. c. The temperature excess over the temperature of the environment plotted with respect to its location on the length and width of the updraft.

adiabatic, and it remained so while the updraft was vigorous, but as the updraft died out the LW decreased as if to indicate mixing of the updraft with drier air.

Figure 6c shows the temperature plot with respect to the updraft column. The temperature base line refers to the temperature of the air outside of the cloud. The temperature trace shows many of the same characteristics as does the liquid water content curve (Fig. 6b). In particular, the early stages of the updraft indicated vigorous undiluted convection with sharply defined excesses, but as the updraft died it became diluted and lost its buoyancy.

The question arises as to how well the updrafts intercepted by the aircraft relate to the towers rising above the cloud tops. A return to Fig. 2a-b shows that there is an immediate apparent relationship. Some details, however, must be interpreted subjectively. There are towers that do not relate to updrafts found by the aircraft. This could be because their updrafts are either north or south of the flight path. There is a down-shear offset of the tower from the updraft deep in the cloud. This offset is dependent on the upward velocity and the shear and is difficult to interpret.

An attempt was also made to relate the towers and the updrafts to their sources. The factors that were considered important in creating a source on this day of clear skies and light winds were: the relative intensity of solar heating, the height of the surface, and the size of the potential source

area. A map (Fig. 7) was constructed relating sloping terrain to the solar angle for 0900 MST on August 10. This was constructed by dividing the Peaks region into areas of like slope as indicated on a topographical map. The slope of these areas was compared to the sun's zenith angle, and the resulting cosine of the solar angle to the terrain was entered for the map region. The cloud updrafts and towers would drift some from the source regions, but for the earliest cloud puffs over each of the mountain masses from the cloud triangulation there seemed little doubt that the rising air could be related to slopes of most favorable sun angle. Comparison of Fig. 2 and Fig. 7 suggests this relationship. The higher the mountain slopes the earlier the cloud puffs appeared. Those over the highest of the San Francisco Peaks appeared about 50 minutes earlier than those over some of the lesser mountains (Elden Mountain and Kendrick Mountain).

As the clouds grew more mature and the visible active parts were higher above the sources the relating of the towers to the sources became less certain because the rate of rise throughout the updraft and the shear across the updraft were uncertain. A little freedom of interpretation still made it possible to relate the towers to the larger regions of favorable solar angle.

6. Discussion.

This sequence of observations has offered an opportunity to study the general features as well as the succession of cloud towers and internal

updrafts of a mountain cumulus as it developed from the first puffs to a cumulonimbus. This cloud developed when the low level winds were light and it is assumed that it was fed primarily by air currents heated on the sun warmed mountain slopes. The location of the active cloud towers seemed to correspond to the slope areas with most favorable sun angle, the higher the slope the earlier it produced an active cloud tower. The active life as well as the total life of the individual cloud towers grew longer as the cloud matured. The successive towers grew gradually wider as the cloud developed, but there was a marked broadening of the towers just prior to and during the development of the first echo. The aircraft found upcurrents deep in the cloud in the same relative position on several consecutive traverses indicating that these updrafts had lives of at least 7 to 18 minutes. They might have lasted longer and been missed by the aircraft if the track did not coincide with the drifting core.

These updrafts within the clouds were found to have significant maximum velocity regions that were approximately 2 or 3 times greater than the maximum rate of rise of the tower tops. From the length of life of the internal updrafts and their vertical velocities it was deduced that typically more than 18,000 feet of air streamed past the flight level through a 3,000 foot wide updraft. This picture invites comparison with a model presented by Turner (1962) which he calls the "starting plume". It consists of a buoyant plume capped by a thermal or vortex, the top of which is rising while the bottom is being fed by its source. Turner's model

is for a neutral surrounding, a source from which the input is of a constant density, and a fluid in which there is no energy introduced by a change of state so there is neither evaporation nor condensation. Any comparison can be only qualitative, but the gross features of a growing cloud tower, with a vortex top being fed by a long buoyant plume which during parts of the life cycle may extend clear to the heat source, seems to correspond to what is observed here. In this model the updraft rate in the buoyant plume should be more than twice the rate of rise of the cloud top; just how much depends upon how far below the top the updraft rate is measured. In the actual cloud, the ratio of these velocities depends not only on the model considerations but also on the buoyancy with respect to the environment. During the life of the updrafts as observed at flight level there were variations in the vertical velocity, liquid water content, and temperature excess of the cloud over that of the environment. These should be reflected in the rates of rise and heights of penetrations of the towers. These sorts of variations are found in the tower histories, but due to the height separation, the flight path, and the visible tower, it was not possible to trace this relationship out on an individual tower basis with certainty.

In some respects the cloud towers seem to be independent of each other, yet in other respects they act as if they were all governed by the same controlling forces. The factors that have to do with the surface heat sources and the surface frictional drag would tend to give updrafts and towers from different slopes individual characteristics of width, length of life, buoyancy,

and vertical velocity. To the extent that all of the towers seem to surge and slacken in growth together, they must be controlled by an environmental characteristic which is varying. This might be related to the amount that the upper air, in which the clouds are growing, is lifted as it flows over the Peaks. The more the air is lifted the more convectively unstable it will be and the more vigorously the clouds will develop.

7. Conclusions.

Observations were made of the growth of a cumulus over a mountain peak on a clear calm morning. The heating of the slopes dominated the convection that occurred, while the dynamic effects of the flow across the mountains imposed only slight modifications. The most interesting feature is that the convection seemed to be analogous to the "starting plume" described by Turner (1962), which are buoyant plumes capped by a rising thermal. Both the towers and the updrafts measured by the aircraft fit the time continuity of flow of Turner's model rather than the short pulses that the bubble theory calls for.

Acknowledgments

The complete crew of the Atmospheric Research Group worked together to achieve the success of this coordinated set of observations. Extra credit goes to Mr. Kenneth Beesmer, who was the aerial observer and exercised the good judgment that made this sequence of traverses possible. The credit for organizing the whole project and designing the aircraft observation system

goes to Dr. Paul B. MacCready, Jr., the Project Director.

This work was supported by the Atmospheric Sciences Section of the National Science Foundation under Grant Nos. G8334 and G11969.

REFERENCES

Braham, Roscoe R., Jr., and Milton Draginis, 1960: Roots of orographic cumuli, Cumulus Dynamics, New York, Pergamon Press, 1-3.

Glass, M., and T.N. Carlson, 1963: The growth characteristics of small cumulus clouds. J. Atmos. Sci., 20, 397.

Silverman, Bernard A., 1960: The effect of a mountain on convection, Cumulus Dynamics, New York, Pergamon Press, 4-27.

Turner, J.S., 1962: The "starting plume" in neutral surroundings. J. Fluid Mech., 13, 3, 356.

APPENDIX C

COMPUTATIONS ON CLOUD GROWTH

RELATED TO SEEDING

by

William L. Woodley

Atmospheric Research Group
Altadena, California

January 1964

Presented at the 225th National Meeting of the AMS, Los Angeles, January 31, 1964, under the title "A computational study of the effects of ice nucleating temperature on convective cloud development".

Submitted to Journal de Recherches Atmosphériques
February 1964

ARG64 Pa-118

ABSTRACT

A statistical study has been conducted investigating the possible cloud growth effects due to heat released when supercooled water is converted to ice. Calculations are made of the heights to which cloud tops would rise assuming that the supercooled water is converted to ice at -10C (the seeded case) or at -30C (the unseeded case). To simplify the computations it is assumed that the cloud parcel rises unmixed with outside air to the level where the buoyancy is zero. 180 cases are treated, for soundings from Flagstaff and Winslow, Arizona, during the summers of 1961, 1962, and 1963. The results imply that height increases of over 5000 ft due to seeding can be expected fairly often, and increases over 15,000 ft are sometimes possible. Despite the simplicity of the model, it is felt that the computed height differences qualitatively represent a reasonable measure of the potential for cloud dynamics changes from seeding. Specific observations of cloud growth due to seeding are noted, but can only be considered as consistent with these concepts rather than verifying them.

1. INTRODUCTION

Conversion of the supercooled water in cloud droplets into ice releases heat which will increase the buoyancy of a cloud. If there is one gram of supercooled water per kilogram of air, the glaciation warming amounts to about 1/3°C. Thus in typical clouds warming of several degrees can occur as the cloud becomes completely glaciated by natural or artificial means. The buoyancy increase from early glaciation by cloud seeding may sometimes cause effects which are large enough to be distinctive, namely a greater growth rate for the cloud, or, subsequently, a greater total height for the cloud.

If the natural cloud moves upward into a markedly stable layer, the small additional buoyancy from glaciation might not have an appreciable effect. However, in certain marginal natural conditions which are only weakly stable, the slight extra buoyancy may be enough to permit considerable growth in the cloud. It is a purpose of this paper to see how frequent these specialm marginal conditions might be.

During the summers of 1961, 1962, and 1963 the Atmospheric Research Group-Meteorology Research, Inc., cumulus cloud studies at Flagstaff involved the seeding of various convective clouds and some of the observations raised the question of possible cloud growth due to the seeding. This paper is an outgrowth of this interest. Although the effect of artificial freezing nuclei materials on cloud dynamics is a complex subject involving cloud dilution and precipitation effects, it has been considered useful to

treat the simple buoyancy effect separately in order to make a start toward solution of the more complex problem.

2. BASIS OF HEIGHT CALCULATIONS

Cloud top heights have been estimated for the following conditions: 1) complete conversion of supercooled water to ice at -10C to represent artificial seeding, and 2) complete conversion of water to ice at -30C to represent natural seeding. The calculations have been based on parcel theory, assuming that the parcel rises from the cloud base without mixing and rises only to the level where the buoyancy is zero. Account is taken in the calculations, however, of release of heat of fusion and changes in buoyancy due to condensate being carried along in the updraft. For simplicity, buoyancies have been estimated from the calculations as temperature differences rather than virtual temperature differences.

Figure 1 shows an example of the height computation scheme. Line A gives the parcel temperature starting at the convective condensation level, assuming a pseudo-adiabatic process with the condensate remaining liquid. Line B includes the buoyancy decrease due to the weight of the condensate, i.e., Line B shows the temperature saturated air should be to have the same buoyancy as the air with condensate. This temperature difference ΔT_v between A and B was calculated by the method of Saunders (1957) who showed the condensate effect, in terms of temperature, to be $-\Delta T_v = T_v \cdot W_{dw}$ where W_{dw} is the saturation

mixing ratio difference between cloud base and the point in question and T_v is the cloud virtual temperature. To the accuracy required here, temperature T instead of virtual temperature T_v can be used in this correction formula.

Lines C add the effect of release of heat of fusion to Line B in Fig. 1. This is shown for two conditions: a) C1 considers that the condensate is converted to ice at -10C, and b) C2 assumes ice conversion at -30C. For the example shown in Fig. 1 at -10C with 5 g/kg of water in condensate form, the heat of fusion raises the temperature by 1.67C while the condensate weight effect lowers the buoyancy by 1.31C for a net buoyancy increase of .36C relative to Line A (pseudo-adiabatic process).

Figure 1 shows the effect of seeding on cloud top height by comparing the cloud top of 24,000 feet (Line B - no release of heat of fusion) with the estimated top of 30,200 feet which would result from converting liquid water to ice at -10C (Line C1). Figure 1 emphasizes that small changes in the temperature of the ascending air can have large effects on cloud top height.

3. RESULTS

Estimates of cloud top heights have been made according to the above techniques for all available soundings from Winslow, Arizona, for the July - August periods of 1961-63 when field studies were being carried out in the Flagstaff area. For the 1963 period special raob soundings

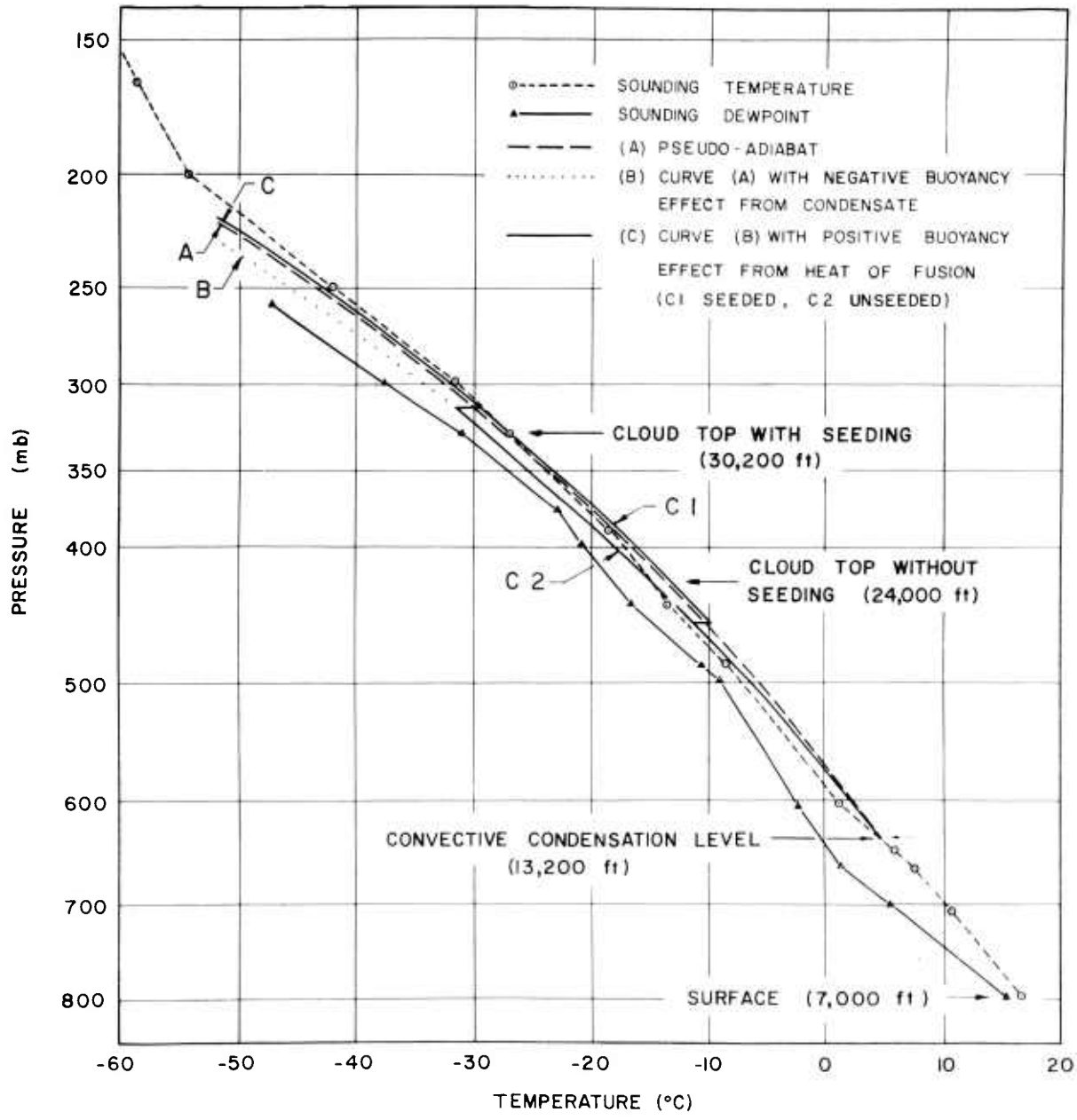

Fig. 1. EXAMPLE OF HEIGHT COMPUTATION METHOD.

were also made at Flagstaff and these have been included in the present study at the appropriate time of day. Results of these calculations of cloud top heights are shown in Fig. 2 for each year.

It is apparent in Fig. 2 that rather spectacular differences in cloud tops may occur for the two cases of converting water to ice at -10C vs. conversion at -30C. For July 22, 1962 at 1700 MST, for example, the cloud top should reach 23,500 feet if conversion to ice does not take place until -30C compared to 39,000 feet if conversion could be accomplished at -10C. Comparable estimates for August 1, 1963 at 1400 MST are 24,000 and 39,000 feet.

Table I summarizes the results of Fig. 2 in terms of cloud top differences which might result from conversion of water in the cloud to ice at -10C.

Table I

CLOUD TOP DIFFERENCES

	Cloud Top Difference (Seeded Case - Unseeded Case)		
Year	% > 5,000 ft	% > 10,000 ft	% > 15,000 ft
1961	47	30.6	4.0
1962	58.2	19.4	7.5
1963	34.5	19.0	4.9

Table I suggests that effects of seeding (conversion to ice at -10C) might frequently be expected to have a small effect on cloud top height

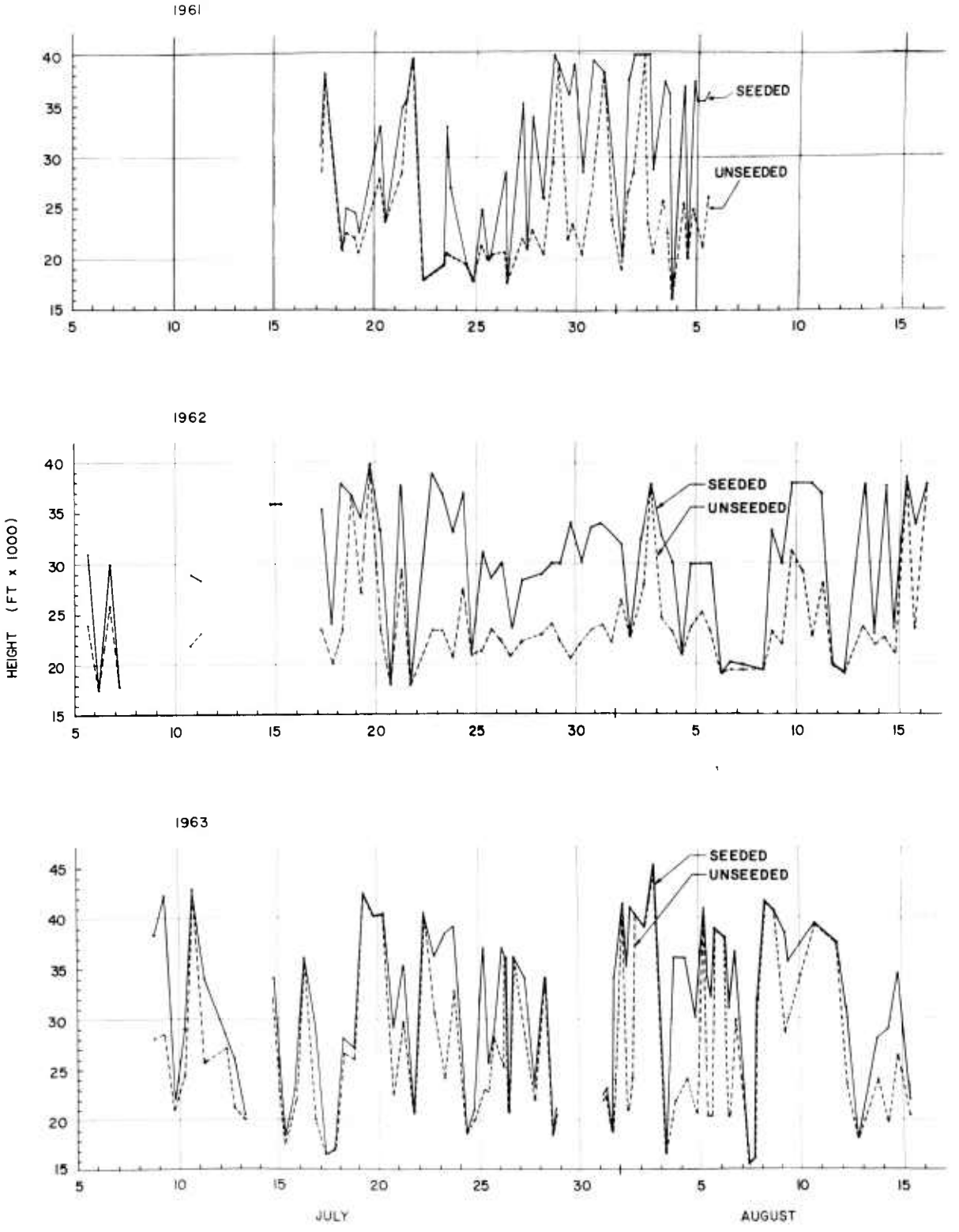

Fig. 2. CALCULATED TOP HEIGHTS OF UNSEEDED AND SEEDED CLOUDS.

and that large effects are comparatively rare. The table also suggests that substantial differences may exist from one year to the next with 1962 apparently somewhat more favorable for detection of seeding effects in the Flagstaff area. Reference to Fig. 1 indicates that favorable periods for detection of seeding effects were of short duration in 1961 and 1963 compared to 1962. In 1962 the period of July 27 to August 1 appears to have been especially favorable for creating these effects.

4. LIMITATIONS OF THE MODEL

A. Limitations of the parcel ascent method for computing cloud top heights are well known and arise from neglect of mixing with surrounding air and neglect of compensating flow in the environment through which the cloud is passing. In addition, no account is taken of rising air parcels overshooting their equilibrium height as given by the parcel method. For strongly rising cores of large convective clouds at Flagstaff, however, MacCready, Smith, Todd, Chien, and Woodward (1963) found undiluted cores to 9000 feet above cloud base and it is suggested that serious cloud dilution effects occur primarily in smaller convective clouds or on the edges of the larger clouds.

B. Cloud top heights computed by a pseudo-adiabatic process would be similar but slightly lower than those shown in Fig. 2 for the cases where glaciation occurs. For this case, increases in buoyancy due to glaciation tend to balance decreases due to weight of the condensate. For non-glaciation cases, the pseudo-adiabatic method will give higher cloud top estimates than those indicated in Fig. 2.

C. The assumptions of conversion to ice at -10C vs. conversion at -30C are idealizations which tend to overemphasize the effects of seeding in some situations. A natural cloud is most likely to remain primarily supercooled to -30C when it is large and vigorous and natural ice nuclei are rare. The assumption that a cloud can be converted to ice at -10C can probably be realized only with the most intensive seeding techniques, particularly for fast growing cumulus where the time for growing ice crystals is short. MacCready (1959) has made estimates of the height of complete glaciation from silver iodide seeding in clouds typical of those at Flagstaff. An assumed silver iodide concentration distribution of $10^5/m^3$ at -5C, $10^6/m^3$ at -10C, $10^7/m^3$ at -15C, and $10^6/m^3$ at -20C would just about glaciate the cloud completely at -10C for weak updraft cases. Such concentrations can probably not be obtained

from typical ground seeding, but even higher ice crystal concentrations have been measured from aircraft silver iodide seeding by Todd (1964).

D. Prediction of the convective condensation level (CCL) for a particular sounding requires subjective judgment and occasionally small changes in this level may lead to large changes in estimated cloud top heights. Local variations in terrain and vegetation may lead to differences in the CCL and cloud formation time such that portions of the atmosphere in the immediate vicinity of Flagstaff may be poised for seeding at different times. The observation sample used in the present study can then be considered as a sample of representative soundings in the area but local variations may exist which substantially influence the possible seeding effects on any particular day.

5. DISCUSSION

Observational verification of the results of seeding are limited in number because of frequent difficulties in obtaining visual observations and because of lack of adequate knowledge of the characteristics and environment of the seeded cloud.

Langmuir (1951) recognized the role of heat of fusion in dynamic seeding effects, and used it to help explain his qualitative observations

of cloud developments in New Mexico. Kraus and Squires (1947) describe a spectacular instance of cloud growth but unfortunately a sounding was not available.

On February 5, 1947, in Australia, Kraus and Squires seeded two cumulus clouds with granulated carbon dioxide. All clouds in the area were based at 11,000 feet, the freezing level at 18,000 feet, and the top of the clouds uniformly at 23,000 feet which would indicate a cloud top temperature of roughly -10°C. The infected clouds were observed to grow spectacularly to produce showers with the second cloud anviling off at 40,000 feet. No other rain showers were observed within a radius of 100 miles of the observing aircraft.

MacCready, Smith, Todd, Chien, and Woodward (1963) examine a seeding event on July 27, 1962 at Flagstaff. This is the start of the period which Fig. 2 shows as being particularly favorable for dynamic cloud changes from cloud seeding. The apparent increased buoyancy from glaciation within the seeded cloud was noted from aircraft penetrations. The seeded cell had a greater tower top rise rate than previous towers (2000 fpm vs. 1400 fpm), and rose 8000 feet higher than the earlier cells. The general experience in Flagstaff, however, has been that individually seeded cumulus grow only slightly in height and frequently collapse shortly after seeding.

The present study indicates that substantial height increases may result from seeding but that favorable conditions for these events occur

only on a relatively small number of occasions. Although a large number of assumptions have been made during the study, the general results appear to be in agreement with results of seeding experiments.

6. CONCLUSIONS

A simple computational procedure has been employed for estimating the heights of the tops of seeded and non-seeded clouds for the Flagstaff area during three summers. The results imply that significant dynamic effects from seeding would not be uncommon for the conditions studied, and that occasionally spectacular effects in cloud growth would be possible from the release of heat of fusion by seeding. The height computations ignore mixing, cloud dimensions, and rise rate and therefore represent a simplified model of the processes occurring in the cloud. The limited observations available on seeding effects in cumulus clouds appear to be in agreement with the results of the study.

ACKNOWLEDGMENTS

This work was supported by the Atmospheric Science Section of the National Science Foundation under Grant G11969. The radiosonde data at Winslow were obtained from the U. S. Weather Bureau, and at Flagstaff from the Air Force Cambridge Research Laboratory, Army Electronic Proving Ground at Ft. Huachuca, and the Army Electronic Research and Development Laboratory of Ft. Monmouth.

The study was performed under the guidance of C. J. Todd of Atmospheric Research Group, whose assistance and stimulus are gratefully acknowledged. P. B. MacCready, Jr. and T. B. Smith of ARG were most helpful in assisting with the detailed interpretations.

REFERENCES

(1) Saunders, P.M. (1957). - The thermodynamics of saturated air: a contribution to the classical theory. Quart. J. Roy. Meteor. Soc., 83, 357, 342.

(2) MacCready, P.B., Jr., Smith, T.B., Todd, C.J., Chien, C.-W., Woodward, E. (1963). - Study and modification of convective storms. Meteorology Research, Inc., Final Report, Contract DA-36-039 SC-89066, U.S. Army Electronic Research and Development Laboratory, Ft. Monmouth, N.J.

(3) MacCready, P.B., Jr. (1959). - The lightning mechanism and its relation to natural and artificial freezing nuclei. Recent Advances in Atmospheric Electricity, Pergamon Press, 369-381.

(4) Todd, C. J. (1964). - Ice crystal development in a seeded cumulus cloud. Meteorology Research, Inc. Submitted to J. of Atmos. Sc.

(5) Langmuir, I. (1951). - Results of seeding of cumulus clouds in New Mexico. Occasional Report No. 24, Project Cirrus, General Electric Res. Lab., Final Report, RL-566, Contract No. W-36-039-sc-38141.

(6) Kraus, E.B., and Squires, P. (1947). - Experiments on the stimulation of clouds to produce rains. Nature, London, 159, 489.

APPENDIX D

ICE CRYSTAL DEVELOPMENT IN A SEEDED CUMULUS CLOUD

By

Clement J. Todd

Atmospheric Research Group
and
Meteorology Research, Inc.
Altadena, California

Submitted to Journal of Atmospheric Sciences

November 18, 1963

ARG63 Pa-103

ABSTRACT

A cumulus cloud was seeded by the aircraft flying 1780 meters below cloud base. The observation plane spiraled up through the cloud base and made replicas of the cloud particles as well as recording pressure altitude, temperature, mixing ratio, liquid water and other factors. In the updraft below cloud base the temperature followed the dry adiabatic potential temperature curve. In the cloud the temperature showed an increase above the pseudo-adiabatic wet-bulb potential temperature. This increase corresponded to the development of ice crystals and was in the amount expected from the release of heat during freezing. The ice crystals were found slightly above cloud base, -9.5C. The concentration increased in a manner which was consistent with the calibrated temperature activation curve of the AgI generator and the diffusion in the column of air above the seeding aircraft. The crystals were primarily unrimed hexagonal plates. The secondary axis growth fits the relationship $2a = K_a t^{3/4}$ where $K_a = f(T)$ which increased five-fold between -9.5C and -13C , and a is the semisecondary axis, T is temperature, and t is time in minutes.

1. Introduction

It is the purpose of this paper to explore existing theory in an attempt to explain ice crystal size, type, and concentration observations made during one cloud-seeding experiment.

Meteorology Research, Inc., and its affiliate, Atmospheric Research Group, of Altadena, California, have been engaged in a program of observing the development of both seeded and unseeded cumulus clouds during the summer at Flagstaff, Arizona. One sequence of observations particularly amenable to some aspects of intensive theoretical analysis was obtained on 15 August 1962. From this cloud a good and clear-cut record of ice crystal development in a seeded cumulus cloud was obtained.

The cloud was over the desert 32 kilometers east of Flagstaff. Unfortunately it was not observed on radar or by time-lapse photography, but it was reported by the aerial observer to be in an early stage of vigorous development. The cloud base was 5,700 km (all altitudes given are pressure altitudes) with temperature -9.5C. It was seeded with AgI from two calibrated airborne Skyfire generators (Fuquay and Wells, 1960) flown one under each wind of a Cessna 180, hereafter referred to as Metro IV. The seeding flight pattern was a circle roughly 1000 m in diameter, flown for 10 minutes in the subcloud updraft at 4000 m. The cloud was observed by the MRI-ARG Cessna 180 cloud physics plane, Metro I. This plane spiraled from 3,300 to 6,800 m in the cloud updraft. During the course of this flight Metro 1 obtained a continuous replica of the cloud particles. These included a large number of specimens of ice crystals due to the seeding. Other meteorological variables were also recorded which, when put together with a summary of the cloud particle replicas, made a revealing meteorological picture of the internal structure of this seeded cumulus cloud.

2. Instrumentation

A light plane was used as the cloud observation instrument platform because it has a short turning radius for cloud spirals, a rapid response to cloud updrafts, operational simplicity, easy maintenance, high reliability, and low operating costs. The light plane is, however, limited in payload and electrical power output. Hence the instrument system had to be designed to fit these constraints. As Metro 1 carried a pilot and one observer, the observational instruments had to be automated to the point that they all could be controlled by one person. The record of some eight variables was taken on a two-channel recorder with four variables sharing each channel. A detailed description of the instrumentation is given by MacCready, Smith, Todd, Chien, and Woodward (1963).

The MRI continuous cloud particle sampler (Todd, 1961, MacCready, 1962a and MacCready and Williamson, 1963) replicates the cloud particles in Formvar on 16 mm clear motion picture leader. The film, freshly coated with a Formvar solution, passes up a tube behind a 2 mm slit through which it is exposed to the airstream. Particles including cloud droplets hit the plastic coating and are captured as the plastic flows over them. The solvent evaporates from the plastic very rapidly leaving a hard, permanent replica. The replicas produce variations in the thickness of the clear plastic which cause a refraction of light that produces shadow images when projected in a 16 mm time-motion projector. These images can be viewed at 100 to 1000-fold magnification, and cloud droplets, ice crystals, graupel, snowflakes, and dust particles are visible with high resolution.

Mixing ratio is measured directly with the MRI Model 901 Mixing Ratio Indicator (MacCready and Lake, 1963). Air is drawn at 5 $cm^3 min^{-1}$ through an electrolyzing tube which is internally coated with phosphorous pentoxide. Current flows between two wires in the tube, which is exactly proportional to the rate of water vapor entering the tube. The mass rate of flow is kept constant with a thermistor flow meter controlling the pump. The time constant is in the order of one second.

Temperature is sensed with a 0.08-second time constant thermistor set in an axial flow vortex housing to provide speed compensation for dynamic heating and to protect the thermistor somewhat from cloud moisture.

The altitude is measured by a standard high-grade sensitive altimeter on which there is a photoelectric follower coupling the 1000-foot hand to a potentiometer. This supplies voltage to the recorder.

Liquid water is measured by a Johnson-Williams hot-wire sensor. One heated wire is transverse to the airflow; the other is parallel to the airflow. These wires are in a bridge circuit with zero output in cloud-free air. In-cloud, the droplets impinge on the transverse wire and are evaporated, cooling the wire. At the airspeed for which it is calibrated the instrument output is linearly proportional to the liquid water content provided the droplets are less than 50 μ in diameter. Evaporation of the larger droplets is incomplete. Low readings which have been observed in completely iced clouds imply that ice crystals bounce off the wire and are not measured.

3. Observations

On 15 August the wind was exceptionally light to 10 km. The early part of the day was characterized by large cumulus clouds building directly over the San Francisco Peaks. In the afternoon, in the flight sequence to be discussed, cumulus were developing over the desert. (The mountain range was no longer a source of suitable clouds for experimentation at that time because the cloud system was too fully developed.)

The cloud chosen for this seeding experiment was growing vigorously and was in an early stage of development. Its exterior had a firm bulging appearance and the base was flat and dark. The seeding plane (Metro IV) flew a circular flight path at 4,000 m in the updraft from 1546 to 1556 MST. Metro I (the MRI Cessna 180 cloud physics plane) entered the updraft at 1546 from the 3,300 m level and ascended at 300 m per minute in a tight spiral turn. The power setting was adjusted so the plane would not climb with respect to rising air. At 5,700 m Metro I entered the cloud base and continued to spiral upward to 6,900 m. The ascent rate decreased with elevation. Above 6,700 m Metro I was unable to stay in the updraft except for brief periods. From 6,900 m Metro I spiraled down outside the cloud.

Of interest is the thermal structure of the cloud and its environment along this flight path. Fig. 1 is a time-height plot of the flight, while Fig. 2 includes further details of the portions above cloud base. In the figures the scales of temperature, mixing ratio, and liquid water content are adjusted to give special meaning as the curves of these variables are compared to the height plot.

As shown in Fig. 1, before Metro I entered the updraft below the cloud, it flew for several minutes until 1543 MST at 3,000 to 3,400 m in air that had a potential temperature θ of 1.5C colder than the θ for the cloud base. The mixing ratio of this air was about 6 gr per kg. The mixing ratio of the cloud base was 3.8 gr per kg. This lower air must have been cooled and moistened by precipitation. Two minutes before entering the updraft, 1543 - 1545 MST, the air had a θ of 0.5C less than at the cloud base. The θ of the updraft from 3,500 m to 5,700 m (cloud base) was within $\pm$ 0.3C of cloud base except at elevation 5,300 m at 5,500 m. At these levels Metro I strayed toward the edge of the updraft and θ dropped to 0.5C less the cloud base. Above cloud base the observed pseudo wet-bulb potential temperature θ_{sw} followed the θ_{sw} of cloud base with only minor departures to 6,200 m. Above this level to 6,900 m (where Metro I left the cloud) θ_{sw} became progressively warmer than cloud base with a maximum excess of 1C. It is interesting to note that this excess of θ_{sw} coincides with the growth of ice particles and a decrease in number of water droplets. When Metro I left the cloud, the θ_{sw} fell sharply to 2.8C below the cloud base value. This difference dropped to 2.0C and then to 1.4C as Metro I descended from 6,900 m to the cloud base at 5,700 m.

The liquid water reading had some noise problems, but it confirmed in a rough way that major portions of the in-cloud flight were made in an undiluted cloud. When ice crystals appear significantly in the cloud particle concentration, it is noted (Fig. 2) that the liquid water meter records less than adiabatic liquid water.

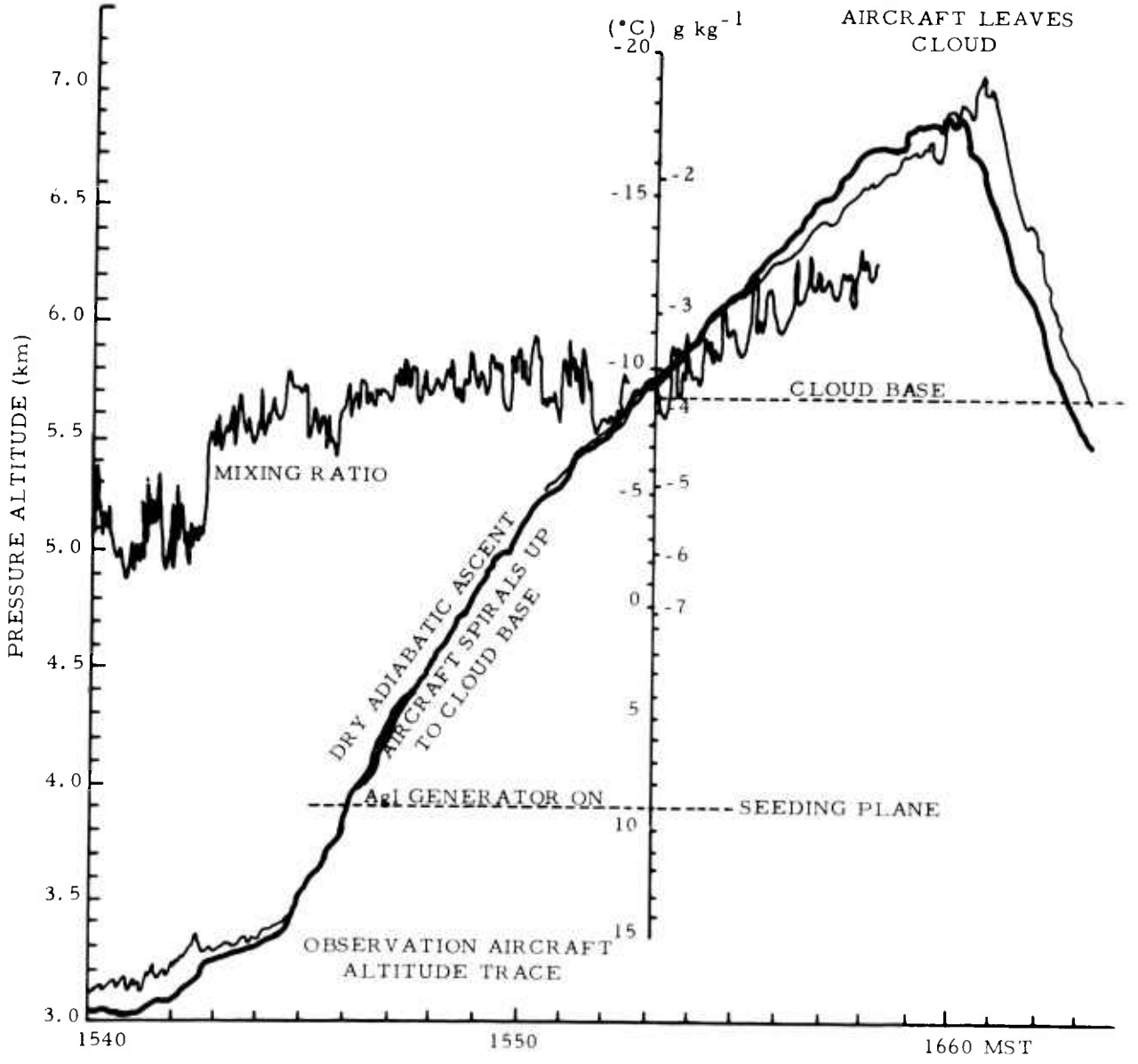

Fig. 1. A TIME-HEIGHT FLIGHT PLOT OF PRESSURE ALTITUDE, TEMPERATURE, AND MIXING RATIO.

The temperature scale is such that the pressure altitude curve corresponds to the potential temperature θ below cloud base and θ_{sw}, the pseudo wet bulb potential temperature, above the cloud base. A comparison of the difference between the temperature and altitude curve shows the departure of flight path potential temperature with that at cloud base. The mixing ratio curve scale is such that mixing ratio curves can also show the height of the condensation level of air taken from the flight path.

Micrographs of the drop samples at positions a-f shown on Fig. 2 are reproduced on Fig. 3. The evolution of droplet size and the growth of ice crystal size and concentration can be seen. The cloud droplet concentration was 500 per cm^3 in what was apparently an unmixed portion of the cloud. The diameter of the droplets increased rapidly immediately above cloud base and then increased more slowly as the diameters became larger. In some places the growth of the ice crystals at the expense of water droplets can be clearly seen as the water droplet size decreases and finally disappears completely. The droplet replica sizes shown in Fig. 3 are somewhat larger than the true droplet diameters due to deformation in replication.

4. Analysis

The long-term objective is to learn how to optimize cloud modification techniques for obtaining chosen goals. It is important to take advantage of all opportunities to learn at what levels seeded ice crystals form, in what concentration they occur, and how fast they grow. During this study it was possible to gain some information on all of these questions.

The first step was to establish the initial dilution of the AgI smoke in the aircraft wake, and then from this, to determine the concentration of nuclei active in ice crystal formation at any temperature T. The following step was to estimate the diffusion of the aircraft wake as it drifted to the sampling altitude, and finally, the third step was to analyze the growth rate of the seeded ice crystals in the supercooled water cloud.

AgI Output. Smoke from the two AgI burners, mounted one under each wing of the seeding aircraft, mixes immediately throughout the turbulent wake. The initial wake of a Cessna 180 is observed to be 25 m in diameter (Smith and MacCready, 1963). Speed of the aircraft is about 50 m^{-1} so the volume of the wake per second is

$$V_0 = 2.5 \times 10^{10} \text{ cm}^3 \text{ sec}^{-1} .$$

Fuquay and Wells (1960) have calibrated the output of the Skyfire AgI generator. Figure 4 shows N(T), the output of active nuclei per second, as a function of temperature. Let n be the concentration of active nuclei per cm^3. Thus, $n = N(T)/V_t$ where V_t is the expanding volume per second of flight path through which the nuclei are distributed. Right behind the aircraft

$$n = \frac{N(T)}{V_0} = \frac{N(T)}{2.5 \cdot 10^{10}} \quad \text{nuclei/cm}^3 . \qquad (1)$$

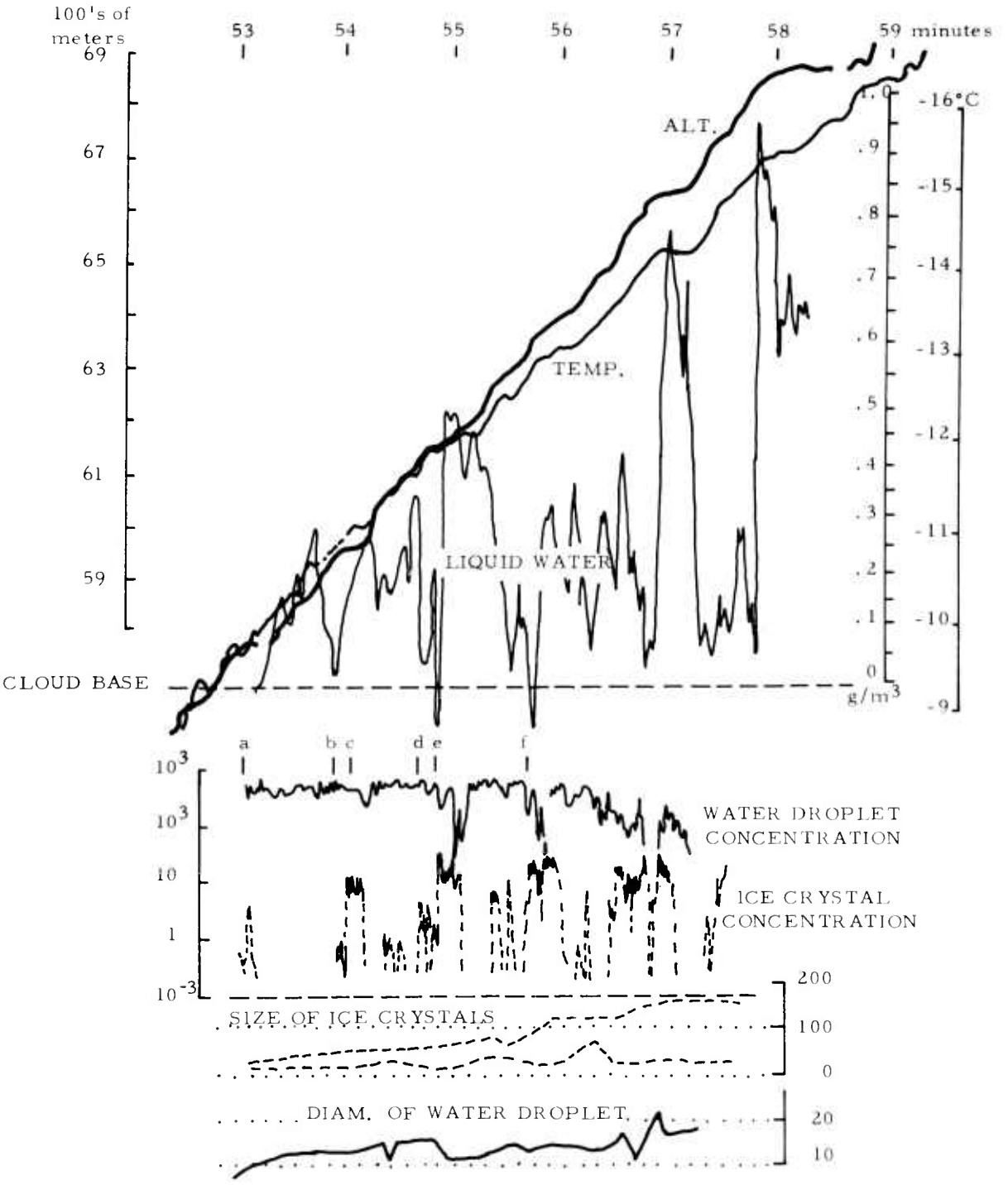

Fig. 2. A DETAILED TIME-HEIGHT RECORD OF THE IN-CLOUD PORTION OF THE FLIGHT IN FIG. 1.

The pressure altitude and temperature scales are the same as in the previous figure. The liquid water curve would coincide with the pressure altitude curve if the parcel ascends adiabatically from cloud base. The concentration and median size of the cloud water droplets and the concentration and range in size of ice crystals are plotted along the same time scale as other flight parameters.

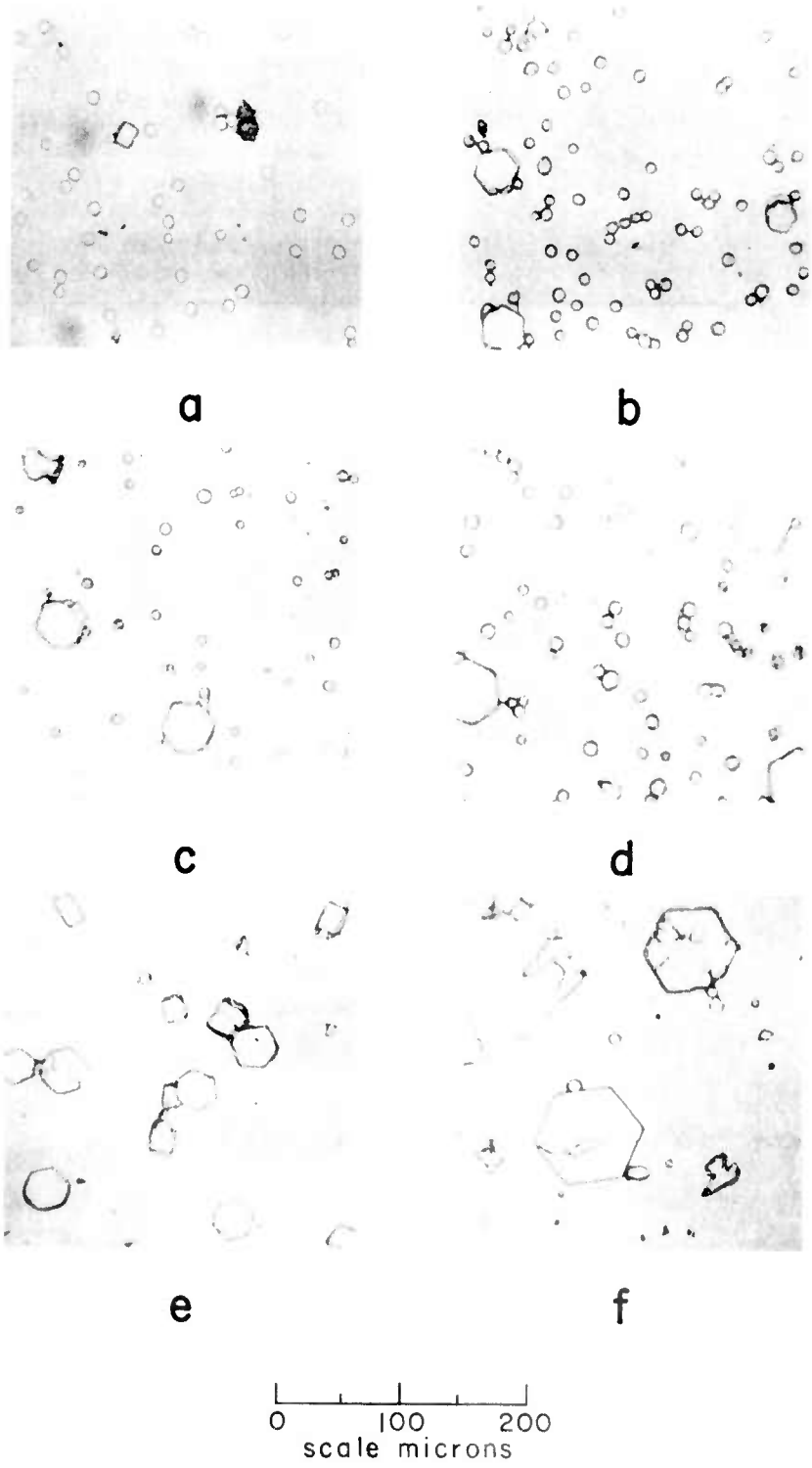

Fig. 3 DEVELOPMENTAL STAGE OF ICE CRYSTALS AT SIX PARTICULAR TIMES INDICATED BY LETTERS a - f ALONG THE WATER DROPLET - ICE CRYSTAL CONCENTRATION CURVES IN FIG. 2.

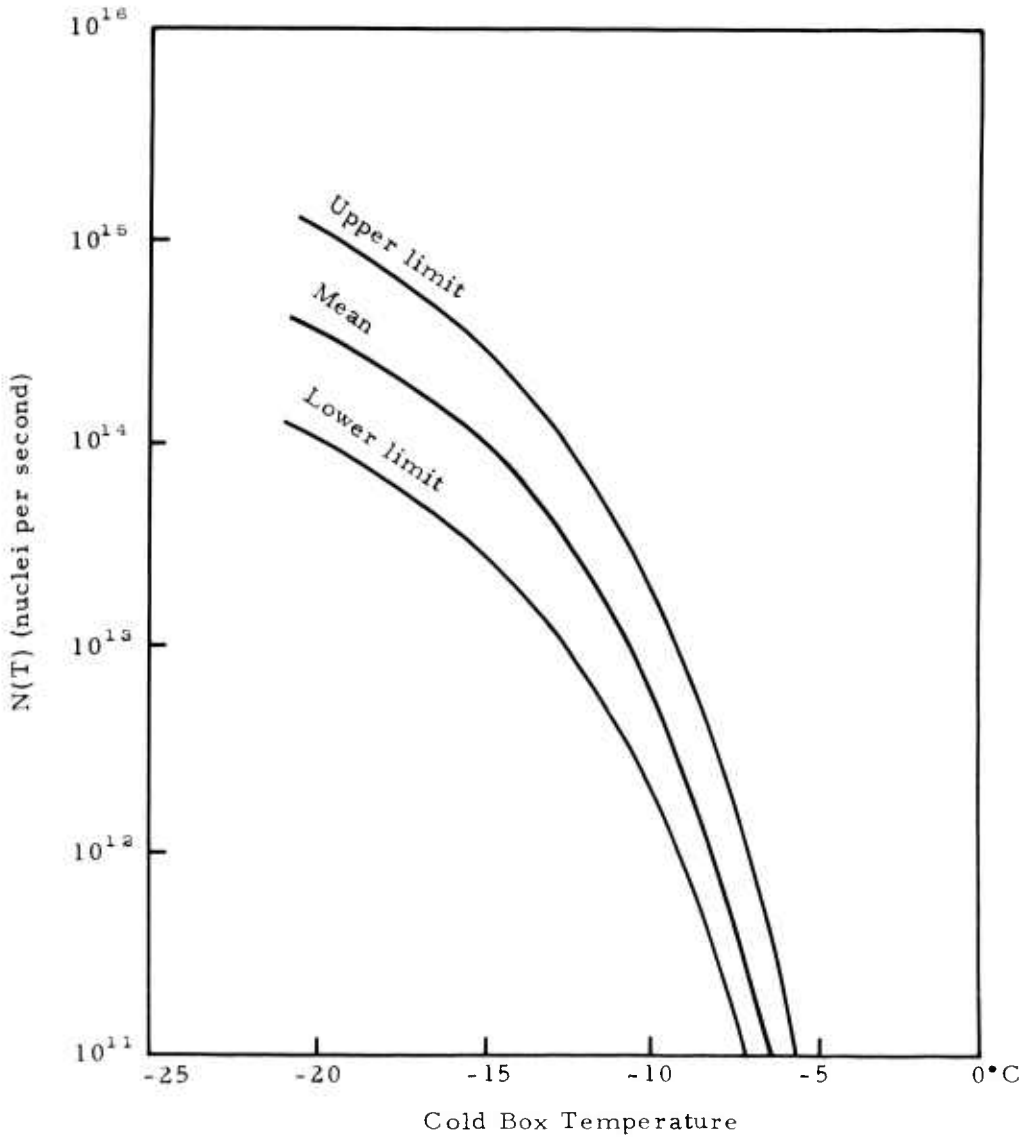

Fig. 4. CALIBRATION OF THE SKYFIRE AgI GENERATOR ADAPTED FROM FUQUAY AND WELLS (1960).

Diffusion of AgI Smoke. An estimate of the diffusion of the wake from the seeding airplane can be easily obtained if it is assumed that eddies, which are dominant in the diffusion process, are of a size within the inertial subrange. This is not strictly a correct assumption (a) because an aircraft wake is long in the longitudinal direction and so some large eddies should be considered, and (b) when the plume breadth grows to a size comparable to the cloud dimension, the inertial subrange is considerably exceeded. However, the inertial subrange concept affords simple computations which should be of the right order of magnitude in the present case. The turbulence during the spiral was rather light and of a fairly constant value. A dissipation rate ϵ of about 1 $cm^2 sec^{-3}$ was estimated from a turbulence meter and is a value comparable to other measurements in convection (MacCready, 1962b). The turbulence was much stronger outside the updraft and at the cloud edges.

Batchelor (1950) has pointed out that the spreading of a cloud puff in the inertial subrange should follow the law

$$\overline{Y^2} = C_4 \epsilon t^3 \qquad (2)$$

where Y is a representative dimension of the cloud (which here we can take as diameter of the wake), C_4 is a dimensionless constant of order unity, and t is time. This equation is of use only after sufficient time has elapsed so that the diffusion is not dependent on the initial distribution of the material (therefore at times considerably longer than $t_1 = (\overline{Y_0^2}/C_4 \epsilon)^{1/2}$, where Y_0 is the initial particle cloud dimension). In the present case, t_1 is small compared to t when the cloud is reached. There are questions as to the exact time origin for t in equation (2), for certainly growth will be somewhat greater if Y_0 is larger. The value of C_4 is not known and will vary considerably whether Y refers to a diameter, radius, or standard deviation. Because of all such indeterminancies the prediction of equation (2) should only be used as qualitative hints rather than quantitative calculations. For the following calculations an arbitrary 25 m, the initial wake diameter, is added to Y to preserve consistency near t = 0 and to allow for some effect of initial size in subsequent growth.

t minutes	Y meters (including 25 m added factor)
6	93
8	130
10	172
12	218

Figure 5 shows a scaled schematic of the diffusion of the wake carrying AgI. This is based on a flight path of one 1000-m diameter turn per minute at 50 m sec^{-1} airspeed in an observed updraft of 5 m sec^{-1} in the lower levels which slows down to 3 m sec^{-1} high in the cloud. The actual plume is, of course, considerably more ragged than the idealized one. There would also be kinks due to irregularities in the large scale cloud motions. The complications of the spreading and mixing at the cloud top are not shown. By comparing the ice crystal concentration regions shown in Fig. 2 with the diffusion patterns in Fig. 5, it can be seen that there is some qualitative correspondence. Low in the cloud the diffused wake is a relatively small part of the cloud, and ice crystals are found in only a small part of the total sample. Higher in the cloud the diffused AgI wake from one spiral begins to meet the adjacent wake's spiral. Within this spiral there are only brief regions without ice crystals.

Table 1. Computed and observed ice crystal concentrations.

a	b	c	d	e	f	g	h
t min	T °C	N(T) nuclei sec^{-1}	n nuclei cm^{-3} at t = 0	$\bar{Y}$ meters	$\frac{V_t}{V_o}$	Computed n at time(t) nuclei cm^{-3}	Obs. ice crystals, cm^{-3}
7.5	-9.5	4×10^{12}	160	120	23	7	8
8.4	-10.7	10×10^{12}	400	138	30	13	20
9.3	-11.5	17×10^{12}	700	157	39	17	50
10.2	-12.5	30×10^{12}	1200	176	49	24	50
11.1	-13.5	50×10^{12}	2000	197	62	32	20

Table 1 is an attempt to see if the generator calibration curve and the assumed diffusion in the inertial subrange can explain the observed concentrations of ice crystals. It can be seen that the computed and observed number of ice crystals, columns g and h, are in fair agreement (column h refers to a smoothed maximum value). This general agreement, however, cannot be construed as a verification of either the generator calibration or the application of the diffusion theory as there is too much freedom of application in dealing with limited data.

Ice Crystals. A great amount of information is available in the cloud particle record which is summarized in Fig. 2. In addition to the regular flight information, the concentration, as well as particle sizes of water droplets and ice crystals, are shown on the same time scale. It is interesting to note from the concentration graph that there are cloud regions without ice crystals at least as high as 6,400 m (-13C). These regions contain virtually the same water droplet concentration as was found at cloud base, 500 cm^{-3}, with diameters of about 17 microns. This would account for all the water that

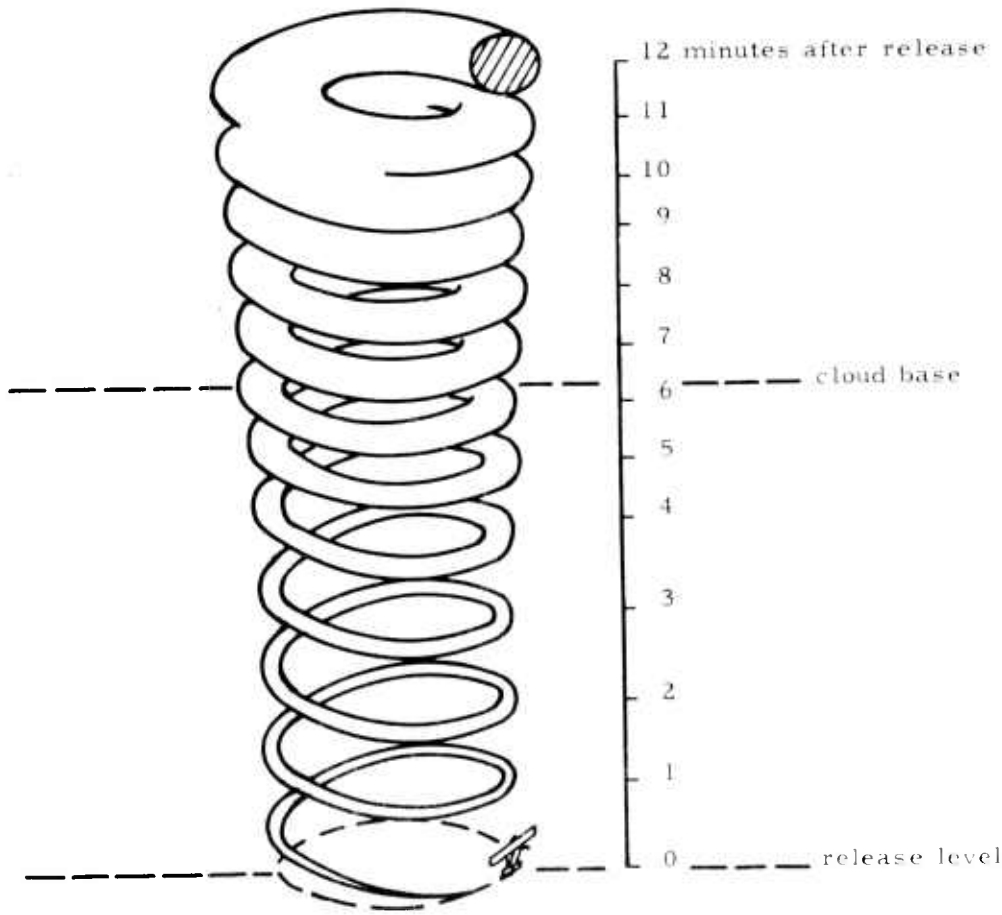

Fig. 5. AN IDEALIZED SCALE DRAWING OF THE RISING AND EXPANDING HELICAL PLUME FROM THE SEEDING PLANE.

The plume is shown to expand as it would appear if it were being diffused by the inertial subrange-sized eddies.

should be found in an undiluted parcel lifted adiabatically from cloud base. So with one cloud there are unseeded control regions as well as seeded regions for comparison of microphysical features.

The replicas show that most of the ice crystals are hexagonal plates, as indeed they should be at temperatures from -9.5C to -13C (Kobayashi, 1958, Hallett and Mason, 1958, Shaw and Mason, 1955, Weickmann, 1957). A surprising feature of the replicas is that there appears to be virtually no evidence of riming.

There is ample opportunity to find crystals growing in a water cloud, though at higher altitudes there are regions where the water cloud has been exhausted by the high concentration of ice crystals. The growth rates of ice crystals in the supercooled water cloud are of particular interest. Each cloud parcel contains ice crystals which are nucleated over a range of temperatures, and hence times. Thus, as the parcel rises and cools in ascent, more and more crystals are nucleated. Here it is then assumed that if the random variations in rate of crystal growth are ignored and if the air is an unmixed parcel so that all elements have the same history, the larger the ice crystal the earlier its nucleation.

Each size category of a given sampling will have a unique starting temperature. Fig. 6 is a graph of sizes of the secondary axis of ice plates plotted against time of sampling. Since this ascent is continuous, there is a unique time-temperature relationship also plotted. The ice crystal concentration at each sampling point is ordered for size and the order is divided according to the proportion assumed to start at a particular prior temperature. The concentration activated at -9.5C was chosen as a base point and from this reference, points occur where concentration doubles, triples, quadruples, etc.

When the sampling points at which the water cloud dissipates are deleted and smoothed curves are drawn for the remaining point, there are a family of curves (Fig. 7). These curves show the growth rate of the secondary axis of an ice crystal as a function of crystal size and temperature in a supercooled water cloud.

In an attempt to separate out the temperature-size factors in crystal growth from Fig. 7, it is noted that Shaw and Mason (1955) were able to describe the growth of the faces by the equations

$$(2c)^2 = U_c t + \alpha$$

or

$$(2a)^2 = U_a t + \beta$$

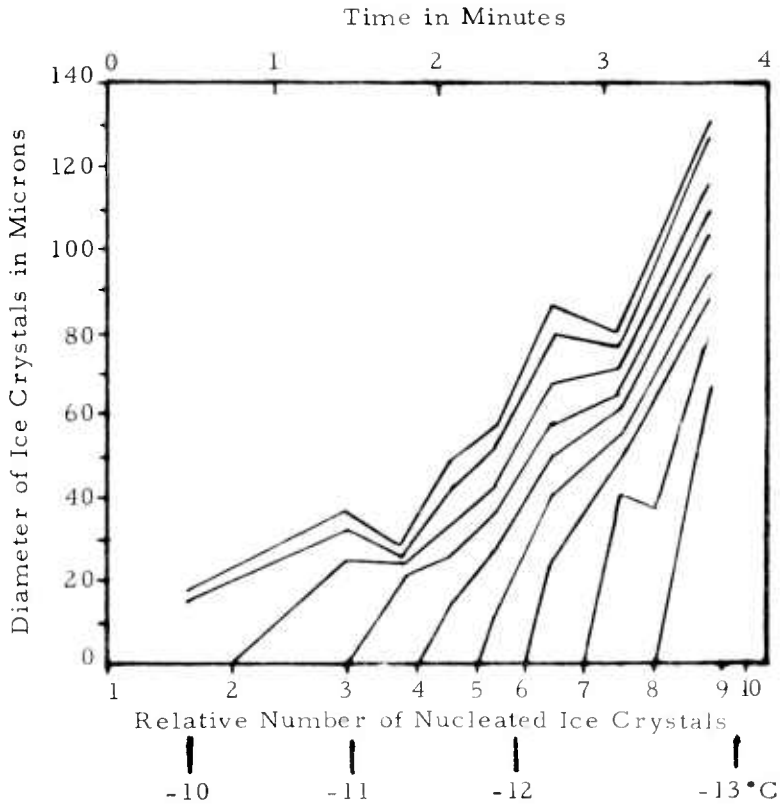

Fig. 6. AN ICE CRYSTAL GROWTH PLOT FOR HEXAGONAL FACE.

Each curve represents growth from a successively colder nucleating temperature as per the activation curve in Fig. 4. The time scale is linear and the temperature correspondence to time is taken from the flight plot in Fig. 2.

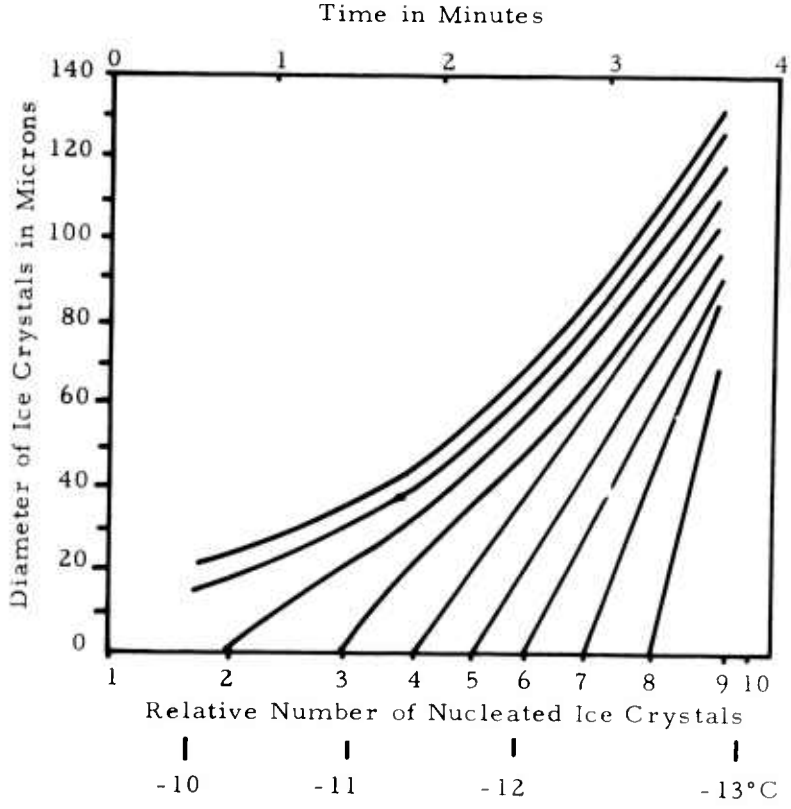

Fig. 7. AN ICE CRYSTAL GROWTH PLOT FOR HEXAGONAL FACE.
Based on the same data as Fig. 6 but the curves are smoothed.

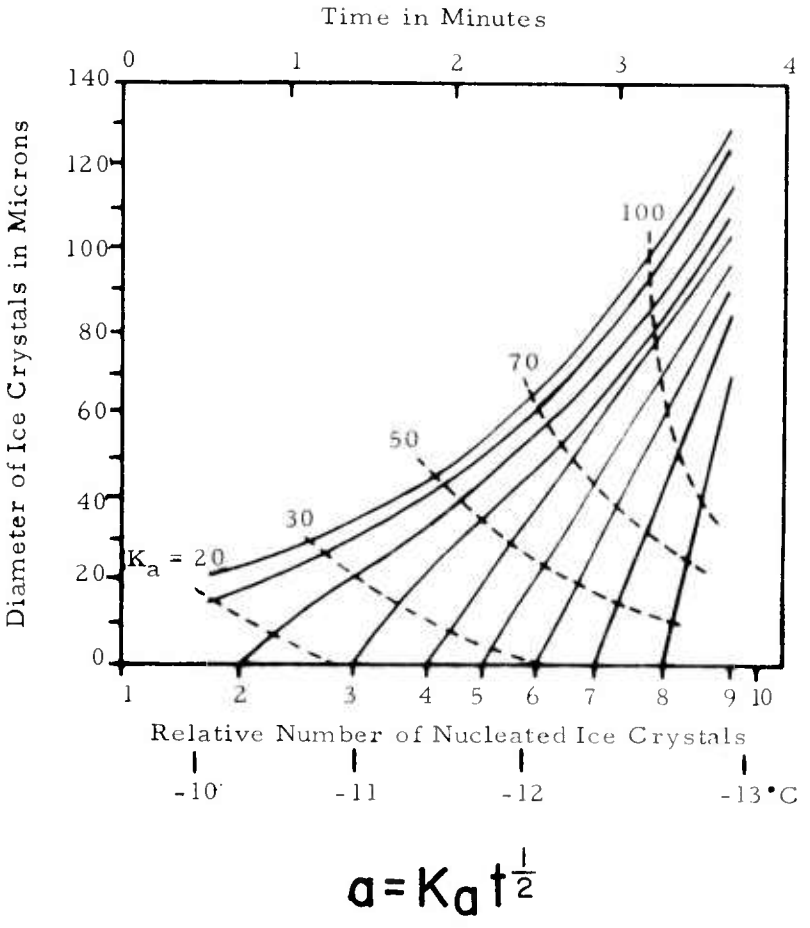

Fig. 8. AN ICE CRYSTAL GROWTH PLOT FOR HEXAGONAL FACE.

The same smoothed growth curves as in Fig. 7 with values of K_a plotted to fit $2a = K_a t^{1/2}$. K_a is not a function of temperature alone.

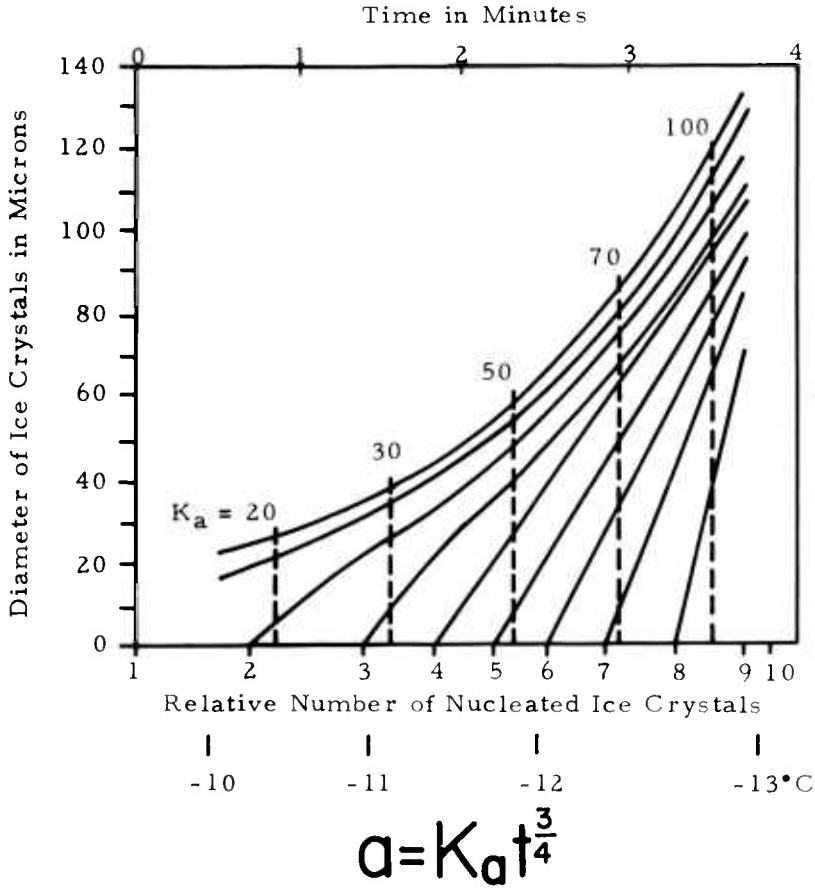

Fig. 9. AN ICE CRYSTAL GROWTH PLOT FOR HEXAGONAL FACE.

The same smoothed growth curve as Fig. 7 but with values of K_a plotted to fit $2a = K_a t^{3/4}$. K_a is a function of just temperature.

where c and a are respectively the semiprincipal and semisecondary crystal axes, U_c , U_a , α , and β are constants. In our observations only the 2a secondary crystal axis of the hexagonal face is observed. The crystal nucleation time is chosen as t_o so that $\beta = 0$. The above equations were rewritten in the form $2a = K_a t^{1/2}$ and a family of curves for a range of K_a from $10_\mu \text{ min}^{-1/2}$ to $150_\mu \text{ min}^{-1/2}$ were drawn with the same linear 2a and t scale as used in Fig. 7. Fig. 7 was placed over the $2a = K_a t^{1/2}$ chart and the K_a values of the tangent points for the curves are recorded in Fig. 8. The K_a values were not constant with temperature (Fig. 8) so there must have been a size or an altitude factor affecting the growth rate if the $t^{1/2}$ law is valid.

A further examination of the literature shows that the growth rates of ice crystal faces may fit other powers of t . Nakaya (1954) finds that the dendritic arms grow as a linear function of time. A log log plot of tabular and graphic information found in Reynolds (1952), Isono (1959), Mason (1953), and Shaw and Mason (1955) indicates that ice crystal axis growth fits rather discretely one of the following $2a = K_a t^{3/4}$, $2a = K_a t^{1/2}$, or $2a = K_a t^{1/4}$. The exponent of t seems to vary as a function of temperature and supersaturation of the environment with respect to ice. On the basis of these findings it was decided to try to fit $2a = K_a t^{3/4}$ to the ice crystal growth of this flight. To do this the parameter K_a (Fig. 9) was plotted along the smoothed growth curves of Fig. 7. Here K_a is a function of temperature, with no systematic residual variation, but K_a increases by a factor of 5 from T = 9.5 to T = 13 .

The power law suggests itself as a useful technique for the description of the growth rate of ice crystals by axis. This could serve as a quantitative technique for making computations of ice crystal growth until the crystallography is better understood and more precise techniques are available. A quantitative technique for computing ice crystal growth would be a valuable link in figuring the conversion rate of a cloud from water to ice, or in estimating the sweep area of ice crystals in precipitation calculations.

5. Conclusions

A study has been made of the flight record taken in one seeded cumulus cloud. It is found that in a real cloud chosen for its simplicity, many of the things predicted in theory do actually occur and can be measured and analyzed although some shortcomings of the theory are clearly evident as well.

Findings of this study are as follows:

a) For this cloud the environment was colder than the cloud updraft both below cloud base and in the air outside the cloud.

b) The potential temperature θ of the cloud updraft below cloud base was almost constant for 1780 m up to cloud base.

c) The pseudo wet-bulb potential temperature θ_{sw} followed the rate expected from unmixed cloud ascent in the strong updrafts above cloud base until ice crystals started to represent a significant volume of the cloud. The θ_{sw} then showed an increase in temperature that is in agreement with the increase expected from the latent heat of freezing.

d) When the expected ice crystal content was computed from laboratory calibrated generator temperature nuclei activation curves and the dispersion was calculated from measured turbulence, there was considerable agreement.

e) Ice crystals were found to be predominantly hexagonal plates and occurred between -9.5C and -13C, as predicted in the literature.

f) When an attempt was made to compare the observed ice crystal growth rates taken from the literature, it was found that present theory is apparently inadequate.

g) It is suggested that the secondary axis of snowflake growth follows $2a = Kt^{3/4}$ $K = f(T)$ which increases five-fold through the temperature range -9.5C to -13C.

Acknowledgments. This work represents the contributions of a major portion of the joint staff of Meteorology Research, Inc., and Atmospheric Research Group in connection with a continuing program of cumulus studies at Flagstaff. Sponsorship of the work came both from the Atmospheric Sciences Section, National Science Foundation, under Grant NSF G11969 to ARG, and from the U.S. Army Electronic Research and Development Laboratory, Contract No. DA 36-039 SC-89066 to MRI. In this particular sequence of tests the U. S. Forest Service cooperated by contributing personnel and airborne seeding generators. Special credit goes to Dr. Paul B. MacCready, Jr., Project Director and developer of many of the instruments and the flight observational system, Dr. C.W. Chien, who worked closely with the author on the ice crystal analysis, and Mr. Dale Smith, who reduced the flight records.

References

Batchelor, G. K., 1950: The application of the similarity theory of turbulence to atmospheric diffusion. Quart. J. Roy. Met. Soc., 76, 328, 133-146.

Fuquay, D. M., and H. J. Wells, 1960: Generator technology for cloud seeding. Irrigation and Drainage Div., Proc. of American Soc. Civil Engineers, 86, 79-91.

Hallett, J., and B. J. Mason, 1958: The influence of temperature and supersaturation on the habit of ice crystals grown from vapor. Proc. Roy. Soc. A., 247, 440-453.

Isono, K., 1959: Microphysical processes in precipitation mechanism, Japanese J. of Geophysics, 2, 49-52.

Kobayashi, T., 1958: On the habit of snow crystals artificially produced at low pressures. J. Meteor. Soc. Japan, 36, 193.

MacCready, Paul B., Jr., 1962a: The continuous particle sampler at the Puy de Dome Comparison Conference. Bull. de l'Obs. du Puy de Dome, 1, 19-30.

_____, 1962b: The inertial subrange of atmospheric turbulence. J. Geophys. Res., 67, 3, 1051-1059.

_____, and J. Lake, 1963: The mixing ratio indicator. Paper presented at the 1963 International Symposium on Humidity and Moisture, Washington, D.C., May 22. Proc. to be published.

_____, and Robin E. Williamson, 1963: Continuous particle sampler study program. Meteorology Research, Inc., Final Report, Contract Nonr-3819(00)(X), Department of the Navy, ONR, Naval Research Laboratory, Washington, D.C.

_____, T. B. Smith, C. J. Todd, C. W. Chien, and B. Woodward, 1963: Study and modification of convective storms. Meteorology Research, Inc., Report No. 2, Contract DA 36-039 SC-89066, U.S. Army Electronic Research and Development Laboratory, Fort Monmouth, New Jersey. ASTIA AD 415347.

Mason, B. J., 1953: The growth of ice crystals in a supercooled water cloud. Quart. J. Roy. Meteor. Soc., 79, 104-111.

Nakaya, U., 1954: Snow crystals, natural and artificial. Harvard Univ. Press, Cambridge, 510 pp.

Reynolds, S. E., 1952: Ice-crystal growth. J. Meteor., 9, 36-40.

Shaw, D., and B. J. Mason, 1955: The growth of ice crystals from the vapor. Phil. Mag., 46, 249-262.

Smith, T. B., and P. B. MacCready, Jr., 1963: Aircraft wakes and enhancement. Meteorology Research, Inc., Part B, Final Report to U.S. Army Dugway Proving Ground, Contract DA-42-007-CML-545.

Todd, Clement J., 1961: A study of cloud composition. Proc. of Ninth Weather Radar Conf., Kansas City, Oct., 280-285.

Weickmann, H., 1957: Artificial stimulation of rain. Pergamon Press, New York, 315-326.

APPENDIX E

A SYSTEM FOR COMPUTING ICE PHASE HYDROMETEOR DEVELOPMENT

by

Clement J. Todd

Atmospheric Research Group
and
Meteorology Research, Inc.
Altadena, California

January 1964

ARG64 Pa-121

ABSTRACT

This is an organization of information prepared for making graphical computations of ice phase cloud modifications. It allows the user to follow through the development of a hydrometeor from (1) the temperature-effectiveness output curves of the nucleating agent to (2) the rate of growth of the ice crystals as a temperature function to (3) the onset of riming as a function of crystal size, fall velocity, and cloud droplet size to (4) the rate of graupel growth as a function of size, shape, density, fall velocity, and cloud droplet concentration, to (5) the development of hailstones as a function of size, density, shape, surface temperature, fall velocity, liquid content of the cloud. The graphical system also gives solutions to the various dependent parameters necessary in the computation, such as: fall velocity, density, shape, and surface temperatures of hailstones. With this computational system it should be possible to solve a wide variety of ice phase cloud modification problems having to do with (a) clearing supercooled fog, (b) opening holes in supercooled stratus, (c) initiating ice phase precipitation, (d) turning a cloud to ice to eliminate aircraft icing, freezing rain, and hail, (e) increasing cloud vertical development by liberating the latent heat of freezing, and (f) increasing the inflow at cloud base by lessening the pressure below the cloud through increases in cloud buoyance brought about by conversion to ice phase.

During this study several gaps in the basic experimental data became apparent. For this work it was necessary to bridge the gaps by interpolation, but they need to be filled. The nature of the gaps and the importance of filling them is pointed out.

This paper stops with the development of the computational system and does not carry out cloud modification model computations.

1. Introduction

There have been a large number of experimental and operational cloud seedings since Langmuir and Schaefer conducted their successful cloud modifications of Project Cirrus. A characteristic of these seedings is that apparent successes are intermingled with a large number of failures. This is a strong indication that there are still important factors in the seeding processes which are not understood.

As yet there has been no really comprehensive organization of present information into a form that can be effectively applied to ice phase cloud modification. There are so many factors that interact in a complicated manner that a mere familiarity with the literature does not allow one to be able to judge the outcome of a seeding experiment in a satisfactory manner. There is a definite need to have all of the important factors organized into a system which shows the various interactions and which can be related directly to cloud experiments.

At this point the basic information hardly seems sophisticated or refined enough to justify using computers. The step appropriate at present is to organize the information found in the literature into a series of graphs which are compatible, reasonably comprehensive, and convenient to apply to cloud experiments. From this it is hoped that it will be possible to map out the potentials of ice phase cloud modification, as well as plan more meaningful field cloud modification experiments.

In the course of this study many specific gaps in present knowledge have become apparent. For the present it has been necessary to bridge these gaps by interpolation and extrapolation. For a lasting and sound foundation these gaps must be filled by experimentation and observation. The gaps are pointed out as they are met in the text, and are summarized in the discussion.

2. Background

The computation of the processes of ice phase cloud modification will be complicated. Much of the technique will have to develop with experience. This will show the relative importance of the various factors involved which will be: (1) the characteristics of the water phase cloud, (2) the cloud dynamics, (3) the natural and artificial ice nuclei, and (4) to some extent the cloud's electrical characteristics. The block diagram in Fig. 1 is an attempt to organize these factors in a manner which shows the various interactions. The blocks that are outlined in heavy black are the ones that are dealt with in this discussion. The items which are underlined are the ones specifically involved in the graphical computation system set up here.

There are important differences in the development of ice hydrometeors, depending upon whether the water cloud in which they form is colloidally stable or precipitating. If the cloud is colloidally stable then the sequence of development is from the nuclei forming an ice crystal, to the growth of the ice crystal, to onset of riming, to graupel development, and hailstone growth.

If the water cloud is precipitating, then the sequence is that nucleation starts ice crystals, which are caught by falling drops. Upon this capture the drop freezes, and because it is large enough, it splinters. These splinters start new ice crystals growing and the process is repeated (Mason and Maybank, 1960), (Browning and Mason, 1963). The effect that this has on clouds is discussed by Koenig (1963). The multiplication of the ice crystals due to splintering plays an important role in increasing the concentration of hydrometeors, and the ice phase develops quite differently from that of the colloidally stable supercooled water cloud.

This discussion will be concerned with ice hydrometeor development in clouds colloidally stable in their liquid phase, and will thus avoid the ice crystal multiplication problem, which brings up the question of discriminating between these two types of clouds. This means that it is necessary to understand the initiation of the all-liquid phase precipitation, which is dependent upon the cloud dynamics, as well as cloud characteristics such as cloud base temperature, depth of the cloud, size distribution and concentration of cloud droplets, and cloud electrical fields. A careful development of this field is needed, but for the present a rudimentary understanding of this will suffice to allow a preliminary exploration of ice phase modification. The rudimentary understanding about which this discussion is oriented is found in MacCready, et al. (1957). Here a precipitation initiation model developed by this writer relates the onset of the all-liquid phase precipitation to the cloud base temperature, rate of updraft, and cloud top

temperature. This model was developed assuming that the initial cloud droplet distribution was typically continental, and that there was no influence of an electrical nature. If the cloud has an oceanic droplet distribution, then this type of precipitation would start sooner. The model also assumes that parcels of air enter the cloud base and rise adiabatically without being diluted by the environment, until finally they are lost out of the cloud top. Crude and out-of-date as this model is, it serves to give a quantitative orientation as to the domain of the all-liquid precipitation, and when the subfreezing temperatures and ice nuclei are considered it indicates the region of splintering of freezing droplets. The ice phase cloud regions in which this splintering does not occur is the region of concern of this study. These are generally the clouds with colder cloud bases, lower liquid water contents, and higher cloud droplet concentrations. If conditions are marginal, then it is important that there be a minimum time for all-liquid coalescence to take place and updraft rate becomes important.

It seems likely that the electric fields play an important role in accretion, but as there is no way to give this quantitative expression yet, it is included in the block schematic but is not incorporated in the computations. The computations of the hydrometeor development are able to delineate several of the conditions that have been indicated to be associated with charge separation, such as the onset of riming and the condition in hailstone development where air bubbles are shed and clear ice develops, or wet growth takes place. A byproduct of this system may then be the determination of conditions

favorable for charge separations, but it is not yet able to take into account the effect of the electric field on hydrometeor development.

3. The Problem

In this report information has been collected and arranged into a convenient and compatible computational form for the following topics:

A. Ice crystal growth rates deduced from the literature

B. Seeding efficiencies of AgI, dry ice, and phloroglucinol as a function of temperature

C. Onset of ice crystal riming

D. Hydrometeor transformation from rimed crystals to graupel to hailstones

E. Energy of ice phase conversion and cloud dynamics.

This information is organized so that it will be useful in analyzing and studying:

1) The development of hydrometeors and the initiation of precipitation that would not have occurred naturally

2) The release of latent heat of the ice phase to stimulate cloud growth

3) The elimination of the supercooled water phase to eliminate aircraft icing, freezing rain, or hail development.

A. Ice crystal growth rates deduced from the literature. This investigation received considerable stimulus when J. Hallett of Imperial College, in private communication, stated that his research showed that ice crystal

growth was a far more complicated function of temperature than had been reported previously. It became apparent that this could well be one of the most important areas of misconception in the understanding of hydrometeor growth, so this study was launched with an intensive review of the literature. Crystal growth information from tables, scatter diagrams, and micrographs was studied and graphed. The lengths of the a and c axes of ice crystals were related to the time of growth (with $t = 0$ the time of nucleation). Then graphs were made of the log of the length of the axes against the log of time. Figures 2a and 2b show these plots for a , the hexagonal, and c , the prism, axes. This information was derived from Mason (1953, 1957), Reynolds (1952), Isono (1959), and Nakaya (1954).

These plots seemed to indicate that crystal growth could be fit to a formula:

$$a = K_a t^{\alpha} \quad \text{and} \quad c = K_c t^{\beta} \tag{1}$$

where α and β apparently fall discretely into 1/4, 1/2, 3/4, or 1. K_a and K_c are functions of temperature, and the environment is always saturated with respect to water.

If formula (1) can be accepted as characterizing crystal growth, then it is possible to use other data where the time of nucleation is in doubt. If the size of a crystal is known at several times but the time of nucleation is not known, then a linear plot of the a and c dimensions against a linear time scale can be compared with a linear plot of formula (1). This was done for ice crystal growth curves found in Shaw and Mason (1955) and for data

taken in a seeded cloud (Todd, 1964). Here the power law seemed to give reasonable fits and a consistent interpretation. The information was therefore added to Figs. 2a and 2b.

There have been several attempts to put forward a quantitative explanation of the changes of habit and rate of crystal growth. The most sophisticated is the work of Marshall and Langleben (1954). The explanations are based on the growth by diffusion formula of Maxwell, and predict that the growth of the linear dimensions will be proportional to $t^{1/2}$. It is apparent that the problem is more complicated than this. Possibly the line of approach being developed by Mason, Bryant, and Van den Heuvel (1963) will be fruitful, where the concern is with the migration distance of water molecules along the crystal surface before being captured at a dislocation, or escaping as vapor molecules. Following this line of reasoning in a qualitative manner an explanation of the power law for crystal axis growth is suggested.

The growth of an axis is proportional to $t^{1/4}$ when the face has a deficiency of dislocations that are active at the given temperature and supersaturation. This would mean that the face would grow as if a line dislocation were sweeping across it. Water molecules landing on the face close to the dislocation would have a high probability of being captured by it. Those landing further away from the dislocation than the length of the path for surface residence of free water molecules would escape (Mason, Bryant, and Van den Heuvel, 1963). Growth is proportional to $t^{1/2}$ when there are a large number of active dislocations so that water vapor molecules landing

anywhere on the face have a high probability of being captured at a dislocation. It is not apparent why these two cases seemed to be discrete or what sort of transition there is between them. The $t^{3/4}$ growth pattern holds when the growth is on a thin edge such as a thin plate. The growth rate becomes proportional to t^1 when points such as needles or dendrite arms are growing. For the most rapid growth it is supposed that the diffusion of vapor is augmented by a convection circulation to the points. This convection apparently could be driven by the vapor pressure gradient to the points (Nakaya, 1955, p 105, Weickmann, 1957, p 320, Schaefer, private communications).

From the slope of the crystal growth-rate curves found in Fig. 2a and 2b there was evidence to suggest that α and β of formula (1) would have to be a function of temperature that would fit Nakaya's (1955, pp 244 and 249) temperature-crystal growth habit chart. It was decided to let the boundaries of the regions on Nakaya's chart determine the temperature for the changes of value of α and β. With α and β functions of temperature, T, determined in a manner consistent with the literature and Nakaya's chart, it was then possible to try to resolve $K_a = f(T)$ and $K_c = g(T)$, for a large number of T values when t and T of the growth of a crystal in a micrograph are given. Some sixty of the crystal micrographs in Nakaya (1955, see Appendix I) were accompanied by suitable information to contribute toward the determination of $K_a = f(T)$ and $K_c = g(T)$. From this and all of the other information points from Figs. 2a and 2b it was possible to develop an estimate for f(T) and g(T) for the range -2.5C to -35C.

Figures 3a and 3b show the above derived estimates of K_a and α and also K_c and β as a function of temperature at water saturation. These curves, of course, are not a satisfactory substitute for carefully observed experimental data. In particular they are ill-defined in the regions of rapid change of growth habit and rate. The data from which the curves were constructed were taken from a number of different authors and were based on work spread over more than 20 years. A wide variety of experimental techniques were used, and there is no real agreement among the authors as to whether satisfactory control of vapor saturation with respect to water was maintained during the experiments.

One other point not yet mentioned is that growth habit seems to have some dependence on the crystal size. For instance, dendrite arms do not appear until the crystal is larger than 50 or 200 microns across.

Figures 4a and 4b show the growth along the a and c axes of ice crystals as a function of time, t, for various temperatures, T. a and c here refer to the dimensions of the crystal diameters along these respective axes. From the Fig. 4 growths it is possible to evaluate the cross section area perpendicular to the direction of fall $A = f(T, t)$ or the gross crystal volume $V = f(T, t)$.

For hexagonal crystals

$$V_{T,t} = \frac{\sqrt{3}}{2} a^2_{T,t} c_{T,t}$$

where $V_{T,t}$ is the gross volume of a crystal grown for t minutes from nucleation at temperature T. (The gross volume is given because it is not yet known how to make the correction to net volume which would take into

account the hollows in prisms, and the open structure in dendritic growth). Figure 5 is a plot of formula (2). This is then transformed to V and T coordinates with isochrones of t in Fig. 6. The fact that the isochrones change shape as t changes illustrates that some of the slow growing crystals have relatively fast starts.

For comparison the ice crystal growth curve received from Hallet (private communication) is shown superimposed on Fig. 6. The agreement is best in general features at t = 6 minutes. The disagreement in the location of maximums and minimums is not hard to understand because Hallett's experimental system is far superior to the deductive system used here for resolving detail.

B. Temperature dependence of the efficiency of AgI, dry ice, and phloroglucinol in ice phase cloud modification. It is of interest to look at the problem of converting a cloud to ice assuming that the crystals do not rime. To start with, a fog or stratus cloud is considered in which the liquid water content is 0.25 g m^{-3}, and it is assumed that 250 active ice nuclei per liter can be introduced into the cloud at any desired temperature. This means that by the time the ice crystals have grown to 1μg all of the cloud water will have been converted to ice. From Fig. 6 it can be seen that the time required for growth to 1μg is:

Table 1.

30	min at -2.5C
5.5	min at -5.0C
32	min at -7.0C
2	min at -15.0C
45	min at -25.0C

A more interesting problem is to find out how many grams of a seeding agent are required to convert fog to ice in a given length of time, but at different temperatures, still assuming no riming. The conditions of this exercise will be (1) a cloud of 1 km^3 with 0.25 g m^{-3} of cloud water, (2) a time limit of 10 minutes. Seeding by AgI smoke, dry ice, and phloroglucinol will be considered.

AgI smoke. Fletcher (1959) has presented a theory for the optimum performance of AgI smoke generators. His curve for this is presented in Fig. 7. It represents the envelope of curves of nucleation temperatures for smoke of uniform size. According to this theory all particles of the same size should nucleate at a given temperature. Presumably then, adjustment of a generator could make it favor either warmer or colder nucleation temperatures, but the curves would stay within the envelope. The calibration curve for the Skyfire generator is given in Fig. 7 as worked out by Fuquay and Wells (1957). It falls below the Fletcher curve as theory predicts, but it shows good efficiency for relative warm temperature nucleation. This curve will be used as indicative of the effectiveness of AgI.

Phloroglucinol. Phloroglucinol is one of several organic crystals discovered to be effective in nucleating ice crystals. It nucleates at temperatures as warm as -2C, and at -3C a 0.5μ particle is effective according to Langer and Rosinski (1962). This is most interesting in light of the ice crystal growth maximum in the -3C to -6C range. It means that phloroglucinol may have substantial advantages over AgI and dry ice as well. It may broaden greatly the range of clouds that can be subject to ice phase modification.

There is still much to learn about seeding with this agent. Experiments done thus far have not been able to test its full potential (Braham 1963). It is important to develop a technique which will put out optimum sizes of phloroglucinol crystals in order to produce large numbers of nuclei. If the 0.5μ crystal can be produced, then it would be possible to make 8×10^{12} cm^{-3} of material. With a density of 0.6 g cm^{-3} there would be 1.3×10^{13} crystals g^{-1}. Such a line is entered in Fig. 7 for phloroglucinol. There is still much left to speculation about this substance and the following questions should be the subject of immediate investigation:

a. What portion of 0.5μ crystals nucleate at -3C?

b. Will the crystals dissolve and become ineffective if they enter a cloud through the condensation level at cloud base?

c. How does the size requirement for nucleation change as a function of temperature?

Dry ice. Eadie and Mee (1963) made a laboratory study to determine the effectiveness of freely falling dry ice particles as a nucleating agent. Here the hypothesis was that the falling particles would not chill the air long enough for nucleation to take place and the ice crystal to grow to a stable size if the temperature were near 0C. Their observations confirmed the hypothesis, and as shown in the curves of Fig. 7, falling dry ice becomes very much less effective as the temperature warms from -7C towards 0C, while dry ice at rest retains its yield rate until nearly 0C. It is noted that Braham (1963) estimates the yield of ice crystals from dry ice 2 to 3 orders

of magnitude higher. It is not known how Braham arrived at his figure, but Mee, in private communications, explains that really objective means of determining the number have not been developed and that their estimate is conservative. For this study the Eadie and Mee curve will be used.

It has been suggested by some that powdered dry ice should be a more efficient seeding agent than cm-sized chunks, but here the cooling time and fall velocity decrease together, and according to Mee (private communication) the problem of insufficient cooling time at warm temperatures is still unsolved by this suggestion.

Comparison of seeding agents. The mass of seeding agent required to transform a cloud into ice with a predetermined size of ice crystal is as follows:

$$M = \frac{V_{LW}}{V_{iTt} \times N_T} \tag{3}$$

where V_{LW} = the volume of liquid water to be converted into ice crystals. $V_{LW} = V_{cloud}$ in m^3 multiplied by volume of cloud water m^{-3}.

V_{iTt} = the volume of an individual ice crystal at T, t minutes after nucleation.

N_T = the number of ice nuclei activated per unit mass of seeding agent at temperature T.

If N_T is plotted on a chart compatible with Fig. 5, that is, with the temperature scales the same and N^{-1} scale the same log scale as V, then once the proportionality factors of V_{LW} have been solved the solution for all T can be found by graphical subtraction of the logs of V_{iTt} and N_T from V_{LW}. This can be accomplished from Figs. 5 and 6.

Table 2.

T	AgI	Dropped CO_2	Maximum efficiency CO_2	Phloroglucinol 0.5μ size particles
-2.5C		10^7 kg	350 kg	50 g
-5.0	4000 g	2300	15	6
-7.5	700	1000	150	80
-10.0	22	90	50	27
-12.5	0.50	5.0	4.0	2.5
-15.0	0.02	0.4	0.3	0.25
-20	0.2	15	15	12.0
-25	1.0	200	200	15.0

Table 2 shows how many g of AgI and kg of dry ice would be needed to turn the one cubic kilometer cloud from water to ice in 10 minutes.

Table 2 illustrates vividly the effect of the relationship of ice crystal growth as a function of temperature and nuclei activation as a function of temperature on modifying fog or stratus. The effect is, however, exaggerated in that the dendrites contain less net volume of water than computed here. The second factor is that growth by riming becomes more important than growth by diffusion after a certain size is reached. This reduces the disparity between the slow and fast growing crystals.

Whereas it may not matter for some types of stratus modification whether it takes 2 minutes or 30 minutes to produce the effects, in cumulus clouds the timing can make a critical difference in producing the desired effect. It is therefore interesting to try to deduce something about the growth of ice crystals in a cumulus cloud updraft. This problem is complicated by the fact that ice crystal growth habits change as crystals change temperature. These changes in habit produce complicated forms of ice crystals (Nakaya, 1954). For this purpose, however, some insight can be gained even though habit changes during growth are not compensated for.

It is assumed the growth of the volume of a crystal in a rising air current can be approximated by a step-wise progression across Fig. 5. From the rate of updraft, the time a crystal grows at each ΔT is determined. A nucleation temperature is chosen for the start of crystal growth. Then the crystal is grown for Δt at the rate determined by T_0 to V_0. Then it is moved to $T_1 = T_0 + \Delta T$ and grows for Δt to $V_0 + \Delta V_1$, and so on to $V_0 + \Delta V_1 + \Delta V_2 \ldots$.

Figures 8a, b, c, d show the growth of crystal volume derived in this manner for updrafts of 1.25, 2.5, 5.0, 10.0 m sec^{-1} . At each updraft rate a range of nucleation temperatures are used. Here can be seen how the speed of the updraft diminishes the growing time for growth by diffusion. But a cloud with 5.0 m sec^{-1} updraft (Fig. 8c) can be completely converted to ice by -16C if it has 1 g m^{-3} of liquid water and if it can be seeded with 2 ice nuclei cm^{-3} active at -11C.

C. Onset of Riming

Riming plays an important part in ice phase growth but the conditions under which it takes place have not yet been bounded by experimental evidence. Both Houghton (1950) and Douglas (1959) have assumed simple solutions to this problem in order to carry out theoretical analyses of ice phase precipitation development. Since Hocking (1959) and Shafrir and Neiburger (1963) have worked out refined solutions to the limits of aerodynamic collision among water droplets, it seems appropriate to look at the riming and graupel development problem again. It would appear that it should be possible to deduce an improved solution based on analogy between ice crystal and water drop collision with cloud droplets. The condition of the analogy must depend on a comparison of fall velocities between water droplets and ice crystals as well as their cross section shapes.

Nakaya (1954) gives the fall velocity of snowflakes, but no fall velocity information on ice crystals of the 20 to 200μ range has been found in the literature. To fill this gap an effort has been made to deduce terminal velocities of ice crystals from their aerodynamic shapes. This is discussed in Appendix II. The results are given in Fig. 9 where they can be compared with the terminal velocities for water drops (Gunn and Kinzer, 1949).

It is assumed that plates fall flat and that needles fall with their c axes perpendicular to the direction of fall. There are two fall velocity curves plotted for needles, one with velocity against the a axis which determines

the rate of fall, and the other against the c axis determined from Fig. 4b for -5C. The c axis is the dimension that is generally observed and discussed. It is interesting to note that the computed fall velocities show rather good agreement with the fall velocities observed for needles by Nakaya (1954, p 114), also given in Fig. 9.

There is a temptation to try to explain the fall velocity of the unrimed dendrites by considering them to be analogous to a composite made of a central plate with needle arms, or branched needle arms. For this to fit Nakaya's (1954, p 114, given in Fig. 9) fall velocity for dendrites, the needles should be 50μ across. Measurement of a number of micrographs of dendrites given by Nakaya indicate that dendrite arms tend to be about 100μ broad. So the explanation must be somewhat more complicated. It is known, however, that the arms are thinner than they are broad, so theoretically it seems likely that the terminal velocity of dendrites can be explained rather simply.

The collection efficiencies E_i for ice crystals sweeping up cloud droplets have not yet been worked out. For the present the best solution to this problem seems to be to deduce E_i by assuming that there is a similarity between E_i and E_w collection efficiency for water drops. It would seem this approach will be most apt to produce large errors in the critical regions between no collisions and the start of collisions. But this uncertainty region for E_i is not as important as it might at first appear, because ice crystals grow rapidly through it. Water droplets, on the other hand,

are apt to slow down in growth as their size approaches this region, so it can be highly critical for water drop coalescence.

The collision efficiencies worked out by Shafrir and Neiburger (1963) have been transformed into coordinates more suitable for this analysis and are presented in Fig. 10. Also in Fig. 10 is a superimposition of the difference in fall velocity between the collecting drop and the cloud droplets.

When neither the overtake velocity nor the cross section area, and hence the collection efficiency, are sufficient to cause collision of water droplets, then it is assumed that there would be no collisions among ice crystals and cloud particles. For the cases where overtake velocity and the cross sections of ice crystals are within the collision range for water droplets, it is assumed that ice crystals will collide with cloud droplets. When either, but not both, the overtake velocity or the cross section for the ice crystals are in range of collision, the problem is indeterminant.

From Fig. 10 it can be seen that cloud water droplets of 15 to 30μ are the ones that will be collected first by a growing ice crystal. By referring to Fig. 9 it can be seen that the crystals that will require minimum growing time to start riming will be those that grow at -15C. These should be both broad enough and fall fast enough to begin riming in a little over one minute after nucleation. The ice needles which grow at -5C gain fall speed rapidly but probably are not broad enough to begin riming until the a axis is 30μ long; this requires more than two minutes of growth. Crystals at -10C must grow about five minutes to achieve falling speed sufficient to catch

cloud particles. At -25C crystals will have a and c axes nearly equal and will fall about as small water droplets of equal size. It will require almost ten minutes of growth before these will start to rime.

An estimate of the time at which riming becomes an important feature in the growth of the ice hydrometeors is added to Figs. 8a, b, c, and d. The estimate assumes that the water cloud is made up largely of droplets in the 15 to 30μ range.

On the other hand, it is interesting to note by a study of Figs. 9 and 10 that: (1) Dendrites may never fall fast enough nor have broad enough arms to collect cloud drops less than 8μ in diameter unless they rime by catching larger cloud droplets and thus gain speed. (2) Needles may have to grow more than 30 minutes in order to become broad enough to intercept cloud droplets less than 8μ in diameter. Cloud droplets smaller than 8μ are almost immune to riming and can be collected only by graupel, hail, or possibly by needles that had grown for more than 40 minutes.

In light of this it is interesting to look at Nakaya's (1954, p 117) frequency curve of diameters of droplets attached to snow crystals. Here he finds the maximum frequency at 28μ and none below 13μ. Of course it could be that the cloud had no smaller droplets.

D. Hydrometeor Transformation from Rimed Crystals to Graupel to Hailstones.

Douglas (1959) computed the growth rates of hydrometeors starting from small ice crystals, but in light of the foregoing analysis of ice crystal growth

rates and the onset of riming as well as recent work done by others, it is worthwhile to look at this problem again. As is well known, the fall velocity and the rate of growth of ice hydrometeors are a function of density. Macklin (1962) has made a study of the density and structure of ice formed by accretion. Important features of this study are shown in Fig. 11 which was adapted from Macklin's Fig. 7 and Fig. 13. These relate density and appearance of a hydrometeor to (a) the size of the accreted particles, (b) the impact velocity with which they are collected, and (c) the surface temperature of the collector. List (1960) has worked out the terminal velocities for hailstones of a variety of densities and shapes. These are added to Fig. 9 to fill out a skeleton chart relating terminal velocities and particle diameters for a wide range of ice hydrometeors. Mossop and Kidder (1962) have studied factors controlling the shape of hailstone development so that a computational guide to the growth of graupel and hailstones during accretion is available. The essence of this guide is incorporated in Fig. 9. Finally List (1963) has filled in the major remaining gap by working out the heat and mass exchange for spherical hailstones. This will be discussed below. There are still many problems in reconciling all of the different assumptions made by the several different investigators and bringing the different contributions into one working model. Yet before this can be completed it is possible to make useful estimates of the appearance, density, size, and fall velocity of ice hydrometeors.

List (1963) gives the expression for thermodynamic equilibrium of a growing hailstone,

$$\frac{1.68k(t_D - t_A) + C_{1,2}\, D_{wa} T_A^{-1}(e_{sh} - e_{sv})}{0.785\left[L_f I - \overline{c}_w(t_D - t_A)\right]} = \nu^{1/2} v^{1/2} D^{1/2} \theta^{-1} E w_f \qquad (4)$$

where the symbols have the following meaning:

k the thermal conductivity of air

t_D surface temperature of the hailstone

t_A air temperature

C_1 207 kcal deg m^{-3} for phase transitions liquid-gas

C_2 235 kcal deg m^{-3} for phase transitions solid-gas

D_{wa} diffusivity of water vapor in air

T_A absolute air temperature

e_{sh} saturated vapor pressure over hailstones

e_{sv} saturated vapor pressure over water

L_f latent heat of freezing

I ratio of frozen water to total water

c_w specific heat of water

ν kinematic modulus of viscosity

D diameter of hailstone

θ heat transfer of a natural rough surface divided by the heat transfer of an ideal smooth surface, found by List to be 1.5

E collection efficiency which is assumed to be 1.0 unless otherwise specified

w_f liquid water content of cloud

List (1963) gives a graphical solution to equation (4) in his Fig. 2. This graphical solution is adapted to the purposes of this paper and is presented in Fig. 12. The coordinates have been changed so that they correspond to those of Fig. 9. This makes it possible to transfer the value for $v^{1/2}D^{1/2}$ directly from Fig. 9 to Fig. 12. List's value $\theta = 1.5$ is retained, but the scale is shifted so that the value for the liquid water content of the cloud can be entered directly. List developed the graph for a hailstone density of 0.917 g cm^{-3}, but this graph has been generalized so that any desired density can be used.

In his Fig. 6 List has solved for the growth conditions under which mass exchange by sublimation and evaporation are zero, $M_{es*} = 0$. He also has a line for mass increase through sublimation equaling the mass increase through accretion, $M_{s*} = M_{cp*}$. These lines have been added to Fig. 12. The altitude has a substantial effect on $M_{s*} = M_{cp*}$ so this curve is given for 800 and 200 mb.

Figures 9, 11, and 12 contain the information necessary for solving hydrometeor growth problems. The solution is obtained by iteration, and involves working with all three charts. In order to work out a convenient method for using the three charts, the following system has been devised: The vertical scale of Fig. 11 is matched to that of Fig. 9, with the value of the diameter of the accreted droplets on the right scale of Fig. 11 set to match the left index on Fig. 9. Fig. 12 is related to Fig. 9 by sliding the left hand edge of Fig. 12 along the diagonal reference line on Fig. 9

until the desired value of liquid water, w_f, matches the w_f index point on Fig. 9. From this alignment of charts it is possible to find $V^{1/a}D^{1/a}$ values from Fig. 9 to solve the heat balance or surface temperatures of Fig. 12. By entering the surface temperature in Fig. 11 the density and shape of the hydrometeor is obtained to solve for a new v and D in Fig. 9, and so on. The solution can be made even more general if the charts of Appendix II are used instead of Fig. 9 for solving terminal velocities.

E. Conversion to Ice Phase and Cloud Dynamics

The conditions in terms of number of nuclei and time required to convert a supercooled water cloud to the ice phase can be found from Figs. 8a, b, c, d. This change of phase will have two immediate effects on the dynamics of the cloud. First, it will increase the buoyancy of the cloud. The amount is given in terms of virtual temperature by Saunders (1957) and is shown in his Figs. 1, 3, and 5. If the increase in buoyancy is sufficient to overcome stability of the environment that is limiting cloud development, then the cloud will develop in the vertical. A classical example of this is reported by Kraus and Squires (1947). Second, the increase of buoyancy in the cloud will decrease the pressure at the cloud base. Figure 14 is a chart for computing this decrease due to seeding ΔP_s. In Fig. 14 are isolines of the difference in pressure ΔP between a cloud transformed into ice at 0C and a similar cloud transformed into ice at a lower temperature T_c. If an unseeded cloud is in water phase below T_i and ice phase at heights above T_i then the cloud's $\Delta P = \Delta P_{top} - \Delta P_{Ti}$.

If a cloud is seeded and transformed into ice at T_s then $\Delta P_s = \Delta P_{T_i} - \Delta P_{T_s}$. In the case where the height of the top of the cloud increases with seeding then the pressure at cloud base is decreased even more.

4. Discussion

A system has been outlined and the graphs have been constructed for solving ice phase hydrometeor growth problems. The system is based on the theoretical and experimental work reported in the literature. There are gaps in the theory and observations, and it is vital to the future of the field that these gaps are recognized and filled by valid experiments and carefully developed theory. The important gaps that became apparent during the development of this study are as follows:

a. Ice crystal growth rates for both a and c axes of ice crystals from the time of nucleation.

This should be a reasonably straightforward problem to solve in terms of experimental techniques now available.

b. Fall velocities of various types of ice crystals.

Though these have been worked out for water droplets, hailstones, and snowflakes, it still remains to be done for ice crystals.

c. Onset of riming of ice crystals.

This apparently has not yet been determined experimentally. It must be a function of the size, shape, and fall velocity of the ice crystals as well as the size of the cloud droplets.

d. The accretion rate of ice crystals once riming has started.

This must be studied experimentally for a wide range of initial shapes of ice crystals in water clouds with droplets of various sizes.

e. Methods of spontaneous nucleation of ice crystals other than with dry ice.

There is an important need to produce nuclei effective at roughly -3C and it would seem that, as falling dry ice particles are very inefficient at this temperature, one of the apparent advantages for dry ice does not exist. For this reason other techniques should be studied, such as producing nuclei in air by compressing, cooling, and expanding the saturated air itself.

f. The effective use of phloroglucinol.

The -2C threshold for ice nucleation, and the apparent potentially large number of active nuclei per gram make this agent of great interest. It is necessary, however, to find out how to produce the optimum number of nuclei active at temperatures warmer than -4C. It is also vital to find out if this agent can be released from below cloud base without its being dissolved and diluted to where it loses its nucleating power as it passes through the condensation level at cloud base.

5. Conclusions

Before laboratory work is completed to fill the above mentioned gaps, much can be learned about the potentialities and limitations of ice phase cloud modification by computing through the effects of proposed modifications. Even without computing some of the more involved hydrometeor growths, it is apparent that there is a substantial advantage in being able to nucleate at

warmer temperatures than those at which AgI is effective. The fact that there is an ice crystal growth maximum at -4C indicates that if there can be effective nucleation at this temperature it should be possible to make a substantial increase in the number of clouds that would be susceptible to ice phase modification. The -4C growth maximum is also in the range in which dry ice pellets poured out of an aircraft are inefficient at seeding. Therefore, a high priority should be given to learning how to use phloroglucinol, and some attention should be given to developing techniques for producing spontaneous nucleation of ice without using dry ice.

It should be possible to develop a reasonable comprehensive model of the present potentials of ice phase cloud modification when a systematic computational exploration can be made using the graphical system outlined here. The structure for such a model could be similar to the one developed by this writer (MacCready, et al., 1957). It was discussed in the background section of this report. This model would predict the effects upon a cloud of varying the concentrations and temperatures of activation of ice nuclei. For simplicity the model would be computed for clouds in which the air flows up through the cloud base, and ascends adiabatically and unmixed with the environment until it mixes with the surroundings as it leaves the cloud top. The model would be computed for a broad range of discrete cloud base temperatures and for a wide range of updraft velocities and cloud top temperatures. The number of cases involved here is large, but because of the similarities among them, the patterns of solution would become apparent

and it would be possible to interpolate results and fill in a comprehensive model with a reasonable amount of work. The rewards for doing this would be tremendous in terms of increased understanding of ice phase cloud modification potentials.

REFERENCES

Braham, R. R., Jr., 1963: Phloroglucinol seeding of undercooled clouds. J. Atmos. Sci., 20, 563.

Browning, K. A., and B. J. Mason, 1963: Production of ice crystals and and electric charge by splintering of freezing droplets in thunderclouds. Quart. J. R. Meteor. Soc., 89, 139.

Douglas, R. H., 1959: Part II, Growth by accretion in the ice phase. Scientific Report MW-30, Alberta Hail, 1958 and Related Studies. McGill University, MacDonald Physics Laboratory, "Stormy Weather" Research Group.

Eadie, W. J., and T. R. Mee, 1963: The effect of dry-ice pellet velocity on the generation of ice crystals. J. Appl. Meteor., 2, 260-265.

Fletcher, N. H., 1959: The optimum performance of silver-iodide smoke generators. J. of Meteor., 16, 385.

Gunn, R., and G. D. Kinzer, 1949: The terminal velocity of fall for water droplets in stagnant air. J. of Meteor., 6, 243-248.

Hocking, L. M., 1959: The collision efficiency of small drops. Quart. J. R. Meteor. Soc., 85, 44.

Koenig, L. R., 1963: The glaciating behavior of small cumulonimbus clouds. J. Atmos. Sci., 20, 1.

Kraus, E. B., and P. Squires, 1947: Experiments on the stimulation of clouds to produce rains. Nature, London, 159, 489.

Langer, G., and J. Rosinski, 1962: A study of organic crystals as ice nuclei. (1963) Organic crystals as icing nuclei, J. Atmos. Sci., 20, 557.

List, R., 1960: New developments in hail research. Science, 132, 3434.

_____, 1963: General heat and mass exchange of spherical hailstones. J. Atmos. Sci., 20, 189.

MacCready, Paul B., Jr., et al., 1957: Final Report of the Advisory Committee on Weather Control, Vol. II, 154-155.

Macklin, W.C., 1962: The density and structure of ice formed by accretion. Quart. J. R. Meteor. Soc., 88, 30.

Marshall, J.S., and M.P. Langleben, 1954: A theory of snow-crystal habit and growth. J. of Meteor., 11, 104.

Mason, B.J., and J. Maybank, 1960: The fragmentation and electrification of freezing water drops. Quart. J. R. Meteor. Soc., 89, 139.

_____, G.W. Bryant, and A.P. Van den Heuvel, 1963: The growth habits and surface structure of ice crystals. Philosophical Magazine, 8, 87, 505.

Mossop, S.C., and R.E. Kidder, 1962: Artificial hailstones. Bull. Obs. Puy de Dome, 2.

Nakaya, U., 1954: Snow Crystals. Harvard University Press, Cambridge, 510 pages.

_____, 1955: Snow crystals and aerosols. J. Faculty of Sci., Hokkaido Univ., Japan, Ser. II, IV, 6.

Saunders, P. M., 1957: The thermodynamics of saturated air: A contribution to the classical theory. Quart. J. R. Meteor Soc., 83, 342.

Shafrir, U., and M. Neiburger, 1963: Collision efficiencies of two spheres falling in a viscous medium. J. Geophys. Res., 68, 13.

Shaw, D., and B. J. Mason, 1955: The growth of ice crystals from vapor. Philosophical Magazine, 46, 249-262.

Todd, C. J., 1964: Aircraft traverses in a growing mountain cumulus cloud. Submitted to J. Atmos. Sci. Atmospheric Research Group, Altadena, Calif.

Weickmann, H., 1957: Artificial Stimulation of Rain. Pergamon Press, New York, 320 pages.

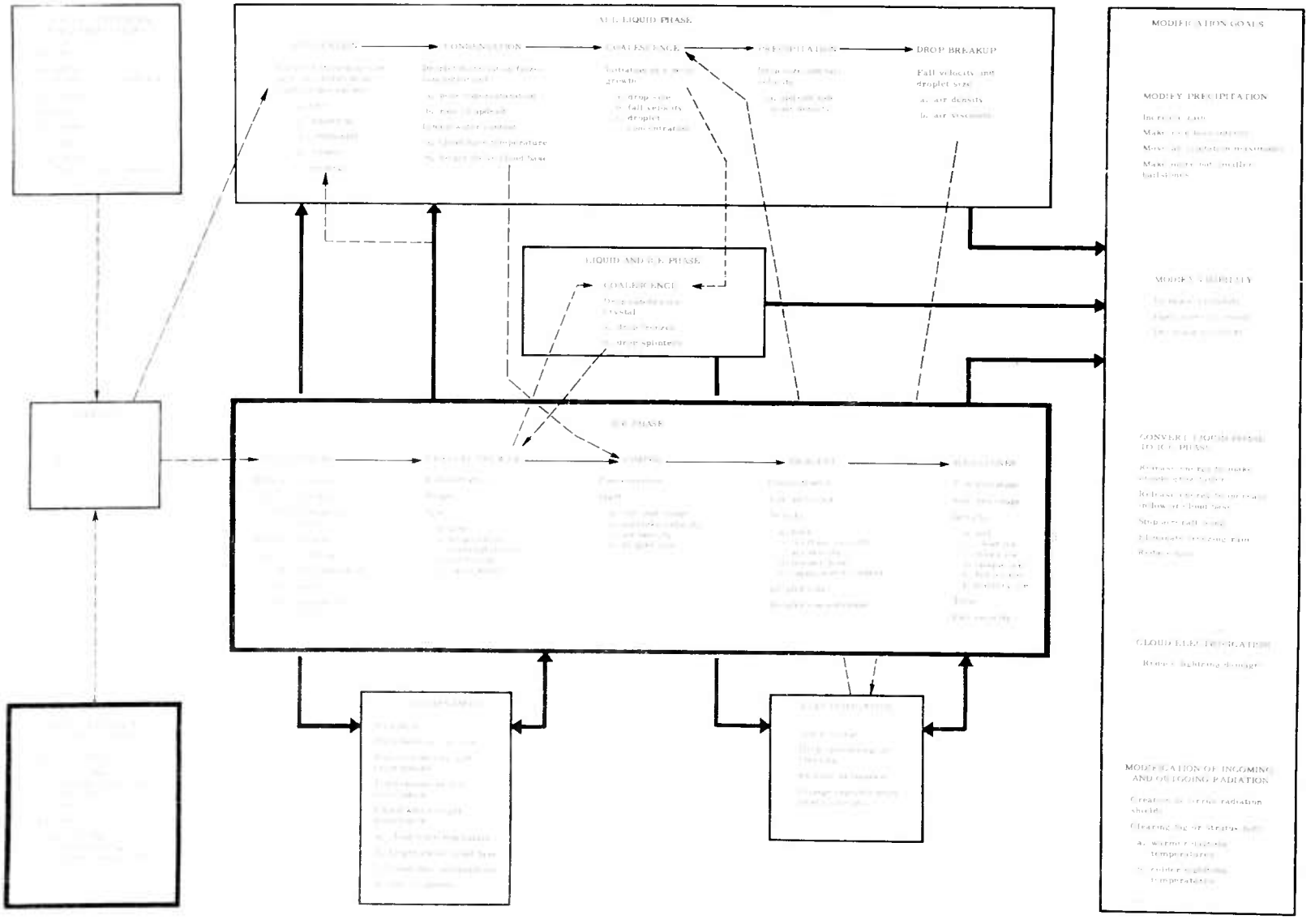

Fig. 1. BLOCK DIAGRAM OF CLOUD PHYSICAL PROCESSES AND CLOUD MODIFICATION.

The darkly outlined blocks are the topic of this discussion.

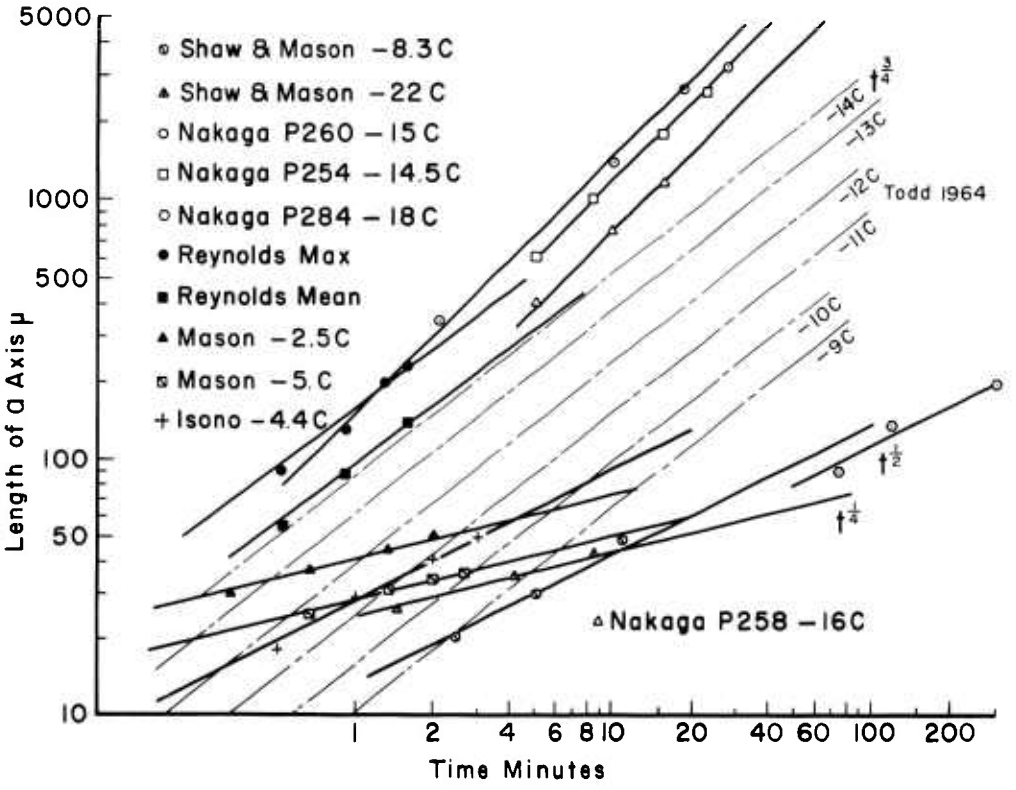

Fig. 2a. GROWTH TIME VERSUS LENGTH OF THE a AXIS OF ICE CRYSTALS TAKEN FROM VARIOUS REPORTS IN THE LITERATURE.

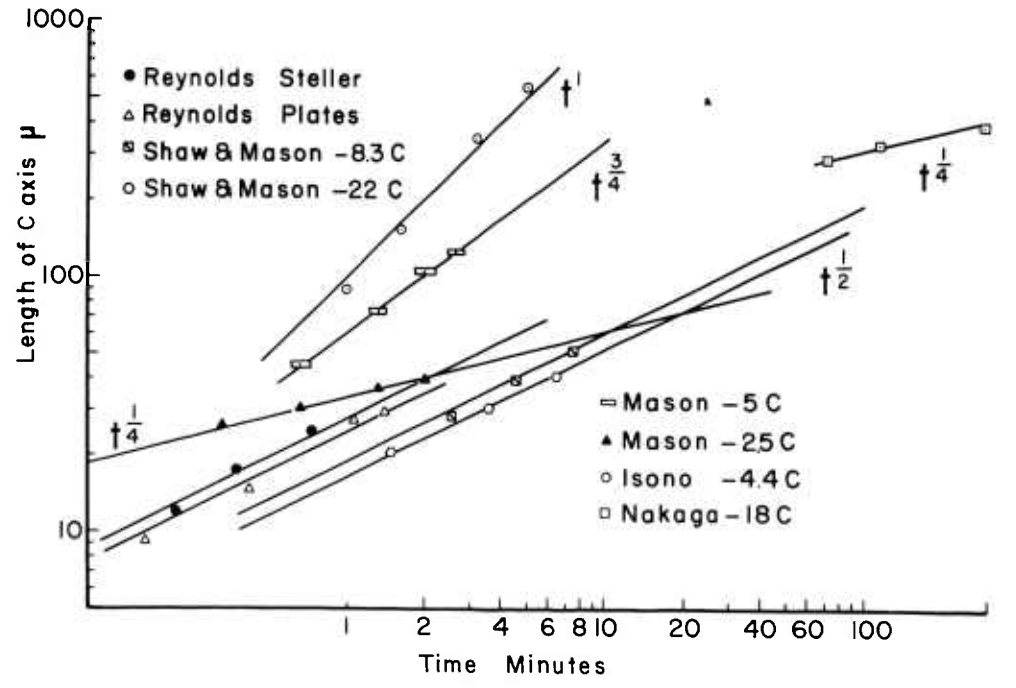

Fig. 2b. GROWTH TIME VERSUS LENGTH OF THE c AXIS OF ICE CRYSTALS TAKEN FROM VARIOUS REPORTS IN THE LITERATURE.

Straight lines are drawn through the data points for slopes of $t^{1/4}$, $t^{1/2}$, $t^{3/4}$, or t^{1}. The points seem to fit these discrete growth rates. All of these observations were presumably at water saturation.

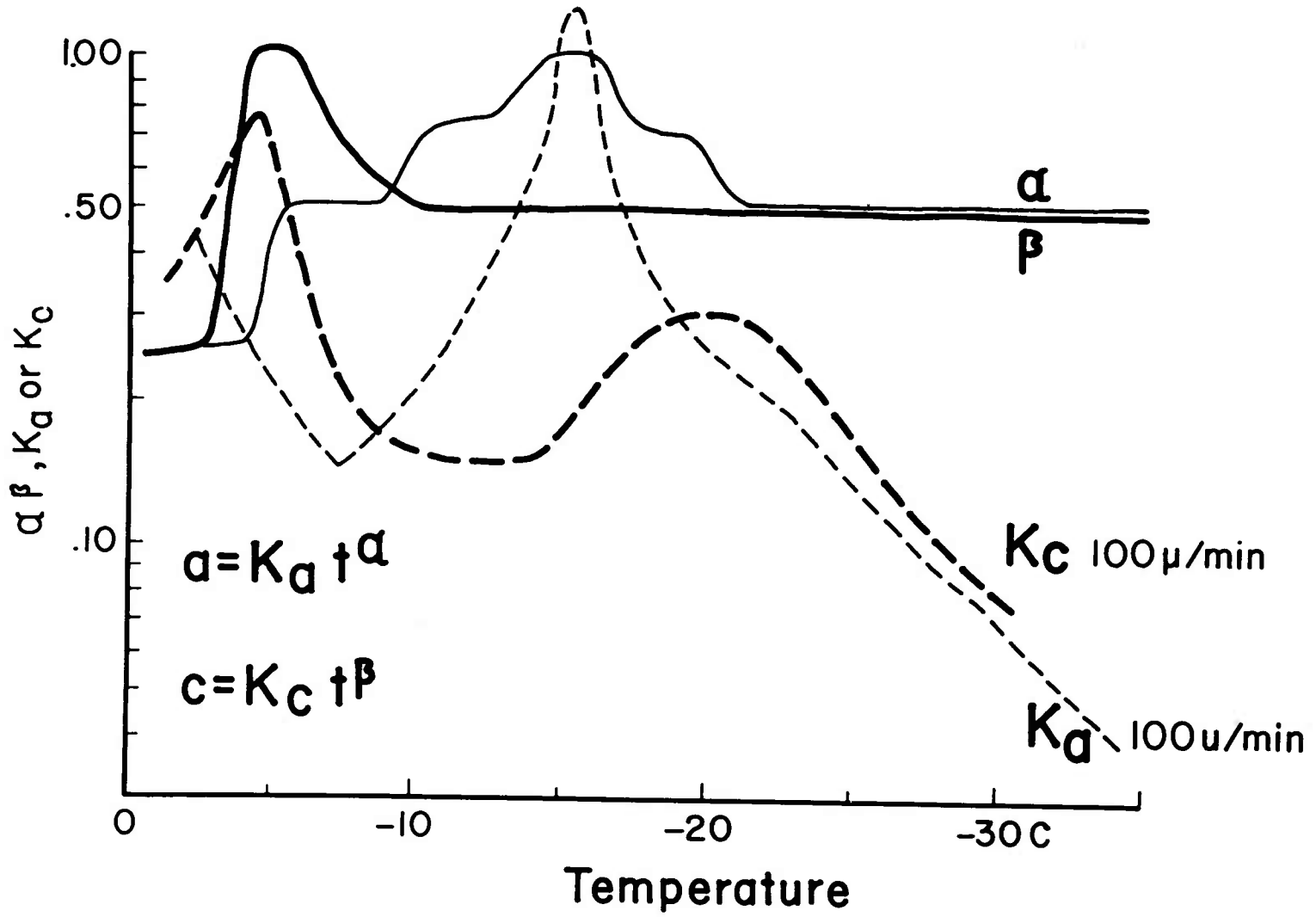

Fig. 3. VALUES OF THE ICE CRYSTAL GROWTH PARAMETERS AS A FUNCTION OF TEMPERATURE.

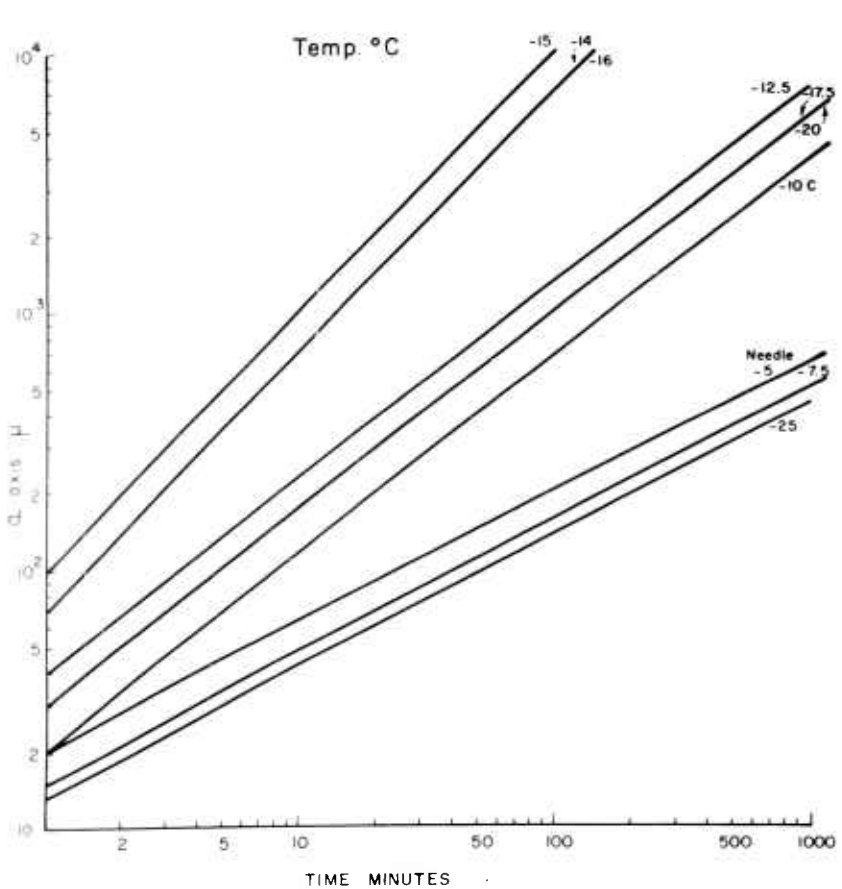

Fig. 4a. LENGTH COMPUTED FROM PARAMETERS OF FIG. 3 FOR THE a AXIS OF ICE CRYSTALS GROWN AT VARIOUS TEMPERATURES PLOTTED AS A FUNCTION OF TIME SINCE NUCLEATION.

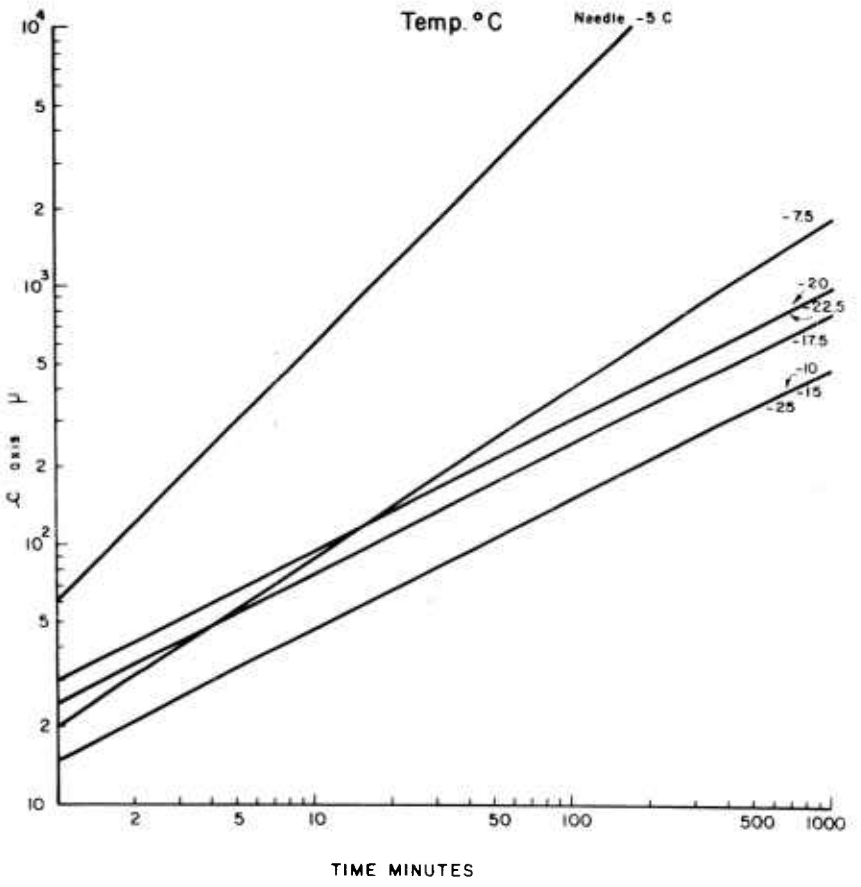

Fig. 4b. LENGTH COMPUTED FROM PARAMETERS OF FIG. 3 FOR THE c AXIS OF ICE CRYSTALS GROWN AT VARIOUS TEMPERATURES PLOTTED AS A FUNCTION OF TIME SINCE NUCLEATION.

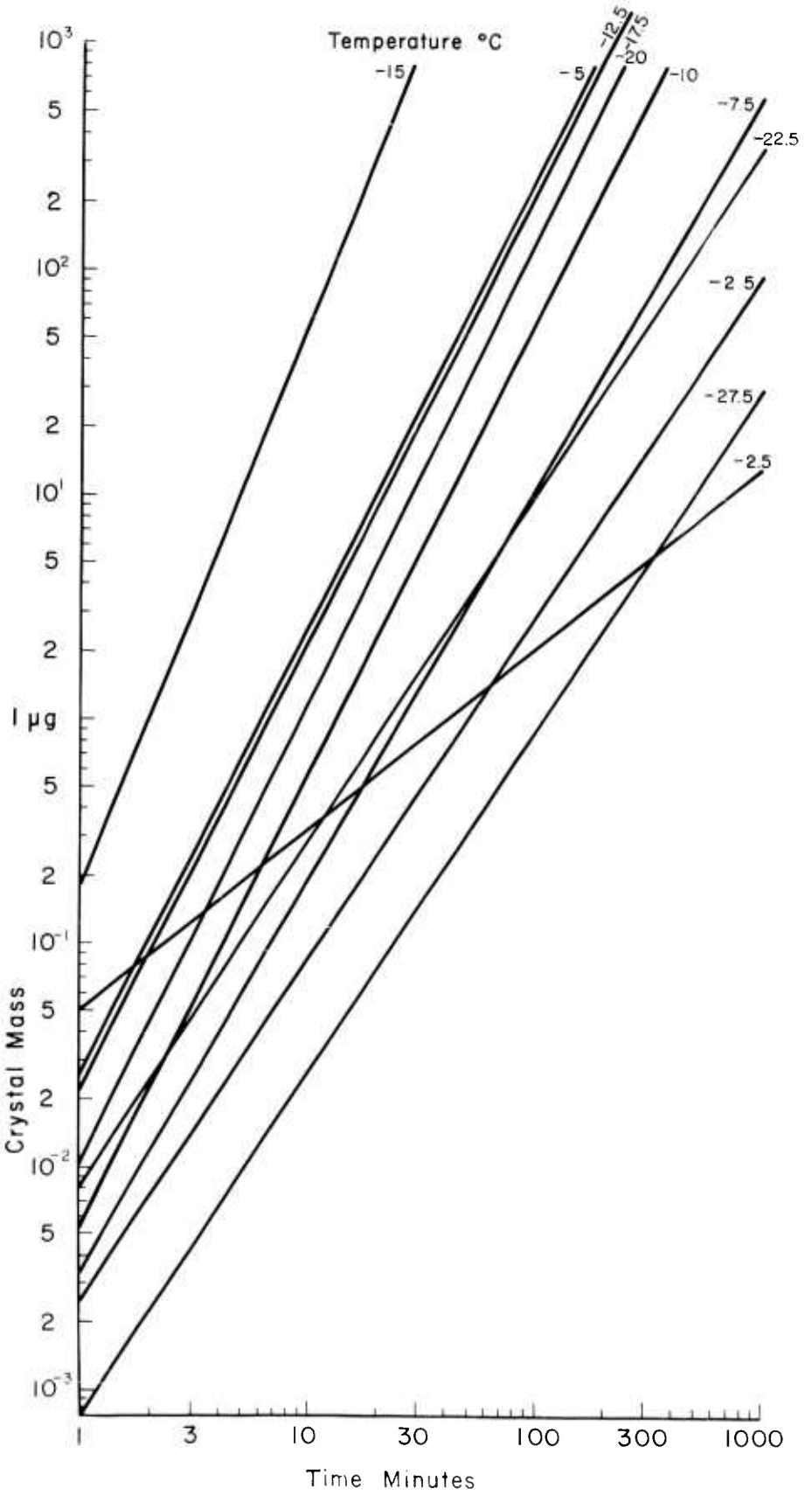

Fig. 5. CRYSTAL MASS COMPUTED FROM FIG. 4a AND FIG. 4b GROWN AT VARIOUS TEMPERATURES PRESENTED AS A FUNCTION OF TIME SINCE NUCLEATION.

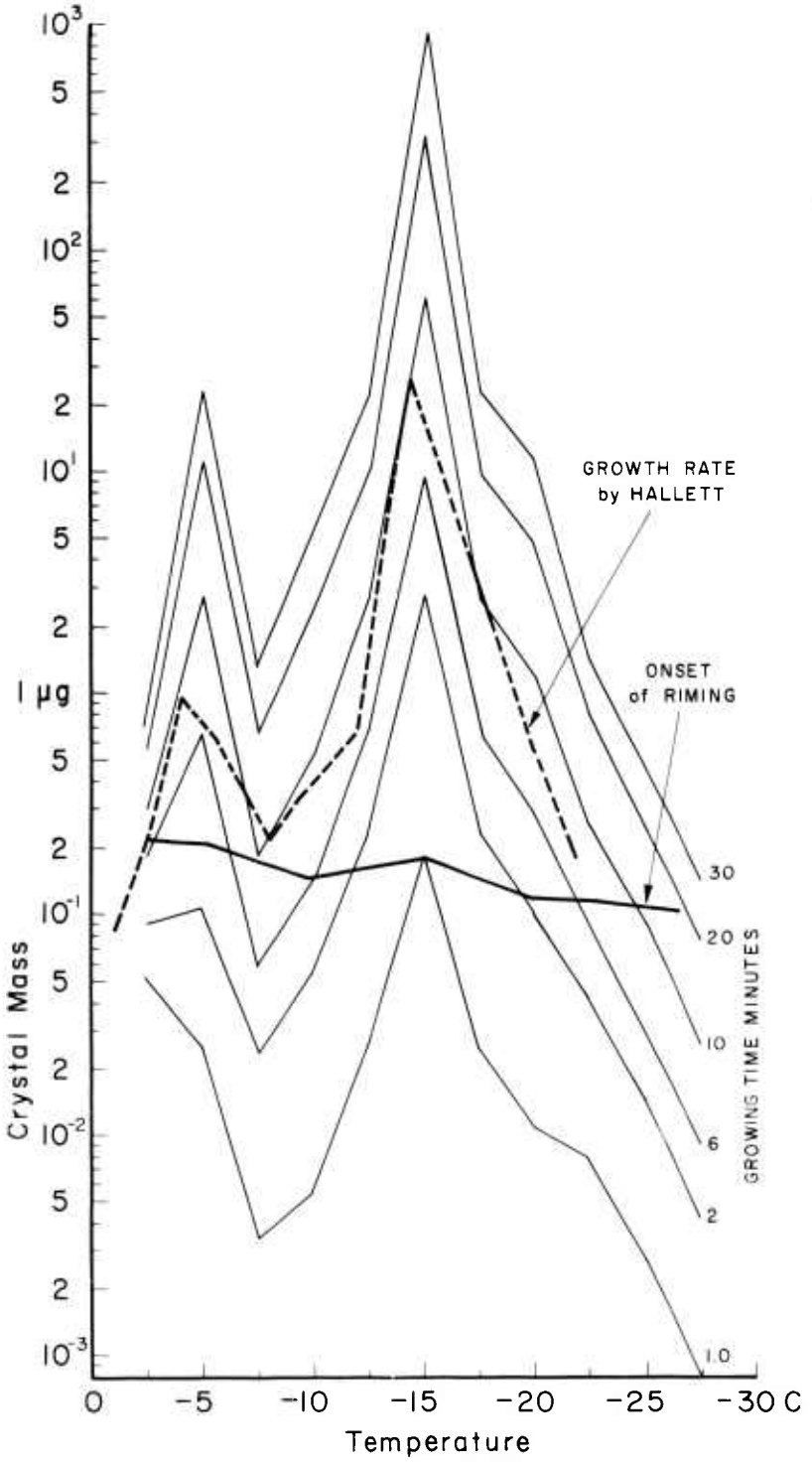

Fig. 6. ISOCHRONES OF CRYSTAL MASS VERSUS GROWING TEMPERATURES, AS DEVELOPED FROM FIG. 5.

Included is the relative crystal growth rate reported by Hallett in private communication. Also included is the deduced onset of riming curve.

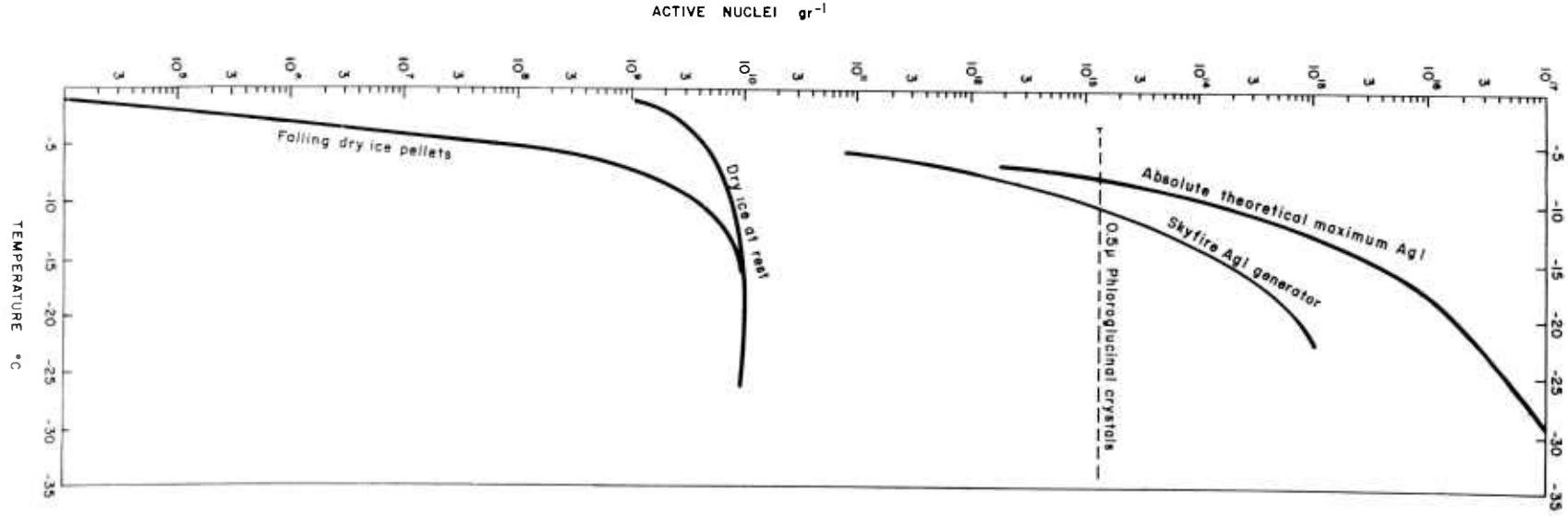

Fig. 7. A COMPARISON OF THE NUMBER OF NUCLEI PER GRAM AS A FUNCTION OF ACTIVATION TEMPERATURE OF AgI, PHLORO-GLUCINOL IN 0.5 μ CRYSTALS, DRY ICE DROPPED FROM AN AIRCRAFT, AND DRY ICE EXPOSED AT REST.

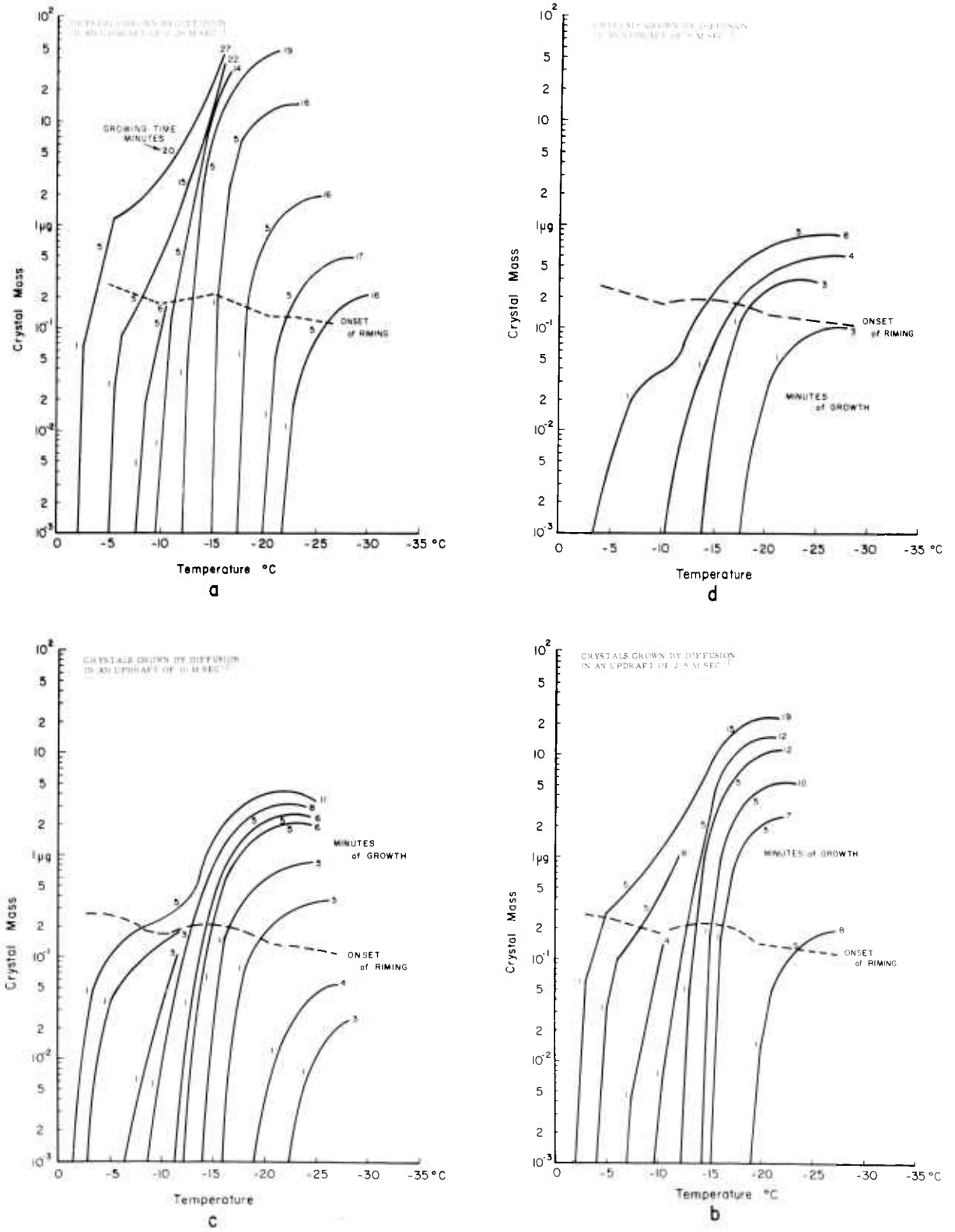

Fig. 8. MASS CRYSTAL GROWTH BY DIFFUSION OF WATER VAPOR IN A RISING CONVECTIVE COLUMN MAINTAINED AT WATER SATURATION.

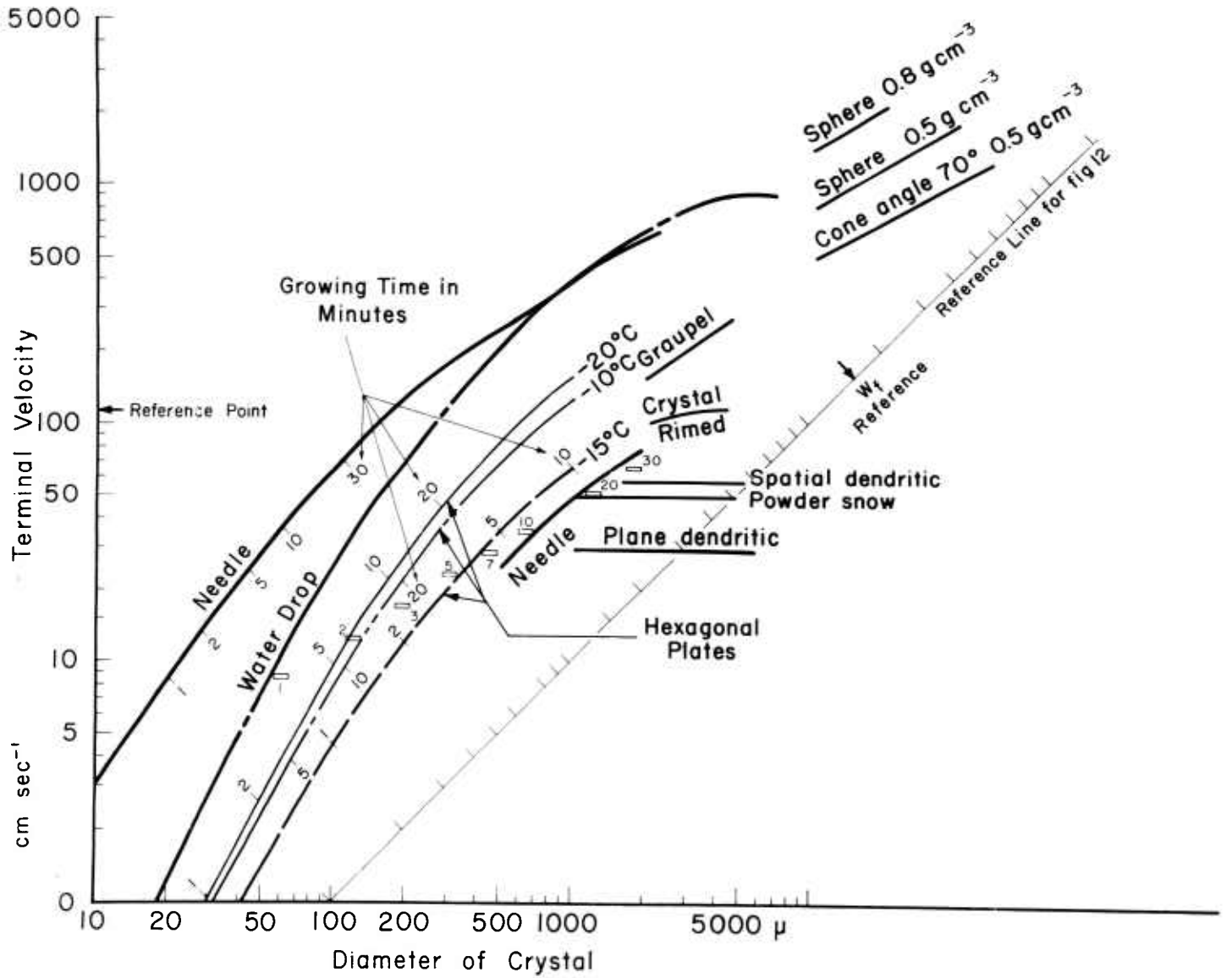

Fig. 9. TERMINAL VELOCITIES OF VARIOUS CLOUD PARTICLES.

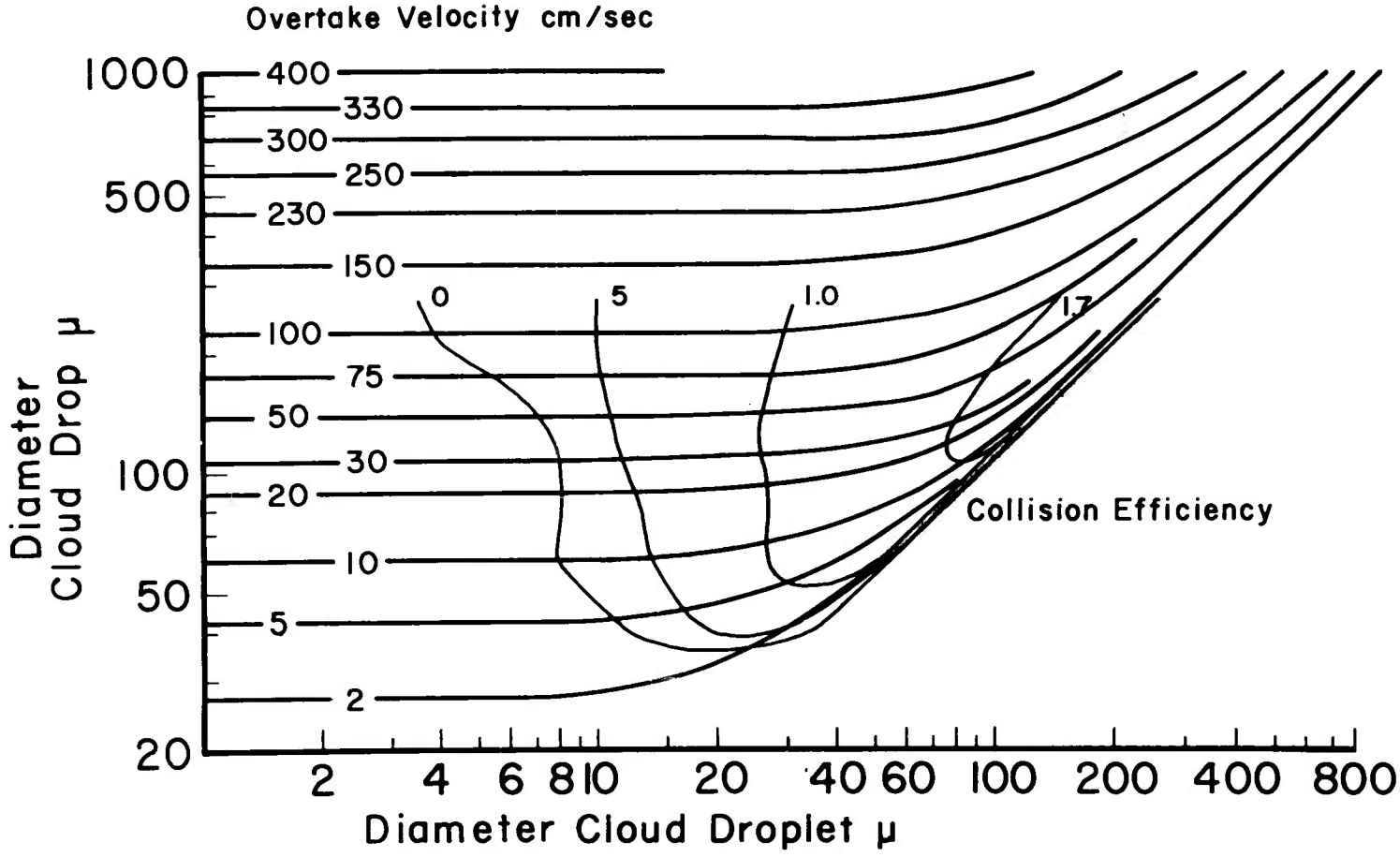

Fig. 10. COLLISION EFFICIENCIES ADAPTED FROM SHAFRIR AND NEIBURGER (1963) WITH AN OVERLAY OF OVERTAKE VELOCITIES.

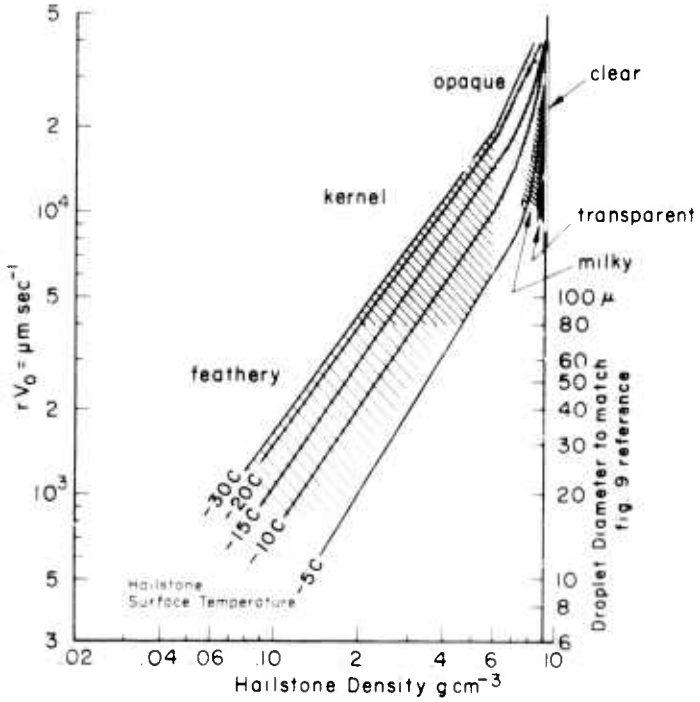

Fig. 11. CHARACTER OF HAILSTONE AND ICE HYDROMETEOR GROWTH, ADAPTED FROM MACKLIN (1962).

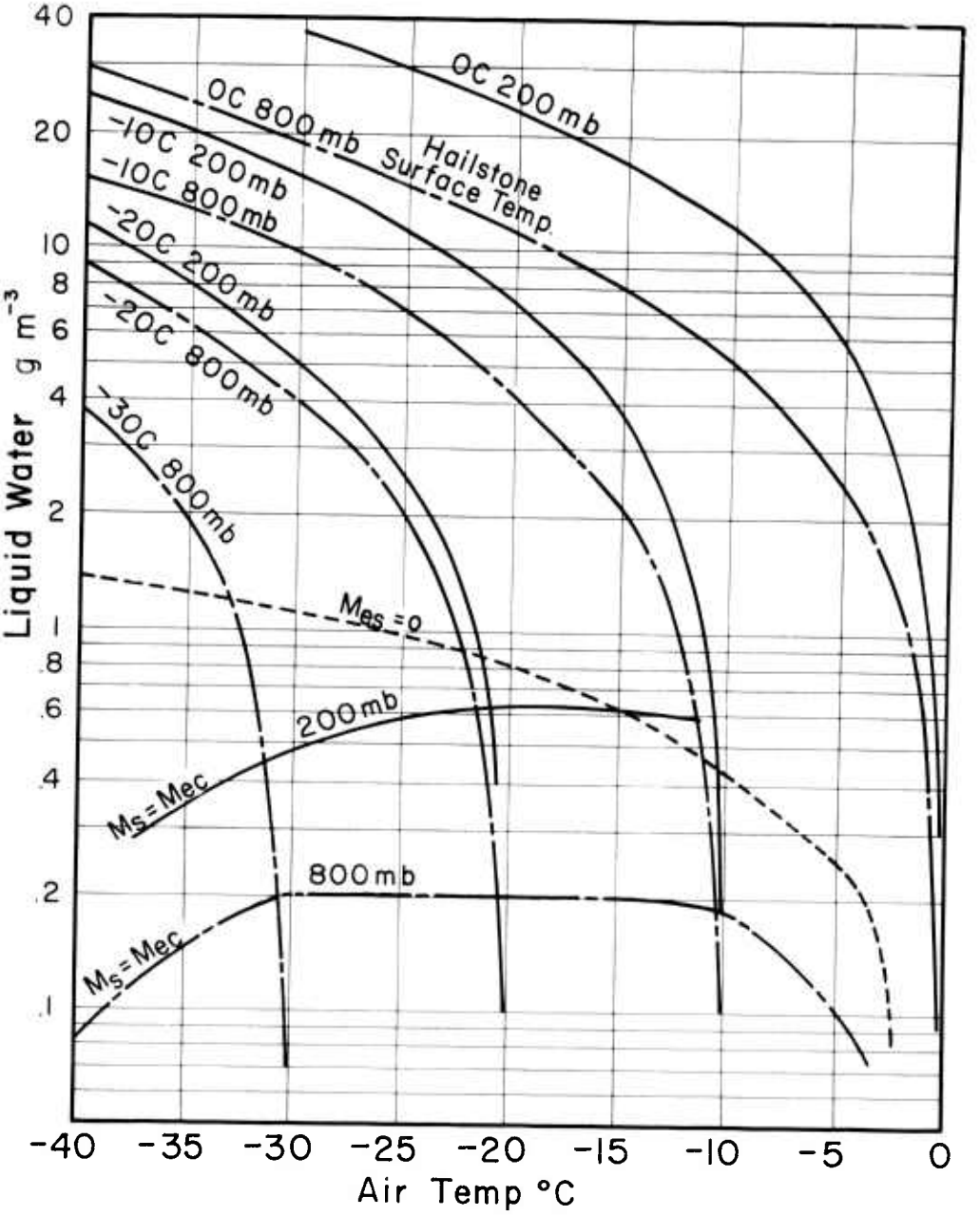

Fig. 12. THIS CHART ADAPTED FROM LIST (1963) IS FOR COMPUTING SURFACE TEMPERATURES OF ICE HYDROMETEORS WHEN USED IN CONJUNCTION WITH FIG. 9.

The value of the liquid water content of the cloud found on the left scale is matched with the W_f reference point on Fig. 9. The size and shape of the ice hydrometeor is entered in Fig. 9 and a line is drawn through this point perpendicular to the reference line to the air temperature of Fig. 12. Here the ice hydrometeor surface temperature is found by interpolating if the air pressure is known. The $M_{es} = 0$ curve indicates the conditions under which evaporation and sublimation are in equilibrium. Above this curve accretion is diminished by evaporation, below it is enhanced by sublimation. The $M_s = M_{cp}$ line shows the conditions in which growth by sublimation equals the growth by accretion.

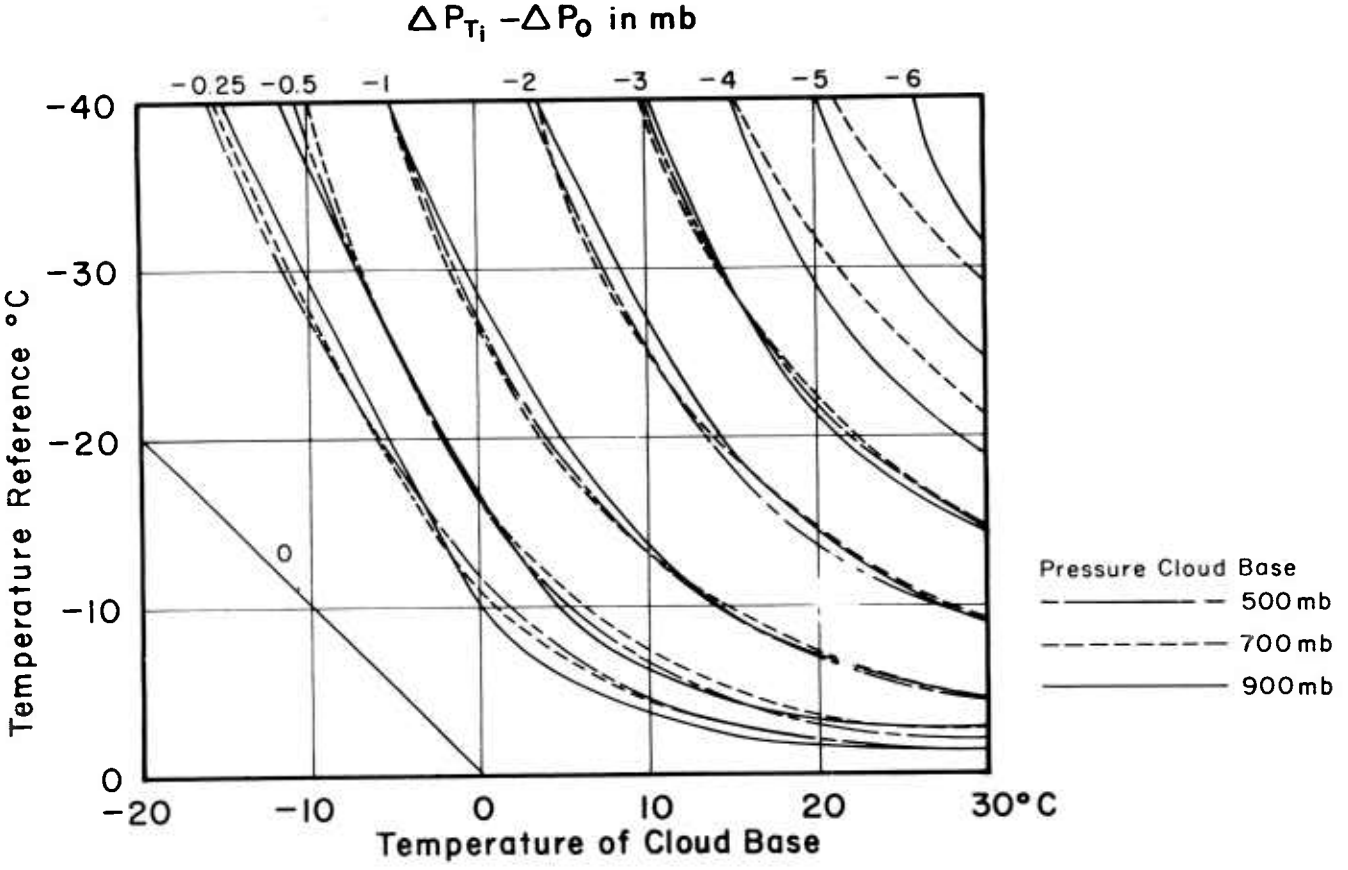

Fig. 13. THE DECREASE IN PRESSURE BELOW THE CLOUD THAT WOULD BE CREATED IF THE CLOUD WERE CHANGED FROM LIQUID PHASE TO ICE PHASE BETWEEN 0C AND THE TEMPERATURE REFERENCE LEVEL.

To find the decrease in pressure created by changing a cloud with the base temperature of 20C to ice at -10C instead of -30C, subtract -1.4 from -4.0 and read ΔP = -2.6 mb.

Appendix I

ICE CRYSTAL MEASUREMENTS MADE FROM NAKAYA (1954)

Nakaya's book was studied carefully and, wherever there was information that could be translated into growth rates of ice crystals or snow crystals at controlled conditions, it was tabulated and analyzed. Table 1 is a tabulation of the information. Column a is Nakaya's reference, figure number, and crystal number. Column b is the time of growth from nucleation. Column c is the length of the a axis measured from the plate. Column d is the length of the c axis measured from the plate. Column e is T_w, the temperature of the water at the bottom of Nakaya's apparatus. Column f is the temperature of the air ambient to the crystal T_a. Columns g, h, i, and j are the coefficients K_a of the equation $a = K_a t^{\alpha}$ for values of α from 1/4, 1/2, 3/4, and 1 respectively, which would give value a column c at time t column b. Columns k, l, m, and n are similar to g, h, i, and j but are for c axis measurement. The units of K_a are hundreds of microns per minute.

Table I

						k_a				k_e			
a	b	c	d	e	f	g	h	i	j	k	l	m	n
	t	a	c	T_w	T_a	1/4	1/2	3/4	1	1/4	1/2	3/4	1
p 370													
1288	20 h	400μ	500μ	+8	-21.5	65	12	1.6		80	15	1.8	
p 371													
1289	2.5	350		+9	-18	120	30	5.8	1.7				
p 379													
1292-3	3	1200	100	+8	-17					27	7.5	1.7	0.5
p 375													
1994				+8	-17								
p 373													
1295	4.5			+11	-20								
p 382													
1298	3	1800		+8	-20		140	32	10				
p 383													
1297	1.7	1200		+17	-13		120	38					
p 218													
1339	1.7	2000		+11	-19		200	60	20				
	0.5	500		+11	-19		90	55	17				
376													
	2.5	1700		+12	-17.5		130	35	12				
1343	1	1500		+10	-23		200	62	25				
1340	2.5	1300	700	-1	-37		120	25	4.7	190	53	13	2.5
402													
1346	20	4000		+6	-24		130	17	3.3				
p 120													
403	20	150	250	+4	-25	25	4.6			45	7.5		
P 222													
1360-1	2.25			+5	-18								
1362	2.75	700	500	+6	-21		55	12			37	8	
1363	1	100	250	+7	-21		13	4.2			42	13	
1364	21.30			+2	-19.5								
1365	22	950	800	+5	-21		26	3.3			22	2.8	

						k_a				k_e			
a	b	c	d	e	f	g	h	i	j	k	l	m	n
	t	a	c	T_w	T_a	1/4	1/2	3/4	1	1/4	1/2	3/4	1
410													
1366-7	0.75	200μ	350μ	+12	-21		30	10			63	19	
411													
1368-9	1	150	300	+7	-21		20	6.2			38	12	
p.191													
343	3.5	10,000	150	-128	-6	40	11						
p 349													
1251	2	150	2300	+26	-5	45	15				200		18
1252	2	300	4200	+29	-5	90	27				350		35
p 193													
1262	2	200	3200	+30	-5	63	18				280		27
p 194													
1269	2.5		800	+26	-8					220	60	22	3.7
p 197													
1273	0.83		250	+27	-9					90	35	12	4.2
p 201													
364	0.75	600		+18	-13	250	90	32	10				
1280	0.75	600		+17	-12	250	90	32	10				
365	2.5	750		+7	-17	200	50	12					
p 165													
7	7	400	150	+7	-27	90	18			35	7		
		200	100	+7	-27	42	10			22	5		
8	15	250		+4	-27	45	8						
9	18	300	300	+3	-38	55	9			55	9		
10	17	500		+4.5	-20	95	27						
11	20	300		+8	-22	50	9						
12	25	40	250	+4	-29	6.5	1			40	7		
p 178													
313	0.75	2500		+15	-15				56				
p 180													
315				+13	-16				73				
316				+12	-16				100				
318				+15	-17.5				59				
319				+17	-15				93				
322				+14	-16				53				

						K_a				K_e			
a	b	c	d	e	f	g	h	i	j	k	l	m	n
	t	a	c	T_w	T_a	1/4	1/2	3/4	1	1/4	1/2	3/4	1
415	15 h	650μ	2000μ	+9	-25	120	20			360	60		
p 225													
416													
1374	4.16	100	350	+8	-26	25	6			56	22		
1376	5.5	550	1000	+8	-26	120	23			230	52		
1377	5.5	200	500	+11	-24	70	12			120	28		
p 238													
434			(	+26	-17								
435		droplets	(	+245	-15								
436			(	+17	-15								
p 250	0.53			+17	-16				100				
p 252			80	+17	-15				100		15		
p 260			100	+20	-13						20		
p 254	0.37	2700		+17	-15				122				
	0.25	700		+17	-14				47				
	0.25	200		+17	-13				13				
p 258	0.23	1200		+14	-15				86				
	0.28	400		+14	-15				23				
	0.3	450		+14	-17				32				
p 260	0.37	3200		+18	-15				146				
	0.58		80	+18	-15					35	15	5	
			120	+20	-12								
	3.0		300	+23	-8								
			400	+32	-6								
p 266	0.25	100		+12	-20		25						
	0.25	300		+14	-15				87				
p 270	1.75	800		+10	-16		80	24					
p 271	0.5	600		+12.5	-16				20				
p 277	4.33	200	1300	+26	-8		12				70	15	
p 279	0.25	120	1800	+35	-6	65	30	15	8				120
p 280	5.33	400	300	+4	-22	120	22	5	1.3	95		3.5	1
p 284	1.10	100	280	+3	-18	35	12			95	21		
	1.83	120	310	+3	-18	38	12			95	30		
	5.0	200	380	+3	-18	50	12			92	22		

A review of this information as related to the T_w T_a diagram of Nakaya led to the empirical derivation of the K_a and K_c curves found in Fig. 3 in the text.

REFERENCES

Nakaya, U., 1945: Snow Crystals, Harvard University Press, Cambridge, 510 pages.

Appendix II

HYDROMETEOR TERMINAL VELOCITY COMPUTATIONS

It facilitates cloud physics analysis to have a convenient method for computing terminal velocities of hydrometeors as they grow, change density and shape, as they pass through different densities of air. The following discussion develops a graphical method for doing this. This graphical system used in conjunction with the graphical system for determining the density, shape, and visual characteristics of ice hydrometeors should make possible a fairly good solution to the hydrometeor development and fall velocity problem once the initial cloud parameters are known.

The terminal velocity V is the velocity at which G = F. That is, the forces of gravity G balance the resistance forces F.

The drag coefficient C_D is a dimensionless quantity defined by

$$F = 1/2\rho V^2 S C_D \tag{1}$$

where F is the force acting on the particle in the direction opposite to its motion, ρ is the density of the surrounding fluid in g cm^{-3}, V is the velocity of the particle in cm sec^{-1} and S is the projected area of the particle in the direction of fall in cm^2.

The gravitational force acting on a particle is:

$$G = gM(\rho_s - \rho) \tag{2}$$

where g is the force of gravity,and M is the mass of the particle, and ρ_s is the density of the particle. V_* is defined as the terminal velocity when the gravitational force and drag force are in equilibrium.

For any shape $C_D = f(R_e)$

$$R_e = \frac{Vd}{\nu}$$

where d is a linear dimension of the particle perpendicular to the direction of fall and is the kinematic modulus of viscosity.

Figure A gives the $C_D = f(R_e)$ for some of the shapes appropriate for the evaluation of terminal velocities of hydrometeors. The water droplet C_D values were taken from Gunn and Kinzer (1949). Values for ice hydrometeors for $R_e \geq 10^3$ were derived experimentally by List (1960). Values for C_D of plates are found by doing a transformation on the resistance for spheres (Menzel, 1960). The C_D for long cylinders is taken from Wieselsberger (1943). These drag coefficients give analogies for most of the hydrometeor forms through the necessary range in R_e. From them it should be possible to make reasonably good estimates of V_* for the hydrometeors that are important to cloud modification. There is a need to extend the experimental results throughout the rest of the range of hydrometeors. This is especially important because of the open and hollow shapes, and because of the roughness of some ice forms.

Equating (1) and (2) gives

$$1/2\rho V^2 S C_D = gM(\rho_s - \rho) . \qquad (3)$$

Because for atmospheric work $\rho_s >> \rho$, ρ_s is substituted for $(\rho_s - \rho)$, and then (3) becomes:

$$1/2\rho V^2 S C_D = gM\rho_s . \qquad (4)$$

The size and shape factors of the hydrometeors determine

$$\frac{S}{M\rho_s} = \frac{k_1 d^2}{k_2 \ell d^2 \rho_s} = \frac{k_3}{\ell \rho_s} \tag{5}$$

where d is the dimension used in determining R_e, ℓ is the dimension in the direction of fall, k_1 and k_2 are constants of geometry, and $k_1/k_2 = k_3$.

For a cube $k_3 = 1$ $\ell = d$

For a sphere $k_3 = 3/2$ $\ell = d$

For a hexagonal plate $k_3 = 1$ ℓ = thickness of plate

For a long hexagonal prism $k_3 = 2/\sqrt{3}$ $\ell = d$

For a 70 deg pyramid with rounded bottom $k_3 = 2.71$ ℓ = distance from top to bottom.

It is desirable to solve for V_* in terms of the independent variables d, $\ell\rho_s/dk_3$ and ρ. To do this a log V_* -- log d diagram, Fig. B, is constructed. The factors of cross section area with respect to mass as related by $\ell\rho_s/dk$ are entered for particular hydrometeors by finding the equivalent cube of proper density and diameter value. A series of lines for constant values of $\ell\rho_s/dk_3$ are drawn for the condition $C_D = \ell$ and $\rho = 0.001$ g cm^{-3}. In order to multiply by C_D and ρ a R_e reference line must be added to Fig. B. The $R_e = 10$ line is used as reference. As R_e is a function of ν which is a function of temperature, the $R_e = 10$ lines are drawn for a range of temperature values. The density of air can be taken into account by shifting the reference for the C_D by a factor ρ. To do this a ρ scale is imposed on the $R_e = 10$ line on Fig. A. Now Fig. B

is overlaid on Fig. A so that the C_D lines are parallel to the V_* lines. The ρ value from the scale on Fig. A is matched with the $R_e = 10$ line for the proper temperature from Fig. B at the same time the C_D line for the proper shape is matched with the intersect of d and ρ_s/dk_3 line. The value of V_* corresponds to the $C_D = 1$ line and a point may be plotted where it intersects d. Curves of V_* -- d for any desired hydrometeor can be plotted quite rapidly as Fig. B is slid over Fig. A.

REFERENCES

Gunn, R., and G.D. Kinzer, 1949: The terminal velocity of fall for water droplets in stagnant air. J. of Meteor., 6, 243-248.

List, R., 1960: New developments in hail research. Science, 132, 3434.

Menzel, D.H., 1960: Fundamental Formulas of Physics, Dover Publications, Inc., New York, 236.

Weiselsberger, C., 1943: Airplane body (non-lifting system) drag and influence on lifting system. Aerodynamic Theory, W.F. Durand, Calif. Institute of Tech., Vol. IV, 142.

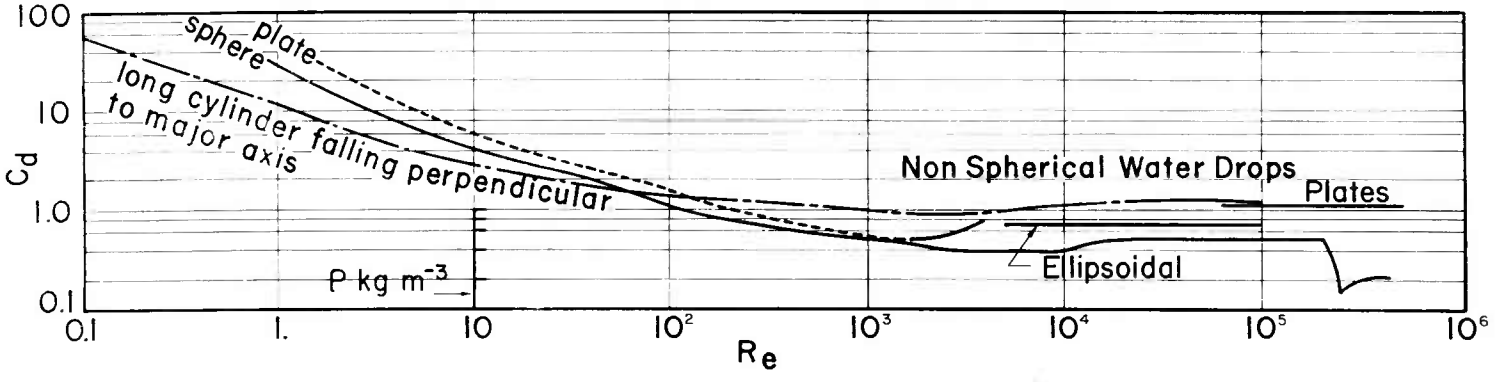

Fig. II-A. DRAG COEFFICIENTS AS A FUNCTION OF REYNOLDS NUMBER FOR DROPS AND CRYSTALS.

ρ scale on Re = 10 line refers to air density and can be matched with temperature on Re = 10 line in Fig. II-B for computing terminal velocities.

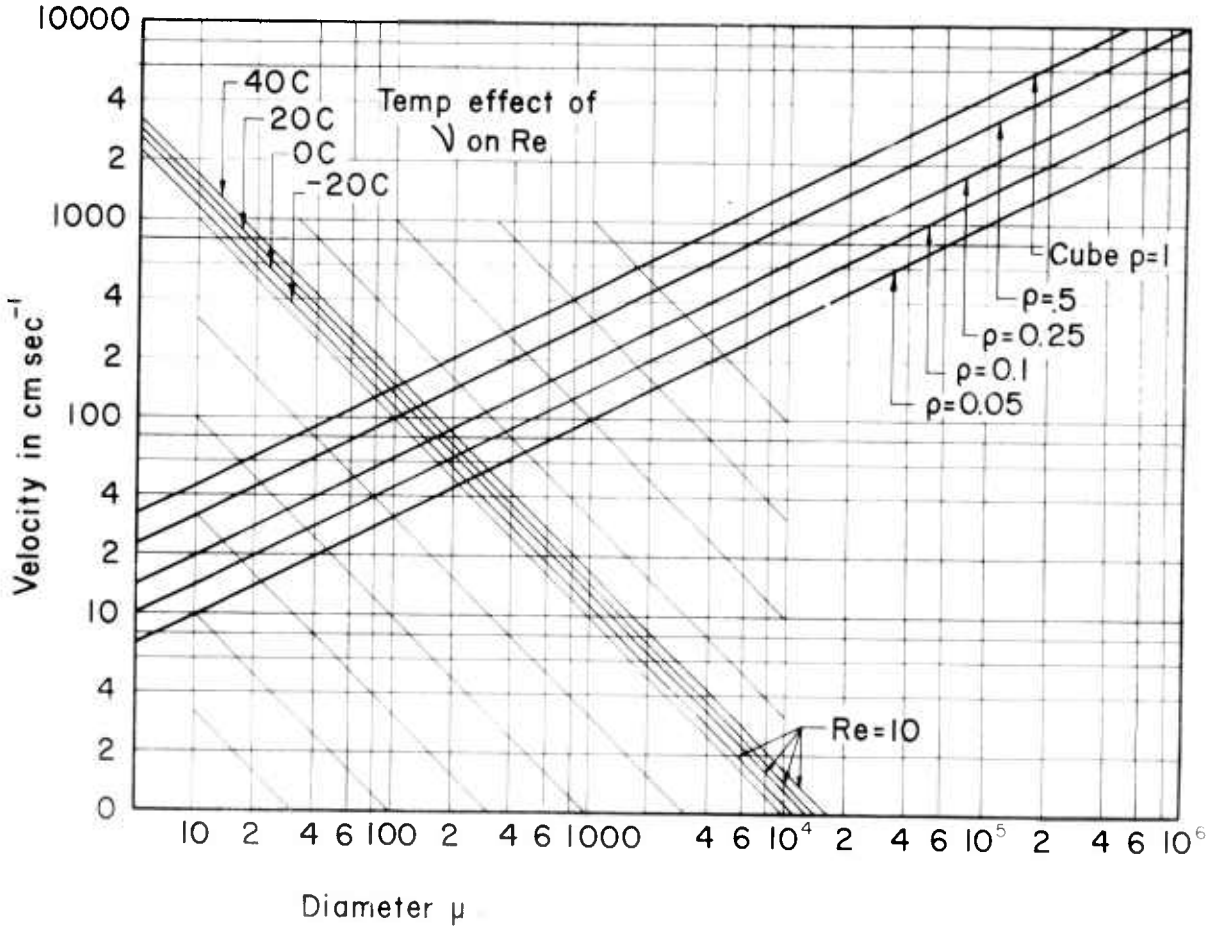

Fig. II-B. TERMINAL VELOCITIES FOR CUBES OF VARIOUS DENSITIES BASED ON THE FICTITIOUS ASSUMPTION $C_d = 1$.

When used with Fig. II-A as described in text, terminal velocities for droplets and crystals can be computed.

Appendix III

BUOYANCY EFFECTS OF HEAT OF FUSION

The latent energy of fusion is released when the water cloud transforms into an ice cloud. As a consequence, a slight increase of cloud temperature and a slight decrease of density is realized. The amount of energy released is controlled by the water content of the cloud which is determined by the pressure and temperature of the cloud base as well as the temperature of ice transformation.

A parameter Φ (in dyne/g) was calculated for a system of clouds with cloud base pressure at 500, 700, and 900 mb and temperature at -20, -10, 0, 10, 20, and 30, while the cloud transformed into ice phase in the temperature range of 0 to -40°C (see Fig. 13 in text).

To obtain the difference in pressure between a cloud which transformed into ice at T_i and a similar cloud with ice transformation temperature of T_i = 1C, it can be evaluated by the integral

$$\frac{1}{g} \int_{p(T_i = 0°C)}^{p(T_i)} \Phi \, dp$$

Should it be desirable to estimate the difference in pressure of a cloud with different temperature of ice transformation, it can readily be evaluated by the integral

$$\frac{1}{g}\int_{p(T_i = 0°C)}^{p(T_{i_2})} \Phi \, dp - \frac{1}{g}\int_{p(T_i = 0°C)}^{p(T_{i_1})} \Phi \, dp \qquad T_{i_2} < T_{i_1}$$

APPENDIX F

CONTINUOUS PARTICLE SAMPLER

By

Paul B. MacCready, Jr.
and
Clement J. Todd

Atmospheric Research Group
and
Meteorology Research, Inc.
Altadena, California

January 15, 1964

ARG64 Pa-117

ABSTRACT

A continuous particle sampler has been developed which captures atmospheric particles in a Formvar solvent liquid film. The Formvar solution completely encapsulates the particle; then as the solvent evaporates the film hardens quickly, preserving a replica of the particle. The method yields exact replicas of ice crystal shapes. Liquid droplets are somewhat flattened by surface tension during replication and so a calibration factor is necessary to ascertain the original droplet size from the replica. This calibration factor has been found experimentally by using spores distributed in the droplets to show the volume of the droplet creating each replica. The sampler provides continuous information on particle concentration, particle sizes, and whether the particles are ice or water. The Formvar solution is ordinarily applied to transparent 16 mm movie leader film, and the replicas are viewed by projecting the film with a stop-motion microscope projector.

Several versions of the instrument have been built and used on cloud physics research aircraft. Special adaptations have been made for ground use: to sample fogs, to measure crystals in a freezing nuclei counter, and to collect snowflakes.

Various design compromises are required in the operational instruments to overcome, over a broad range of meteorological conditions, problems such as those associated with film coating, droplet encapsulation, droplet

migration, and spurious crystal growth. These factors and others associated with particle collection, data reduction, and interpretation are discussed. Examples of the field use of the sampler are given.

1. Introduction

The continuous particle sampler was developed primarily to provide a method for ascertaining quantitatively the coexistence of ice crystals and supercooled water droplets in a cloud being seeded by natural or artificial freezing nuclei. It has turned out to handle this job particularly well, and also perform other valuable related tasks.

The device is a continuous version of the Formvar[1] method developed by Schaefer (1956) for making ice crystal replicas. Its main virtue is that it makes permanent replicas of the shapes of particles which impinge on a liquid-plastic surface. The Formvar plastic solution flows over the particle, completely enclosing it, and then the solution hardens as the solvent evaporates. The encapsulated particle may then evaporate or sublimate away, but its replica is preserved.

In the airborne continuous sampler, the liquid-plastic Formvar-solvent film is put on transparent 16 mm film which is continuously drawn past a slot exposed to the ambient airflow. The Formvar solution then hardens before the exposed portion reaches the take-up reel. Conceptually, the instrument is simple. However, the practical instrument requires that many design compromises be made to give proper coating, proper hardening, and good particle collection and replication.

---

[1] Trade name, Formvar 15-95E, Shawinigan Resins Corp., Springfield, Mass.

The active development of this sampling method has been proceeding for three years, through both the Atmospheric Research Group and Meteorology Research, Inc., with sponsorship by the National Science Foundation, the Army Electronic Research and Development Laboratory[2], and the Naval Research Laboratory[3], as well as MRI. This paper reviews the development, shows the present state of the technique, and considers the numerous interrelated factors on which the technique depends. It is felt that the method has general applicability for studies in which knowledge of the size spectra and particle types of aerosols are needed.

2. Background

In 1961, trials with various droplet collection methods showed that Schaefer's Formvar replication technique could lead toward an operational continuous sampler. An important factor in the development of the system has been the availability of a 16 mm film[4] which would not dissolve in the

---

[2] A first final report "Study and Modification of Convective Storms", MacCready, P. B., Jr., T. B. Smith, C. J. Todd, C.-W. Chien, E. Woodward, Meteorology Research, Inc., to Army Electronic Research and Development Laboratory, Ft. Monmouth, N. J., Contract No. DA 36-039 SC-89066, 1963, gives some details about the sampler and data obtained with it during the summer of 1962.

[3] Final report "Continuous Particle Sampler Study Program", by MacCready, P. B., Jr., and R. E. Williamson, Meteorology Research, Inc., NRL-ONR Contract Nonr-3819(00)(X), December 1963, gives details on many of the items reviewed in this paper, and describes the latest version of the sampler.

[4] Cronar, P40A Leader, Polyester Photographic Film Base, duPont, Wilmington, Delaware.

solvents used (chloroform or ethylene dichloride). This meant that 16 mm film handling methods could be adapted to the sampler, which was a great convenience for the drive mechanism as well as in the subsequent viewing of the replicas.

The first complete sampler system was used successfully in the summer of 1961 on the Atmospheric Research Group Flagstaff studies. In this dipper tank system the Formvar coating was precoated on the leader film, and then softened before exposure by running the film through a solvent bath maintained at a particular level by means of a float valve. System design and some results were presented by Todd (1961).

In the fall of 1961 the unit was taken to a droplet collector comparison conference in France organized by H. Dessens. A miniature wind tunnel, consisting of a tube and a blower, provided the air flow on the ground to substitute for the airplane motion. This device was operated satisfactorily in-cloud on a mountain peak, along with collector equipment of other investigators. The results were given by MacCready (1962).

In the summer of 1962, two improved units were installed on two aircraft, one unit being the precoated film variety, the other using uncoated film and applying the Formvar-solvent mixture just before exposure by means of a coating wheel (see Fig. 1). The coating wheel method seemed the more practical (more controllable, and less likely to stick), and an adaptation of it was used for the 1963 summer measurements (see Fig. 2). Research results for the summer studies obtained with the device have been

Fig. 1. COATING WHEEL VERSION MOUNTED ON A CESSNA 180.

The tank at the bottom contains the Formvar-solvent solution and applies it to the film via the coater wheel. The cylindrical tank above is not used; it was only employed for the dipper tank version. The drying tubes can be seen extending under the wing to give extra drying time before the film reaches the take-up reel. The lips around the exposure slot are heated for de-icing. The supply and take-up reels are both mounted on one shaft.

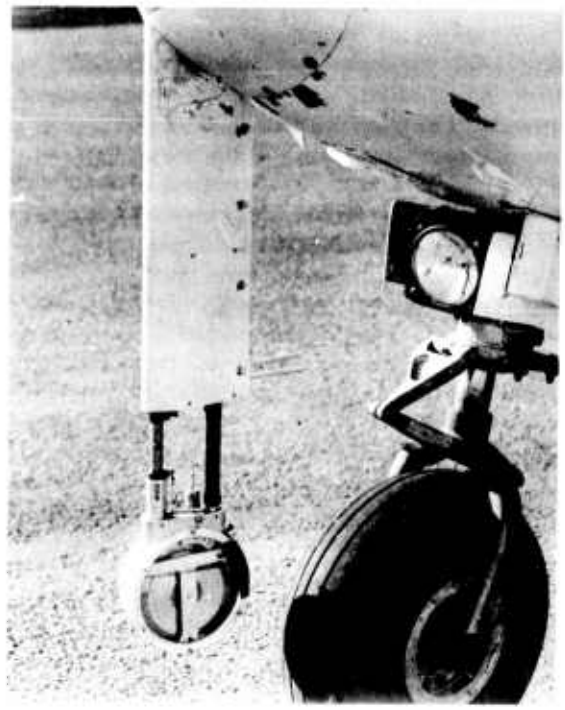

Fig. 2. COATING WHEEL SYSTEM INSTALLED IN THE NOSE OF A TWIN ENGINE APACHE AIRCRAFT.

The drying tubes leading the film from exposure area to take-up reel were electrically heated to stop blushing and spurious crystal growth, and, around the slot, to prevent icing. The drying tubes went into the cockpit area, where a projector showed the replicas on a small screen so as to permit in-flight evaluation.

presented in the MRI report of Footnote #2 and by Todd (1964). Still another coating wheel version (Figs. 3 and 4) was developed in the fall of 1963, utilizing the knowledge obtained from the field studies with the previous units.

Hindman (1964) has presented two versions of continuous sampling by the Formvar method for particles impacting by gravity settling. For one version the particles collected were ice crystals grown from freezing nuclei in a continuous cold box, while in the other case the particles were tiny hydrometeors falling from the ambient air. In either case the particles land on a dry Formvar coating which is subsequently softened during passage through a chamber with chloroform vapor. This is a continuous analog of the vapor replication technique investigated by Schaefer (1962).

Figure 5 gives some representative results of the use of the continuous sampler. Most experience with the technique so far has been derived in summer at Flagstaff, Arizona, in cumulus clouds with rather cold bases.

3. Design Factors and Compromises

The Formvar coating on the film must be soft during the impaction process, and flow readily so as to encapsulate the particle, but still be stiff enough to resist being blown off by the wind, and stiff enough to keep the droplets from clumping together (here called flocculation). The coating hardens as the solvent evaporates. This hardening must not take place before the film passes the slot, but must occur before the film reaches the take-up reel and before the particle size or shape is significantly altered.

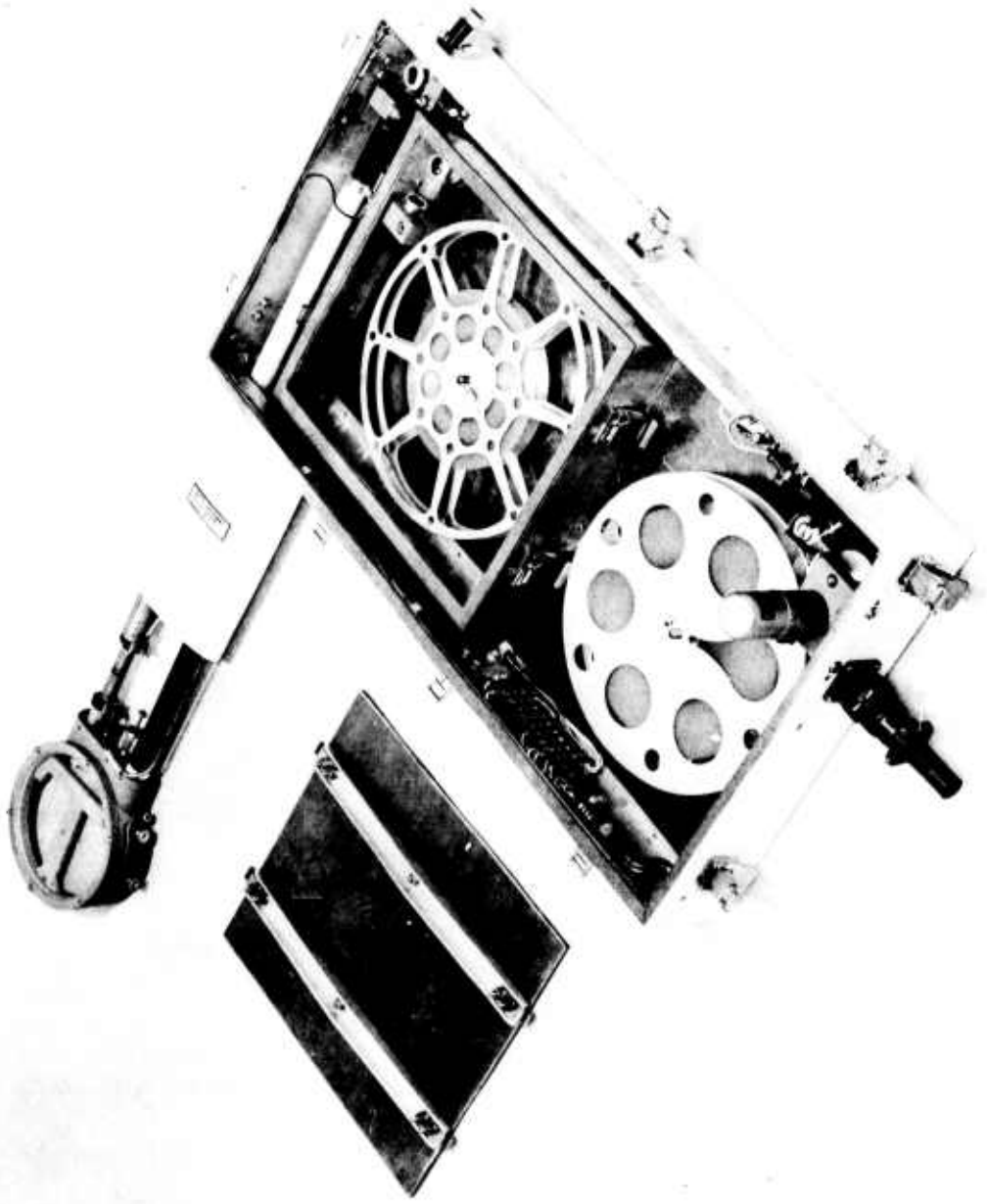

Fig. 3. LATEST CONTINUOUS SAMPLER

This uses the coating wheel principle and heated drying tubes. The supply reel compartment is sealed tightly to prevent air backflow down from the slot which could preharden the coating and also permit moisture from the air to contaminate the tank.

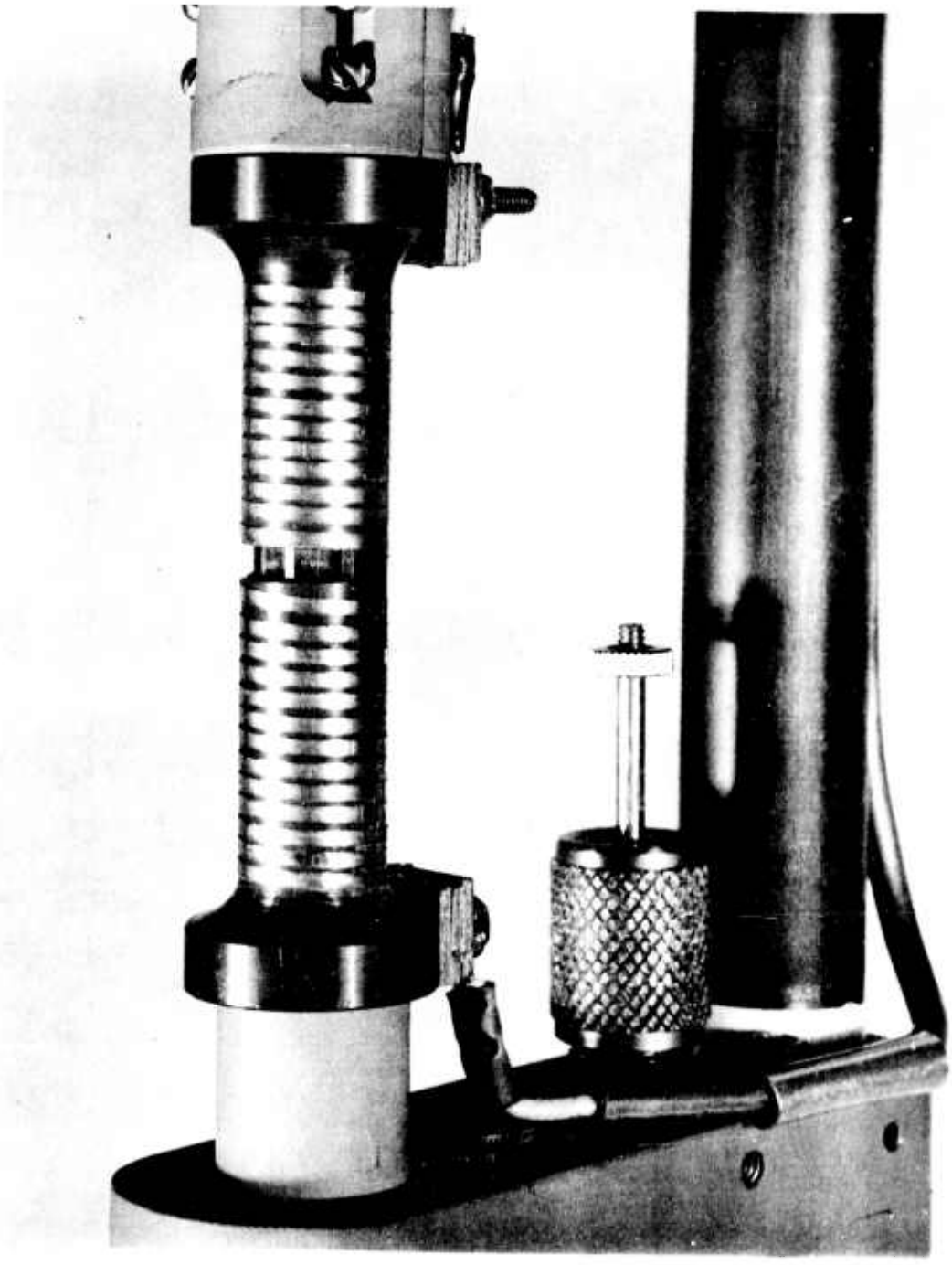

Fig. 4. DETAIL OF THE WINDOW SHOWING THE DE-ICING WIRE.

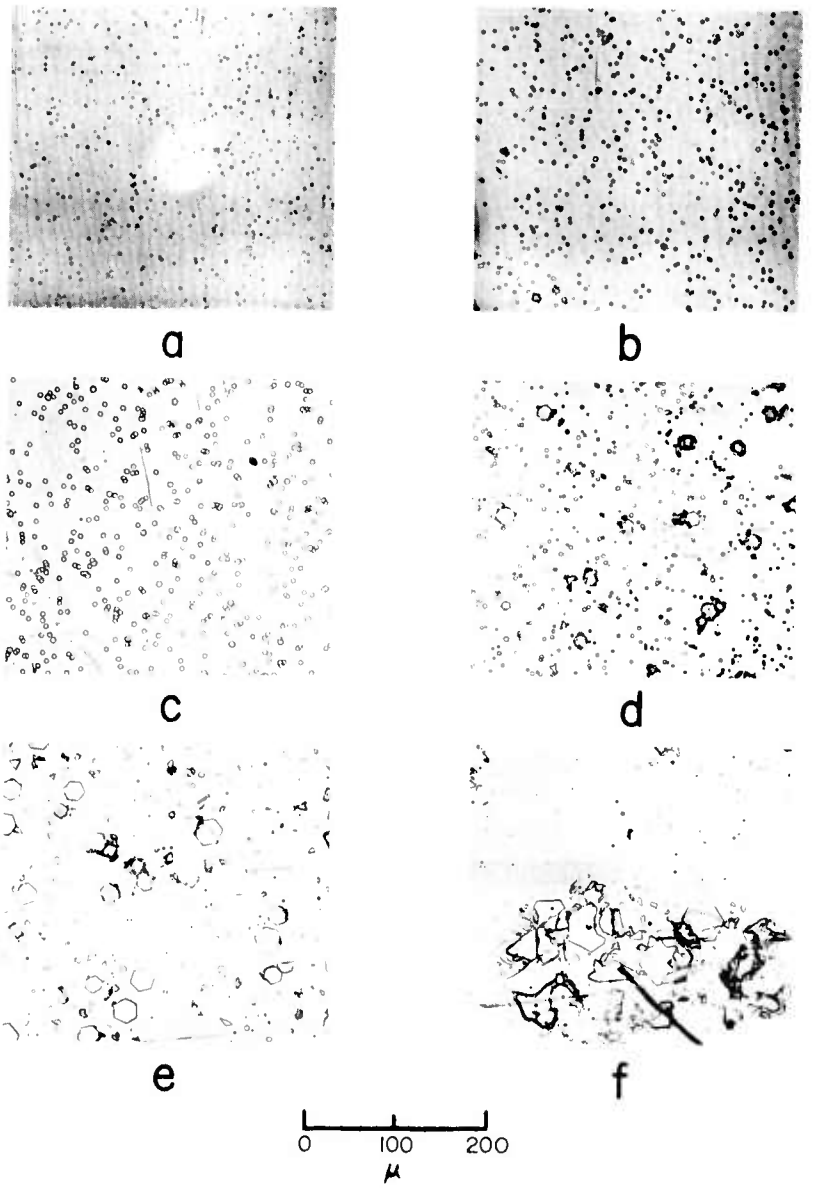

Fig. 5. REPLICAS DURING SPIRAL ASCENT IN THE CORE OF A CUMULUS CLOUD BEING SEEDED WITH SILVER IODIDE, FLAGSTAFF, AUGUST 15, 1963.

a. 5,720 m, -9.8C. Just at cloud base. Small droplets approximately 3μ diameter.
b. 5,735 m, -10.0C. Droplets larger, 5-7μ, 12μ ice crystal.
c. 5,795 m, -10.3C. Droplets to 9μ. Unseeded portion, no crystals.
d. 5,870 m, -11.0C. Crystals and smaller droplets.
e. 6,405 m, -13.9C. Hexagonal, square, and triangular plates, with small droplets.
f. 6,618.5 m, -15.4C. Large cracked and broken crystals.

The evaporation cools the film, and water from the ambient air can condense on the film (here called blushing) or can cause spurious growth of ice crystals. This cooling effect can be eliminated by adding heat to the system, but excessive heat can melt the ice crystal or even evaporate water droplets before replication is complete. These interrelated factors require careful design compromises. The task gets harder as the range of operating conditions is increased to cover higher air speeds and colder temperatures, and the task is further complicated by mechanical problems such as film sticking and elongation of sprocket holes.

Mechanical Coating Considerations. The first continuous cloud particle collector used a method in which the film was precoated and dried in the laboratory, and then the hardened coating was softened by immersion in the solvent dipper tank just before the film was exposed to the air stream. The coating in the laboratory was accomplished with a broad (6 mm wide) slit pen, siphon fed from the Formvar solution supply bottle. It was found that if a solution of at least 6 per cent Formvar was used the coating would not orange-peel or wrinkle during the drying process. In general the thicker solution produced smoother and more uniform coatings.

Considerable effort was expended in attempting to develop a continuous applicator using a wick, but the results were not encouraging. The wick or pad always left a streaked surface, large feed pressures were required in order to produce acceptable coating rates, and the method involved numerous operational difficulties.

The roll-on coating wheel (Figs. 1 - 4) proved to be reliable operationally. In the coating wheel method the moving film is pressed against the top edge of a thin, large diameter wheel causing it to rotate. The bottom portion of a wheel lies in a reservoir of the coating solution, and as the wheel rotates a stripe of this solution is transferred to the film at the point of contact. In practice the edge of this wheel, which is about 3 mm wide, is machined to form a trench on the order of 300μ deep. In order to minimize the deposition of excess Formvar at the edges of the stripe, an adjustable scraper was fitted. This scraper consists of thin, stainless steel blades which are in contact with the perimeter and sides of the wheel and serve to wipe off any excess solution which adheres to these surfaces.

The vapor pressure of the solvents used is very high and any flow of air over the solution surface causes rapid evaporation. To prevent a flow of unsaturated air over the solution, the tank and film magazine portion of the system should be pressurized or sealed so that their atmospheres are in equilibrium with the stagnation pressure (see Fig. 3). This configuration also minimizes hardening of the Formvar solution and evaporative cooling prior to exposure at the window slot.

Coating Factors. Both chloroform ($CH\,Cl_3$) and ethylene dichloride ($C_2H_4Cl_2$), as well as mixtures of both, have been used as solvents for the Formvar. The chloroform is the more volatile solvent, by a factor of 2-1/2 or 3. The melting point of chloroform is -63.5C, while it is only

-35.5C for ethylene dichloride, and thus the use of chloroform is indicated at cold temperatures. Replication with a continuous sampler at -43C has been achieved. The rapid cooling by solvent evaporation during Formvar hardening can be severe with chloroform, and so sometimes the use of ethylene dichloride is preferable.

Ice crystals seem to replicate best with a thin film (minimizing evaporative cooling and making the regulation of heat less critical) and dilute Formvar concentration (which gives the best replica resolution). Such a thin film tends to magnify troubles of skinning over the film before reaching the impaction area, which can have a bad effect on droplet replication and, to a lesser extent, on crystal replication. The conditions which are best for ice crystal replicas tend to permit flocculation of water droplets. Thick concentrations minimize flocculation. Thick film provides less droplet distortion but tends to blow off more in the air stream, especially when of dilute concentration.

It appears from flight tests that, with adequate drying heat, a concentration of between 2.5 per cent and 4 per cent of either solvent in the coater tank is about optimum. When the concentration is less than 2.5 per cent the air stream displaces the coating at relatively low air speeds, except for very thin films (as was the case for Fig. 5). When the concentration is greater than 4 per cent the replication efficiency appears to decrease.

There seems to be a reasonably broad range of film thickness and concentrations for good droplet collection and replication, or alternatively

for good ice crystal collection and replication, with either chloroform or ethylene dichloride. The ranges are extended with careful control of drying heat. There is a much more limited range of film thickness and concentration for good simultaneous collection and replication of coexisting droplets and crystals. Both droplets and crystals have been obtained at once with thin 1 per cent ethylene dichloride (used for samples on Fig. 5), and on other occasions with thicker film of 2-1/2 per cent chloroform (65 per cent) and ethylene dichloride (35 per cent) mixture. More field tests are required to show if the ranges for collection and replication of both droplets and crystals are so critical that a dual instrument would be needed for reliable field investigations.

Neither the drive motor nor the rest of the electrical system may be considered spark-proof, and therefore, in order to eliminate the possibility of what could be quite a violent explosion, it is recommended that a non-inflammable solvent such as chloroform be used rather than the ethylene dichloride. Since the chlorinated hydrocarbons and in particular chloroform are toxic and their effect is to some extent cumulative, the equipment should be mounted and vented in such a way that personnel are not exposed to sensible concentrations of vapor.

Blushing and Ice Crystal Growth. Blushing and spurious ice crystal growth can be completely controlled by using heat at the window and along the drying tubes. Even without heat, very thin films have provided good crystal replicas because the total amount of solvent causing evaporative

cooling is small. The particles put on the film by blushing are small, on the order of 1 or 2μ, and often irregularly shaped. The larger droplet replicas can be evaluated even in the presence of blushing except in severe cases. Blushing is not a problem when droplets are replicated with Formvar solution on a glass slide, presumably because the thermal inertia of the slide keeps the temperature up. This thermal inertia effect is not easy to apply in the continuous sampler.

Flocculation. Flocculation is the term used to describe the adhesion of several droplets to one another beneath the Formvar film. Flocculation has been most frequently observed when thin, low percentage solutions are employed, and when the droplet diameters are greater than the thickness of the coating. Considerable flocculation can occur apparently without coalescence, and so the droplet size and concentration information is not lost by flocculation.

High Aircraft Speeds. The coater system replicated reliably at speeds up to 80 m per sec. High speed can result in partially blowing off the liquid film; speed is also sometimes associated with the presence of bubbles in the film; and speed intensifies the problem of film hardening prior to reaching the exposure slot. All these effects are minimized by the use of a narrow (in the film movement direction) window slot rather than a wide one. The slot width and film speed (often 5 to 20 cm/sec) are adjusted to keep the number of droplets collected, in clouds with the maximum liquid water contents, down to where flocculation or overlapping of droplets is

statistically insignificant. It has proved advantageous to seal the supply reel to prevent large air flows from the slot along the tube toward the supply reel (see Fig. 3). This minimizes prehardening of the film, and avoids putting contaminants from the ambient air in the coater tank. For high speed aircraft it is likely that the best technique for sampling would be to introduce a diffuser to slow the flow at the window slot, although this would complicate the collection efficiency calculations.

4. Absorption and Evaporation of the Vapor

From the foregoing discussions it is apparent that vapor softening of a precoated Formvar film might be desirable, to permit more quantitative control of the film characteristics and to avoid the complexities of dipping or coating the film in flight. Therefore simple tests were conducted to provide some data on the rate at which precoated film can be softened by vapor. Chloroform vapor was used because it has a much higher vapor pressure than ethylene dichloride at any given temperature. The same laboratory setup used for the absorption tests served to give information on the evaporation rate of the chloroform from the Formvar-chloroform film.

A short piece of film with a precoated Formvar strip on it was suspended from a sensitive analytical balance down in a cold chamber at -20C. A vapor chamber (a container lined with chloroform-soaked blotters) was kept at a given warmer temperature, say -11C, and then placed around

the film. The rate at which vapor was absorbed was noted. For the evaporation tests the vapor chamber was withdrawn and the weight decrease noted as a function of time. Figure 6 gives the absorption results for a thin coating about 2μ thick. It is evident that the absorption takes place in two regimes: a) the first 30 seconds, during which the rate depends almost directly on the initial temperature difference between film and ambient air, and b) the period after 30 seconds when the rate is slow and is rather constant no matter what the starting temperature. During period (a) presumably the film is much cooler than ambient. During period (b) presumably the film temperature is close to the vapor chamber ambient temperature.

The results point out that the rapid absorption of vapor will take place only if the vapor is substantially warmer than the film on which it is to condense. Extrapolating from the figure, it is possible that dry Formvar 1μ thick could be softened sufficiently in 30 seconds by the vapor method if the vapor-film temperature difference were kept at 30C. Thus the vapor softening technique may be feasible for a continuous sampler, but it will not be particularly convenient.

The tests showed that the initial absorption rate for 5μ film is about the same as for the 1μ film, although both eventually will reach the same concentration with the thick film absorbing more solvent. Thus the thinner film will reach a particular softness much more quickly than will the thicker film.

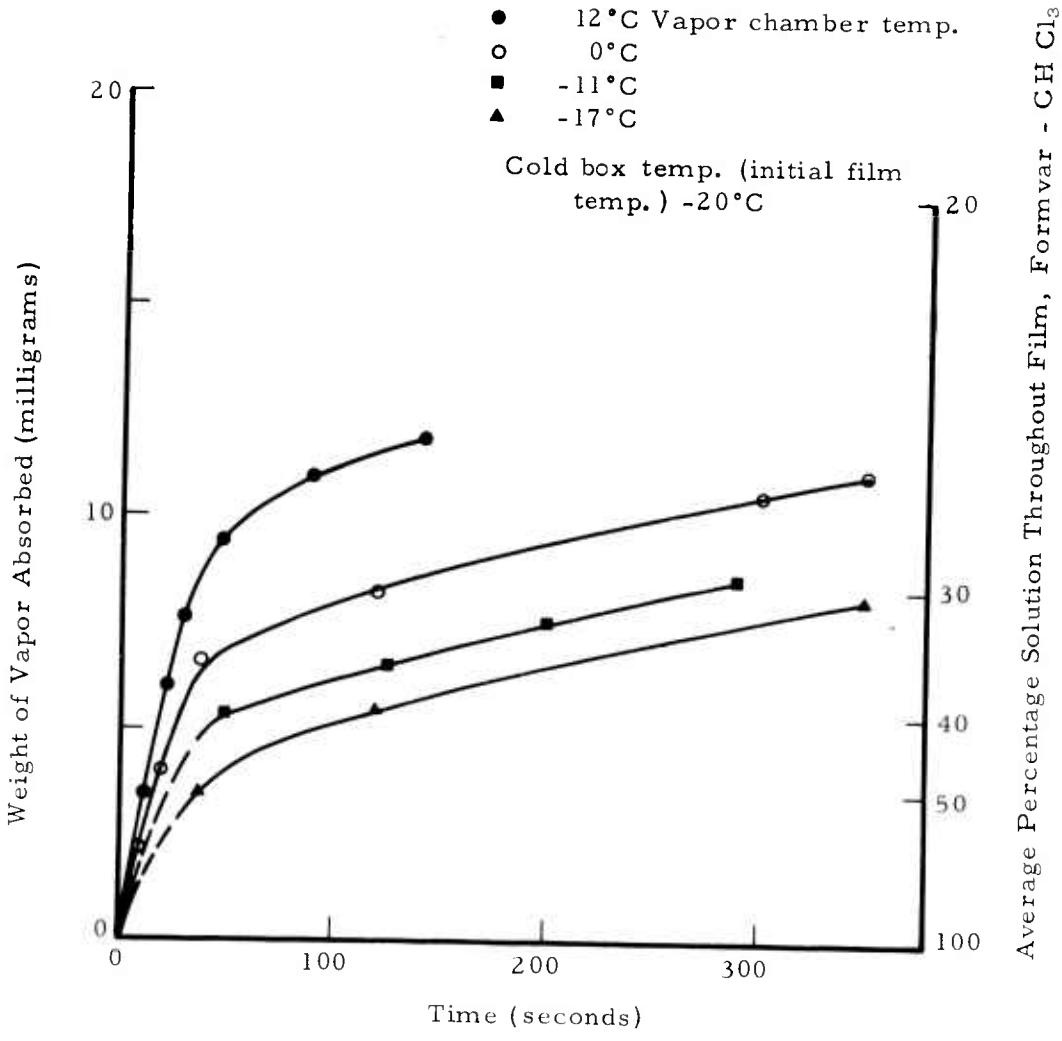

Fig. 6. $CH\,Cl_3$ VAPOR ABSORPTION INTO FORMVAR (1%)

The evaporation rate test results proved to be virtually mirror images of the absorption tests. They thus verified that thin film will stiffen much more quickly than thick film. The data suggest that the vapor pressure of the ambient air must be kept low (presumably by ventilation) when rapid evaporation is desired.

5. Droplet Distortion

When an ice crystal impacts on the softened Formvar film, the subsequent replica is a perfect, hollow, three-dimensional casting of the crystal in the Formvar. If the impacting particle is a liquid droplet, the situation is much more complex because the droplet will distort. The Formvar will still encapsulate the droplet (probably in a millisecond for small droplets), the solvent will evaporate and leave a Formvar replica, and the droplet will eventually disappear by evaporating through the thin Formvar skin. However, the exact shape the droplet assumes will depend on the original spherical droplet diameter, the thickness of the Formvar coating, and the surface tensions of the Formvar solution to air and to water. As the solvent evaporates, the Formvar coating thickness changes, and the surface tensions change as the Formvar solution gets denser (and the solution concentration will get denser more quickly in the thin skin over the droplet than in the main film). These varying factors will keep readjusting the droplet shape until the Formvar solution viscosity increases to the point where no further shape change will take place (the Formvar

gets so viscous it is effectively solid). For the practical utilization of the continuous sampler it is essential to establish the calibration factor, replica radius divided by original droplet radius, for various conditions of film thickness, film material, and droplet size.

In the foregoing it has been assumed that the droplet and solvent do not merge with each other. Actually the solvent may dissolve in the water to the extent of about 1 per cent of the water mass. Thus an indeterminacy in true original droplet mass can arise, but the amount is negligible compared to other errors associated with the measurement and correction of droplet diameters.

A mathematical calculation of the distortion of the droplet was made, by equating surface tension energies, based on a very simple picture: the droplet, originally spherical with radius r, falls into a Formvar solution of thickness h, and is distorted to an elliptical cross section with semi-major axis a and semi-minor axis b; the Formvar skin or cap which coats over the top of the droplet has radius c. These relationships are shown in Fig. 7. In the actual case the droplet is flattened but not in such an ideal oblate spheroid shape, and the Formvar solution and Formvar cap skin have varying strengths as the solvent evaporates.

When the spherical droplet, with surface area S_S is distorted into the oblate spheroid shape, its area will be increased to S_E and energy

$$\gamma_{F/W} (S_E - S_S)$$

will have to be added. $\gamma_{F/W}$ refers to the surface tension of the Formvar

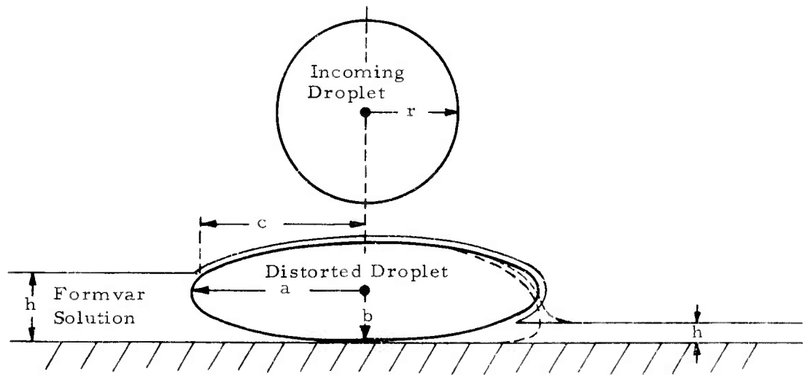

Fig. 7. SIMPLIFIED MODEL OF THE DISTORTED DROPLET.

The left side of the picture gives the case for $h > b$, while the right side of the picture gives the case for $h < b$. For $h > 2r$ the droplet is entirely beneath the flat Formvar surface, $c = 0$, and the droplet remains spherical so $a = b = r$. The dashed lines show a more realistic shape of the droplet and Formvar solution, but a shape which is more difficult to treat mathematically.

solution with respect to water. The energy available to cause this distortion is considered derived from raising the Formvar skin which flows over the top of the droplet. The film which originally had area A_c is distorted into a cap which has area S_T, and so the energy is

$$\gamma_{F/A}\,(S_T - A_c)$$

$\gamma_{F/A}$ refers to the surface tension of the Formvar solution with respect to air.

Equating the energies,

$$\frac{\gamma_{F/A}}{\gamma_{F/W}} = \frac{S_E - S_S}{S_T - A_c}$$

The ratio $\gamma_{F/A}/\gamma_{F/W}$ was measured for some Formvar-chloroform solutions. It reaches a peak of 1.4 at 2 per cent, and decreases to 0.4 at 10 per cent; it is presumed to be somewhat lower at the more pertinent higher concentrations. $(S_E - S_S)/(S_T - A_c)$ was computed as a function of the desired r and the measurable h and a. A computer assisted in the rather complex calculations required. The results cannot be deemed quantitatively informative, due to the oversimplification of the picture on which they are based, as well as due to a lack of accurate knowledge of the $\gamma_{F/A}/\gamma_{F/W}$ ratio for very thick solutions. Nevertheless, the calculations do show that the correction factor a/r does depend on the surface tension ratios $\gamma_{F/A}/\gamma_{F/W}$ but that for normal values of $\gamma_{F/A}/\gamma_{F/W}$ the dependence is not very strong. The computations also served to assist in understanding the results of the absolute calibration study.

The method chosen for a rough absolute calibration was an adaptation of the one employed by Farlow and French (1956). It provides for the simple and rapid determination of micro-drop volumes by the inclusion of uniform size solid particles in the water drops. The principle involves the use of a suspension, in water, of solid particles of uniform size. If the suspension is vigorously stirred, any small droplet will contain the same concentration of particles as the suspension from which it originated, and so the original droplet volume can be estimated from the number of particles observed in the replica.

Several types of inorganic particles were tried, but they either dissolved or had too broad a size spectrum. A survey of available natural particles led to the selection of the spores of the common mold, aspergillus niger. The density of the particles is greater than that of water but the particles are practically insoluble in chloroform-Formvar solutions. The particles were quite uniform with a diameter of about 3μ. The spores were shaken from the mold and placed in suspension in distilled water. The stock solution was vigorously stirred and maintained in the bath of an ultrasonic cleaner. Some of the stock solution was aspirated at the window of the coater system equipment, with an air speed of about 35 meters/sec. Because of the small quantity of the stock solution only two test runs were possible, one run on a solution of 3.5 per cent Formvar-chloroform and one on 6 per cent Formvar-chloroform. The thickness of the dried coating of Formvar (h_f) from these two runs was arrived at by averaging many readings of a

micrometer screw gauge and also by deducing the thickness by gravimetric procedures (10μ for the 3.5 per cent solution, 23μ for the 6 per cent solution). The original volume of the droplet was taken to include that occupied by the particles. A total of 320 counts were made for calibration of the stock solution. The concentration of particles per unit volume in the stock solution was determined by means of a hemacytometer. Somewhat over a hundred counts were made for calculation of replica droplet volume. Counts were averaged for replicas having the same diameter. The small number of replicas counted was due to the poor yield of usable sizes stemming from the crudeness of the aspiration equipment and the small volume of calibration suspension produced. The probable error for computations of volume from single points on the presented curves must be considered to be slightly over 20 per cent based upon the mean deviations of the experimental data, however the apparently good fit of the curves indicate that this might be pessimistic. The results are presented on Fig. 8.

Consideration of Fig. 8 shows an important point, namely, that the curve for the 6 per cent solution and the curve for the 3.5 per cent solution are about the same when plotted in terms of r/h_f or a/h_f. Such a plot has been made as Fig. 9. As would be predicted from the model discussed previously, for $a/h_f < 0.5$, the droplet is entirely below the surface and is undistorted, $a/r = 1$. For larger droplets there is distortion and $a/r > 1$. Both the 6 per cent curve and the 3.5 per cent curve are the same, to within the accuracy of the measurements on which they are based. One would

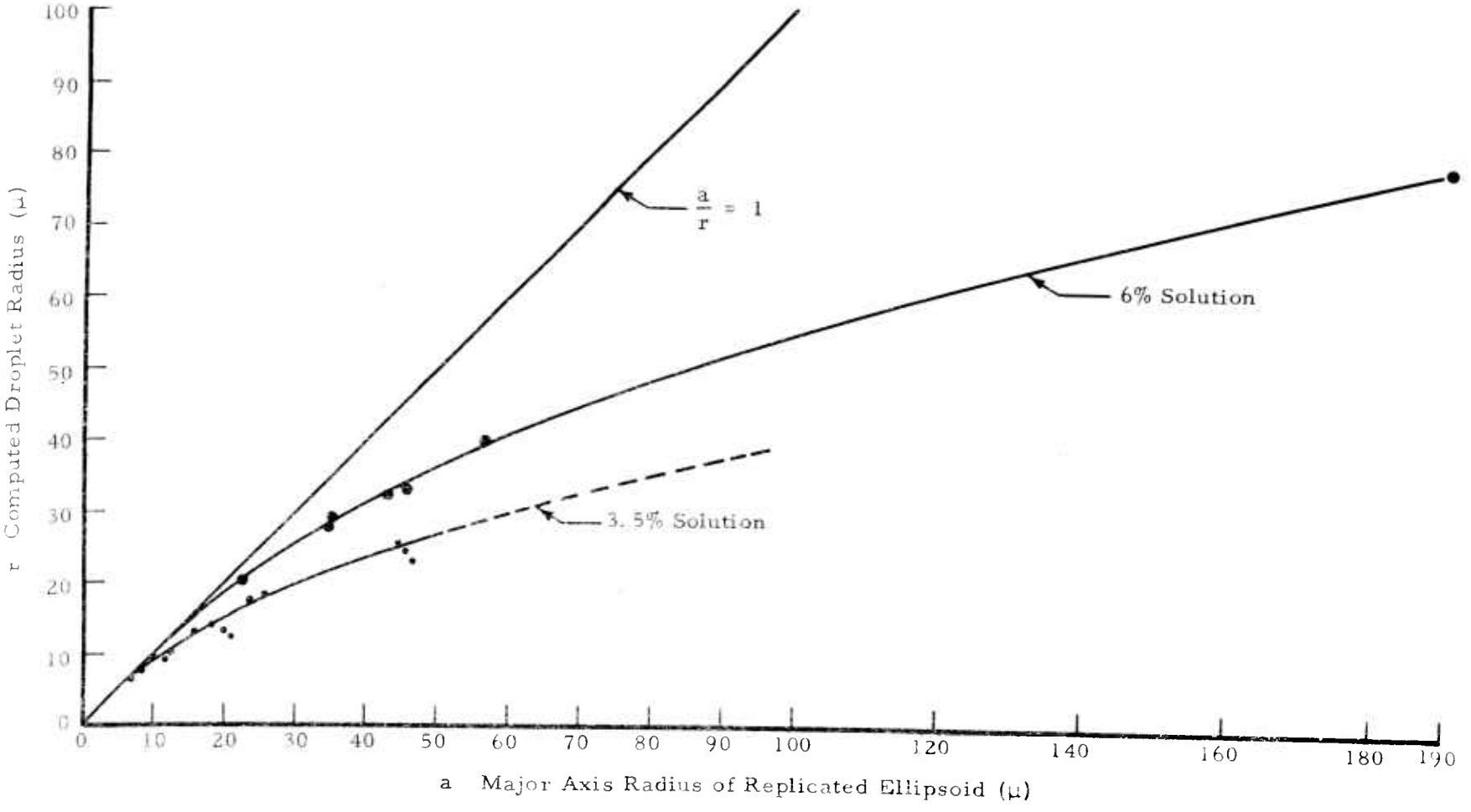

Fig. 8. DISTORTION CALIBRATION WITH ASPERGILLUS NIGER SPORES.

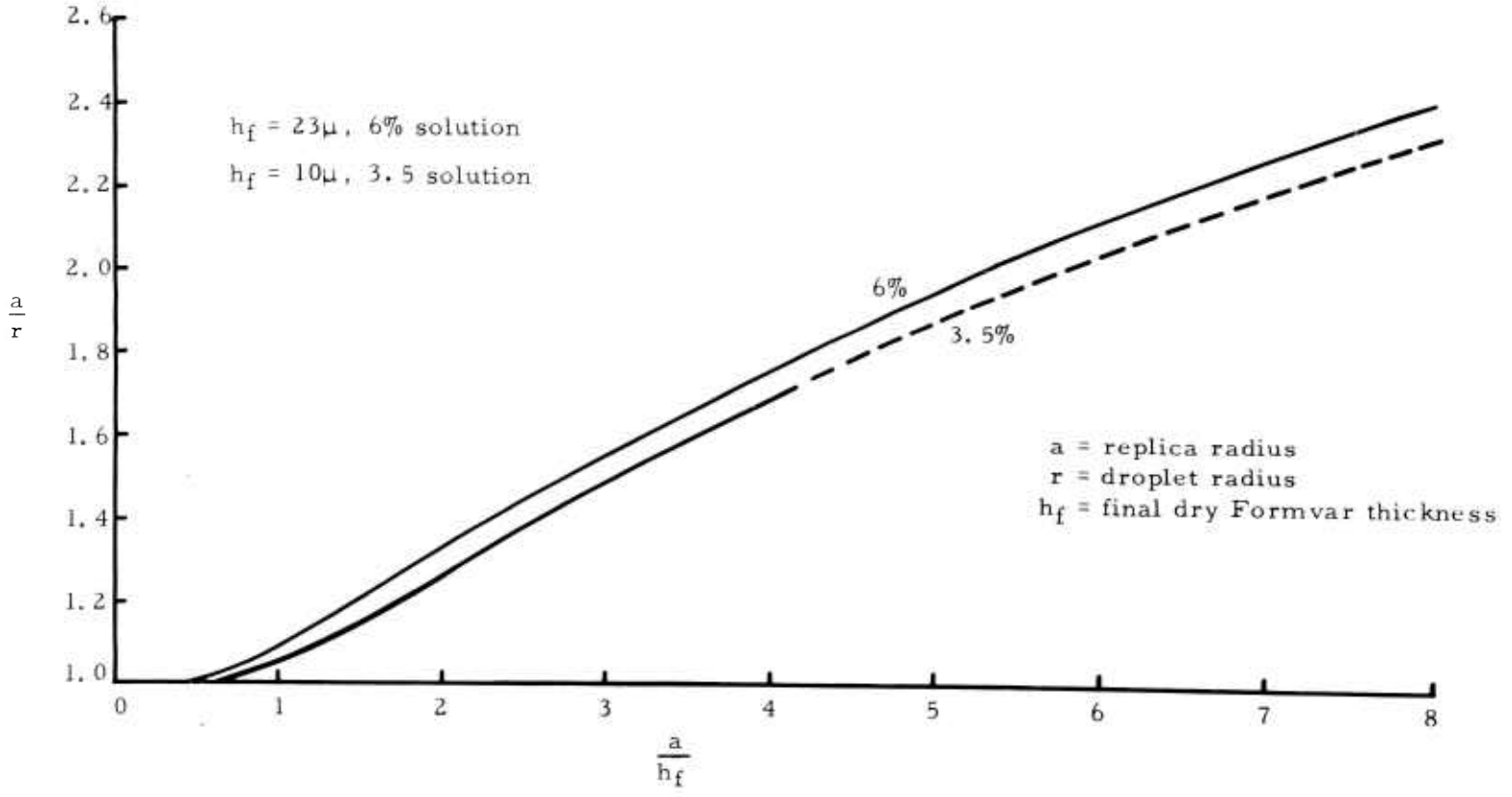

Fig. 9. CALIBRATION FACTOR RELATED TO DRY FORMVAR THICKNESS

hypothesize that, as a reasonable first approximation, the same relation holds for other Formvar solution concentrations.

The curves for various concentrations will be a unique function of a/h_f only if the original wet solution thickness is of no importance. Apparently the final shape of the droplets is determined by droplet size and the Formvar solution details after the solution has evaporated until it is considerably more concentrated than 6 per cent. Therefore the initial concentration is of no concern (except for other problems such as film coating, complete encapsulation, flocculation, blushing, etc.).

When the calibration factors shown on Fig. 8 were examined with respect to the theoretical computations on distortion, another factor became evident. For thick films, where a/h_f is not much larger than unity, the final distortion is in agreement with theory for rather low $\gamma_{F/A}/\gamma_{F/W}$ ratios -- ratios which imply a very thick solution from which almost all the solvent must have evaporated. This will of course come about because until the concentration of the evaporating film is thick, the film thickness will exceed the spherical droplet diameter. For thin films (or large droplets) where a/h_f is large, the final distortion is in agreement with theory for higher $\gamma_{F/A}/\gamma_{F/W}$ ratios -- ratios which imply a rather thinner solution. It is presumed in this second case that the Formvar cap gets stiff, from evaporation, rather quickly; thus the shape and hence the calibration ratio a/r is determined by the stiff cap while the main solvent film is still not very stiff.

The mean curve of Fig. 9 can be considered as the basic calibration for chloroform solutions of any starting concentration. In a practical case,

h_f can be measured from the film and then Fig. 9 used to find r for the values of a encountered. In actual use, h_f will be found to be rather constant, and so from Fig. 9 a family of curves resembling those of Fig. 8 can be derived. From this plot, r can be read off directly from a on the appropriate concentration line.

The absolute calibration has been done only for chloroform solutions. For ethylene dichloride, one calibration is available from MacCready (1962). For the droplets studied, a = 15μ, and r = 10μ, a/r = 1.5. The film thickness was estimated at 10μ. If it had been 6μ, this point would fit perfectly on Fig. 9. The ethylene dichloride would be expected to have a somewhat different calibration than the chloroform, because of the differing surface tension ratios, but the theoretical calculations imply that the effect should not be large.

For very thin films the droplet distortion should vary only slightly with film thickness. This is consistent with the physical picture shown by the dashed curve in Fig. 7. Observations of replicas on a film with varying thickness (from uneven coating) implied that the replica size at the thinnest portions was not much greater than that where the film was thicker. This would suggest that a/r does not increase indefinitely with a/h_f on Fig. 9, perhaps reaching a limit below 3.

6. Size Ranges

The small end of the size range of particles which can be treated by this sampler depends essentially just on collection efficiency. In all the

versions of the continuous sampler, as shown in Figs. 1 through 4, the film is curved around a longitudinal axis and fits snugly behind the slot. Thus to a first approximation the collecting surface represents a section of a circular cylinder, and so its collection efficiency can be computed from the curves presented by Langmuir and Blodgett (1945).

To illustrate typical values, Fig. 10 shows the collection efficiencies computed for conditions which were representative of those on the Flagstaff cumulus studies. The curve for the stagnation point of the 1.2 cm diameter cylinder is one actually used in data reduction; the other two curves demonstrate the differences caused by using a larger cylinder or considering the whole cylinder rather than the stagnation point. Normally the particles are counted near the center of the film, near the stagnation point. When low concentrations of ice crystals are being detected, sometimes a much greater width of the film is used to increase the sampling volume. Ice crystals do not have spherical shapes and so for them a simple collection efficiency curve such as on Fig. 10 is not appropriate. However, by far the majority of ice crystals in natural clouds have sizes for which the collection efficiency is greater than 0.8, and so the exact curve used for them is not important.

Fig. 10 indicates a practical lower limit of 3μ diameter for droplets collected by the units as presently used. Figure 5 shows particles at about this size limit. A smaller diameter collector or higher air speed would permit small particles to be collected; 1 or 2μ diameter seems a practical limit for future designs.

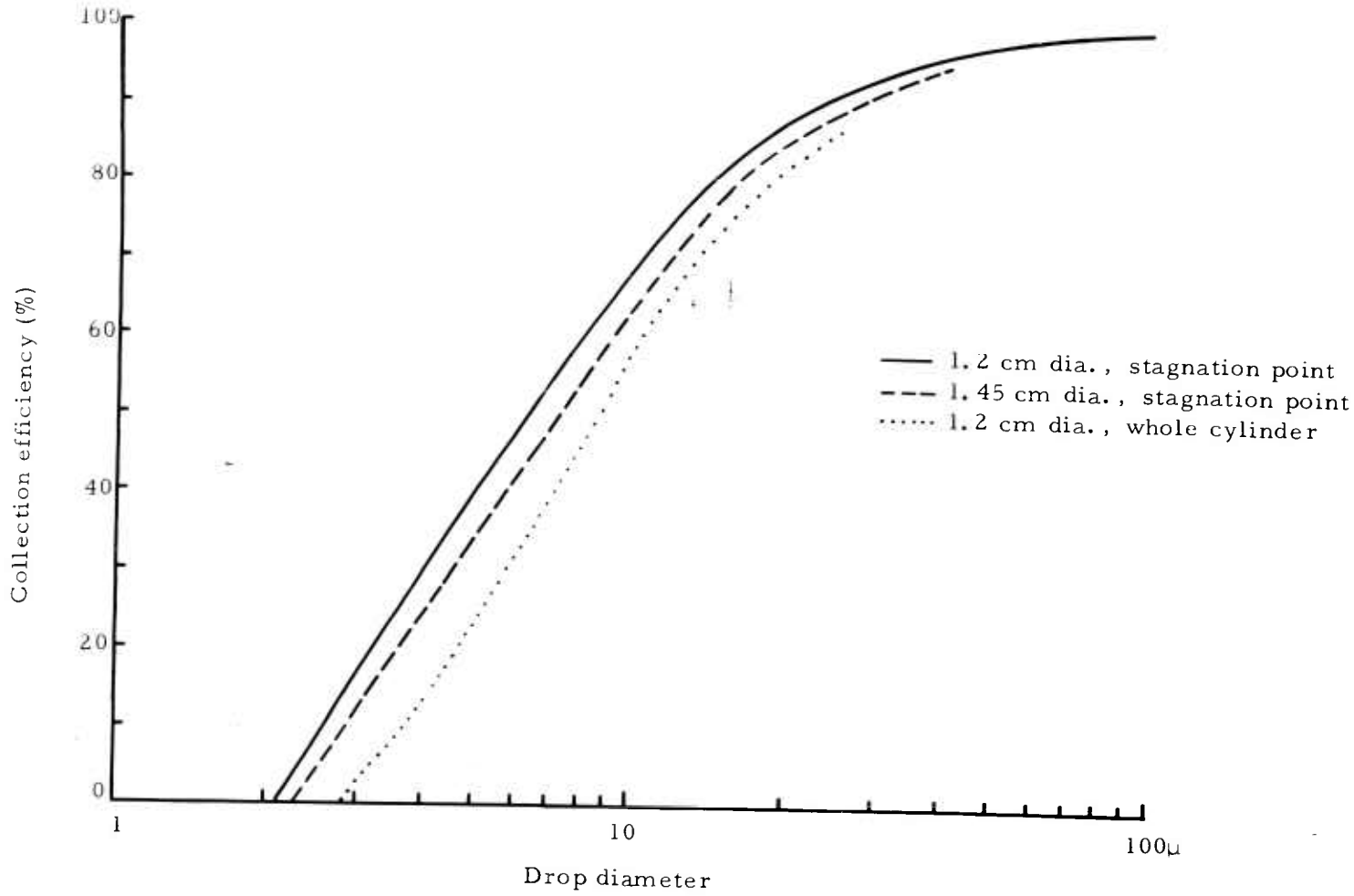

Fig. 10. COLLECTION EFFICIENCY FOR DROPLETS IMPACTING ON A CYLINDER.

Curves representative of conditions at Flagstaff in summer cumulus clouds: true air speed 50 m per sec, temperature 0°C, pressure 500 mb.

The large end of the size range depends primarily on breakup during collection. Ice crystals of 100μ may be cracked and 200μ crystals broken (see Fig. 5); ice needles as long as 600μ have been collected unbroken. When a graupel pellet hits the film the replica has the appearance of a snowball which has struck a windshield; the number of graupel pellets can be counted, but the size of each is difficult to interpret.

Circular droplet replicas of even 150μ diameter have been found on the film. The size of the corresponding droplets is not known, because the size correction factor for such extremes has not been found, but possibly the impinging droplet was on the order of 50μ diameter. In the ground measurements in France (MacCready, 1962) replicas larger than 25μ diameter were not completely encapsulated, leaving a hole in the replica center. The maximum size having complete encapsulation must vary with concentration, but in any case the correction factor for the largest droplets will probably be somewhat indeterminate. Rupe (1950) found that the formula:

$$\text{diameter (microns)} = \frac{1725}{\text{impact speed (m/s)}}$$

gives the largest size of a droplet which would not break on penetrating a kerosene surface. At 50 m per sec this corresponds to a diameter of 34.5μ. Weickmann (1953) found the constant in the above formula to be increased by an order of magnitude for collection in castor oil. From considering and viewing many of the records from the continuous sampler,

it seems likely that droplets under about 50μ diameter are unbroken, and perhaps this is true even for substantially larger droplets.

7. Data Reduction

It has turned out to be most convenient to analyze the film by projecting it on a screen with a modified version of a standard stop-motion projector. For counting large particles such as big snow crystals and graupel the standard 16 mm projection lens system is used. For counting and examining small particles the lens system is replaced by a tube with the optics system from a microscope, usually set at 500 or 1000 power.

The main problem is to cope with the large amount of data generated each flight. At the present stage of development of the system, automatic data reduction of these replica records does not yet seem justified. Some of the droplet records are of a quality for which automatic counting and sizing would be possible, but manual methods can give concentrations and spectra quickly and without intricate apparatus. Human interpretation is necessary during data reduction of complex snowflake replicas and of poor quality droplet replicas.

The film records are first examined crudely by running them through at 16 frames per second. The eye and mind react quickly enough to ascertain the general distribution of drop sizes, the presence of ice crystals and graupel, and the general quality of record.

The next step for general cloud studies is to get the concentrations of droplets and crystals and the general size ranges. These counts can be

made rapidly from representative frames. The droplet counts must be corrected for droplet distortion, and then the collection efficiency factor used to determine true concentration. These corrections are especially quick to apply when the droplet spectra are narrow. To facilitate correlating these data to the other cloud parameters recorded on an analog chart during the airplane traverse, it has proved convenient to plot the data on a chart driven from a gear on the projector. The gear ratio is adjusted to put the particle information on the time scale of the cloud parameter records. When the sampler is run in the aircraft, three event markers on the cloud parameter chart record every 1, 10, and 100 rotations of an idler wheel on the film. Thus the sampler data can easily be exactly correlated to the cloud data.

For detailed case studies complete size spectra and accurate concentrations are required. A data compilation technique worked out by the second author which has proved simple and effective is to move a strip of paper around the projected frame, putting the strip's left edge on the left edge of each replica image and making a mark on the strip at the right edge of the replica image. Then the dots are counted in the size categories, to provide spectra after the droplet distortion and collection efficiency corrections are applied. Rather than recording complete spectra it is often satisfactory to record only the concentration and the mean and standard deviation of the distribution. Obtaining the standard deviation is facilitated by putting a micron scale vertically on the strip (perpendicular to the droplet

size scale which goes horizontally from left to right). Then slide a probability scale down the strip, with the 50 per cent cumulative probability line matching the horizontal position of the median droplet. Mark the strip at drop sizes corresponding to various cumulative probabilities, and make a best fit line through these points. Read off the micron size of one standard deviation (50 per cent to 84 per cent or 50 per cent to 16 per cent cumulative probability).

8. Conclusions and Recommendations

The unique value of the continuous Formvar collection principle has been established over the last three years of development. In its most efficient form, it collects solid and liquid particles in a manner which permits relatively easy analysis. Some collection scheme such as this seems to be the only satisfactory approach to measuring small ice crystals on cloud physics research programs; the shape of the crystals is desired, as well as size (which must be defined with respect to shape) and concentration. For droplet measurements, the Formvar technique is good but some other optical method is a possibility. The optical method, light scattering or light shadow, measures the droplets in the air, avoiding some collection efficiency problems as well as avoiding droplet distortion and breakup on a surface; also in some cases the data acquisition is electronic and so further data reduction is unnecessary. The continuous collector is simpler than optical methods, and convenient to carry in small vehicles. In

summary, the measurement of ice crystals apparently requires the continuous collector, and the same device is effective for droplet measurements Although competitive systems are a possibility.

The most basic problem with the continuous sampler is that, although in final form the device is relatively simple, it is based on many complex factors and interrelationships (nonlinear viscosity and surface tension variations in coating and encapsulations, various contradictory requirements for rapid evaporation of solvent without blushing or crystal melting, etc.). From the development studies it is apparent that all of these practical problems are solvable, because all have been solved at one time or another. The difficult matter is to find a compromise which solves them all simultaneously over a broad range of atmospheric situations with adjustments which are not impractically critical.

Experience with the present units of course has created ideas of how future designs can be improved. One suggestion to make the design requirements less critical is to give the film two separate parallel coatings, one of a type optimized for droplet collection, the other optimized for crystal collection. It would appear that the technique of vapor softening of precoated film warrants further consideration.

Any system, whether substantially new or merely an adaptation of the present one, requires a series of systematic tests at various air speeds and ambient temperatures with various solution concentrations, with various amounts of drying heat, for collecting both crystals and droplets. A final

version, if made to cover a wide meteorological range, will have controllable heaters (initially controlled manually, later automatically).

The simple counting techniques associated with projecting the film by a stop-motion 16 mm projector and counting by hand have worked well. Even quantitative measurements take only a few minutes per frame, a time which is so short that the development of automatic techniques to cut down the time is hardly justified now.

The absolute calibration technique described in this report shows that one of the primary questions pertaining to this collector method has been solved in principle. More detailed calibrations using the same method should be made, including tests at various temperatures and Formvar concentrations.

Acknowledgments

The initial development of the continuous sampler and the continuity for its continued development were made possible by the support extended to the Atmospheric Research Group by the Atmospheric Sciences Section of the National Science Foundation (Grant 11969). The laboratory studies and development of the latest unit were sponsored by the Naval Research Laboratory (Contract Nonr-3819(00)(X). Mr. Robert Ruskin of NRL has been particularly helpful in the cooperative phases of the work. The program has been materially aided by concurrent sponsorship of cloud physics studies at MRI using and developing this type of sampler by the

U.S. Army Electronics Research and Development Laboratory (Contract DA 36-039 SC-89066). Some of the development was sponsored by MRI internal research funds.

Many ARG-MRI people have participated actively in the development of the continuous droplet sampler. Mr. J.A.K. Lake handled the development of the early versions of the sampler; Mr. R. Sloane developed the computer program associated with the theoretical distortion calculations and did much of the laboratory work on materials; Mr. E.E. Hindman, II, aided in the laboratory investigations and had primary responsibility for the operation of the collectors at Flagstaff in 1962 and 1963; Mr. R. Williamson completely handled the absolute calibration procedure and the design of the latest mechanical unit.

REFERENCES

Farlow, N.H., and F.A. French, 1956: Calibration of liquid aerosol collectors by droplets containing uniform size particles, J. Colloidal Science, 11, 21, 177-183.

Hindman, E.E., II, 1964: Continuous sampler for settling particles, J. de Recherches Atmosphériques, I.

Langmuir, I., and K.B. Blodgett, 1945: Mathematical investigation of water droplet trajectories, General Electric Co. Report No. RL-225, Final Report Army Contract W-33-038-ac-9151.

MacCready, P.B., Jr., 1962: The continuous particle sampler at the Puy de Dome comparison conference, Bull. Obs. du Puy de Dome, 1, 19-30.

Rupe, J.H., 1950: Critical impact velocities of water droplets as a problem in injector-spray sampling, Prog. Report #4-80, Jet Propulsion Lab., Calif. Inst. of Tech., Sept.

Schaefer, V.J., 1956: Preparation of snow crystal replicas - VI, Weatherwise, August.

_____, 1962: The vapor method for making replicas of liquid and solid aerosols, J. Appl. Meteor., 3, 413-418.

Todd, C.J., 1961: A study of cloud composition, Proc. of Ninth Wea. Radar Conf., Kansas City, Mo., Oct.

_____, 1964: Ice crystal development in a seeded cumulus cloud. Submitted to J. Atmos. Sci.

Weickmann, H.K., and H.J. aufm Kampe, 1953: Physical properties of cumulus clouds, J. of Meteor., 10, 3, 204-211.

APPENDIX G

CONTINUOUS SAMPLER FOR SETTLING PARTICLES

by

Edward E. Hindman II

Atmospheric Research Group
Altadena, California

November 10, 1963

To be published in Journal de Recherches Atmosphériques, Vol. I, 1964

ARG63 Pa-104

ABSTRACT

An instrument has been developed which continuously collects particles which fall by gravity and makes replicas of them by embedding them in a liquid plastic coating which quickly hardens. The plastic coating is on transparent 16 mm movie leader material and the replicas can be conveniently examined by projecting the leader with standard projection equipment. Chloroform is the solvent vapor which softens the plastic coating.

In one version, the continuous collector is installed in a continuous flow cold box and thus samples the ambient freezing nuclei concentration. In another version, the film unit is set outside and collects the small hydrometeors which fall on it. Records taken with this latter unit are presented in this paper showing the effects of silver iodide seeding of a supercooled geyser.

1. INTRODUCTION

In various cloud physics research studies, continuous sampling of the variables has proven desirable because of the rapid variations that occur. For capturing and preserving ice crystals and droplets for convenient subsequent analysis, the Formvar* technique developed by Schaefer (1), (2) has been particularly effective. This method has been adapted to the collection of particles from an airplane by Todd (3) and MacCready (4). It was also used by MacCready on the ground with a wind tunnel substituting for the aircraft motion. The present paper describes the adaptation of these principles to the continuous measurement of gravity settling particles. In one case the particles are the ice crystals grown from natural nuclei in a continuous cold box. In the other case, the particles are the tiny hydrometeors falling out from a geyser plume.

2. THE TECHNIQUES

The method, as originally developed by Schaefer (1), uses a liquid plastic material (Formvar, dissolved in a suitable solvent). The particles settle on a glass slide that is coated with liquid Formvar solution, and as the solvent evaporates, permanent replicas of the particles remain in the plastic. A later modification by Schaefer (2) uses a precoated slide that is dry at the time of particle collection. After the particles have settled on the slide, the plastic is then softened by using solvent vapor. Todd (3) noted Schaefer's methods became suitable for continuous operation with the advent of a 16 mm film base** which is not affected by the solvent. In this paper the collection of settling particles is done on precoated moving 16 mm film with the coating then softened by the vapor method. Replicas of the particles can be conveniently counted and studied by projecting the film with a standard stop-motion 16 mm movie projector. In this manner the sizes of ice crystals are accurately preserved, and the two-dimensional sizes measured; however liquid droplets are flattened on the film and so the replica diameter exceeds the original droplet diameter.

3. DESIGN OF THE VAPOR SYSTEM

Ethylene dichloride ($C_2H_4Cl_2$), ethylamine ($C_2H_5NH_2$), and chloroform ($CHCl_3$) were all tried as solvents. The rate of solvent absorption on the Formvar film is a function of the solvents, temperature, and temperature differential between the film and the vapor. The chloroform turned out to be most convenient because of its low freezing point (-63°C) and good vapor

*Formvar (trade name) 15-95E, Shawinigan Products Corp., Springfield, Mass.

**Cronar P-40A Leader (trade name), Polyester Photographic Film Base, E.I. duPont de Nemours & Co., Wilmington, Delaware.

pressure in the typical temperature range of 0°C to -30°C. Ethylamine did not dissolve the Formvar coating. Ethylene dichloride, with its low vapor pressure and a freezing point of -36.5°, is relatively unsuited for general vapor softening. To overcome this problem, the vapor pressure of ethylene dichloride could be increased by heating, but since the evaporation from the Formvar must take place at ambient conditions (here 0°C to -30°C), the heating process would be too slow.

Chloroform seemed to be the most suitable solvent and so it was used during tests on plastic film thickness. The first plastic coating, in the 1- to 5-micron region, was obtained by a continuous coating device using a one per cent (by weight) solution of Formvar in the solvent; a coating with a thickness of 10 to 20 microns remained after using a 10 per cent solution. The thinner coating turned out to be much more sensitive to solvent vapor and produced a sharper, more clearly defined replica edge than the thicker coating. It was also found that the chloroform did not affect the crystal structure in any way.

4. THE FREEZING NUCLEUS COUNTER

Figure 1 is a schematic of the freezing nucleus counter. The bottom of the box is cooled with dry ice and the copper plates extend up the sides to conduct cold temperature upward. This serves to maintain a good "head" of cold air and drive the gravity flow. The air enters through the top coming down through a wet sponge which has been pierced to permit some air flow. The air leaves the box from an exit tube located near the bottom at one end. The inside box dimensions are: width 5 cm, height 25 cm, length 30 cm.

The film has a Formvar coating of 1 to 5 microns thick. It moves at about 8 cm per minute which gives the film sufficient time for the softening process to take place in the solvent container. Any crystals which fall on the film as it moves horizontally to the right are thus replicated. As the inverted film moves back to the left, there is ample time for the solvent to evaporate.

So far the freezing nucleus counter has been operated only to test the feasibility of the technique, not to obtain routine data. The results are encouraging. Ice crystal replicas are clear and easy to count. The replicas average about 10 microns in diameter. Even the larger supercooled liquid cloud droplets can also be seen. Crystal growth continues somewhat after settling on the film as evidenced by the lack of droplets in a replica's immediate vicinity. The softening of the Formvar would be made more reliable if the wick were heated slightly; this improvement is recommended in future units.

The unit has one major drawback: it can sample only a small volume flow of air, on the order of one liter per minute, and so can only give useful crystal counts when the nuclei concentration is well over 10 per liter. This limits its utilization for natural nuclei counting although the sensitivity is fine for monitoring silver iodide plumes. By redesign, the sampling volume rate could be increased by almost an order of magnitude, but it would still be too low for conventional natural nuclei studies.

5. THE CONTINUOUS SMALL PARTICLE SAMPLER

The techniques of the freezing nucleus counter were applied to making continuous replications of small hydrometeors. Essentially the film and solvent components of the nucleus counter were removed from the cold box and the film exposed to falling particles in the atmosphere. The physical setup is shown in Fig. 2. This device is presumably suitable for quantitative measurements during light wind conditions.

In the cold box the volume of sampling is given by the film area and the height of the temperature where nucleation is initiated. In the outdoor version, the height from which the volume is calculated is the vertical distance the particle would fall during the sampling time. Thus, larger particles are sampled from a larger volume. This appears to be more convenient because there are generally fewer larger particles per unit volume. Considering spherical particles of unit density, the sampling volume for the range of particle sizes was computed from standard fall rate data. For example, during a one-minute exposure, particles 3, 25, and 800 microns in diameter will settle from 0.01 cm^3, 1 cm^3, and 1 liter, respectively.

6. THE SAMPLER AT YELLOWSTONE

The continuous small particle sampler was operated on the 1962 Yellowstone Park Expedition organized by Dr. V. J. Schaefer through the State University of New York with the support of the National Science Foundation.

On the morning of January 12, the sampler was operated around Old Faithful geyser to sample the supercooled cloud produced by the geyser. The sample was continuous from 0824 to 1200, except for brief periods when the unit was brought inside to warm the batteries. The results of the sample are illustrated in Fig. 3, with examples of the replicas given on Fig. 4. All the pictures of Fig. 4 are negative prints; when viewed in a microscope the particle outlines are dark. During this run the unit was occasionally moved about the area and was sometimes downwind of hot pools, but nevertheless the main features of the run are not obscured.

The portion of the sample taken between the first and second eruptions (0824 to 0925) was within a short distance of the geyser The ambient temperature was below -40°C, or the "Schaefer Point" (5), so as a result frozen droplets were the main particle form (Fig. 4a). The supercooled particles that were present came from the warm steam rising off hot pools which form near the geyser immediately after an eruption (Fig. 4b).

A short time after each eruption the concentration of ice crystals appeared to increase and then taper off. This is possibly a result of the increase in liquid water after each eruption. Since a majority of the sampled drops are greater than 10 microns, and each eruption was below -33°C, the drops were subjected to spontaneous nucleation as summarized by Fletcher (6). During the period between eruptions the ice crystals gradually settled out, reaching a minimum just prior to the next eruption.

Figures 4c, 4d, and 4e show the typical crystals at times not close to eruptions, as the temperature slowly increased.

The effects of Schleusener's (7, 8) AgI generator are illustrated by Figs. 3 and 4. Before seeding, the crystals were growing but at a slow rate. A substantial increase in the growth rate of the ice crystals occurred after seeding, and they also became more regular and time-free (Fig. 4f, 4g, and 4h). Natural ice crystals are rimed when there is a deficiency of freezing nuclei which allows large amounts of supercooled water to remain (Fig. 4b). Further proof of the seeding effects was obtained from visual observations. Optical effects (22° halo and parhelia) were observed after the seeding and none before.

7. SUMMARY

The continuous sampler for settling particles has been developed to the point where it has demonstrated its feasibility as a technique. Improved versions can serve as operational devices for continuously recording freezing nuclei and for collecting particles settling by gravity at temperatures at least as low as -30°C. The particle replicas on 16 mm film can be conveniently handled, examined, and counted.

ACKNOWLEDGMENTS

The major portion of this work was supported under NSF Grant G11969 for the Atmospheric Sciences Program of the National Science Foundation. Special appreciation is extended to Mr. C. J. Todd of Atmospheric Research Group for his counsel throughout the work, and to Mr. J. McQuerry of El Camino College for his ideas and encouragement during the initial stages.

REFERENCES

(1) Schaefer, V. J. - Preparation of snow crystal replicas VI. Weatherwise, August 1956.

(2) Schaefer, V. J. - The vapor method for making replicas of liquid and solid aerosols. J. Appl. Met., 3, 413-418, 1962.

(3) Todd, C. J. - A study of cloud composition. Proc. Ninth Wea. Radar Conf., Kansas City, October 1961.

(4) MacCready, P. B., Jr. - The continuous particle sampler at the Puy de Dome Comparison Conference. Bull. Obs. Puy de Dome, 1, 19-30, 1962.

(5) Schaefer, V. J. - Condensed water in the free atmosphere in air colder than -40°C. J. Appl. Met., 4, 481-488, 1962.

(6) Fletcher, N. H. - The Physics of Rain Clouds, Cambridge University Press, London, 207, 1962.

(7) Schleusener, R. A. - Preliminary tests on a non-combustion type silver iodide generator. CER63RAS15, Colorado State University, Fort Collins, Colorado, 1963.

(8) Schleusener, R. A. - Third Yellowstone Field Research Expedition. Atmospheric Sciences Research Center, State University of New York, Albany, 82-84, 1963.

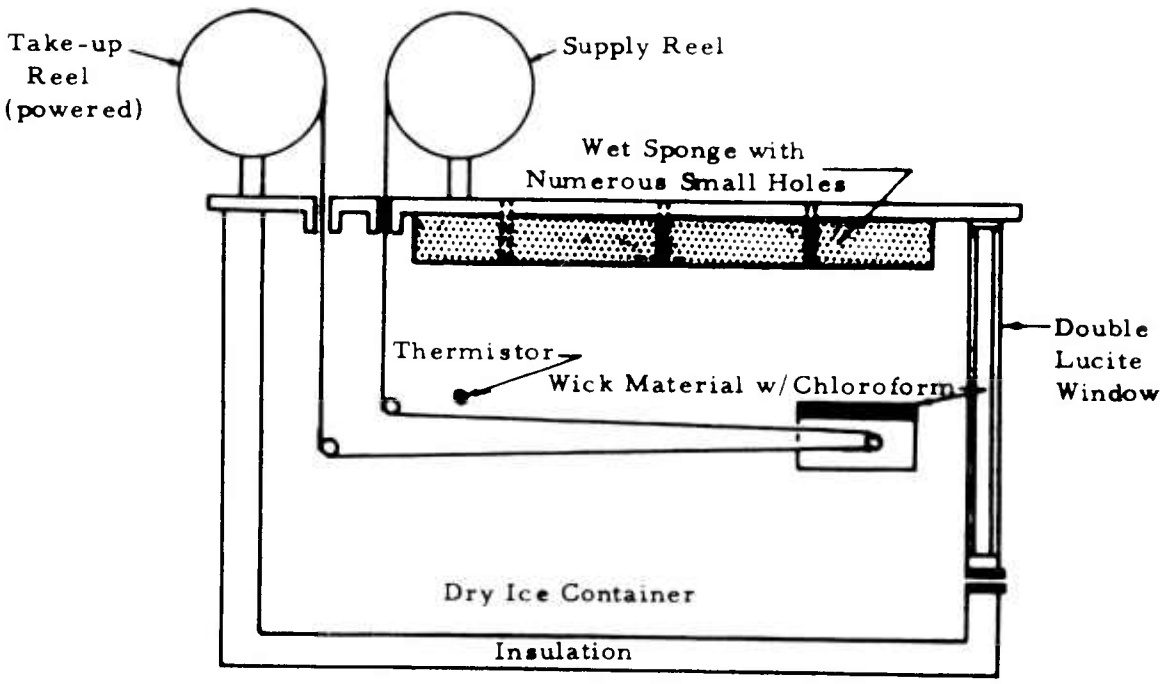

Fig. 1. A SCHEMATIC OF THE FREEZING NUCLEUS COUNTER.

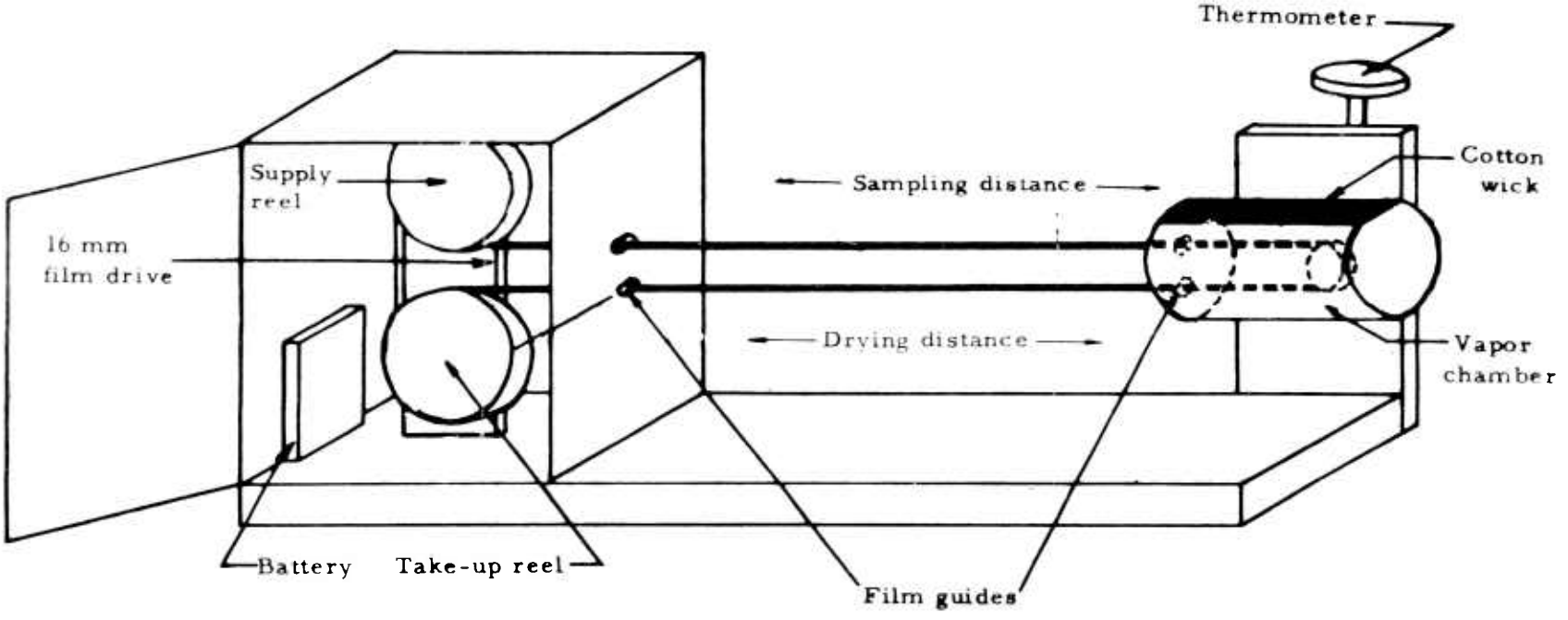

Fig. 2. DIAGRAM OF THE SUPERCOOLED GEYSER PLUME SAMPLER.

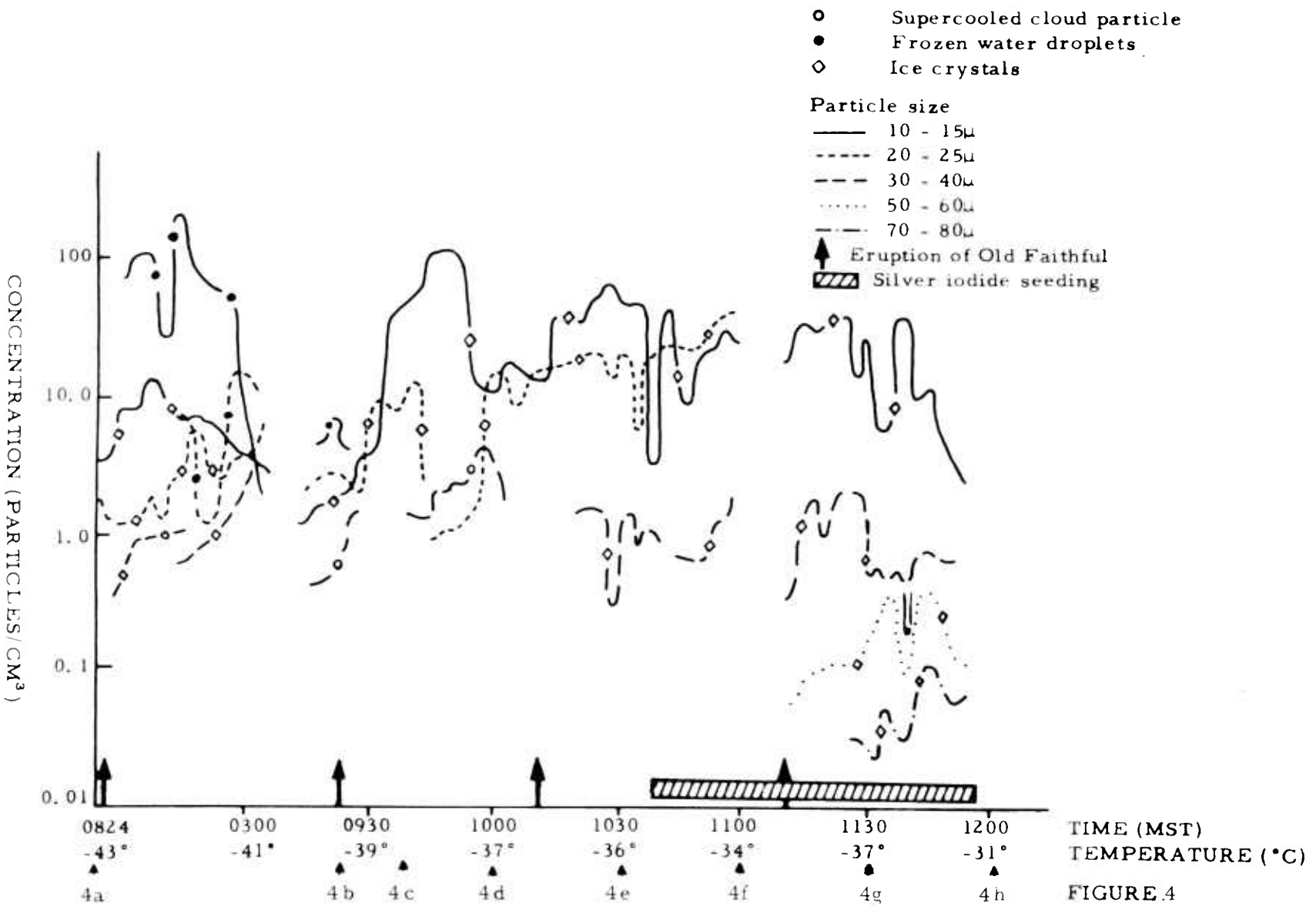

Fig. 3. RESULTS OF THE SAMPLE TAKEN ON JANUARY 12, 1962

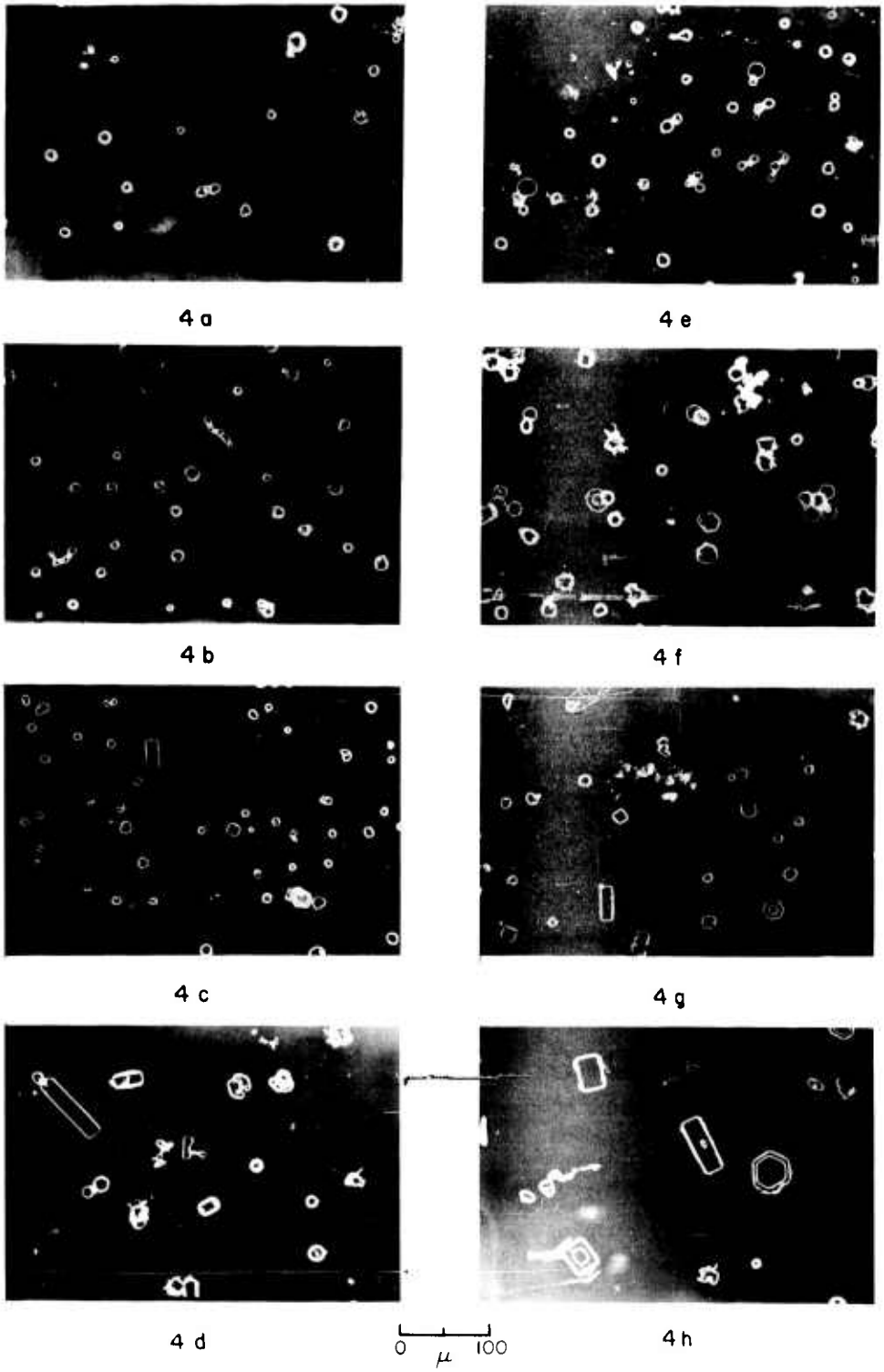

Fig. 4. YELLOWSTONE REPLICAS. 4a. 0830 frozen droplets, -43°C. 4b. 0923 frozen droplets (dark spheres) supercooled droplets (light spheres), -39°C. 4c. 0937 hexagonal plates and prisms (rectangles), -38°C. 4d. 1000 hexagonal plates, -37°C. 4e. 1030 irregular ice crystals, prisms, -36°C. 4f. 1100 irregular ice crystals, hexagonal plates, prisms, -34°C. 4g. 1130 hexagonal plates, prisms, -33°C. 4h. 1200 hexagonal plates, prisms, -31°C.

APPENDIX H

OBSERVATIONS OF HYDROMETEOR CHARGE EVOLUTION IN THUNDERSTORMS

By

Paul B. MacCready, Jr.

and

Alexander Proudfit

Atmospheric Research Group
Altadena, California

March 1964

ARG63 Pa-85a

SUMMARY

Systematic observations were made of hydrometeor charges associated with thunderstorms at Flagstaff, Arizona. All the measurements took place in and below clouds which were entirely supercooled. From these limited cases, a rather consistent picture emerged: (a) generally, charges on graupel and hail within the supercooled clouds were positive (measurements made as high as the -17.5°C level), (b) below the cloud at the +2° to +8°C level, just where the melting of the hydrometeors was apparently complete, the hydrometeors became abruptly negative, (c) at still lower, warmer levels the charge magnitudes were consistently smaller, with both signs represented but predominantly negative. The data suggest that a strong hydrometeor charging mechanism is associated with the melting of ice hydrometeors outside the cloud. The maximum charge magnitudes appeared comparable to the amounts which would be limited by breakdown gradients at the hydrometeor surface.

The measurements were made from a light plane by the standard induced-charge method. The aircraft would spiral within the central upcurrent up into the cloud and later spiral down through the precipitation shafts.

1. INTRODUCTION

The mechanisms which provide the dominant electrification in thunderstorms are not yet known, although there are many suggested theories. Measurements of pertinent variables in actual clouds are especially vital because all the conditions cannot be duplicated within the confines of a laboratory even if the conditions which should be duplicated are known. This paper describes field measurements made in convective clouds and thunderstorms at Flagstaff, Arizona.

The main feature of the measurements is that a consistent pattern seemed to emerge from them. The measurements are here reported without detailed interpretation, because many more measurements are required before the complete picture is defined.

Numerous studies have emphasized the correlation between the growth and fall of ice hydrometeors and the development of strong cloud electrification, the most likely inference being that the hydrometeors are instrumental in causing the electrification. Thus the direct measurement of the charge on hydrometeors becomes particularly important in understanding the fundamental electrification mechanism, and fortunately the measurement is relatively simple. Potential gradient measurements are useful, but their interpretation tends to be ambiguous because various charge distributions can cause the particular gradients as observed at particular times and places. Eventually space charge measurements and particularly cloud droplet charge measurements must be obtained in

conjunction with other electrification and meteorological data before the electrification mechanism problem can be given a quantitative solution.

2. MAIN FEATURES OF THE FIELD MEASUREMENTS

1. Potential gradient measurements at the ground at Flagstaff have demonstrated that the electrified clouds seem to be typical of many electrified clouds found elsewhere; the predominant electrification is associated with a vertically oriented charge dipole having the positive charge on top. Measurements of both steady-state gradient and lightning discharge gradient change support this model. The electrified clouds studied had relatively cold bases, colder than 0°C, assuring that the significant growth of large hydrometeors occurred in the ice phase. The supercooled droplets were generally smaller than 20 μ in diameter. Some of the clouds studied were being seeded with silver iodide (introduced into the vertical current rising into the cloud) [MacCready et al., 1963].

2. The charge on graupel, encountered in the -10° to -15°C range during spirals upward in the cell center and during traverses, was generally positive.

3. On downward spirals in the precipitating area under the cloud it was noted generally that the ice hydrometeors at colder than freezing temperatures were positive, that at some point where the particles were completely melted the charge on the liquid hydrometeors changed to

negative, the sign change often being rather abrupt, and that at still warmer temperatures the hydrometeor charges were mixed and much smaller. These changes of charge imply that a strong negative charging mechanism is associated with melting.

The downward spirals of the sampling airplane did not accurately follow the descent of the hydrometeors being measured. The charge evolution described above was derived by assuming that the charges encountered at each level were characteristic of that level; e. g., the main charge evolution from plus to minus depends on temperature (altitude). It is not impossible that the variations in the sign of the hydrometeors could be ascribed to a variation in time rather than temperature or height. However, the systematic variation with temperature was encountered ten times in 9 flights, while no correlation with the timing or stage of the precipitation was apparent. Thus the data best support the concept of the charge evolution being basically temperature dependent.

4. The maximum plus and minus charge magnitudes were more than 1000 picocoulombs (3 esu), and the charge on typical graupel pellets was in the range of 50 to 500 picocoulombs. For both the water and the ice hydrometeors, these observed charges were of the order of the maximum which can be held on a hydrometeor before breakdown gradients are built up at its surface.

5. Although the charge pattern was generally consistent, there were some exceptions. Some of the graupel showed no measurable charge,

although most of it registered positive. Where the hydrometeors were predominantly of one sign, there was an occasional charge of the other sign intermingled. Negatively charged ice hydrometeors were found at colder than freezing temperatures at cloud base on several occasions.

3. MEASUREMENT TECHNIQUES

The hydrometeor charge measurements were obtained as part of a continuing field program of cloud physics studies in summertime cumulus clouds at Flagstaff. A coordinated system of ground and airborne instruments are used. On the ground, concentrated around the isolated San Francisco Peaks, are radars, a network of time-lapse cameras, and a network of miscellaneous meteorological instruments including potential gradient sensors. The aircraft are equipped to sample cloud droplets and measure vertical velocities, turbulence, altitude, temperature, water vapor, and liquid water content, as well as atmospheric electricity.

The measurements reported here were made with instruments installed on a Cessna 180 aircraft, with background data coming from the rest of the field system.

The hydrometeor charge was found through the use of an open Faraday cage [Gunn, 1947]. Hydrometeors pass through a conducting tube or ring, open at each end. While the hydrometeor is in the charge ring, most of the charge appears on the ring and can be measured by an appropriate electrometer circuit. Because of the speed of the aircraft (50 m/sec) and the

length of the ring, each charged hydrometeor causes a voltage pulse of about 1-msec duration. The decay side of this pulse is electronically slowed or stretched so that the pulse can be registered on a Brush recorder, which does not respond above several hundred cycles per second.

Figure 1 shows a cross section of the ring cage unit. A Kistler model 555 charge amplifier was modified by the manufacturer to have three sensitivity ranges: 10, 100, and 1000 picocoulombs producing 1-volt output. The sensor sensitivity and the characteristics of the pulse stretcher and the rest of the electronics system combined to give three sensitivity ranges of ±10, ±100, and ±1000 picocoulombs full scale with the Brush recorder set at zero center and ±0.4 volts full scale. Instrument noise was never a problem; thus charges under 5 per cent of full scale could be read. Charges considerably beyond full scale on the recorder did not overload the electronics; they could be estimated by noting the pulse width at a given amplitude. Primary calibration came from discharging known capacitances into the ring. An over-all absolute error of less than 25 per cent is estimated for the system.

There are three possible events when the hydrometeor with charge Q enters the sensor:

1. The hydrometeor passes through the open-ended Faraday cage, termed the ring. Imyanitov [1958] has shown that the maximum charge appearing on the ring is αQ, where

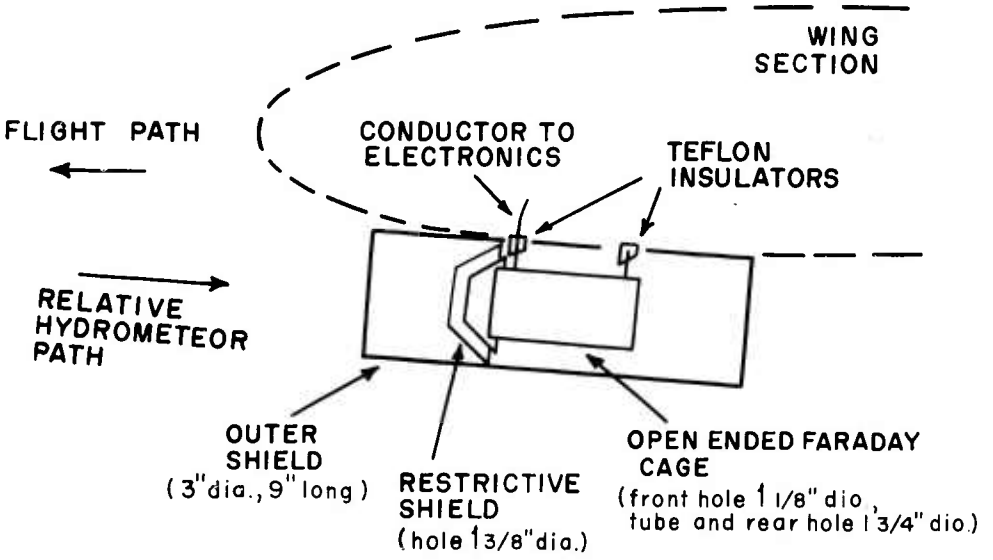

Fig. 1. CROSS SECTION VIEW OF HYDROMETEOR CHARGE SENSOR.

$$\alpha = \frac{h}{2\sqrt{\frac{h^2}{4} + r^2}}$$

h is ring length

r is ring radius

In the present case, with h = 9 cm and r being assumed to be 1.6 cm as a representative value, considering the 1.4 cm radius entrance and the 2.2 cm radius exit, $\alpha \sim 0.94$. α actually varies somewhat with the radial position of the hydrometeor, but not by an amount that is significant in the present study.

2. The hydrometeor strikes the ring and transfers the total charge Q to it. For small particles passing through the restrictive shield, the geometry shows that about two-thirds will go through the ring and one-third will strike the ring (ignoring collection efficiency). For larger particles, some will strike the ring but part of the particle will break off and pass through the ring. In either case, between 94 and 100 per cent of the charge will appear on the ring. The time constants of the system determine the decay shape of the pips on the recorder. There is a longer decay for the pips which result from collisions than for those from a charge passing through the ring. Preliminary flight checks showed that both types of pips gave comparable magnitudes in several representative meteorological situations; this implies that no large spurious readings are being created because of hydrometeors striking the ring at the 50 m/sec flight speed.

3. Particles passing between the ring and the shield will also give a

momentary charge to the ring. The sensor is designed so that no major particles can move through this area.

Most recordings were made at a chart speed of 10 mm/sec, at which speed the shape of the pips could be examined. After confidence was gained with the unit, a speed of 0.4 mm was occasionally used; the magnitude and number of pips could be ascertained, but not the shape.

In a region of numerous charged particles, a new hydrometeor could enter the ring before the trace had decayed to zero, and then the zero level would show a bias. The ring processed about 40 liters of air per second, so this was troublesome only in precipitation having more than about 200 particles per m^3. Sometimes some zero drift occurred without large charges being present. It seems logical that this was caused by a dense cloud of many very small charges, essentially the cloud charge. On the medium sensitivity setting a cloud charge of the order of 5 esu per gram of droplets could account for this. Cloud charges of this magnitude would be expected in regions of charged hydrometeor growth.

The aircraft was equipped with three radioactive probes and associated electrometers for measurement of airplane charge and vertical potential gradient. The apparatus was crude and simple, but still it appeared to have some value inside clouds. Two probes were put at mid-fuselage, one at the top and one at the bottom, and their voltage difference was noted for vertical (relative to the aircraft vertical) gradient measurements. An electrically floating electrometer was used, its output signal being

transferred to recorder potential by converting the output to alternating current, sending it across a special isolating transformer, and reconverting to direct current. The third probe was on the side of the fuselage under the wing, where it was relatively unaffected by vertical gradients; thus it pertained mostly to airplane charge. A corona current charger was used to charge the aircraft occasionally in clear air to check that the two vertical gradient probes were properly balanced so they would not respond to aircraft charge. The probe positions would be altered to provide balance, and if some imbalance remained the error due to aircraft charge could still be estimated in the resulting data.

The potential gradient and aircraft charge measurements are not reported in detail here because (a) the instrumentation is considered somewhat crude and (b) their rapid variations in steep spiraling flight in nonsmooth cloud conditions tend to obscure the main points. It was noted that the aircraft charge and the charge on hydrometeors were sometimes the same sign and at other times of opposite sign, implying that vertical potential gradients were not involved in a dominant hydrometeor charging outside the cloud. The aircraft charge arises from the charges both on small droplets and on larger hydrometeors, and so it is closer to the net charge, which in many instances should have the opposite sign from the hydrometeors.

4. SUMMARY OF HYDROMETEOR CHARGE MEASUREMENTS

In August 1962 nine flights were made in electrified cloud situations with the hydrometeor charge unit in operation.

August 13. 1. At the melting level positive hydrometeors switched abruptly to negative. The airplane was in a downward spiral below cloud base. This spiral is shown completely in Figure 2.

August 14a. 1. Dense graupel of +20 pcoul was encountered at -14.5°C at the top of an upward spiral in a cloud with a base temperature of -6°C.

August 14b. 1. At -13.5°C at the top of an upward spiral in a cloud with -8.8°C base, +10 to +50 pcoul charges were found on light graupel.

2. In a downward spiral below cloud base, in very light ice particles so small they could not be seen individually but could be heard striking the plane, +1 to +5 pcoul were measured down to 4,300 m, at about +2.5°C; then -1 to -15 pcoul at 4,100 m and lower, warmer than +4.5°C, in very small raindrops.

3. In a horizontal traverse at the +2°C to +4.5°C level, many +3 to +5 pcoul charges were encountered, and just one negative charge, -5 pcoul. Some hydrometeors showed no measurable charge.

4. In a downward spiral, in soft graupel at +2°C, measured positive charges were +10 to +30 pcoul, decreasing in charge as the plane descended. At +6°C the hydrometeors were termed light rain; at +6.5°C the charges began being negative, about -2 pcoul.

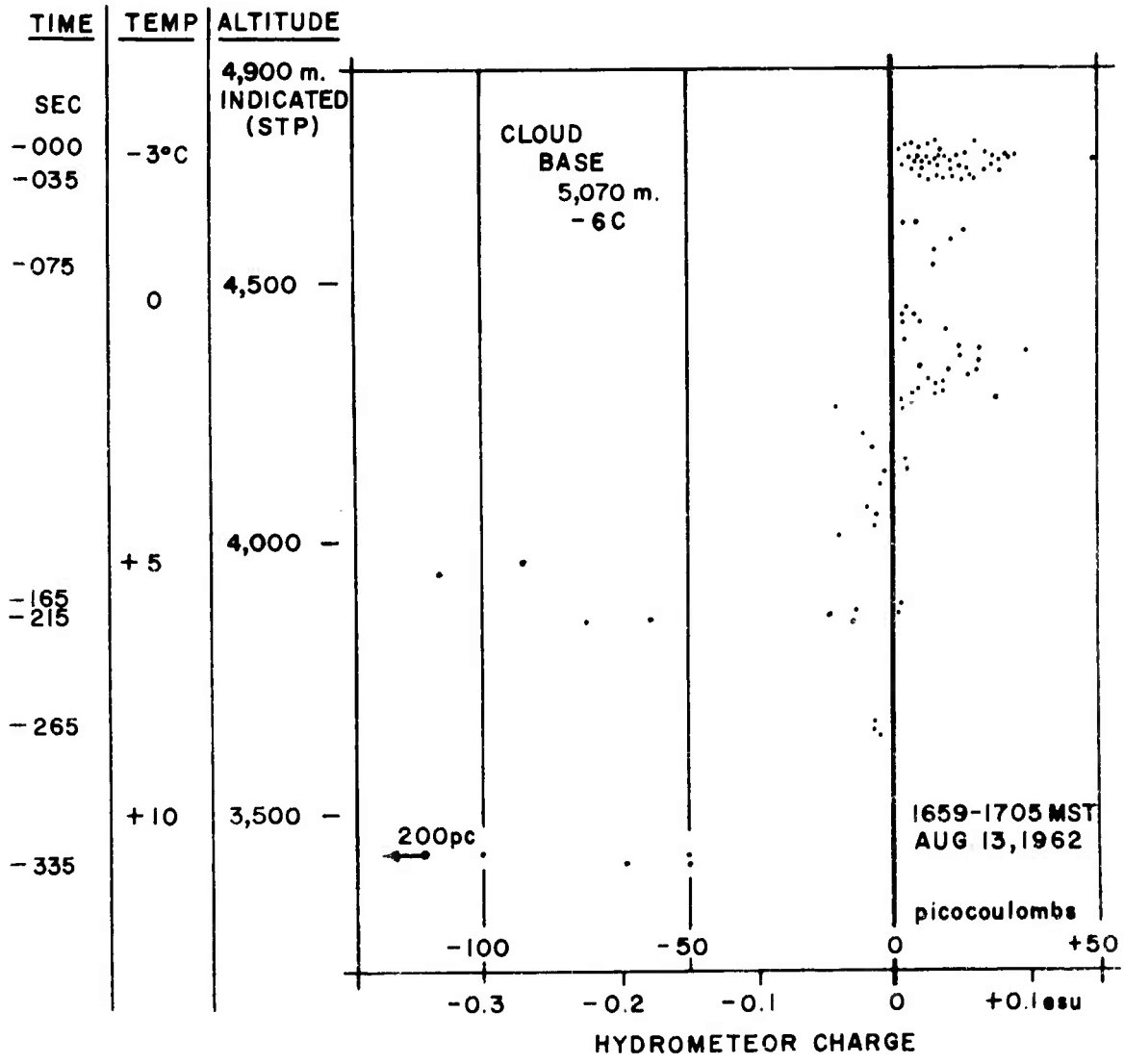

Fig. 2. HYDROMETEOR CHARGE MEASUREMENTS DURING SPIRAL DESCENT, 8/13.

At +12°C there were some -15 pcoul charges.

August 15a. 1. In a seeded cloud (base -6.7°C) at -17.5°C at the top of an upward spiral, a few negative charges were found on graupel, probably of the order of -500 pcoul (scale setting indeterminate).

2. In a horizontal traverse at the 0 to +4°C level, at +2 to +4°C in 'noisy graupel with no water in it' there were predominantly positive charges of +200 pcoul, just one out of 100 being negative. In heavy rain at +4°C there was no appreciable charge. In light graupel the charge was +30 to +100 pcoul, then in melting graupel -100 to -200 pcoul. At 0°C -25 pcoul was noted on small hydrometeors.

August 15b. 1. In a slow downwind spiral below cloud (base -6°C), in virga, at -5°C there were a few positive charges of +5 and +10 pcoul, and at -3°C a few stronger positive charges, then more small positive charges. At +8°C there were a few strong negative charges in light rain, of uncertain magnitude.

2. At the top of an upward spiral in a seeded cloud, at -14°C there were many positive charges exceeding +100 pcoul in graupel.

3. In a subsequent spiral down through precipitation below this same cloud, base -8.8°C, strong positive charges were found on moderate hail turning to negative when melted at +9°C, with weak

charges of both signs at warmer temperatures. The detailed measurements in this spiral are given in Figure 3. During this descent lightning was noted about 500 m away.

4. In flight through and below some other thin clouds, many +5 and +7 pcoul charges were noted in small snow flakes at -8°C, to +20 pcoul at -4°C. At +3°C in melting drops the charges were -300 pcoul, and in rain at +11°C to +13°C they were -150 to -300 pcoul.

August 16a. 1. In a brief upward spiral into a cloud (base -1°C) at -4°C the measurements showed small positive and negative charges as the aircraft was at the cloud edges.

2. At the top of another spiral, in leaving the cloud mass at -11°C, the charges were +10 to +110 pcoul, and there may have been some smaller charges some of which could be negative.

August 16b. 1. At +8°C in light precipitation a few ±2 pcoul charges were found.

2. At +0.5°C to -2°C positive charges predominated, in the +5 to +60 pcoul range, with the stronger charges at the colder temperatures. The hydrometeors were termed light ice ones which showed wetness on the airplane. In the same area negligible charge existed at +6°C. At +8°C in an adjacent precipitation area with a mixture of graupel and rain, the observer noted +300 pcoul when some melting was apparent, no measurable charge in some of the rain,

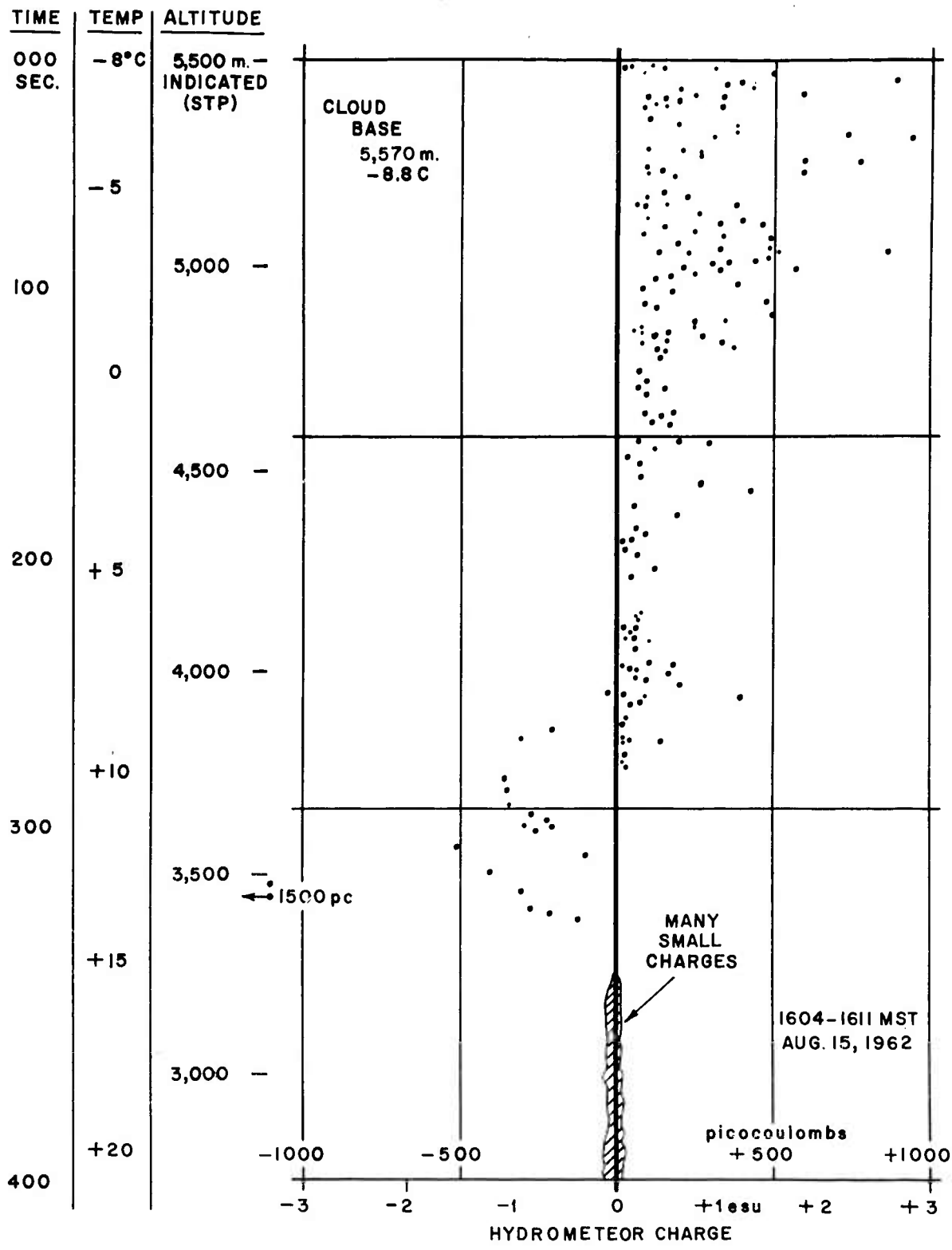

Fig. 3. HYDROMETEOR CHARGE MEASUREMENTS DURING SPIRAL DESCENT, 8/15.

and some ±50 pcoul charges in the area. At 13.5°C there were many -100 to -300 pcoul charges, and two +200 pcoul charges, and then primarily ±4 pcoul in a downcurrent and in an upcurrent at 19.2°C.

3. In a slow climb up through the precipitation area and another descent the following distributions were noted. In rain at +16°C to +6.5°C charges were both signs, ±2 to ±10 pcoul, being stronger at higher altitudes. At +1°C there was a group of +20 to +50 pcoul charges. At temperatures warmer than +2°C there were many negative charges, -5 to -15 pcoul, and negligible charge at temperatures warmer than +10°C.

August 22. At Fort Collins, Colorado, a spiral was made down through a thunderstorm precipitation region. Although no detailed notes are available, the records show positive charges at +1°C to -1°C, and negative charges in the +7 to +19°C range.

5. CHARGE MAGNITUDES

The sizes of the hydrometeors were only estimated very crudely in this study, and yet it was apparent that the maximum charges on the hydrometeors were not far from the maximum charges which could be held on the particles without breakdown gradients at the edges. The important point is that the charging mechanisms, both positive and negative, are strong enough so that the charge on a hydrometeor is often

limited by the breakdown gradient rather than by the charging rate. Figure 4 shows in a convenient form the charges which can be held on various sizes of spherical hydrometeors. The relationship employed is

$$Q = Fr^2$$

where Q is charge in esu, F is field strength in esu/cm, and r is in centimeters. For Q in coulombs (1 coul = $3 \cdot 10^9$ esu), F in volts per centimeter (1 v/cm = 1/300 esu/cm) and r in centimeters, the equation is $Q = 1.11 \cdot 10^{-12} Fr^2$. In terms of charge density, Q/m where m is the mass (grams) of a spherical particle,

$$r = \frac{3F}{4\pi q/m\ \delta}$$

where δ is the relative density of the particle, and q and F are in electrostatic units. In other units, with charge in picocoulombs and the field strength in volts per centimeter, the above equation becomes

$$r = \frac{0.264\ F}{q/m\ \delta}$$

For a graupel or hail pellet, the rough surface should intensify the field at some portions of the surface, and so the mean limiting gradient may be well under the 10,000 to 15,000 v/cm usually assumed. A limiting gradient of about 7000 v/cm is suggested for a typical rimed particle, graupel, or small hail. A water drop will have a smoother surface, and thus a higher limiting surface gradient of, say, 10,000 to 15,000 v/cm. The largest stable liquid drops are about 0.6 cm in diameter. Considering

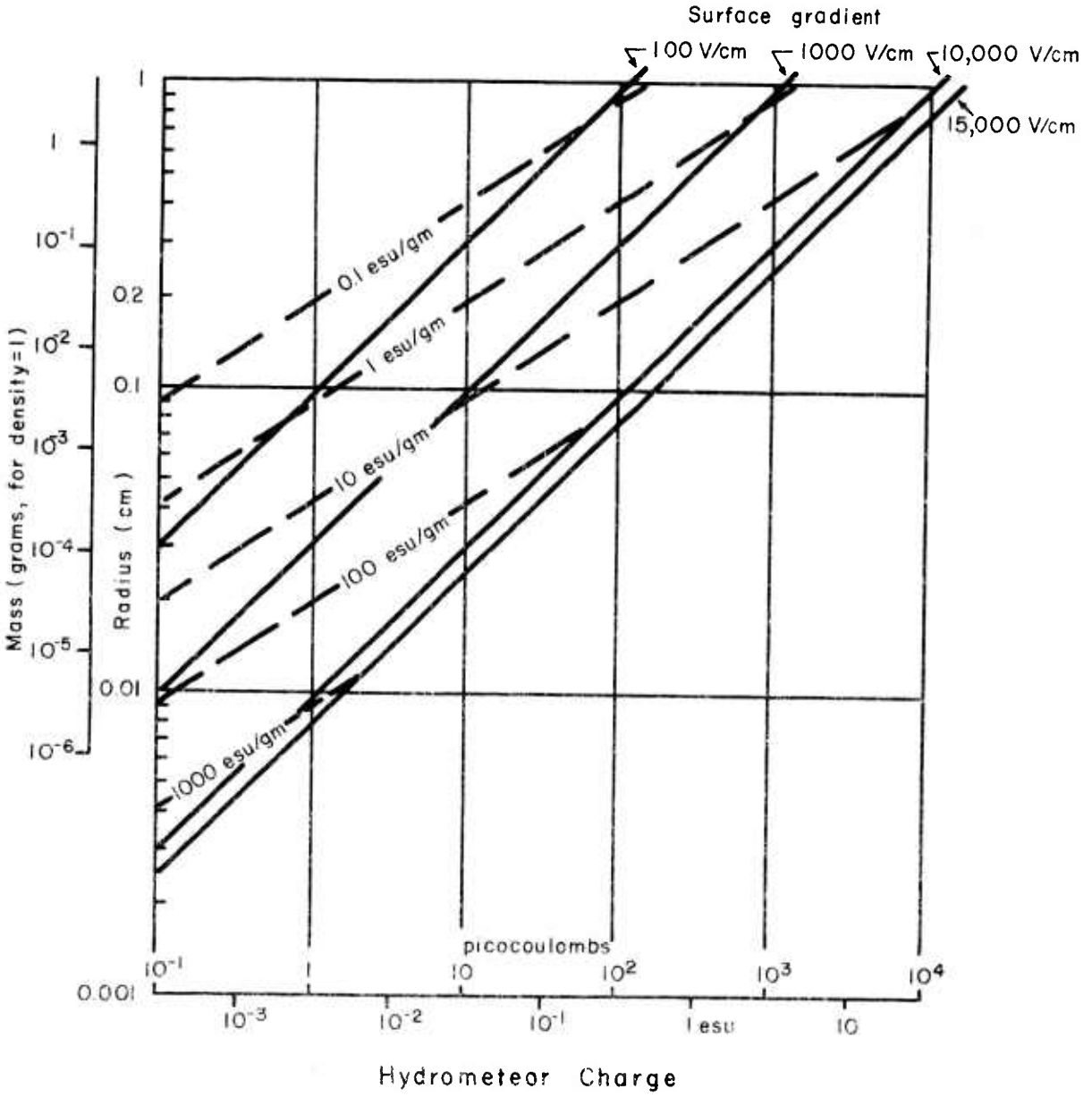

Fig. 4. VARIOUS CHARGE-RADIUS RELATIONSHIPS. Solid lines show the surface gradient for spherical particles. Dashed lines show the charge density in esu/gm, for a particle density $\delta = 1$. For other densities the charge density lines can be relabeled using a factor δ^{-1}.

such a drop to be spherical, for a 10,000 v/cm surface gradient the charge is 3 esu or 1000 picocoulombs, and the charge density 26.5 esu/g. A 15,000 v/cm breakdown gradient gives a maximum charge of 4.5 esu or 1500 picocoulombs. If this drop of 0.1132 g mass had melted from a small hail pellet of $\delta = 0.7$ and the same mass, from the previous assumptions the maximum charge on the hail, would have been 2.66 esu, and the charge density 23.5 esu/g. The hail sphere is larger, but the surface breakdown gradient on the hail is lower.

Gunn [1949] examines the subject of charge limits with respect to measured values of size and charge for liquid raindrops measured at the ground under thunderstorms. He points out that drop deformation may significantly lower the charge limit on the drop. For some drops he found charges which would lie just a bit beyond the 10,000-v/cm line of Figure 4, although most were an order of magnitude less. Thus his measurements demonstrate a logical charge versus size limit, although he was dealing with considerably smaller hydrometeors than those shown in Figure 3, and the peak charges were under 0.1 esu.

In summary, a suggested rule of thumb for maximum hydrometeor charging is, during riming

$$Q = +7.8 \cdot 10^{-9} r^2$$

Q = charge in coulombs
r = radius in centimeters

and after melting, the maximum charge would be

$$Q = -1.11 \cdot 10^{-8} r^2 \text{ (here } r < 0.3 \text{ cm by drop instability).}$$

Kuettner [1956] has pointed out that the electrostatic force on a drop in a 1000-v/cm gradient will equal the gravitional force for a charge density of 300 esu/g. Figure 4 shows that drops smaller than about 200 μ in radius can hold such a charge. These electrostatic effects could appreciably accelerate or retard the coalescence growth of small hydrometeors having the maximum charge. They could also be instrumental in expelling small charged hydrometeors from a cloud or in somewhat readjusting the positions of charged areas, even though the change in net velocity of the hydrometeors is small compared with the main dynamic motions in strong cumulus situations. The effect is greatest on small hydrometeors; larger ones have less charge density, and in any case gravity effects will predominate. For smaller ones, such as cloud droplets moving in the Stokes flow regime, the velocity of maximum charged droplets will vary linearly with r and thus be small.

6. DISCUSSION

The hydrometeor charge observations at Flagstaff imply that a strong charging mechanism (or first discharging and then charging with the opposite sign) is closely associated with melting. How the effect depends on falling speed, space charge, conductivity, potential gradient, chemical and mechanical structure of the ice hydrometeor, etc., is not known. In any case, since the change from positive to negative during melting occurred entirely outside the cloud, the charging is not associated with collisions with droplets.

The sign reversal at Flagstaff occurred often around +3°C or +4°C, the hydrometeors being relatively small. In some cases of heavier precipitation and larger particles, the reversal was at +6°C, +8°C, or even warmer. During one spiral descent the observer was carefully noting the condition of the hydrometeors and he observed that the sign reversal did correlate very well with the point, at 6.5°C, at which the drops first showed no characteristics of containing any ice. The temperature at which an ice hydrometeor will be completely turned to liquid depends on many factors, especially hydrometeor size and structure, vertical air velocity, and local humidity. The Flagstaff measurements seem reasonably consistent with the concept that the main charging is associated with the final stages of melting.

Mason [1957, p. 443] calculates the final melting level of ice and graupel in some representative cases. The distance below the 0° level turns out to be almost directly proportional to the particle radius. A radius of 2 mm would correspond to a melting level of 6°C to 8°C, which is not inconsistent with the Flagstaff data.

The existence of a negative hydrometeor charging level associated with melting was found long ago from gradient measurements. For example, Kuettner [1956], discussing the Simpson-Scrase model, the Simpson-Robinson model, and Kuettner's own measurements on the Zugspitze, states, 'in nature a new charging effect takes over in the melting zone, adding negative charge to the precipitation particles at a faster

rate than the pure ionic discharge currents would do.' The positive charge below the negative charge of the main thunderstorm dipole might be related to the positive charge released to the air in the melting regions as the hydrometeors lose positive charge and acquire negative charge.

Figure 3 shows a deep descent made in precipitation (termed 'soft hail' by the observer) below cloud base during a strong electrification situation. It is worth examining in detail, although it is not wise to try to infer too much from the details of any individual case. The aircraft descent rate is not greatly different from the fall speed of the larger hydrometeors in still air.

The maximum positive charges just below cloud base appear to be about the maximum which could be maintained on the observed hydrometeors before breakdown, as discussed in the preceding section. The magnitude of the maximum charges decreases steadily. The rate of decrease is not inconsistent with the charge which would leak off by conductivity; at 5,500 m the standard air conductivity would be expected to drain off 50 per cent of the charge in 2 to 4 minutes. There is no marked effect at the 0°C level.

The switch from positive to negative takes place abruptly and completely at +8° to +10°C, presumably about the level at which melting of these hydrometeors is completed. The flight notes verify that the particles still had ice characteristics at +6.5°C. The maximum negative charges are at a bit warmer level, +12° to +13°C; the melting of the very largest

hydrometeors could reasonably have been delayed to this temperature.

As derived in the preceding section, the largest charge on a stable liquid water drop should be of the order of -1500 picocoul. This figure results from assuming a maximum radius of 0.3 cm and a maximum surface field of 15,000 v/cm. This agrees with the maximum negative charge shown in Figure 3, 1500 picocoul.

At even higher temperatures, even though the rain was still strong, the observed charges were small. This could be attributed to a combination of conductivity loss, ionic charging due to the presence of space charge (primarily positive charge, brought to this level by a downcurrent from the melting level where the hydrometeors release positive charge or brought up from the ground where corona currents provide charge), and ionic charging due to ion mobility effects in the presence of a strong electric field. The abruptness of the change at +14°C from strong negative charges to weak charges of both signs is not necessarily significant; it must be remembered that the aircraft operation provides sampling variations in both time and space and so, as operated, is not exactly following the evolution of a particular group of hydrometeors.

Figure 2 shows a similar descent made in a situation where the ice hydrometeors were termed 'light and heavy graupel'. Some of the graupel had no appreciable charge. As shown by the time scale on

Figure 2, the descent was made somewhat erratically. Considering charges greater than 5 pcoul, the change from positive to negative was very abrupt at +2°C, at which level the melting of standard graupel could be complete. The maximum negative charges were found at even warmer temperatures.

It is worth noting that the riming process in the Flagstaff thunder storms studied involves only hydrometeor coalescence with small supercooled droplets, less than 20 μ in diameter. Droplet measurements were made with a continuous film Formvar droplet sampler during the electrification flights [MacCready et al., 1963]. Thus the mechanism proposed by Latham and Mason [1961], involving splintering effects on electrification with larger droplets, does not seem applicable here. No physical reason is given here for the ice hydrometeor charging mechanism. As pointed out by Latham and Mason, except for Findeisen's measurements, studies of charging by riming have regularly shown the rime deposit to be negative. However, none of the studies exactly duplicated the conditions on a graupel pellet growing in a thunderstorm.

Kuettner [1956] considered cloud dynamics and masking charges on cloud droplets, as well as hydrometeor charging to introduce the concept that the fall of positive hydrometeors could give rise to the observed thunderstorm main vertical dipole with negative polarity on the bottom.

His interpretation of his own measurements on the Zugspitze and of available vertical gradient information within thunderstorms required the existence of just the sort of charge evolution during riming and melting which was found during these limited measurements at Flagstaff. Kuettner's picture of the over-all charge separation mechanism is not clear to us, especially as regards the complete mechanism for providing a net positive charge in the upper portions of the cloud. Nevertheless, his concept that the charge distribution must tie in closely with temperature levels is consistent with these field data.

The data presented here do imply that a strong hydrometeor charging mechanism is associated with the melting of ice hydrometeors. They further suggest that the hydrometeors are predominantly positively charged while in the ice phase. It must be reemphasized that the clouds which were investigated comprise only a very limited sample, with very cold bases and small droplet sizes; this must be recognized in any extrapolation of the results to other situations. Similar measurements on a brief subsequent project in the summer of 1963, not yet analyzed in any great detail, suggest that with warmer cloud bases the signs of the hydrometeors form a much more complex picture than the simple results given here. Laboratory tests on charging during melting [Dinger and Gunn, 1946; MacCready, 1964] support a positive charging during melting rather than the negative charging suggested by the flight data.

Gunn [1957] mentions that the region in the vicinity of the zero isotherm is a region of maximum electrification activity (65 per cent of lightning strikes to aircraft were in air in the temperature range of 0° to +5°C). Gunn [1947] shows a figure indicating a preponderance of positively charged hydrometeors at cold temperatures and negative ones at warm temperatures. In measurements within an active thunderstorm [Gunn, 1950] he found that the electrification was at a maximum 'where the temperature approximates 10°C and where the melting of snow or graupel formed above the freezing level probably takes place.' The measurements reported here are not inconsistent with his measurements, but there can be broad latitude in interpretation.

In summary, it does seem likely that the melting level represents a layer in which substantial charge is liberated by hydrometeors. The details of the whole cloud charge generation picture will be complex, because of the great complexity of the flow field, hydrometeor and droplet distributions, and chemical contaminant factors. Quantitative field investigations of charges on hydrometeors and droplets throughout a cloud system at various times are required before the cloud charge picture can be deemed to be adequately described.

ACKNOWLEDGMENTS

The main part of this study has been supported by the Atmospheric Sciences Section, National Science Foundation, under grant NSF G11969 to the Atmospheric Research Group. Beginning

in 1955, additional support for the long-range Flagstaff cumulus studies has been provided to Meteorology Research, Inc., affiliated with the Atmospheric Research Group, by the U.S. Forest Service (Project Skyfire), the AEC Division of Biology and Medicine, the Air Force Cambridge Research Laboratory, and, most recently and in the largest part, the U.S. Army Electronic Research and Development Laboratory (Contract DA 36-039 SC-89066).

The contributing work of Mr. Thomas Lockhart and Mr. Ross Beesmer as well as others of Meteorology Research is gratefully acknowledged. The instrumentation and the interpretation of measurements benefited materially from various discussions with Dr. Heinz Kasemir and Dr. Helmut Weickmann.

REFERENCES

Dinger, J. E. and Gunn, R. 1946 Terrest. Mag. Atmos. Elect., 51, p. 477.

Gunn, R. 1947 Phys. Rev., 71, p. 181

Gunn, R. 1949 J. Geophys. Res., 54, p. 57.

Gunn, R. 1950 J. Geophys. Res., 55, p. 171.

Gunn, R. 1957 Proc. IRE, 45, p. 1331.

Imyanitov, I. M. 1958 Instr. & Expl. Tech. USSR, English Translation, No. 2.

Kuettner, J. 1956 J. Met., 13, p. 456.

Latham, J. and Mason, B. J. 1961 Proc. Roy. Soc. A., London, 260, p. 537.

MacCready, P. B., Jr. Smith, T. B., Todd, C. J., Woodward, B., and Chien, C. W. 1963 Meteorology Research, Inc., Final Report to U.S. Army Electronics Research and Development Laboratory, Fort Monmouth (ARPA), Contract DA36-039 SC 89066.

Mason, B. J. 1957 The Physics of Clouds, Oxford University Press, London.

APPENDIX I

SELF-CHARGING OF MELTING ICE

by

Paul B. MacCready, Jr.

and

Alexander Proudfit

Atmospheric Research Group
Altadena, California

March 1964

ARG63 Pa-81a

SUMMARY

A laboratory investigation was initiated to try to duplicate a phenomenon which had been repeatedly observed in certain flight measurements during the Flagstaff cumulus studies: the apparent strong negative charging of ice hydrometeors at the final stage of melting during their fall outside of the cloud. Sample ice structures of 1 cm^3 from distilled water were melted in an 8 m/sec air stream at ambient temperatures. Regardless of the technique of measurement used (current into the sample, charge into the sample, or charge into an open Faraday cage around the sample), certain features were observed consistently: (a) a positive charge was acquired by the sample, (b) the magnitude of the charge was on the order of 30 picocoulombs (0.1 esu), and (c) the acquisition of charge occurred primarily during the later portion of the melting process. Generally similar but more erratic results were obtained with actual hail samples.

The sign of the charging was opposite to that observed in the flight measurements, and the magnitude of the charging was far less, but the correlation of the charging with the final stage of melting agreed with the results of the flight tests. Laboratory tests previously reported by Dinger and Gunn also showed positive charging during melting, and the charging correlated with the amount of dissolved gas and hence bubbles. It is felt that the charging effect is real and is probably

primarily associated with effects from bubbles during melting, and that the disagreement in sign between the laboratory and flight measurements may be attributable to the differences in ambient conditions and hydrometeor properties.

1. INTRODUCTION

During the 1962 field program of the cumulus cloud investigation at Flagstaff, Arizona, some of the hydrometeor charge measurements were made as the research aircraft spiraled rapidly down below the cloud through the precipitation. The charges on the hydrometeors in the limited conditions studied generally showed a consistent pattern: the hydrometeors were positively charged while in the ice phase and had become negatively charged by the time they were completely melted. In an attempt to gain further insight into this phenomenon, a laboratory experiment was initiated in late 1962. The aim of this laboratory study was to try to duplicate this apparent hydrometeor charging during melting. This report describes these preliminary laboratory studies.

2. THE PHENOMENON

The observations in the field at Flagstaff (see MacCready, 1964) can be summarized qualitatively as follows:

(a) The charge on ice hydrometeors (small to large graupel) both within and below convective clouds was found to be predominantly positive, with a maximum charge strength apparently approaching the limit which can exist on a particle of that size before breakdown gradients are reached at its surface.

(b) After melting (at the +3°C to +10°C level, depending principally on the hydrometeor type, size, and the air vertical

velocity) the hydrometeors would have negative charges of maximum magnitude comparable to the previous maximum positive charges.

(c) The switch from plus to minus was often very abrupt, and within the accuracy of the qualitative measurements coincided well with the level at which the last ice-characteristic of the hydrometeors disappeared.

In the cases studied the change from plus to minus took place completely below (outside) the clouds, and so a mechanism related to the collisions or near misses with droplets was not operating.

3. EXPERIMENT 1

In all cases the experiments consisted of making simulated ice hydrometeors by freezing distilled water in the desired shape, placing the ice in a small wind tunnel through which air at room temperature was drawn, and monitoring any charging as the ice melted. The velocity through the tunnel was measured by a Pitot tube-manometer system; the speed was about 8 m/sec. The electrification measurements were reproducible. The overall absolute error of the charge and current measurements was under 10 per cent of the indicated value. The laboratory setup was simple, but considerable attention to technique and calibration was required because of the very low currents involved.

For the first series of experiments, ice spheres of approximately 1.6 cm diameter were employed. The spheres were obtained by using glass molds (small Christmas tree ornaments), which were cracked off after freezing had been completed. A wire was inserted in the filling neck of the mold in order to enable the specimen sphere to be connected to the measuring equipment. The mold was filled by means of a hypodermic needle. Freezing took place in a cold box partially filled with dry ice.

The spheres were removed from the cold box and inserted in the wind tunnel through a hinged section and the fan and measuring equipment turned on. As the air caused the ice to melt, the rate of change of charge (i.e., current) was measured by a Keithley 600A electrometer, used in its 'fast' current measuring mode. The output of the electrometer drove one channel of a Brush mark II chart recorder. The setup is diagrammed in Fig. 1a.

During the initial series of runs some reproducible indication of a change of charge as a function of the ice sphere's change of state existed. As would be expected, drops of water were dropped or blown off during the melting process which tended to produce spurious results. This fact, coupled with the tedious nature of molding the spheres, led to an alteration of the setup and procedure.

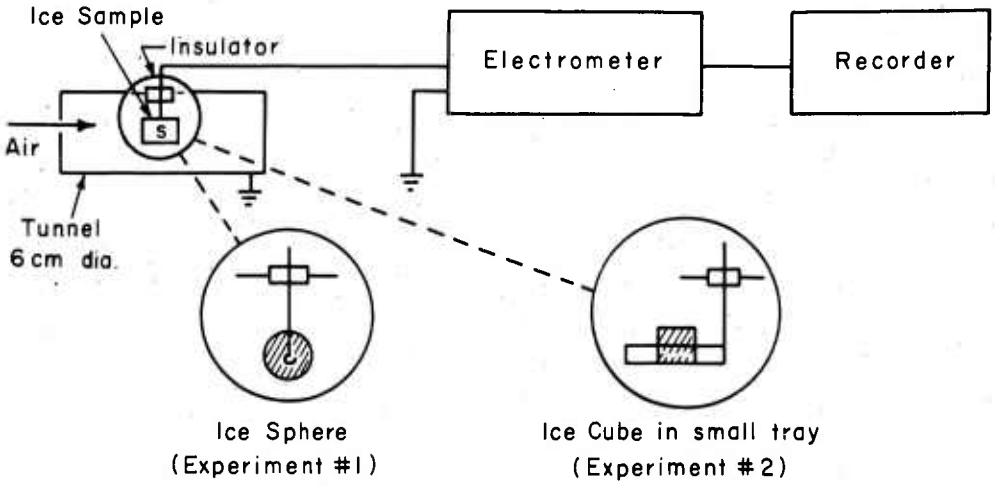

Fig. 1a. DIRECT CURRENT MEASUREMENT (EXPERIMENTS 1 & 2)

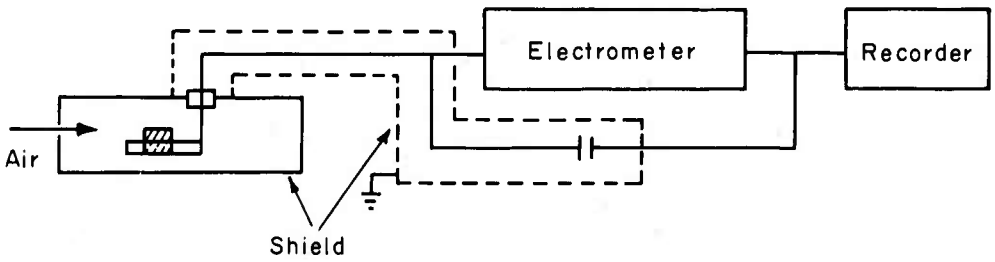

Fig. 1b. DIRECT CHARGE MEASUREMENT (EXPERIMENT 2)

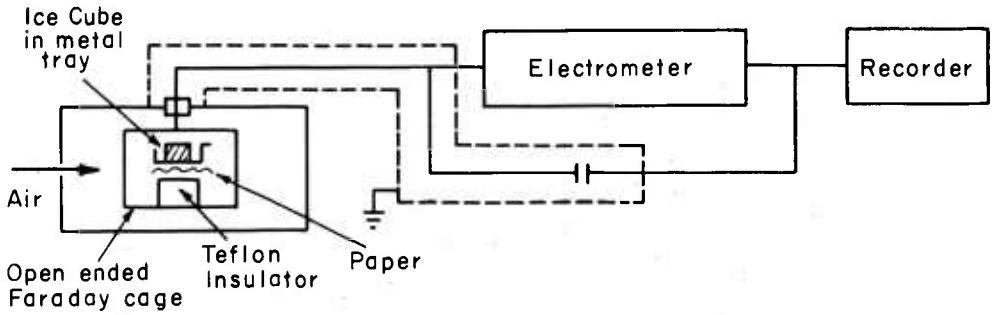

Fig. 1c. INDUCED CHARGE MEASUREMENT. (EXPERIMENT 3)

4. EXPERIMENT 2

Ice cubes, approximately 1.2 cm on an edge, were now used, being obtained from conventional small ice trays. Freezing took place in a commercial electric deep freeze. A small brass tray, approximately 2 cm by 2 cm with a 0.6 cm lip (the volume of the tray was sufficient to contain all of the melted ice cube's water), was mechanically and electrically connected to the feedthrough of the tunnel (center terminal of a teflon-insulated UHF coaxial cable connector).

The cube was removed from being stored in a dry ice-cooled cold box and placed in the tray via the trap, and the air and equipment turned on. The measuring equipment had two modes of operation. The first, I, as before, shown in Fig. 1a, measures the current flowing as a change of state occurred. The second mode, Q, shown in Fig. 1b, measured the total charge acquired by the cube/water (plus tray) during the change of state.

Figure 2a shows two sample results for the I mode of operation. The melting of the surface apparently does not play a role in the charging; it is only several minutes later that the charging current becomes appreciable. The maximum current comes near the end of the melting, and when the melting is completed, there is no more charging. Observation of the sample during this period gave evidence that some of the stronger current effects were related to the release

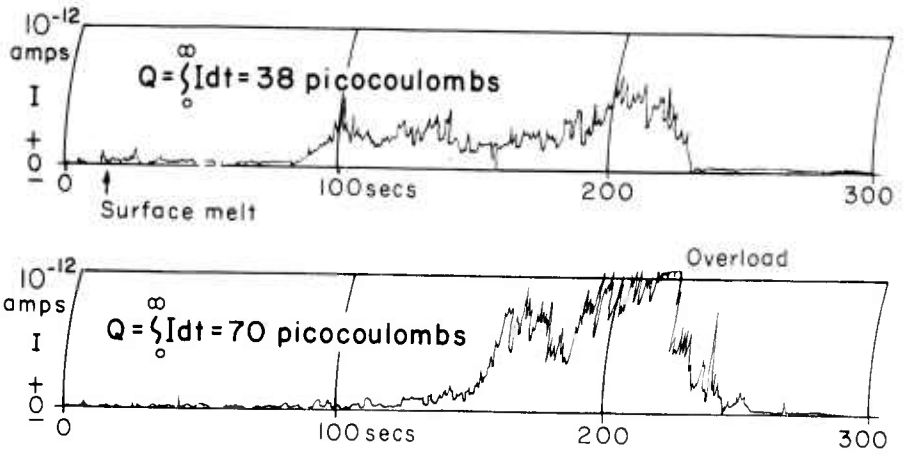

Fig. 2a. I MODE CHARGING, EXPERIMENT 2

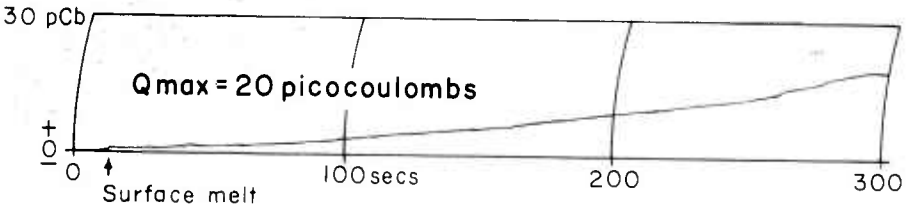

Fig. 2b. Q MODE CHARGING, EXPERIMENT 2

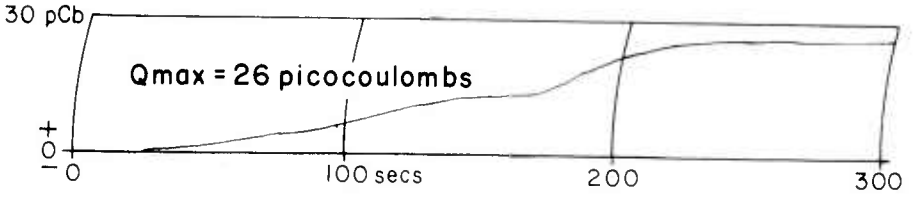

Fig. 2c. 'Q INDUCED' MODE CHARGING, EXPERIMENT 3

of bubbles from the sample. All of the I records illustrated these same overall characteristics, although the details of the current magnitudes and timing of events would vary somewhat. On some occasions there was a bit of extra random 'noise' before the surface melting which was attributed to the frosting of the cold surface in humid conditions, and in some cases the charging current grew a bit more smoothly beginning about half a minute after surface melting.

Figure 2b shows a sample of the Q mode of operation. It is evident that the Q mode is consistent with the I mode, the charge being the integral of the current. The best charging rate is usually near the end of the charging. Tests without an ice cube in the tray showed that the instrumentation setup itself yielded an apparent charging or drift of about 0.5 picocoulomb/min, which should be subtracted from the indicated charge. After the peak charge has been accumulated, it can be observed to leak off slowly because of air conductivity. There were differences in the details of the results of individual Q runs, but all the runs showed the same predominant characteristics.

The I and Q tests all indicated total charges of the order of 30 picocoulombs, with a spread from about 10 to 90 picocoulombs. Such charges are one or two orders of magnitude less than those which would limit further charging because of breakdown gradients at the hydrometeor surface.

5. EXPERIMENT 3

Both the I and the Q techniques discussed above involve continually removing the charge from the ice-water sample and keeping the sample close to ground potential. A different technique, 'Q induced', was therefore used next which left the charge on the sample throughout the change of state. The physical setup is diagrammed in Fig. 1c. The sample is set inside an open-ended Faraday cage, and the charge on the cage is measured. In effect, for the tray of the previous experiments there was substituted the Faraday cage. The sample was placed on a smaller tray, set on paper thermal insulation, on top of a teflon insulating block within the cage.

The results were identical in every way to those for the Q mode in Experiment 2. One example is shown in Fig. 2c. Nineteen tests were run. The average total charge was 26 picocoulombs, and the extremes were 9 and 70 picocoulombs (about 2 picocoulombs should be subtracted from these values to correct for the instrumentation bias).

6. MEASUREMENTS WITH HAIL

A brief series of measurements of charging during melting of hail was conducted at Flagstaff during August, 1963. Since the three separate measurement schemes described earlier had previously all given comparable results, the simplest, (Experiment 2) was used

for the hail study. Although there was considerable scatter to the data and there were not enough tests made to give as much significance as would be desired, several features of the results were distinct and are worth noting here. All the hail was dirty from being collected on the ground.

(a) With zero wind, the charging effect was greatly diminished. The charging was relatively unaffected by wind variations from 3 to 10 m/sec.

(b) Pea to grape size hail gave positive charging during melting of 10 to 20 picocoulombs; the larger sizes were generally associated with the larger charges, but the data show much scatter. The maximum charge densities for the smaller hailstones were on the order of 100 picocoulombs/gm.

(c) A clear hailstone containing very few bubbles showed negligible charging. All the other hailstones appeared whitish because of the many bubbles within them.

7. COMPARISON OF FIELD AND LABORATORY MEASUREMENTS

The laboratory studies reported here agree with the flight observations in that the simulated laboratory hydrometeors became charged during the melting without any cloud particles being present. Further, in the laboratory and in the flight tests the charging was strongest toward the end of the melting. Thus the laboratory tests, and those of Dinger and Gunn (1949) help substantiate the hypothesis that a real

electrification phenomenon is associated with melting. However, the laboratory tests provide only a few clues as to the details of the mechanism, other than to hint that bubbles in the hydrometeor may play a dominant role in the transfer of charge to the air, that the charge is not being transferred by any evaporation effect or by the breakup of hydrometeors, and that a potential gradient in the environment is not essential for the charging. The laboratory tests did not duplicate the ambient temperature, pressure, density, air flow speed, conductivity, space charge, or potential gradient, or the physical structure, internal motions, and gaseous and chemical composition of the hydrometeors (even the tests with hail did not duplicate natural hail properly, using instead hail which was dirty and which had been stored for days or weeks). The laboratory studies also placed the hydrometeors in a relatively confined space, which could attenuate the net electrification from droplets emitted from bursting bubbles by preventing the droplets from blowing downstream. Thus it may not be surprising that the laboratory investigation showed different details of charging from that found in the field.

Dinger and Gunn (1946) relate their charging observations (which were more detailed than those reported here) to the bubbling effects of dissolved gases during melting. They also show the effects of contaminants. The type of ice sample used in the present laboratory tests

did not have many bubbles and so might not be expected to show large effects. Natural graupel or hail has a much more porous structure and offers the opportunity for many more bubbles. In addition, the large surface area of the droplets from which graupel and hail form implies that the natural hydrometeors may contain relatively large amounts of absorbed gas, some of which can be released during warming to create more bubbles. The tests with hail gave results not much different from those with the artificial ice, but it is perhaps significant that the hail data were more erratic, did include the highest charge density case, and showed small charging from clear hail.

Blanchard (1961) has considered the possibilities of hydrometeor charging during melting by the bubble process, in connection with studies on the electrification of the atmosphere from bubbles in the sea. He suggests (a) that the sign of net charging should be independent of the external field except for very strong storm fields, (b) that a net positive charge may be acquired by the main drop, and (c) that the temperature may have a great influence on the charging of drops of low salinity.

Kikuchi and Magono (1961a, b) measured charges on natural snow crystals before and after artificial melting during snowfall and found they acquired considerable positive charge during melting.

Matthews and Mason (1963) examined the charging from melting snow in the laboratory and did not find significant effects. They concluded from their measurements that any charging was less than 3 picocoulombs per gram of melting ice, from one to two orders of magnitude less than the charging found by Dinger and Gunn, found in the present paper, and found in the field by MacCready and Proudfit (1964). The test setups for all these studies were different, but nevertheless the discrepancy in results is hard to explain. The lack of effect in the Matthews and Mason tests might relate in some cases to the type of ice used, to a relatively low sensitivity limit on their electrometer, or to low rates of airflow past the test specimens. In the present study in the tests on hail the rate of airflow was found to affect the results greatly, giving low charging when the airflow was slow. The main factor may be the re-collection of emitted tiny charged droplets back on the large ice-water mass, from the combined effects of gravity and electrostatic forces; such an effect would depend strongly on the wind and on the physical laboratory setup.

8. CONCLUSIONS AND RECOMMENDATIONS

In summary, the evidence seems good that appreciable charging can be associated with hydrometeor melting. It seems likely that some phenomenon pertaining to the release of bubbles is of primary importance in the charging (although the tests of Kikuchi and Magono showed charging with crystals which presumably did not have many bubbles),

but the details of the sign and magnitude of the charging would be expected to vary in some manner with temperature, melting rate, drop size, internal circulation, and the details of physical and chemical composition.

The strength of the charging-during-melting effect is large enough so the phenomenon could conceivably play a significant role in the overall thunderstorm charge distribution picture and in an ice phase. Further studies are warranted, especially in view of the discrepancies between the results of different investigators.

Future laboratory tests should include an emphasis in two areas, (1) a more basic study about the mechanism, with particular attention to the charging of the individual droplets released by bubbles of the size and type encountered in melting ice hydrometeors, and (2) tests which duplicate more closely the actual atmospheric conditions. One approach to the latter area for hail studies would be to employ a tunnel-electrometer in an aircraft, using immediately ice hydrometeors obtained in flight and melting them with ambient air as the plane descends. In this manner most natural conditions would be duplicated.

ACKNOWLEDGMENT

This study has been supported by the Atmospheric Sciences Program, National Science Foundation, under Grant NSF G11969.

REFERENCES

Blanchard, D. C.	1961	Reference No. 61-9, Woods Hole Oceanographic Institution, Tech. Report to ONR, Contract Nonr-798(00)(NR-082-124), April. UNPUBLISHED MANUSCRIPT.
Dinger, J. E. and Gunn, R.	1946	Terrestrial Magnetism and Atmospheric Electricity, 51, p. 477.
Kikuchi, K. and Magono, C.	1961a	Journal Japanese Society of Snow and Ice, 23, p. 41.
Kikuchi, K. and Magono, C.	1961b	Journal Japanese Society of Snow and Ice, 23, p. 155.
MacCready, Jr., P. B. and Proudfit, A.	1964	Submitted to Quart. J. R. Met. Soc.

Atmospheric Research Group, and Meteorology Research, Inc., Altadena, California
FLAGSTAFF CUMULUS STUDIES
P. B. MacCready, Jr., T. B. Smith, C. J. Todd
Joint Report by ARG to Atmospheric Sciences Section, National Science Foundation, Grants No. NSF G8334 and No. NSF G11969, Spring 1959 - Spring 1964
and by MRI to USAERDL, Study and Modification of Convective Storms, Report #4A, 1 April 1963 - 31 March 1964, 245 p. incl. illus. tables photographs (Rept. No. MRI64 FR-134) (Contract DA 36-039 SC-89066, Proj. No. 3A99-27-005-06) (ARPA Order No. 265-62) Unclassified report.

This report describes objectives, instrumentation, analysis techniques, conclusions, and recommendations resulting from four field seasons of basic research field investigations of cloud physics, cloud dynamics, and cloud electrification at Flagstaff, Arizona. The natural outdoor laboratory for natural and seeded clouds was instrumented by use of several aircraft thoroughly equipped for cloud physics measurements, two radars for monitoring precipitation and tracking the aircraft, and a ground photographic network. Results include: a) The instrumented outdoor laboratory technique was developed to a satisfactory stage and cloud seeding proved useful as a research tool, b) A persistent convective wake and associated precipitation was found downwind of the isolated peaks, and necessary conditions for the formation of the phenomena were determined, c) Cloud cross sections were observed by systematic aircraft traverses, and showed continuity consistent with the "starting plume" concept, d) Radiosonde records were analyzed for the height differences which the heat of fusion from cloud seeding could cause, and it was found that conditions often permitted differences exceeding 5000 ft, e) The Formvar type continuous particle sampler was developed and used in the aircraft for quantitatively

UNCLASSIFIED
1. Clouds-Physical properties.
2. Clouds-Electrical properties.
3. Cumulus Clouds-Growth.
I. Title: Flagstaff Cumulus Studies
II. MacCready, P. B., Jr.
III. U. S. Army Electronic R&D Lab., Ft. Monmouth, N. J.
IV. Contract DA 36-039 SC-89066

Atmospheric Research Group, and Meteorology Research, Inc., Altadena, California
FLAGSTAFF CUMULUS STUDIES
P. B. MacCready, Jr., T. B. Smith, C. J. Todd
Joint Report by ARG to Atmospheric Sciences Section, National Science Foundation, Grants No. NSF G8334 and No. NSF G11969, Spring 1959 - Spring 1964
and by MRI to USAERDL, Study and Modification of Convective Storms, Report #4A, 1 April 1963 - 31 March 1964, 245 p. incl. illus. tables photographs (Rept. No. MRI64 FR-134) (Contract DA 36-039 SC-89066, Proj. No. 3A99-27-005-06) (ARPA Order No. 265-62) Unclassified report.

This report describes objectives, instrumentation, analysis techniques, conclusions, and recommendations resulting from four field seasons of basic research field investigations of cloud physics, cloud dynamics, and cloud electrification at Flagstaff, Arizona. The natural outdoor laboratory for natural and seeded clouds was instrumented by use of several aircraft thoroughly equipped for cloud physics measurements, two radars for monitoring precipitation and tracking the aircraft, and a ground photographic network. Results include: a) The instrumented outdoor laboratory technique was developed to a satisfactory stage and cloud seeding proved useful as a research tool, b) A persistent convective wake and associated precipitation was found downwind of the isolated peaks, and necessary conditions for the formation of the phenomena were determined, c) Cloud cross sections were observed by systematic aircraft traverses, and showed continuity consistent with the "starting plume" concept, d) Radiosonde records were analyzed for the height differences which the heat of fusion from cloud seeding could cause, and it was found that conditions often permitted differences exceeding 5000 ft, e) The Formvar type continuous particle sampler was developed and used in the aircraft for quantitatively

UNCLASSIFIED
1. Clouds-Physical properties.
2. Clouds-Electrical properties.
3. Cumulus Clouds-Growth.
I. Title: Flagstaff Cumulus Studies
II. MacCready, P. B., Jr.
III. U. S. Army Electronic R&D Lab., Ft. Monmouth, N. J.
IV. Contract DA 36-039 SC-89066

sampling droplets and crystals in clouds. Also a ground based version was created to replicate settling particles. f) From the records of the sampler operated in a seeded cloud, the concentration and size of crystals were obtained, showing concentration consistency with a diffusion theory and providing quantitative information on crystal development rate. g) An extensive, complete system was generated for computing ice phase hydrometeor development. h) Hydrometeor charges below cloud base were found to change abruptly as ice hydrometeors melted completely, and the observed effect was duplicated in the laboratory but with opposite sign.

sampling droplets and crystals in clouds. Also a ground based version was created to replicate settling particles. f) From the records of the sampler operated in a seeded cloud, the concentration and size of crystals were obtained, showing concentration consistency with a diffusion theory and providing quantitative information on crystal development rate. g) An extensive, complete system was generated for computing ice phase hydrometeor development. h) Hydrometeor charges below cloud base were found to change abruptly as ice hydrometeors melted completely, and the observed effect was duplicated in the laboratory but with opposite sign.

sampling droplets and crystals in clouds. Also a ground based version was created to replicate settling particles. f) From the records of the sampler operated in a seeded cloud, the concentration and size of crystals were obtained, showing concentration consistency with a diffusion theory and providing quantitative information on crystal development rate. g) An extensive, complete system was generated for computing ice phase hydrometeor development. h) Hydrometeor charges below cloud base were found to change abruptly as ice hydrometeors melted completely, and the observed effect was duplicated in the laboratory but with opposite sign.

sampling droplets and crystals in clouds. Also a ground based version was created to replicate settling particles. f) From the records of the sampler operated in a seeded cloud, the concentration and size of crystals were obtained, showing concentration consistency with a diffusion theory and providing quantitative information on crystal development rate. g) An extensive, complete system was generated for computing ice phase hydrometeor development. h) Hydrometeor charges below cloud base were found to change abruptly as ice hydrometeors melted completely, and the observed effect was duplicated in the laboratory but with opposite sign.

DISTRIBUTION LIST

Address	No. of Copies
ARDC Liaison Office, U.S. Army Electronics Laboratories, Attn: AMSEL-RD-LMW, Fort Monmouth, New Jersey 07703	1
USCONARC Liaison Office, U.S. Army Electronics Laboratories, Attn: AMSEL-RD-LMP, Fort Monmouth, New Jersey 07703	1
Director, U.S. Army Electronics Laboratories, Attn: AMSEL-RD-DR, Fort Monmouth, New Jersey 07703	1
Director, U.S. Army Electronics Laboratories, Attn: AMSEL-RD-ADT, Fort Monmouth, New Jersey 07703	1
Director, U.S. Army Electronics Laboratories, Attn: AMSEL-RD-ADJ, (Responsible File & Record Unit), Fort Monmouth, New Jersey 07703	1
Director, U.S. Army Electronics Laboratories, Attn: AMSEL-RD-NR, Fort Monmouth, New Jersey 07703	3
Director, U.S. Army Electronics Laboratories, Attn: AMSEL-RD-SMA, Fort Monmouth, New Jersey 07703	13
OASD (R&E), Room 3E1065, The Pentagon, Attn: Technical Library, Washington, D.C.	1
Office of the Chief, Research and Development, Department of the Army, Attn: CRD/M, Washington, D.C.	1
Commanding General, U.S. Army Electronics Command, Attn: AMCRD-RE, Washington, D.C.	1
Commanding General, U.S. Army Materiel Command, Attn: AMCRD-RE, Washington, D.C.	1
Commanding General, U.S. Army Electronics Proving Ground, Attn: Technical Library, Fort Huachuca, Arizona	1
Commander, Defense Documentation Center, Attn: TISIA, Cameron Station, Bldg. 5, Alexandria, Virginia 22314	20
Chairman, U.S. Army Chemical Corps Meteorological Committee, Fort Detrick, Frederick, Maryland	1
Chief, Meteorology Division, U.S. Army Chemical Corps Proving Ground Dugway Proving Ground, Utah	1

Address	No. of Copies
Director, Atmospheric Sciences Programs, National Science Foundation Washington, D.C.	1
U.S. Army Corps of Engineers, Waterways Experiment Station, P.O. Box 631, Vicksburg, Mississippi	1
Commanding Officer, U.S. Army Signal Missile Support Agency, White Sands Missile Range, New Mexico, Attn: Missile Geophysics Div.	1
Director, Federal Aviation Agency, Attn: Mr. Hilsenrod, Pomona, New Jersey	1
Climatic Center, U.S. Air Force, Annex 2, 225 D Street, S.E. Washington, D.C.	1
Director of Meteorological Research, Office of the U.S. Weather Bureau, Washington, D.C.	1
Department of Meteorology, University of Wisconsin, Madison, Wisconsin	1
Meteorology Department, University of Chicago, Attn: Dr. R. Braham, Jr., Chicago, Illinois	1
Department of Meteorology and Oceanography, New York University, College of Engineering, University Heights, New York 53, N.Y.	1
Meteorology Department, Pennsylvania State College, State College, Pennsylvania	1
Dr. W. Saucier, University of Oklahoma, Norman, Oklahoma	1
Commander, Air Force Command & Control Development Division, Air Research & Development Command, USAF, Attn: Dr. R. Cunningham, Laurence Hanscom Field, Bedford, Massachusetts	1
Director, Bureau of Research & Development, Federal Aviation Agency, Washington, D.C.	1
Chief, Bureau of Naval Weapons (FANE), U.S. Navy Department, Washington, D.C.	1
Officer-in-Charge, Meteorological Curriculum, U.S. Naval Post Graduate School, Monterey, California	1
U.S. Naval Research Laboratory, Attn: Dr. J.E. Dinger, Washington, D.C.	1

Address	No. of Copies
Commanding General, Army Ordnance Missile Command, Attn: ORDXM/RRA, Dr. O.M. Essenwanger, Redstone Arsenal, Alabama	1
Mr. C. Gentry, National Hurricane Research Project, Aviation Bldg., Rm 517, 3240 N.W. 27th Avenue, Miami 42, Florida	1
Institute for Geophysics, University of California, Los Angeles, California, Attn: Dr. M. Neiburger	1
Dr. E.B. Kraus, Woods Hole Oceanographic Institute, Woods Hole, Massachusetts	1
Illinois State Water Survey, University of Illinois, Attn: Mr. Glen Stout, Urbana, Illinois	1
Commanding Officer, U.S. Army Natick Laboratories, Attn: Earth Sciences Division, Natick, Massachusetts	1
Office of Naval Research, U.S. Navy Department, Washington, D.C.	1
Dr. Vincent Schaefer, Schermerhorn Road, Schenectady, New York	1
Texas Water Commission, P.O. Box 2311, Capitol Station, Austin 11, Texas, Attn: Mr. John T. Carr, Jr.	1

UNCLASSIFIED